Department of Natural Resources, Mines and Energy
Office of Groundwater Impact Assessment

Groundwater Modelling Report

Surat Cumulative Management Area

October 2019

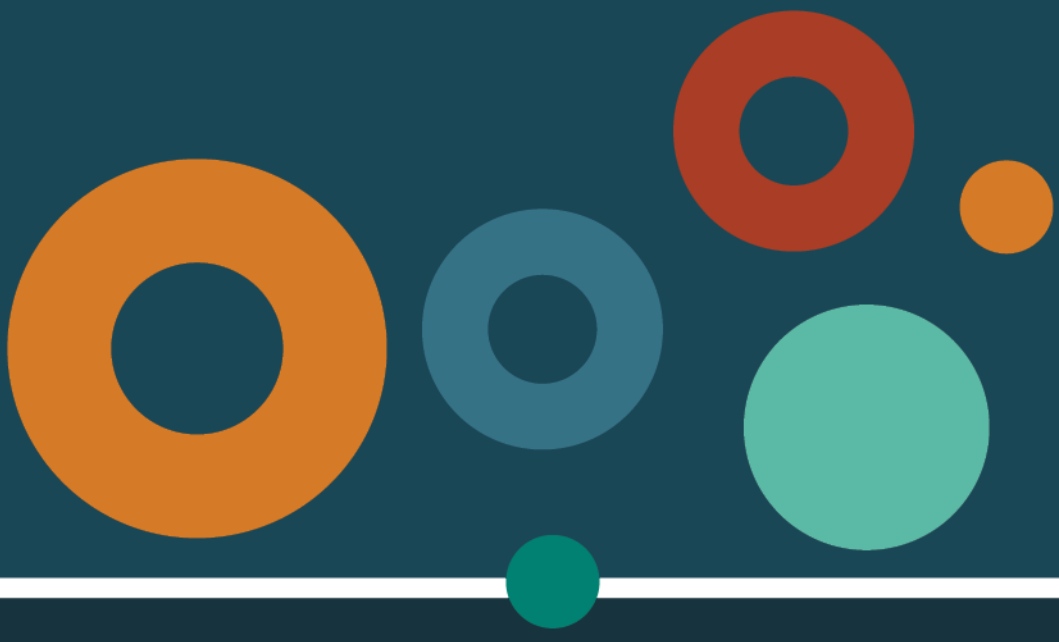

Queensland Government

This publication has been prepared by the Office of Groundwater Impact Assessment, Department of Natural Resources, Mines and Energy.

Bibliographic reference:

OGIA, 2019. *Groundwater Modelling Report – Surat Cumulative Management Area*. OGIA, Brisbane.

Interpreter statement:

The Queensland Government is committed to providing accessible services to Queenslanders from all culturally and linguistically diverse backgrounds. If you have difficulty in understanding this document, you can contact us within Australia on 13QGOV (13 74 68) and we will arrange an interpreter to effectively communicate the report to you.

Contents

Tables

Figures

Appendices

Abbreviations

C	degrees Celsius
Arrow	Arrow Energy Pty Ltd (including subsidiaries and joint venture partners)
CMA	cumulative management area
CSG	coal seam gas
DNRME	Department of Natural Resources, Mines and Energy (Queensland)
DST	drill stem test
GAB	Great Artesian Basin
IAA	Immediately Affected Area
KCB	Klohn Crippen Berger
km	kilometres
L	litres
LAA	Long-term Affected Area
m	metres
ML	megalitres
ML/yr	megalitres per year
mm	millimetres
mm/yr	millimetres per year
OGIA	Office of Groundwater Impact Assessment
Origin	Origin Energy Ltd (including subsidiaries and joint venture partners)
P&G	petroleum and gas
PEST	model-independent parameter estimation and uncertainty analysis software
psia	pressure, pound-force per square inch absolute
QDEX	Queensland Digital Exploration Reports System
QGC	Queensland Gas Company Pty Ltd (including subsidiaries and joint venture partners)
Santos	Santos Ltd (including subsidiaries and joint venture partners)
USGS	United States Geological Survey
UWIR	underground water impact report
Water Act	*Water Act 2000*

This page is intentionally left blank

1 Introduction

1.1 Modelling objectives and purpose

The regional-scale groundwater flow model described in this report is a numerical tool developed by the Office of Groundwater Impact Assessment (OGIA) for the purpose of predicting changes in regional water pressures and water levels in aquifers within the Surat Cumulative Management Area (CMA) in response to extraction of groundwater associated with petroleum and gas (P&G) production. Figure 1-1 shows the extent of the Surat CMA. This model, documented herein, has been used to generate impact predictions to underpin the 2019 Underground Water Impact Report (UWIR) for the Surat Cumulative Management Area (OGIA, 2019a) and is henceforth referred to as the UWIR 2019 model.

More specifically, the UWIR 2019 model is designed for regional cumulative impact assessment to:

- define the immediately affected area (IAA) for each consolidated aquifer present within the model domain – the area where water pressures are predicted to decline by more than 5 m within the next 3 years
- define the long-term affected area (LAA) for each consolidated aquifer present within the model domain – the area where water pressures are predicted to decline by more than 5 m at any time in the future
- identify potentially affected springs – springs where the water pressure in aquifers underlying the sites of these springs is predicted to decline by more than 0.2 m at any time in the future
- predict the rate and volume of water movement between formations
- estimate the quantity of groundwater that is expected to be extracted as a result of P&G developments in the CMA.

The domain of this model covers an area of around 460 × 650 km encompassing the entire Surat CMA. The model domain is discretised into cells of 1.5 × 1.5 km areal extent, 34 layers deep, for the purpose of simulating the flow of groundwater within the Surat Basin sequence and overlying alluvial formations within the Surat CMA, and within the CSG-producing Bandanna and Cattle Creek formations of the Bowen Basin.

1.2 General modelling approach

OGIA's approach to modelling has evolved since the UWIR 2012. The UWIR 2019 model represents the third iteration of conceptualisation, development of customised methods and tools, construction and calibration. Each iteration of the model is informed by a revised understanding of key hydrogeological processes or concepts operating within the Surat CMA at the time.

The first model iteration to predict impacts in the UWIR 2012 was largely based on information from previous studies. Relatively little primary data interpretation was undertaken and the groundwater flow model was developed using a standard version of MODFLOW 2005.

A new model was constructed for the UWIR 2016, which differs significantly from the UWIR 2012 model in terms of both its philosophy and approach. This is reflected in its specifications, construction, parameterization and calibration using a number of innovative modelling techniques developed by OGIA's team and a revised conceptualisation of the groundwater flow system based on primary data

interpretation. This, for example, includes access to an abundance of lithological and other data from CSG wells which is used to undertake regional hydraulic property upscaling for both the CSG target coal reservoir and potentially impacted aquifers using numerical permeameters which are subsequently used to parameterize the regional groundwater model. MODFLOW-USG was the modelling platform for the UWIR 2016 model and a number of revisions were made to the standard MODFLOW-USG modelling code to address unique challenges in the Surat CMA, including:

- simulation of water desaturation due to gas production in coal seams around CSG wells
- more accurate representation of CSG wells using a descending MODFLOW drain methodology
- simulation of reinjection of treated CSG water into the Precipice Sandstone.

This work was undertaken by OGIA in collaboration with one of the primary developers of the MODFLOW code. History matching against historical heads and recent water extraction rates was used for the UWIR 2016 model to constrain predictions of both short and long term CSG impact. In contrast to the UWIR 2012 model, no uncertainty analysis was undertaken for the UWIR 2016 model.

The UWIR 2019 model represents a revision of the previous model and includes a number of further refinements to the modelling approach based on additional data and a revised understanding of key hydrogeological processes and concepts that are operating within the Surat CMA. In the development of the UWIR 2019 more emphasis has been placed on model uncertainty and constraining modelled impact predictions with available groundwater monitoring data. This is achieved through a substantially revised model calibration workflow and inclusion of a predictive uncertainty analysis. A comprehensive list of model improvements is now provided.

1.3 Key improvements in the UWIR 2019 model

Key improvements incorporated into the UWIR 2019 model compared to the previous model include:

- revision of the model structure based on a revised regional geology model at 250 m grid based on geophysical log data from about 7,000 P&G wells, updated geological mapping and other revised data sets ((OGIA, 2019b), section 3.2)
- revised and updated initial model parameterisation drawing on expanded lithological and hydraulic parameter data sets (Chapter 4)
- incorporation of additional major faults (section 3.2.5.7) and open cut coal mines at regional scale (section 3.3.4)
- simulation of CSG well completions in the Surat Basin which extend into the overlying Springbok Sandstone and which required further revisions to the MODFLOW-USG modelling code (sections 2.3.5 and 3.3.3)
- inclusion of a more detailed representation of permeability of the upper Walloon Coal Measures aquitard based on detailed stochastic modelling of the lithology of this key unit (section 4.4.1)
- more accurate simulation of the Origin Energy Ltd (Origin) Precipice re-injection scheme and its impacts on heads in the Precipice (sections 2.3.6 and 5.4.6.3)

- an updated and improved model calibration workflow incorporating time series groundwater level data for more than 470 UWIR WMS and non-UWIR groundwater head monitoring points in CSG reservoirs and key aquifers (section 5.4.6.3)
- completion of a predictive uncertainty analysis (Chapter 7).

Other improvements incorporated into the UWIR 2019 model include:

- representation of a revised contact zone between the Bandanna Coal Measures and Precipice Sandstone (section 3.2.5.5)
- an increase in the number of layers from 32 to 34, to allow representation of the Boxvale Sandstone which forms part of the Evergreen Formation and represents the source aquifer for a number of springs in the area (section 3.2.1)
- a more detailed representation of outcropping Cenozoic age units present within the model domain which was developed as part of the regional geology model build (OGIA, 2019b). Previously only major alluvial sediments associated with the main river systems had been represented in the model
- the use of numerous updated and revised input data sets including initial estimates of recharge (section 3.3.1) and non-CSG groundwater extraction (section 3.3.2)
- extension of the Condamine Alluvium model to the end of December 2017 to provide updated boundary conditions for the Condamine Alluvium area (section 3.3.1).

1.4 Model review

All model development work undertaken since the UWIR 2016 has been subject to ongoing review and endorsement by an independent technical advisory panel established by OGIA. In addition, a formal review of the calibration and uncertainty analysis results presented in this report, undertaken in May 2019, concluded that the UWIR 2019 model is “fit for purpose” for use as a quantitative tool for assessing cumulative impacts of water extraction from coal seam gas bore fields and exceeds national standards for a regional groundwater flow model.

The approximation used to represent coal desaturation and dual-phase flow effects, using a modified Richards equation implemented in the modified version of MODFLOW-USG (section 2.2.3), was also previously subject to academic peer review prior to a research article describing the method (Herckenrath et al., 2015) being accepted by the Journal of Hydrology.

1.5 Report structure

This report provides a description of the UWIR 2019 model which was used to generate the impact predictions for the UWIR 2019. This report is structured as follows:

- Chapter 2 outlines some of the capabilities of the MODFLOW-USG modelling platform that are of relevance to its use in the present context. Information on a number of alterations made to MODFLOW-USG by OGIA for the purpose of better simulating CSG impact is also provided.
- Chapter 3 describes how the basic geometry and boundary conditions for the UWIR 2019 groundwater flow model were developed.

- Chapter 4 describes methodologies developed to generate initial model parameter values, and the likely ranges of these values, for subsequent adjustment during model calibration and uncertainty analyses.
- Chapter 5 describes calibration of the UWIR 2019 groundwater flow model and presents the final calibrated model parameters.
- Chapter 6 describes the configuration of the predictive version of the UWIR 2019 model.
- Chapter 7 outlines the methodology used to undertake a predictive uncertainty analysis in order to generate the probabilistic impact predictions presented in the UWIR 2019.
- Chapter 8 presents the overall conclusions of the work undertaken, identifies the main sources of uncertainty inherent in the model and outlines some potential further work packages.

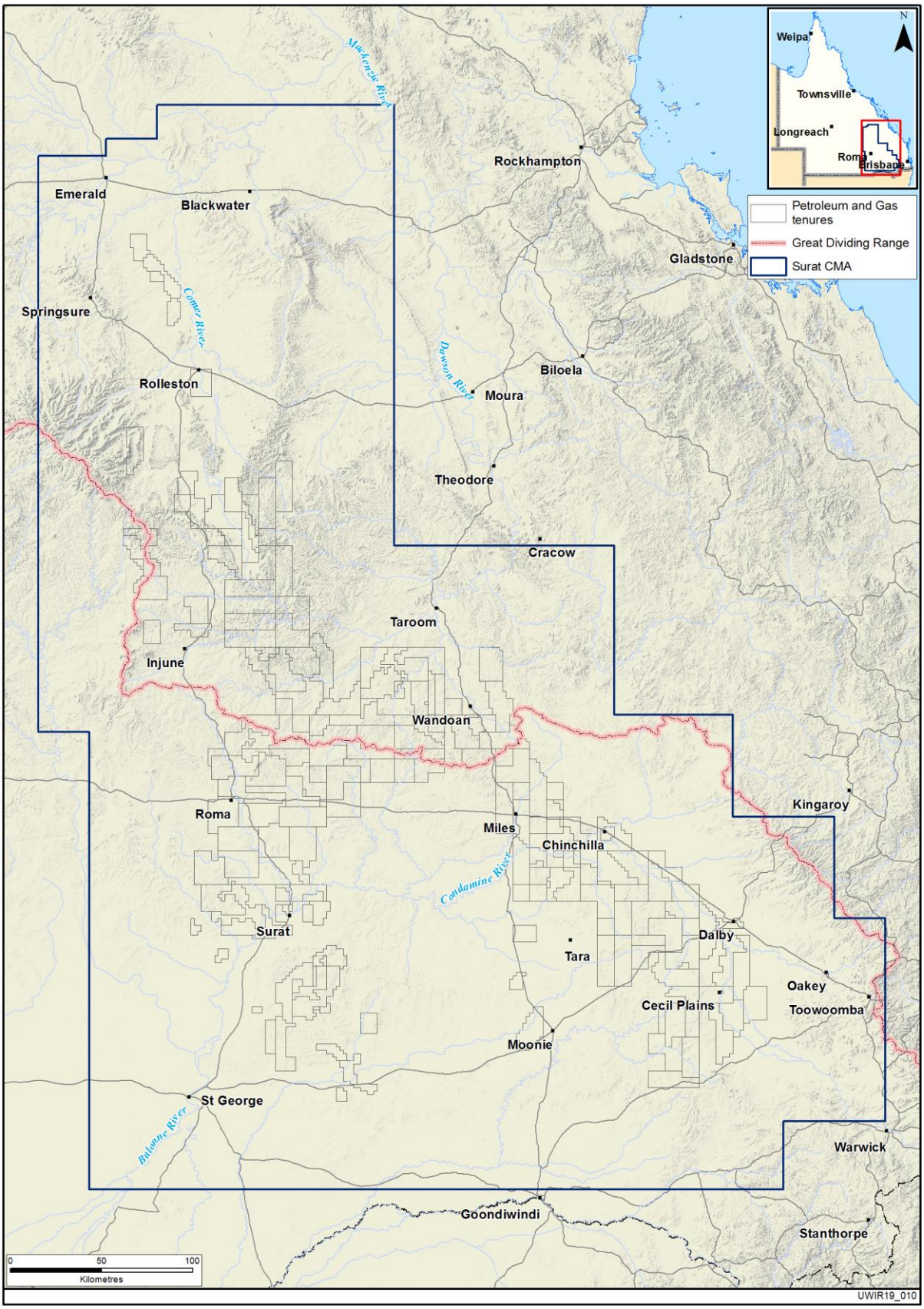

Figure 1-1 The extent of the Surat CMA

2 Modelling software

2.1 In this chapter

The UWIR 2019 model was developed using the MODFLOW-USG groundwater modelling software. This section outlines some of the capabilities of this modelling package that are of relevance to its use in the present context. It also describes:

- alterations made to MODFLOW-USG by OGIA to enhance its ability to simulate regional CSG impact
- some implementation details unique to OGIA's impact assessment.

Similarly, calibration of the UWIR 2019 model was also undertaken using the model-independent parameter estimation and uncertainty analysis software (PEST) package. Some pertinent capabilities of PEST, and its utility support software, are also briefly outlined.

Construction, calibration and deployment of the UWIR 2019 model relied heavily on software developed by OGIA. Mention is also made of some of the tasks performed by these programs. Particular attention is paid to the handling of regional faults.

2.2 MODFLOW-USG

2.2.1 General

The "USG" in MODFLOW-USG stands for "unstructured grid". Its release in 2014 marked a break with previous versions of MODFLOW in which numerical solution of the finite difference equations for groundwater flow required a rectilinear grid. The United States Geological Survey (USGS) version of MODFLOW-USG is described by Panday et al. (2017) and is downloadable from the USGS website: http://water.usgs.gov/ogw/mfusg/.

Since the release of MODFLOW-USG by the USGS, the official USGS version of MODFLOW-USG has remained relatively static. However its principal developer, Dr Sorab Panday (who is not a USGS employee) has continued its development. As he expands the capabilities of MODFLOW-USG, Dr Panday makes updated versions available to the public through the Groundwater Vistas modelling platform. These versions are colloquially referred to as MODFLOW-USG "beta" to distinguish them from the official USGS version of MODFLOW-USG. Dr Panday also makes source code available to collaborators so that project-specific alterations to MODFLOW-USG can be made if required.

The simulator used for OGIA's impact assessment is a modified version of MODFLOW-USG beta, however it is referred to simply as "MODFLOW-USG" herein. Some capabilities of MODFLOW-USG that are salient to regional CSG impact assessment are described in the remainder of section 2.2. Modifications made to MODFLOW-USG by OGIA that enhance its use in CSG impact assessment are described in section 2.3.

2.2.2 Unstructured grid

In contrast to previous versions of MODFLOW, the unstructured grid formulation of MODFLOW-USG allows inactive cells to be extinguished rather than simply deactivated. In a traditional rectilinear grid, inactive cells occur outside areas where flow simulation takes place, but are nevertheless situated within a rectangle that completely encloses the active part of the model domain. Inactive cells also occur in model layers up-dip from formation outcrops. The change in status of such cells from inactive to non-existent reduces model memory requirements considerably, at the same time as it reduces the

size of model input and output files. This can be an important consideration where a model has a large areal domain and possesses many layers, as does the UWIR 2019 model. The elimination of inactive cells also demonstrably increases the execution speed of models developed using MODFLOW-USG.

Use of an unstructured grid brings pronounced benefits to the numerical representation of unconformities wherein stratigraphic layers are removed by erosion prior to deposition of later stratigraphic units. In the UWIR 2019 model, this occurs under the Condamine Alluvium and Main Range Volcanics (see Figure 3-4), as well as at other locations within the model domain. Eroded model layers must be retained in a structured grid; beneath unconformities, they are generally ascribed small thicknesses together with hydraulic properties that pertain to the closest underlying non-eroded model layers. The introduction of awkwardly thin cells in this manner introduces the potential for numerical instability in the model simulation process. In contrast, eroded cells can be eliminated in an unstructured grid. Direct hydraulic connections (sometimes referred to as “non-neighbour connections”) are then made between cells which abut each other across the unconformities.

Regional faults are represented in the UWIR 2019 model through displacement of affected model layers at fault planes. Concomitant enhancement of up-fault permeability and suppression of cross-fault permeability is implemented (refer section 2.5 for details). Use of an unstructured grid allows non-neighbour connections to be made between cells belonging to different model layers that are juxtaposed by fault displacement. At the same time, connections between cells in the same model layer can be broken where fault displacement eliminates contact between cross-fault cells. Meanwhile conductances associated with cross-fault stratigraphic unit connections can be reduced where cross-fault contact areas are reduced, but not eliminated, through fault displacement.

A side benefit of unstructured grid usage is that the introduction, elimination and/or modification of inter-cell connections to reflect the presence of a fault can be undertaken without having to actually modify model layer elevations. Hence, the presence of a fault can be simulated without having to alter model geometry in accordance with displacements that exist in the real world. This allows a model such as the UWIR 2019 model to be used in simulating the local effects of smaller faults whose specifications (or even whose presence) may not be accurately known. Furthermore, such exploration can be readily undertaken in a stochastic sense in a way that only requires alteration of cross-fault connections and associated conductances, as well as adjustments to vertical conductances of fault-abutting cells (to reflect the presence of fault-promulgated vertical flow).

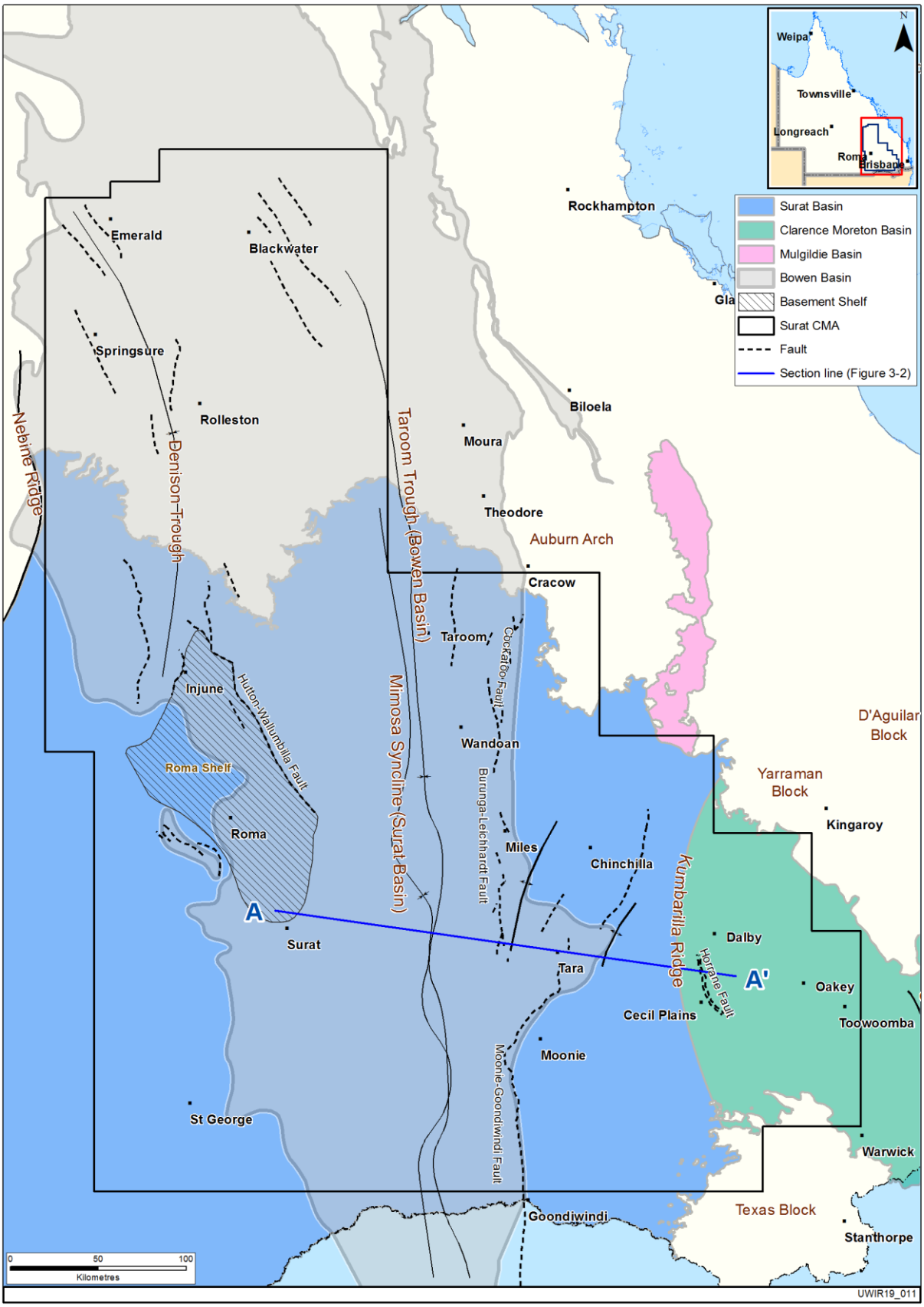

Figure 2-1 Geological basins and major structural features in the Surat CMA

2.2.3 Desaturation

As discussed in Moore et al. (2015), the presence of a gas phase in the vicinity of CSG production wells has a profound effect on flow of water towards those wells, and on lateral propagation of cones of depression away from those wells. In particular:

- more water is extracted from pore storage than from elastic storage in the vicinity of CSG production wells
- the relative permeability pertaining to water is reduced as water saturation of coal seams diminishes.

Some modelling approaches to account for these effects in the context of regional CSG groundwater impact assessment include the use of the reservoir simulator ECLIPSE (Howell et al., 2013) and the use of response functions (Cui et al., 2018). The modelling approach of Herckenrath et al. (2015) was adopted to approximate dual-phase flow effects as a result of coal seam depressurisation. This method is implemented into MODFLOW-USG using a modified form of the van Genuchten equation that allows desaturation to commence at a user-specified pressure head. In the CSG context, this pressure normally coincides with the saturation pressure of the Langmuir isotherm that governs gas desorption, or the natural groundwater head, whichever is smaller.

A series of synthetic studies in which pressures calculated by MODFLOW-USG were compared with those calculated using the ECLIPSE reservoir simulator (Herckenrath et al., 2015) demonstrate that, with proper parameterisation of the van Genuchten relationship, CSG-extraction-induced pressures calculated using MODFLOW-USG can approximate those calculated using ECLIPSE. The accuracy of approximation increases with distance from a well field, and with time since commencement of water and gas extraction; at high times and large distances, which are of primary interest in a regional model such as the UWIR 2019 model, a quasi-equilibrium saturation vs. pressure relationship is attained which can be well-matched by an appropriately parameterised van Genuchten curve.

Herckenrath et al. (2015) demonstrate that if this van Genuchten curve is then employed by the MODFLOW-USG single phase simulator, the latter is able to reproduce ECLIPSE-calculated pressures with reasonable accuracy if both models employ otherwise identical water-pertinent hydraulic properties. They further demonstrate that only a mild deterioration of fit between MODFLOW-USG and ECLIPSE-calculated pressures is experienced in dipping formations where buoyant movement of desorbed gas takes place (a phenomenon that cannot be simulated using a single phase model). However while reproduction of the areal and temporal distribution of ECLIPSE-generated water saturations using MODFLOW-USG is good where coal measure layers are flat, reproduction of water saturations is not as good where coal measures dip.

Herckenrath et al. (2015) conclude that while MODFLOW-USG cannot reproduce ECLIPSE-generated pressures exactly, its reproduction of these pressures is more than good enough for regional CSG impact assessment. In particular, errors in pressure simulation are smaller than errors and uncertainties that are likely to be incurred by the following unavoidable aspects of CSG regional impact assessment modelling:

- the use of model cells of large lateral extent
- vertical integration of complex coal measure stratigraphy into a small number of regional model layers

- uncertainties and spatial variability associated with the many coal measure properties that govern gas desorption and gas and water flow
- the need to upscale these properties to a regional scale where parameterisation is based on pilot points (see section 4.1.2).

In the 2019 regional impact assessment model, desaturation in response to depressurisation can occur in any layer in which CSG extraction takes place, with the exception of the Walloon Coal Measures non-productive zone (layer 11) and lower Springbok Sandstone (layer 10) which are screened by CSG wells at a number of locations throughout the Surat CMA (see sections 2.3.5 and 3.3.3.3).

2.2.4 Dual porosity

Moore et al. (2013) and Moore et al. (2015) suggest that upscaling of coal measures should follow a principle of lithological segregation whereby separate layers of an upscaled regional model are employed to individually represent coal and interburden material. They point out that failure to do this will result in a distortion of the relative water permeability curve. However a strategy of lithological segregation is difficult to implement in a regional impact assessment model, particularly for coal measures in which coal seams are thin and discontinuous. This problem can be overcome to a large extent through adoption of a dual porosity formulation whereby a permeable, porous medium is assumed to possess mobile and immobile domains which are separate in function but not in space. For the UWIR 2019 model, the mobile domain represents coal while the immobile domain represents interburden material comprised predominantly of silt and shale. Water flows through the mobile domain, its rate of flow being governed by the permeability ascribed to the material comprising this domain.

Water can be stored, both elastically and in pores, in both the mobile and immobile domains. In the UWIR 2019 model, only elastic storage is simulated in the immobile domain as it is not allowed to desaturate. However water does not undergo lateral flow in the immobile domain; it can only be transferred to and from the mobile domain at a rate that is proportional to the head difference between these domains in any model cell. In coal measures, such inter-domain water transfer simulates vertical flow of water from interburden material to the nearest coal seam that is connected to a CSG extraction well.

MODFLOW-USG supports the use of dual porosity media. The UWIR 2019 model ascribes a dual porosity formulation to all layers from which CSG extraction takes place. The two domains are linked through what is called a “dual domain flow transfer rate” (DDFTR). An initial value for DDFTR can be calculated from vertical interburden permeability and average spacing of coal seams within an overall model layer that represents part of a coal measure sequence. See section 4.6 of this document for further details.

2.2.5 Other useful MODFLOW-USG capabilities

Other attractive features of MODFLOW-USG that support its choice for regional CSG impact simulation include the following:

- its use of adaptive time stepping in transient simulations contributes to numerical stability in nonlinear simulation contexts such as those which prevail during cell desaturation

- access to source code allows modifications to be made to enhance the performance of MODFLOW-USG in CSG impact assessment; some such modifications are discussed in the following subsections
- inclusion of the Connected Linear Node (CLN) package in MODFLOW-USG simulation functionality.

In early versions of the UWIR 2016 model, the CLN package was employed to simulate extraction from non-CSG wells that tap multiple model layers. Support for multi-layer extraction was, in fact, an important design consideration for the CLN package, as part of its purpose is to replace the older (and often performance-limited) MODFLOW Multi-Node Well (MNW) package. Unfortunately, when employed in the UWIR 2016 model, performance of the CLN package was disappointing as solution convergence was slow and simulation times were large. As a result, the UWIR 2019 model dispenses with the use of the CLN package. Instead it employs separate well boundary conditions in all layers tapped by the same bore. Extraction rates from these separate MODFLOW-USG wells are distributed between layers in proportion to transmissivities encountered by the bore.

2.3 Alterations to MODFLOW-USG

2.3.1 General

During development of the UWIR 2016 model, OGIA collaborated with Dr Sorab Panday (author of MODFLOW-USG) in enhancing its capabilities where necessary to improve its performance in the CSG impact assessment context. Dr Panday made himself available for discussions, altered some aspects of dual porosity simulation to accommodate OGIA's needs, and fixed minor bugs. He also made source code for the beta version of MODFLOW-USG available to OGIA.

The availability of MODFLOW-USG source code allowed OGIA modellers to alter it in minor ways to further enhance its performance in the CSG modelling context. These modifications are described in the remainder of section 2.3; further details can be provided on request. The majority of these modifications were made during development of the UWIR 2016 model and also used in the UWIR 2019 model. Some further modifications to the MODFLOW-USG drain package were, however, required for the UWIR 2019 model to allow simulation of CSG wells which extend into units overlying the target coal reservoir (section 2.3.5).

2.3.2 Derating of pumping

MODFLOW-USG allows pumping from a groundwater node or connected linear network (CLN) node to be reduced if the head in the node falls to a level that is close to the bottom elevation of the cell or linear segment in which the node lies. As programmed in MODFLOW-USG, derating of extraction commences if the head in the node falls to a level that is greater than the bottom of the cell or segment by 1% of the total thickness of the cell or length of the segment.

Experience in using MODFLOW-USG has revealed that derating of extraction from its prescribed value to zero over a short distance can lead to convergence difficulties in the MODFLOW-USG solver. This, in turn, can lead to greatly increased run times. The MODFLOW-USG well package was therefore altered to allow use of an increased derating distance. Alterations allow a modeller to specify the head at which derating commences, as well as that at which extraction diminishes to zero. OGIA software which writes the well package input file for MODFLOW-USG calculates the derating length as the cell-to-well correction length derived from the Peaceman equation (Peaceman, 1978) for the well operating at full extraction. With the zero-extraction elevation coinciding with the elevation of

the pump, derating occurs in a way that effectively maintains the head in an extraction well at or above the level of the pump intake.

Further alterations to the MODFLOW-USG well package allow derating of injection in addition to derating of extraction. This is critical to operation of the MODFLOW-USG reinjection package developed by OGIA; see section 2.3.6 below. Reinjection rates can thus be limited to those that can be sustained by realistic pressures applied to an injection well.

2.3.3 Descending drains

CSG production wells are open to multiple model layers. Extraction of co-produced water (but not gas) from these wells is simulated by the UWIR 2019 model.

Simulation of extraction from a multi-layer well in a standard groundwater model requires that the head ascribed to the well be the same at all places where it connects to groundwater model nodes. Near-hydrostatic conditions are thus assumed to prevail in the well at any instant in time; meanwhile, the head in the well can change over time as drawdown is induced by extraction. Enforcement of such a condition supports appropriate partitioning of extraction between model layers which are tapped by the well.

The hydrostatic condition which underpins simulation of multi-layer extraction of water from a typical groundwater model is inappropriate for simulation of gas extraction. This is because gas wells are not filled with water; instead they have a high gas content, with this gas content increasing over time. If a well is almost completely gas-filled, then conditions in the well approach that of uniform pressure rather than that of uniform head. Where a single phase model such as MODFLOW-USG is employed to simulate gas extraction, boundary conditions that govern movement of water towards the well have more in common with a seepage face than with a traditional groundwater extraction well.

With this in mind, water extraction from CSG wells is simulated in the UWIR 2019 model using a “descending drain” methodology. Suppose that a single CSG well taps five model layers. Then five MODFLOW-USG drains are assigned to that well. The MODFLOW-USG drain boundary condition allows flow out of a model cell, but not into a model cell; flow from each drain-affected cell is governed by a drain-specific head in association with a drain-specific conductance. The elevations of these five drains are originally equated to the head in the highest model layer that is tapped by the CSG well, or the pressure head equivalent of the saturation pressure of the Langmuir isotherm that governs gas adsorption, whichever is lower. Once gas extraction commences from the well, all five drains descend at the same rate, this rate being set by the modeller. Each layer-specific drain ceases its descent at a certain, drain-specific elevation. This is normally the elevation of the centre of the model layer to which each drain is assigned plus the water head equivalent of the bottom hole pressure of the CSG well. However the elevation of the drain assigned to the bottommost layer descends to an elevation equal to that of the bottom of the well screen plus the water head equivalent of the bottom hole pressure. In the uppermost layer tapped by the CSG well, the terminal elevation of the pertinent drain is the top of the well screen plus the water head equivalent of the bottom hole pressure. Addition of the bottom hole pressure term acknowledges well operating conditions as supplied by gas companies. It accommodates the fact that wells are partially gas-filled and partially water-filled.

Software developed by OGIA writes the MODFLOW-USG drain package input file which implements CSG pumping in the manner described above according to extraction schedules supplied by gas companies. Modifications to MODFLOW-USG made by OGIA automate calculation of the conductance associated with each drain boundary condition. This conductance is calculated internally

by MODFLOW-USG using the Peaceman formula. Expanded drain package input functionality supported by the OGIA-modified MODFLOW-USG simulator allows a modeller to provide the diameter of each CSG extraction well. Internally, the revised code ascertains the “enhanced hydraulic conductivity” ascribed to the cell in which each drain is located (see section 2.3.4 below), as well as the water saturation of the cell. Drain conductance is calculated accordingly.

2.3.4 Hydraulic conductivity enhancement

Descending drains representing layer-specific portions of CSG extraction wells are connected to the mobile domain of dual porosity media that occupy model layers representing coal measures. As is described in Chapter 4 of this document, upscaled hydraulic conductivities calculated from numerical permeameters are ascribed to this mobile domain. These hydraulic conductivities reflect the discontinuous nature of coal seams within a coal measure sequence. The “regional hydraulic conductivity” that is calculated using these permeameters is considerably less than that of coal. The transmissivity assigned to a model cell within a coal measure sequence at any location is thus considerably less than the sum of individual coal seam transmissivities at that same location.

What is appropriate for regional transmissivity, however, is not appropriate for the transmissivity that is “seen” by an individual CSG extraction well. The latter is, in fact, the sum of transmissivities intersected by the well. In coal measures, this is dominated by the sum of coal seam transmissivities.

Alterations made to MODFLOW-USG by OGIA implement the reading of a file containing horizontal cell hydraulic conductivities which the extended drain package, discussed above (section 2.3.3), uses for calculation of drain conductances using the Peaceman formula. OGIA software calculates these conductivities through weighted arithmetic averaging of lithology-based hydraulic conductivities; weighting reflects local lithological proportions. The conductance ascribed to a drain that occupies a particular cell is thus representative of the transmissivity with which the well portion simulated by that drain is in contact. In deployment of the UWIR 2019 model, the conductance calculated in this way is modified by a user-supplied factor; the latter is adjusted through the model calibration process.

2.3.5 CSG production from non-coal measure layers

As is discussed above, accommodation of CSG extraction from coal measure layers is realised by endowing these layers with a dual porosity status and a capacity to dewater. However, some CSG wells are understood to be screened into model layers representing the “non-productive” part of the Walloon Coal Measures, as well as from the layer above this which represents the lower Springbok Sandstone. Further alterations to MODFLOW-USG were therefore made to accommodate extraction of co-produced water from these layers. A different approach is required from that used to simulate water extraction from coal measure layers because:

- Only a small amount of water is extracted from these layers, and because the lower Springbok Sandstone in particular contains only a small amount of coal, the UWIR model does not allow these layers to desaturate.
- Wells which extract gas from the lower Springbok Sandstone typically only partially penetrate this layer.

For CSG wells in non-coal-measure layers, cell-to-well conductance is calculated as the inverse of the sum of two resistances. Each of these resistances is, of course, the reciprocal of a pertinent conductance. The two conductances are as follows:

1. The conductance between the casing of the well and the centre of a notional cell that is situated at the base of the partially penetrated layer. The top of this notional cell has the same elevation as the top of the screen of the CSG extraction well.
2. The vertical conductance between the centre of this notional cell and the centre of the MODFLOW-USG model cell from which extraction actually takes place. Where a well fully penetrates the notional (and relatively thin) Walloon Coal Measures non productive zone layer, this second conductance is not needed.

The first conductance is calculated using the Peaceman equation. The second is calculated using the standard formula for conductance of a prism. The base of the prism is at the centre of the notional cell from which gas is extracted (the top of this cell is at the top of the well screen). The top of the prism is at the centre of the actual model cell from which gas is extracted.

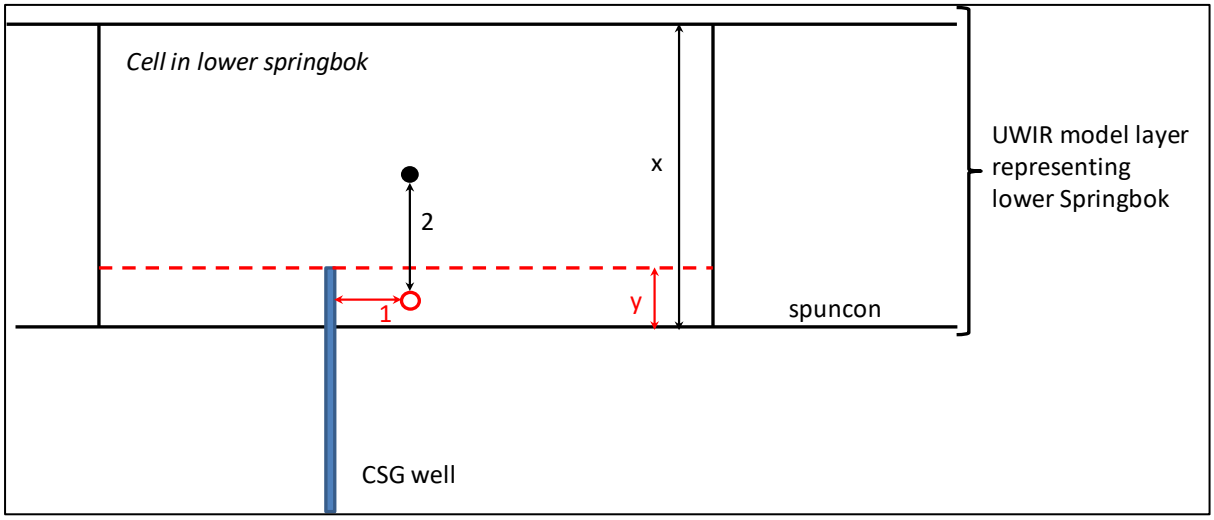

Figure 2-2 Model implementation of a CSG well completion into the Lower Springbok Sandstone

2.3.6 Reinjection package

Simulation of regional CSG impact assessment must accommodate the fact that some of the water extracted from CSG wells is reinjected into other stratigraphic units. OGIA has developed a "reinjection package" for MODFLOW-USG that can simulate this facet of water management. Operation of this package is described as below.

The reinjection package keeps track of water extracted from user-specified groups of drains (i.e. from user-specified groups of CSG extraction wells). Each such group is linked to one or more model nodes through which reinjection of drain-extracted water can take place. Internally, a "reinjection stack" is introduced to MODFLOW-USG wherein a user-specified fraction of group-specific, drain-extracted water can be stored for a user-specified time. Water is placed into a level of the stack that is determined by the amount of time over which it is stored before being reinjected; this storage time can be as small as one stress period if desired. During any stress period, water is withdrawn from the bottom of the stack. As it is withdrawn, it is reinjected into the node or nodes that are associated with the pertinent group of CSG extraction wells. Fractionation of injected water amongst multiple reinjection nodes is undertaken according to the cell transmissivity associated with each node. Reinjection is simulated using the (appropriately modified) MODFLOW-USG well package.

The reinjection package allows the modeller to specify the fraction of CSG co-produced water that is reinjected. However the hydraulic properties associated with cells into which water is reinjected may limit the reinjection rate to a value that is below this. For nodes at which reinjection takes place, the

modeller can supply a head elevation at which the injection rate starts to diminish and a (greater) head elevation at which reinjection ceases altogether. As stated above, this is the converse of functionality added to MODFLOW-USG in which water extraction, rather than injection, is similarly derated. If desired, the difference between these two elevations can correspond to the Peaceman-calculated cell-to-well head difference at full injection rate. Meanwhile the larger of the two heads can correspond to the surface, or to the pressure head imposed on the reinjection well by gas company infrastructure. Code added to the modified MODFLOW-USG well package keeps a record of the difference between requested and actual injection. An "observed value" of zero for this difference can therefore be used as a model calibration target.

2.3.7 Other minor changes

If the user-supplied specific storage for a particular node is negative, MODFLOW-USG has been programmed to reinterpret it as a value for storage coefficient rather than as a value for specific storage. Hence, internally MODFLOW-USG multiplies this value by the area of the cell, but not by the thickness of the cell. This allows specific yield to be supplied to outcropping cells in layers which are otherwise specified as "confined".

MODFLOW-USG saves cell saturations in its drawdown file; where cells can desaturate, drawdown itself is therefore not recorded. To overcome this inconvenience, rudimentary drawdown output protocol was introduced to MODFLOW-USG by OGIA, this providing information used in the model calibration process. The altered MODFLOW-USG is programmed to record binary drawdowns (as well as saturations) at user-nominated stress periods. The stress period for which MODFLOW-USG heads are denoted as reference heads for drawdown calculation can also be supplied by the modeller.

2.4 PEST software suite

Calibration of the UWIR 2019 model was implemented using the PEST software package (Doherty, 2019), downloadable from the website http://www.pesthomepage.org.

As is discussed in Chapter 5 of this document, calibration of the UWIR 2019 model required the adjustment of over 14,000 parameters on the basis of nearly 65,000 observations and penalty conditions. Aspects of advanced PEST functionality required for calibration of the UWIR 2019 model included the following:

- extensive use of Tikhonov regularisation to maintain maximum adherence to upscaled hydraulic property values calculated prior to the calibration process
- invoking SVD-assist functionality to ease the numerical burden of Jacobian matrix assemblage by calculating sensitivities for combinations of parameters that have been identified through singular value composition as being uniquely estimable on the basis of the current calibration dataset
- estimation of parameter upgrades by solving the inverse problem using LSQR which is a numerically efficient scheme when the number of parameters is high
- parallelisation of model runs over hundreds of cores using run management capabilities provided by PEST_HP (Doherty, 2019).

Spatial parameterisation of the UWIR 2019 model employs pilot points. Interpolation from pilot points to MODFLOW-USG nodes employs radial basis functions whose characterisation accommodates spatial variability in pilot point density. All computations associated with pilot point parameterisation

are undertaken using the PLPROC parameter list processor that is downloadable from the PEST web pages (John Doherty, 2018). PLPROC also supports other aspects of complex model parameterisation such as parameter value limiting, cross-layer parameter assignment and mathematical operations between parameters at both the pilot point and model node level.

Also downloadable from the PEST web pages are a suite of programs which automate PEST setup in calibration of groundwater and other models. Some of these programs perform tasks unrelated to parameter estimation, such as facilitating visualisation of model parameter fields and outputs. See (John Doherty, 2018). Model construction tasks which were implemented or assisted by programs of the PEST Groundwater Utilities Suite included the following:

- parameter pre-processing and manipulation such as, for example, calculation of cell-based vertical hydraulic conductivities from cell-based horizontal conductivities and a layer-specific vertical anisotropy ratio
- two-dimensional spatial interpolation from pilot points to MODFLOW-USG grid cells and imposition of cell-based parameter bounds
- building of covariance matrices for use in Tikhonov regularisation
- addition of Tikhonov regularisation constraints to PEST input datasets
- conversion of binary MODFLOW-USG output files from double to single precision (a double precision version of MODFLOW-USG was employed in order to reduce the propensity for solver convergence failure)
- extraction of heads and water budget information from binary MODFLOW-USG output files
- interpolation of MODFLOW-USG outputs to the locations and times of measurements
- processing of model outputs and corresponding observations on the basis of user-supplied equations for use in the calibration process
- exporting MODFLOW-USG cell geometries and properties for use by the PARAVIEW open-source, multi-platform, data visualisation package.

2.5 Regional faults

Twenty two of the 32 active regional fault segments identified in the regional geology model (OGIA, 2019b) are explicitly represented in the UWIR 2019 model. Ten small faults which were previously identified by UQ but which only appear to affect the base of the Walloon Coal Measures were not included in the groundwater model. The exclusion of these small faults is consistent with the overall approach to the explicit inclusion of only major faults in the regional model structure.

Model layers are offset at regional fault planes; cross-fault model node linkages are removed, modified and/or introduced to accommodate layer abutment relationships induced by vertical fault slip.

The UWIR 2019 model also accommodates outcomes of faulting that can extend beyond those induced simply by layer displacement along a fault plane. These are:

- smearing of fault-entrained material over the fault plane
- inter-formational flow along the fault plane
- enhancement of vertical permeabilities within the damage zone adjacent to the fault.

The effect of faulting on fluid migration in petroleum reservoirs has received a great deal of attention in the petroleum literature. Studies have related the nature and amount of fault-entrained material to displacement of the fault (see for example (Manzocchi et al., 2010; Yielding, 2002)), and have related fault and damage zone widths to fault throw (see for example, Bense et al. (2013); Faulkner et al. (2010); Manzocchi et al. (1999); Sperrevik et al., (2002).

In the UWIR 2019 model, fault plane and damage zone properties are represented in a manner similar to that described by Bense and Person (2006). Cross-fault and near-fault properties represented in the model are modified using software specifically developed to implement this representation. A brief description of the methodology follows.

Using software developed by OGIA, a modeller nominates the width of a fault and the width of the damage zone associated with a fault; these can vary along the length of a fault if desired. At any point along the fault, this software calculates the throw of the fault from local layer displacement as represented in the UWIR 2019 model. Fault-entrained material at that point is assumed to be comprised of all lithologies that are within a throw-length of the point; the entrained proportion of each material is assumed to be the same as local lithological proportions encountered along the throw length, these being obtained through interpolation between geophysical logs, where available, or inferred from other geological evidence and provided as inputs to OGIA software. The cross-fault hydraulic resistance at any point within the fault plane is obtained by summing the resistances of entrained lithologies at that point. The resistance of each entrained lithology is calculated as its entrained thickness divided by its vertical hydraulic conductivity. This cross-fault resistance is introduced to the model using the MODFLOW-USG horizontal flow barrier (HFB) package for model layers that are thick enough for their continuity to be preserved across the fault. MODFLOW-USG does not support HFB between cells that do not belong to the same layer; so this option is not available for cells that are juxtaposed across a fault entirely as a result of fault displacement.

Up-fault conductance is calculated through summation of entrained lithological conductances. The conductance of each entrained lithology is calculated as its horizontal hydraulic conductivity times its entrained thickness. The vertical conductivity of the damage zone is calculated under the assumption that vertical hydraulic conductivity anisotropy within this zone has been reduced to 1.0 through catalysis. Fault zone and damage zone vertical conductances are summed to yield total up-fault conductance. The vertical conductivity of cells on either side of the fault is adjusted to accommodate this conductance. The following should be noted:

- calculation of cross-fault resistance and up-fault conductance employs lithological hydraulic conductivities rather than upscaled hydraulic conductivities; the latter are translated to lithological equivalents using three “downscaling factors” in each faulted layer computed from numerical permeameters described in Chapter 4 of this document. The derivation and role for each of these factors are as follows:
    1) when multiplied by the upscaled horizontal hydraulic conductivity, achieve a number that approaches the arithmetic average of lithological horizontal hydraulic conductivity; these are used in the calculation of fault width contributions to upscaled vertical conductance
    2) when multiplied by the upscaled horizontal hydraulic conductivity, achieve a number that approaches the harmonic average of lithological horizontal hydraulic conductivity; these are used for calculation of fault damage zone contributions to upscaled vertical conductance

3) when multiplied by the upscaled vertical hydraulic conductivity, achieve a number that approaches the harmonic average of lithological vertical hydraulic conductivity; these are used for computation of fault horizontal flow barrier characteristics.

- OGIA software allows cross-fault resistances and up-fault conductances calculated in the manner described above to be modified by user-supplied factors which can diminish or enhance the degree to which they alter background hydraulic properties.

2.6 Other in-house software

Other software written by OGIA facilitated UWIR 2019 model development, calibration and processing in ways that include the following:

- translation of model inputs in structured grid format to unstructured grid format
- construction of all MODFLOW-USG input files
- introduction of non-neighbour connections (and adjustment of original neighbour connections) to accommodate regional faulting in the model domain
- modification of node-to-bore interpolation factors used in attributing model-calculated heads to specific bores to account for potential loss of connection across faults
- processing of historical and projected CSG-related and non-CSG-related pumping data
- processing of historical borehole water level data.

3 Model setup

3.1 In this chapter

This chapter describes how the basic geometry and boundary conditions for the UWIR 2019 model were developed. Specifically, information is provided on the following model features:

- horizontal and vertical model discretisation
- model layer types
- model boundary conditions
- assignment of input stresses.

This chapter also makes reference to various calibration simulations which are detailed in Section 5.3. In summary, they are as follows:

- a steady state simulation of hydraulic conditions which existed prior to the commencement of any significant groundwater extraction from the Surat CMA, referred to as the *1947 steady state simulation*
- a steady state simulation of hydraulic conditions which existed prior to the commencement of CSG extraction from the Surat and Bowen basins within the CMA in 1995, referred to as the *1995 steady state calibration*
- a transient simulation representing the post CSG development period from January 1995 to December 2017, referred to as the *transient calibration.*

Parameterisation of the model is described in Chapter 4.

3.2 Model geometry and layering

3.2.1 Model layer specification

The hydrostratigraphy of the Surat and Bowen basins within the model domain (see Figure 3-1) has been represented numerically using the 34-layer system shown in Figure 3-2. Two further layers have been added compared to the UWIR 2016 model (OGIA, 2016a) to allow simulation of the Boxvale Sandstone which forms part of the Evergreen Formation. Otherwise the layering system is the same as that employed in the previous model with at least one regional model layer used to represent each of the main stratigraphic units present within the Surat CMA.

A number of stratigraphic units are also represented by multiple model layers. In particular the main target coal reservoirs (the Walloon Coal Measures, Bandanna Formation and Cattle Creek Formation) are represented using a minimum of three layers to allow a more accurate representation of aquifer geometry in key areas such as the Condamine Alluvium, where coal seams subcrop beneath other aquifer layers, as well as allowing for improved simulation of vertical gradients induced by CSG extraction.

The Springbok Sandstone and Hutton Sandstone are also subdivided into two layers to accommodate vertical variation of hydraulic properties within these units, based on geophysical log interpretations that show distinct differences in lithology and hydraulic properties in the upper and lower parts of these formations (OGIA, 2019b).

The specifics of the construction of various model layers from the updated OGIA's revised geological model (OGIA, 2019b), including the approach to layer subdivision, are discussed in section 3.2.5.

3.2.2 Model extent

The regional groundwater model domain encompasses the entire Surat CMA and includes representations of coal seam formations and potentially connected aquifers within the Surat, southern Bowen and Clarence-Moreton basins. It covers an area of around 300,000 km^2. Figure 3-1 shows the location of the model domain in relation to the Surat CMA.

The domain of the UWIR 2019 regional groundwater flow model is the same as that employed in the previous UWIR 2016 model.

As previously noted, the model includes 34 layers to represent the full Great Artesian Basin (GAB) sequence, alluvial formations within the Surat CMA and the CSG-producing Bandanna and Cattle Creek formations of the Bowen Basin (refer to Figure 3-2). An illustrative cross-section of the model layering is provided in Figure 3-3.

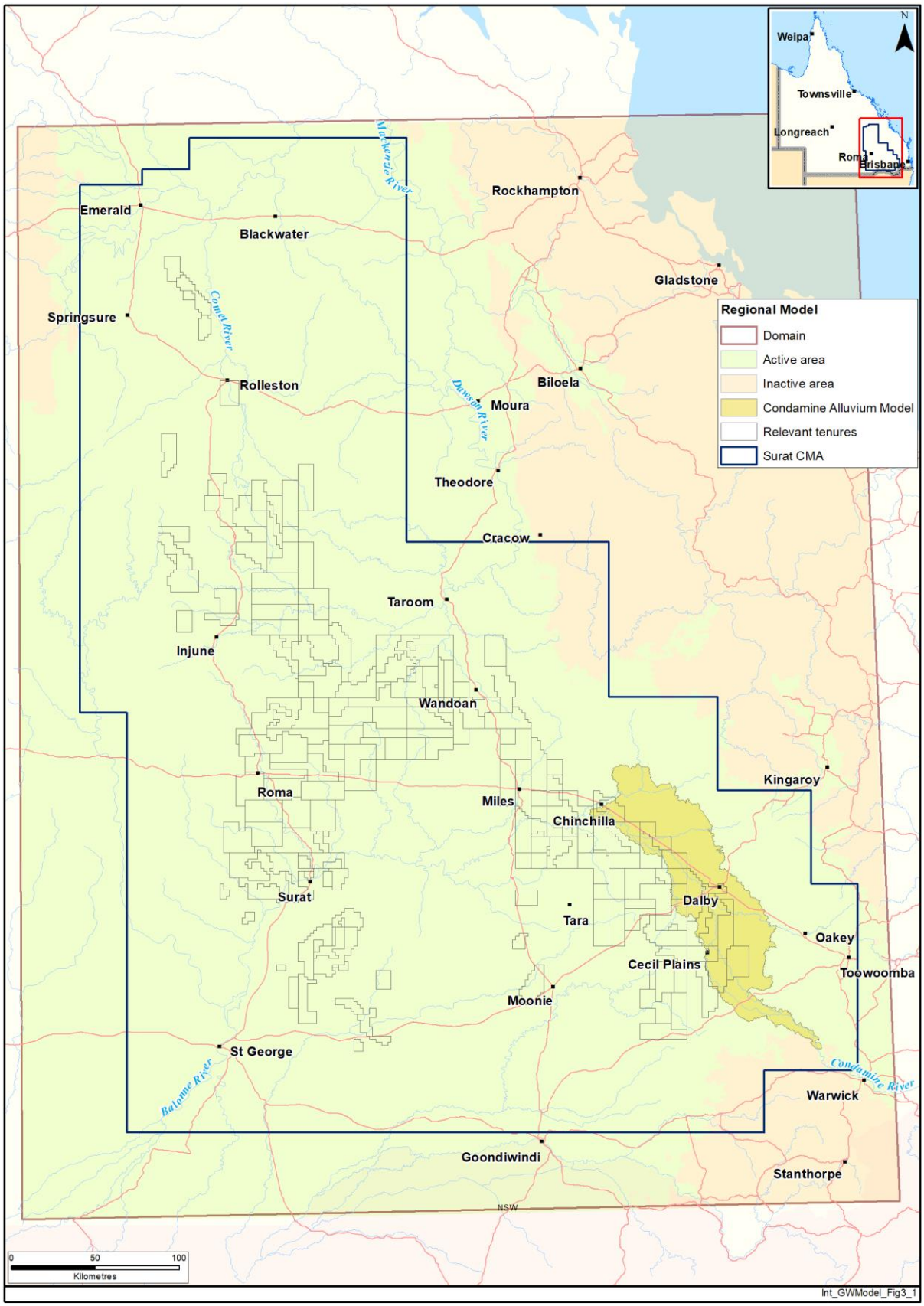

Figure 3-1 Regional groundwater flow model domain

Model layer	Formation	
1	All Alluvium and Basalt (including Main Range Volcanics)	Surat & Clarence-Moreton basins
2	Upper Cretaceous (Griman Creek Formation & Surat Siltstone) / Cenozoic Sediments *(including the Condamine-Walloon transition zone)	
3	Wallumbilla Formation	
4	Bungil Formation	
5	Mooga Sandstone	
6	Orallo Formation	
7	Gubberamunda Sandstone	
8	Westbourne Formation	
9	Upper Springbok Sandstone	
10	Lower Springbok Sandstone	
11	Walloon Coal Measures non-productive zone	
12	Upper Walloon Coal Measures	
13	Middle 1 Walloon Coal Measures	
14	Middle 2 Walloon Coal Measures	
15	Middle 3 Walloon Coal Measures	
16	Lower Walloon Coal Measures	
17	Durabilla Formation	
18	Upper Hutton Sandstone	
19	Lower Hutton Sandstone	
20	Upper Evergreen Formation	
21	Boxvale Sandstone	
22	Lower Evergreen Formation	
23	Precipice Sandstone	
24	Moolayember Formation	Bowen Basin
25	Clematis Group	
26	Rewan Group	
27	Bandanna Formation non-productive zone	
28	Upper Bandanna Formation	
29	Lower Bandanna Formation	
30	Lower Bowen 1	
31	Cattle Creek Formation non-productive zone	
32	Upper Cattle Creek Formation	
33	Lower Cattle Creek Formation	
34	Lower Bowen 2	

Regional aquifer Partial aquifer Tight aquifer Interbedded aquitard Tight aquitard

Figure 3-2 Layers and corresponding aquifers represented in the regional groundwater flow model

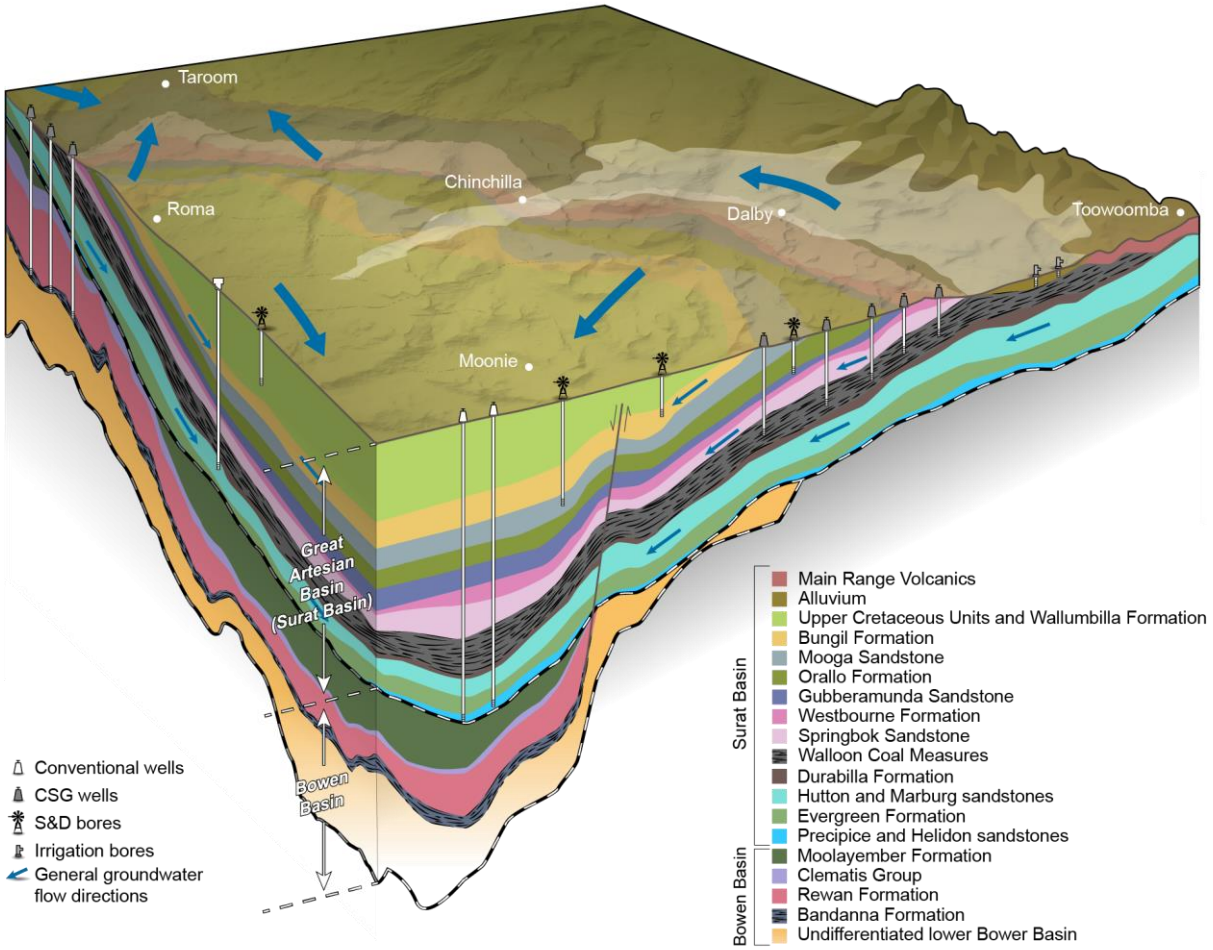

Figure 3-3 Conceptual model of groundwater systems in the Surat CMA

3.2.3 Grid specifications

The numerical model grid is assigned a horizontal datum and spatial grid reference conforming to the Geocentric Datum of Australia (GDA) for the Map Grid of Australia (MGA) 1994 (Zone 55). The top-left corner of the grid is located at 551,000 m E and 7,445,000 m N; the principal axes of the model grid are oriented in the northerly and easterly directions. A model domain of approximately 650 km length in the north-south direction and 460 km length in the east-west direction was discretised using 433 rows and 306 columns of uniformly sized 1.5 × 1.5 km cells. In total, the model comprises 1,305,003 active cells or nodes; the number of active cells or nodes for each layer, the starting and ending nodal indices, and the associated horizontal planar area for each model layer are provided in Table 3-1. Furthermore, the model grid was strategically placed to ensure that cell centres of the model are concordant with the cell centres of the previous two iterations of UWIR model. The influence of spatial interpolation on comparisons made between outputs of the three models is thereby avoided.

Table 3-1 Model layer extent and node specifications

Stratigraphic unit(s)	Model layer	Horizontal planar area (km^2)	Number of nodes	Node starting index	Node ending index
Alluvia, basalt and Cenozoic Sediments	1	119,480	53,102	1	53,102
Upper Cretaceous	2	60,854	27,046	53,103	80,148
Wallumbilla Formation	3	76,300	33,911	80,149	114,059
Bungil Formation	4	81,659	36,293	114,060	150,352
Mooga Sandstone	5	86,848	38,599	150,353	188,951
Orallo Formation	6	93,337	41,483	188,952	230,434
Gubberamunda Sandstone	7	96,095	42,709	230,435	273,143
Westbourne Formation	8	98,939	43,973	273,144	317,116
Upper Springbok Sandstone	9	104,369	46,386	317,117	363,502
Lower Springbok Sandstone	10	104,897	46,621	363,503	410,123
Walloon Coal Measures non-productive zone	11	59,004	26,224	410,124	436,347
Upper Walloon Coal Measures	12	72,709	32,315	436,348	468,662
Middle 1 Walloon Coal Measures	13	86,114	38,273	468,663	506,935
Middle 2 Walloon Coal Measures	14	98,156	43,625	506,936	550,560
Middle 3 Walloon Coal Measures	15	110,570	49,142	550,561	599,702
Lower Walloon Coal Measures	16	120,341	53,485	599,703	653,187
Durabilla Formation	17	122,211	54,316	653,188	707,503
Upper Hutton Sandstone	18	135,041	60,018	707,504	767,521
Lower Hutton Sandstone	19	135,335	60,149	767,522	827,670
Upper Evergreen Formation	20	114,955	51,091	827,671	878,761
Boxvale Sandstone	21	57,458	25,537	878,762	904,298
Lower Evergreen Formation	22	116,339	51,706	904,299	956,004
Precipice Sandstone	23	83,716	37,207	956,005	993,211
Moolayember Formation	24	69,638	30,950	993,212	1,024,161
Clematis Sandstone	25	73,271	32,565	1,024,162	1,056,726
Rewan Group	26	78,721	34,987	1,056,727	1,091,713
Bandanna Formation non-productive zone	27	86,882	38,614	1,091,714	1,130,327
Upper Bandanna Formation	28	91,382	40,614	1,130,328	1,170,941
Lower Bandanna Formation	29	83,104	36,935	1,170,942	1,207,876
Undifferentiated Bowen Basin	30	109,872	48,832	1,207,877	1,256,708
Cattle Creek Formation non-productive zone	31	23,441	10,418	1,256,709	1,267,126
Upper Cattle Creek Formation	32	23,468	10,430	1,267,127	1,277,556
Lower Cattle Creek Formation	33	23,468	10,430	1,277,557	1,287,986
Undifferentiated Bowen Basin strata	34	38,288	17,017	1,287,987	1,305,003

3.2.4 Model boundaries

3.2.4.1 No flow

As shown in Figure 3-1, three areas towards the northwest, northeast and southeast of the model domain have been deactivated by defining no-flow boundary conditions in all model cells within these areas. These are areas where the principal stratigraphic units of both the Surat and Bowen basins are absent and early Permian units or basement bedrock is present at outcrop. There is no data to suggest that groundwater interaction occurs across these basin boundaries; hence negligible flow is anticipated into both the Bowen and Surat basins from areas to the northwest and northeast of the modelled area (GHD, 2012). The no-flow area towards the northeast of the CMA also excises the Mulgildie Basin from the active domain of the UWIR 2019 model. This is a small, elongated basin which extends northward towards Monto. There is no evidence of significant hydrological interaction between this sub-basin and the Surat Basin proper; as such, it is unlikely to be affected by P&G production from the Surat Basin (GHD, 2012). The northern model boundary is also a no-flow boundary for the Bowen Basin, as little or no interaction between the northern and southern halves of the Bowen Basin is anticipated (GHD, 2012). The eastern model boundary coincides with a hydrogeological flow divide along the Helidon Ridge which has been represented as a no-flow boundary which therefore prevents any ingress of water from the Clarence-Moreton Basin to the east of the model domain.

3.2.4.2 General head boundaries

Only minor, if any, interaction occurs between groundwater within the CMA and waters to the west of the Nebine and Eulo ridges. A north-south aligned GHB was therefore ascribed to the western edge of the UWIR 2019 model. Use of this boundary in the manner now described accommodates uncertainties associated with the location of the regional groundwater divide.

A GHB specifies the head at some distance from the designated boundary. It also specifies a conductance that represents aquifer materials between the model boundary and the distant head. Prior to calibration of the UWIR 2019 model, all cells along the western GHB were assigned head values consistent with calibrated steady state heads along the western boundary of the UWIR 2012 model. Values of conductance for each western GHB cell were computed on the basis of (i) the horizontal distance and (ii) the arithmetically averaged transmissivity, between the respective western boundaries of the UWIR 2012 and UWIR 2019 models along each pertinent model row for equivalent aquifers or productive coal units represented by the model. These are layers 4-5, 7, 9, 10, 12-16, 18-19, 21 and 23 of the UWIR 2019 model.

The southern boundary of the UWIR model domain is approximately aligned with the Queensland State border. It is not associated with any identifiable hydrogeological boundary. In fact, groundwater flow within the Surat Basin is believed to flow southward into the GAB through this boundary. However, the general lack of data on groundwater pressures in this area precludes the assignment of heads to the boundary on the basis of historical observations. A GHB was therefore ascribed to cells along the southern extent of the model to simulate connectivity of the model domain with the wider GAB. The heads associated with this boundary were all ascribed the topographic surface elevation at each model cell. This involved model layers 4-5, 7, 9, 10, 12-16, 18-19, 21 and 23 of the UWIR 2019 model. GHB conductance values were then calibrated to ensure respect for steady state heads observed in bores near the boundary.

GHB cells comprising the southern and western boundaries of the UWIR 2019 model are depicted for pertinent model layers in Appendix A1.

3.2.5 Groundwater model layer construction

Most layers of the UWIR 2019 model were defined by extraction of pertinent surfaces extracted from the revised and updated regional geological model constructed by OGIA (OGIA, 2019b). Maps of the lateral extents and thicknesses of the geological layers which these surfaces define are provided in the related technical report (OGIA, 2019b).

These geological model reference surfaces formed the main input to the numerical groundwater flow model. Grid construction for the latter involved the following steps:

- Merging of the reference surfaces pertaining to the base of alluvial strata, base of Cenozoic sediments and the base of basalts (which includes the Main Range Volcanics) into a single surface so that they could collectively comprise a single layer of the groundwater flow model.
- Upscaling the DEM-1S (approx. 30 × 30 m) used to define the ground surface in the geological model to the 1.5 × 1.5 km groundwater flow model grid using bilinear resampling. This resampled surface forms the top surface of the UWIR 2019 model.
- Upscaling the 250 × 250 m gridded geological formation reference surfaces to the groundwater flow model grid using bilinear resampling.
- Extraction of a 1 m thick layer from the base of the Condamine Alluvium to represent the Condamine transition zone (see section 3.2.5.1).
- Subdivision of the Springbok Sandstone and Hutton Sandstone units using surfaces that delineate the estimated depth at which discernible transitions in hydraulic characteristics occur (see section 3.2.5.2).
- Subdivision of coal-bearing units into multiple model layers (see sections 3.2.5.3, 3.2.5.4 and 1.1.1.1)
- Ensuring that unconformable relationships between stratigraphic layers were respected by removal of cells up-dip of stratigraphic layer outcrop areas and up-dip of layer subcrop areas under unconformities. As noted in section 2.2.2, the unstructured grid employed by MODFLOW-USG supports elimination, rather than deactivation, of cells that are not required in a simulation by virtue of an unstructured formulation. Beneath unconformities, cell elimination is accompanied by the introduction of vertically-oriented, non-neighbourhood cell connections that "bridge" eliminated cells. Cell elimination was undertaken for cell thicknesses of less than 0.5 m.
- Insertion of the Cattle Creek Formation into the undifferentiated Bowen Basin strata underlying the Bandanna Formation. This was specified using a pair of surfaces representing spatially-varying estimates of the distance from (i) the base of the Bandanna Formation to the top of the Cattle Creek Formation and (ii) from the top of undifferentiated Bowen Basin strata to the base of the Cattle Creek Formation. These surfaces were interpolated from CSG company picks and control data along the extent of the Cattle Creek Formation. The thickness isopach was subdivided into three layers; the uppermost layer comprised a non-productive zone of 10 m overlaying two layers of equal thickness.
- Introduction of non-neighbourhood connections and/or removal of existing connections between cells as a result of layer juxtaposition incurred through stratigraphic displacement by regional faults (see section 3.2.5.7).

- Translation of structured grid surfaces to an unstructured nodal geometry as required by MODFLOW-USG; this was accomplished using utility software developed by OGIA.

Isopach maps showing the extent and thickness of each model layer resulting from this process are included in Appendix B1.

3.2.5.1 Representation of the Condamine Alluvium transition zone

The Condamine Alluvium is incised into the Walloon Coal Measures by up to 120 m in the south-eastern region of the model domain. Over most of this area, the contact between the formations is dominated by undifferentiated clays comprising basal alluvial clays of the Condamine Alluvium and/or the weathered upper part of the Walloon Coal Measures. This contact zone forms the "Condamine Alluvium transition zone". The transition zone is considered to be discontinuous; where present, the transition zone ranges from less than 1 m to just over 15 m in thickness. In areas where the transition zone is absent and the Springbok Sandstone does not subcrop, coal seams of the Walloon Coal Measures may come into direct contact with the overlying Condamine Alluvium; see (OGIA, 2016c) for a more detailed discussion on the conceptualisation of Condamine Alluvium connectivity with the Walloon Coal Measures and the transition zone.

Vertical flow between the Condamine Alluvium and the underlying Walloon Coal Measures is largely controlled by the properties of transition zone clays, and of mudstone and siltstone that overlies the uppermost coal seams of the Walloon Coal Measures. A collaborative research project was undertaken to improve understanding of the degree of connectivity between the Condamine Alluvium and strata of the Surat Basin which it unconformably overlies (OGIA, 2016c). This study provided estimates of the range of vertical hydraulic conductivities which characterise the transition zone; it concluded that connectivity is generally low.

The undifferentiated clay transition zone at the base of the Condamine Alluvium is represented in the UWIR model as a hydraulic resistance term. This was done by first excising a 1 m thick zone from the base of the Condamine Alluvium. This zone was then assigned to layer 2 of the model. Parameterisation of this layer is described in section 4.3.1 and comprises spatially varying resistance values calculated from available estimates of vertical hydraulic conductivity and thickness isopachs inferred from available logs.

3.2.5.2 Layer subdivision of the Springbok and Hutton sandstones

Analysis of available geophysical log data suggests that lower parts of the Springbok Sandstone tend to be dominated by coarse to very coarse-grained sandstones. In contrast, the upper portion of the Springbok Sandstone is typically comprised of fine to coarse-grained, felspathic to lithic sandstone interbedded with siltstone and mudstone. Conversely, upper parts of the Hutton Sandstone are typically characterised by thick, indurated sandstones compared to the more thinly interbedded sandstone/siltstones which underlie them (OGIA, 2019b). Both the Springbok Sandstone and the Hutton Sandstone were therefore subdivided vertically to allow these observed differences in lithological composition to be represented in the groundwater flow model. Each formation was divided into two layers on the basis of lithology proportion maps inferred from geophysical logs. Interpolation from boreholes where logging data is available to the grid of the UWIR 2019 model was constrained to respect inferred formation boundaries and mapped outcrop areas.

Isopach maps showing the extent and thickness of the model layers representing the upper and lower Springbok Sandstones are provided in Figure B1-9 and Figure B1-10 of Appendix B1, and the upper and lower Hutton Sandstones are provided in Figure B1-18 and Figure B1-19 of Appendix B1.

3.2.5.3 Layer subdivision of the Walloon Coal Measures

The Walloon Coal Measures comprises a sequence of discontinuous permeable coal seams interbedded with low-permeability material consisting of siltstones, mudstones and fine-grained sandstones. As discussed previously in section 2.2.4, Moore et al. (2013) and Moore et al. (2015) suggest that a strategy of lithological segregation should be adopted when representing coal measures in a regional model, in which coal seams and interburden are represented individually. This approach can account for the stark contrast in hydraulic properties of both units and preserve the relative permeability functions as the water saturation of coals is lowered by gas extraction, whereas water saturation of the interburden remains relatively static. Lithological segregation can be implemented through assimilation of the many different coal seam and interburden units which occur in reality into a much smaller number of discrete units in the model. A better alternative, however, is adoption of a dual porosity formulation whereby both coal seams (the mobile domain) and interburden (immobile domain) are represented within the same upscaled regional model layer. The assumption that underpins this approach is that flow in the interburden is primarily vertical (towards depressurised coal seams) and flow in coal is predominantly lateral (towards CSG wells). Given the significant differences between permeability of coal and the interburden, this is considered to be a reasonable assumption.

A discrete model layer is also employed by the UWIR 2019 model to represent the unproductive portion of a coal measure sequence that overlies CSG well screens. For the Walloon Coal Measures, this is layer 11 and represents effectively an aquitard.

As was discussed in Chapter 2 of this document, after a few months of depressurisation, gas wells contain more gas than water. Hence pressures within these wells, and in coal measure layers that abut them, are not much greater than atmospheric pressure. It follows that the head at the top of a coal measure sequence in a depressurising gas field is greater than that at the bottom of the sequence by an amount that is roughly equal to the thickness of the sequence. This has important repercussions for calculation of impact in underlying layers, which experience substantially more drawdown than layers with overly the target coal reservoir. Simulation of the effects of CSG extraction on layers other than the coal measure sequence must take this into account. This requires that an upscaled representation of any coal measure sequence from which CSG extraction takes place must employ at least two model layers (together with an overlying non-productive layer as discussed above). As is discussed below, this is done for the Bandanna and Cattle Creek formations in the UWIR 2019 model. However more layers than this are required for the Walloon Coal Measures because of the thickness of this unit (it is about 300 m thick in areas of existing and proposed CSG extraction), and in order to serve the requirement that vertical head gradients be well-represented in areas where the Walloon Coal Measures subcrops below the Condamine Alluvium. In particular, the use of multiple layers allows CSG-induced pressure changes at larger depths within the Walloon Coal Measures to propagate up-dip to their zone of contact with the Condamine Alluvium. In total, the Walloon Coal Measures is represented by a maximum of six model layers, the top layer of which is non-productive.

More specifically, the productive Walloon Coal Measures is split into a maximum of five layers (layers 12 to 16 of the UWIR 2019 model) of roughly equal thickness in areas where the total formation thickness exceeds 150 m. However in areas towards the east and west of the model domain where the productive thickness is less than 150 m, layers are gradually “eroded off” from top to bottom as this thickness reduces. The uppermost and lowermost layers of the productive Walloon Coal Measures are configured to be relatively thin (not exceeding 50 m) to ensure that the conductance

which connects the upper and lower heads in these layers to the neighbouring Springbok Sandstone and Durabilla Formation respectively is not unduly low. A cross-section showing the detail of the final adopted Walloon Coal Measures layering system in the Condamine Alluvium area is shown in Figure 3-4. Isopachs of resulting Walloon Coal Measures layer thicknesses are presented in Figure B1-11 to Figure B1-16 of Appendix B1.

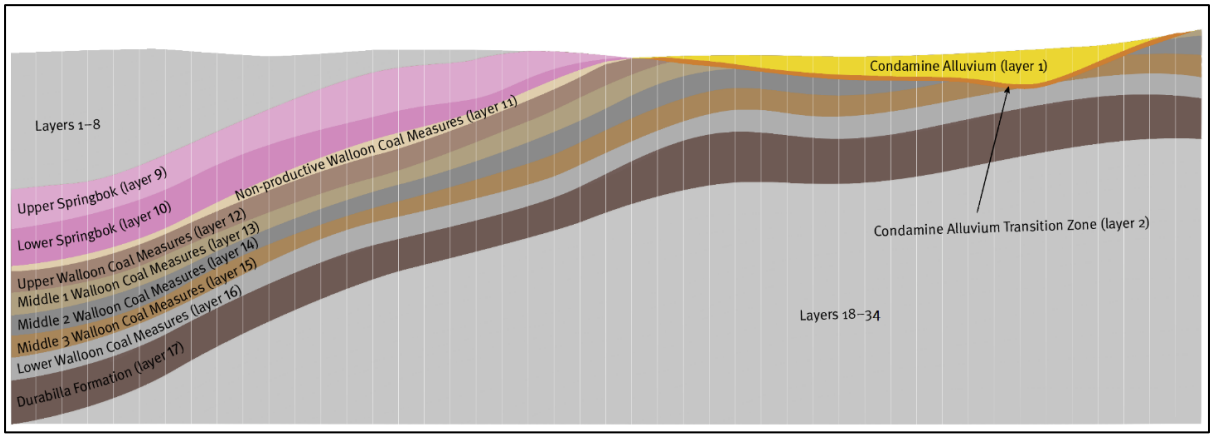

Figure 3-4 Illustrative cross-section of model layering for the Walloon Coal Measures beneath the Condamine Alluvium

3.2.5.4 Layer subdivision of the Bandanna Formation

The Bandanna Formation is the uppermost CSG reservoir in the Bowen Basin. As for the Walloon Coal Measures, coal (of moderate to high permeability) exists within an interburden of generally fine-grained sandstone, mudstone and siltstone. Coal seams within the Bandanna Formation have an average thickness of less than 2 m. However, individual coal seams may be up to 8 m thick, and can also be laterally more continuous than coal seams within the Walloon Coal Measures. CSG is produced from this formation at the Peat and Scotia gas fields on the eastern limb of the Taroom Trough, and at the Fairview and Spring Gully gas fields in the Denison Trough (OGIA, 2016d).

Three numerical model layers are used to represent the Bandanna Formation. These are as follows:

- As for the Walloon Coal Measures, material which overlies the uppermost productive coal seam in the Bandanna Formation forms an effective aquitard over most of subcrop area of this formation. This non-productive part of the Bandanna Formation is represented using a single model layer (layer 27 of the UWIR 2019 model), the thickness of which was defined using well screening data supplied to OGIA by tenure holders and validated using well completion reports lodged onto the Queensland Digital Exploration Reports System (QDEX). A thickness of zero was also ascribed to this layer in areas where the Bowen Basin sediments have been uplifted and eroded, which can bring the Precipice Sandstone into direct contact with coal seams from the Bandanna Formation at some places, referred to as contact zones. Delineation of these contact zones are further described in section 3.2.5.5.
- The remaining thickness of the Bandanna Formation was split into a maximum of two layers (layers 28 and 29 of the UWIR 2019 model). These layers are of equal thickness in areas where they do not outcrop or subcrop. However in outcrop/subcrop areas, a similar convention was adopted to that employed for the Walloon Coal Measures whereby the upper layer is eroded off as the total layer thickness is reduced.

Isopachs of layer thickness for the Bandanna Formation are provided in Figure B1-27 to Figure B1-29 of Appendix B1.

3.2.5.5 Contact zones between Bandanna Formation and the Precipice Sandstone

As Surat Basin sediments were deposited over the erosional surface of the Bowen Basin, there is potential for the coal seams of the Bandanna Formation to come in contact with the Precipice Sandstone in areas where faulting has caused uplifting of the coal formation to the erosional surface of the Bowen Basin. As described in the geological modelling report (OGIA, 2019b), new seismic survey and drilling data have become available since the release of the UWIR 2016 leading to a revised interpretation of the area of these contact zones.

Figure 3-5 shows the extent of two Precipice-Bandanna contact zones that are of significance for CSG impact modelling, including:

1. an area immediately east of Injune near the Fairview and Spring Gully fields, in the vicinity of the Hutton-Wallumbilla Fault (the western contact zone)
2. an area 5 km south of the Peat gas field, near the Burunga Fault (the eastern contact zone).

In comparison with the UWIR 2016, the interpreted area of the western contact zone has reduced from around 520 km^2 to around 210 km^2, whereas the eastern contact zone has increased from around 18 to 36 km^2. Interaction between model layers representing the Precipice Sandstone and Bandanna and Cattle Creeks formations in these areas is simulated through the introduction of non-neighbour connections.

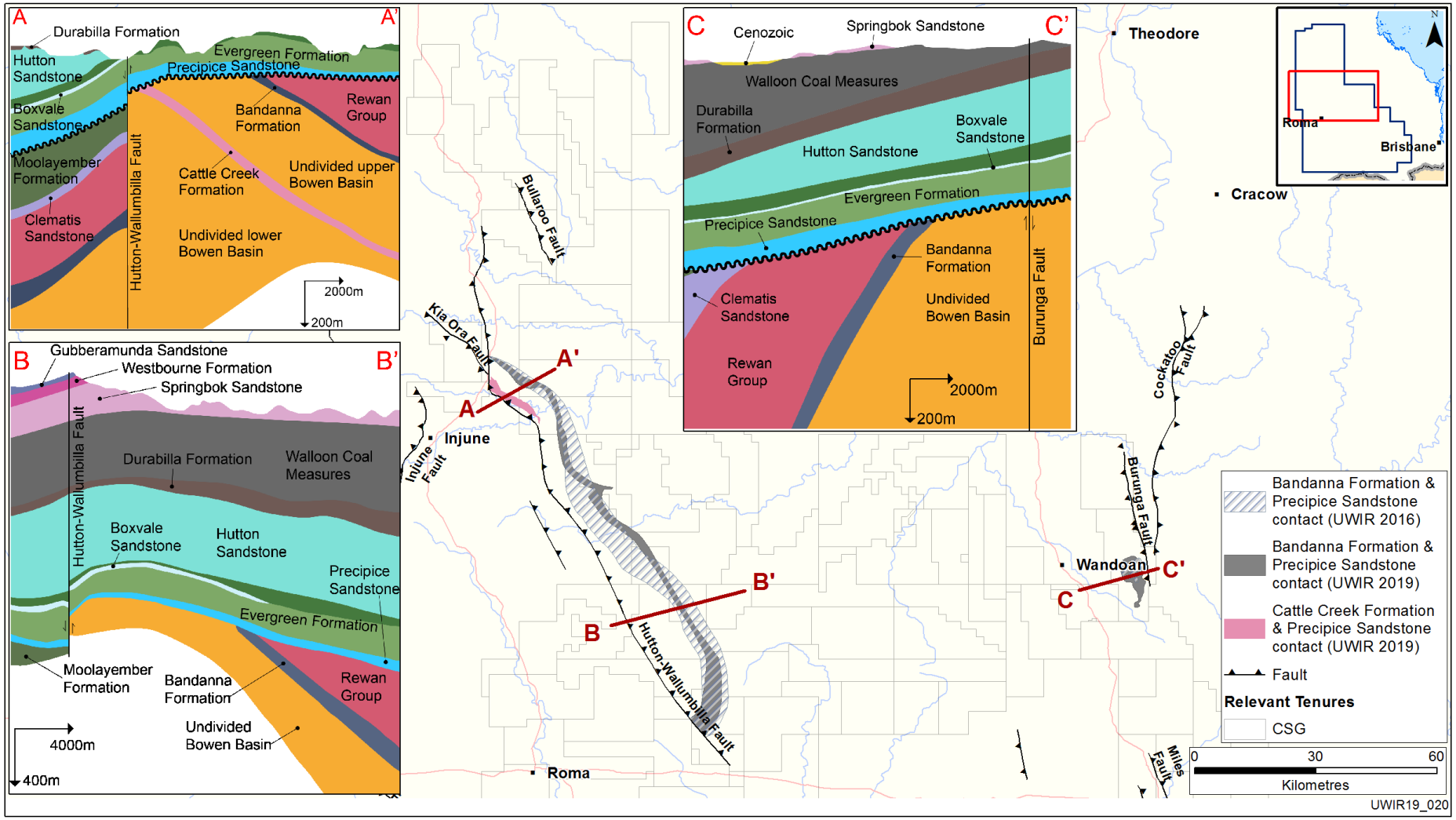

Figure 3-5 Location of interpreted contact zones between the Bandanna Formation and overlying Surat Basin sediments

3.2.5.6 Layer subdivision of the Cattle Creek Formation

The deepest CSG target reservoir within the model domain is the Lower Permian Cattle Creek Formation. This is located within the Denison Trough of the Bowen Basin. It is largely comprised of dark grey mudstone with interbeds of quartzose sandstone, calcareous siltstone, silty limestone and coal (OGIA, 2019b). The Cattle Creek Formation is not considered to be laterally extensive across the Bowen Basin, although only limited exploration of this formation has occurred to date.

The Cattle Creek Formation is represented in the 2019 OGIA model using a similar approach to that adopted for the Bandanna Formation. A single layer (model layer 31) represents the non-productive upper portion of this formation while a further two layers (model layers 32 and 33) represent the remainder. At the time of construction of the UWIR 2019 model, CSG extraction takes place from only a few bores in this formation; the non-productive zone has therefore been ascribed a constant thickness of 10 m, this being based on limited information on well screen locations.

Thickness isopachs for model layers representing the Cattle Creek Formation are provided in Figure B1-31 to Figure B1-33 of Appendix B1.

3.2.5.7 Inclusion of faults

OGIA (2019c) provides a detailed overview of OGIA's fault characterization project, which outcomes are used to support the representation of faults in the UWIR 2019 model. The methodology for inclusion of faults in the UWIR 2019 model was discussed in section 2.5. Details pertaining to the parameterisation and computation of inter- and cross-fault permeability are provided in section 5.5.2.4. A brief description of the manner in which layer displacement and modification of inter-cell connections were handled during model construction is provided below.

Since the grid resolution of the groundwater flow model is somewhat coarser than that of the geological model on which layering of the groundwater model was based, it was not possible to map faults directly from one model to the other. Bespoke code was therefore developed to equate vertical fault plane displacements in the groundwater model to their counterparts in the geological model, and to remove artefacts introduced to near-fault groundwater model layering by interpolation from the geological model.

The location of the faults, which are also represented using the MODFLOW horizontal flow barrier (HFB) package are shown in Figure 3-6. It should be noted that the hydraulic conductivity applied to HFB cells within the model is such that they typically act as only partial barriers to flow. The range of model layers associated with each regional fault was derived from the geological model. These are listed in below in Table 3-2.

Table 3-2 Affected model layers in regional fault representation

Fault	Uppermost affected model layer	Lowermost affected model layer
Horrane	11	34
Hutton-Wallumbilla	18	34
Bullaroo	25	34
"Fault 10"	21	34
Injune	26	34
Merivale	25	34
Arbroath - West	26	34

Fault	Uppermost affected model layer	Lowermost affected model layer
Consuelo	26	34
Burunga - South	25	34
Wambo	25	34
Leichardt - Central	26	34
Cockatoo	26	34
Arbroath - East	26	34
Leichardt - North	26	34
Leichardt - South	26	34
Kia Ora	18	34
Miles	26	34
Moonie Goondiwindi (s1)	11	34
Moonie Goondiwindi (s3)	11	34
Moonie Goondiwindi (s5)	11	34
Moonie North Fault	17	34
Cockatoo-Connection	26	34

Six additional fault segments are represented compared to the UWIR 2016 model, predominantly comprising additional segments in the vicinity of the Moonie Goondiwindi and Cockatoo regional fault systems. The representation of all of the other modelled fault segments have also been reviewed and where necessary revised as part of the geological model development (OGIA, 2019b).

Figure 3-7(a-c) shows a cross-section through the Hutton-Wallumbilla fault for the (a) conceptual, (b) geological and (c) numerical models respectively. In the last of these figures, arrows represent cross-fault, non-neighbour connections introduced to the unstructured grid. Note that the model layers appearing in Figure 3-7(c) have been coloured by associated formation for consistency with Figure 3-7(a-b).

Figure 3-8 shows an interpreted seismic section (Figure 3-8a) and modelling layering (Figure 3-8b) through the Horrane fault system south of Dalby. As shown in Figure 3-8b along parts of this fault the displacement is assessed as exceeding the thickness of the Durabilla Formation thereby juxtaposing the upper part of the Hutton Sandstone with the lower part of the Walloon Coal Measures. This has been simulated in the regional model through the introduction of non-neighbour connections between layers 16 and 18 at this location.

Further code was developed by OGIA to alter the connections between model cells affected by regional faulting. Four different data arrays featured in the MODFLOW-USG input dataset for its unstructured discretisation (DISU) package were modified by this software. These are as follows:

- FAHL – the overlap area between neighbouring cells
- CL12 – the perpendicular length between the centre of a node and boundary of the cell which holds the node
- IAC – the number of connections for each node
- JA – the list of nodal indices connected to each node.

See Panday et al. (2017) for further details of data required by the DISU package.

If the displacement of a fault is such that it completely offsets a cell from its cross-fault neighbour in the same layer, then the cross-fault connection between pertinent nodes was removed. Otherwise the element of the FAHL array corresponding to that connection was reduced in accordance with the revised cross-fault, intra-layer juxtapositional area of the displaced cells. If the displacement of a fault is such that it puts a cell in connection with a cell from an upper or lower layer, then a new connection was introduced. Elements pertaining to this connection were added to the FAHL, CL12 and JA arrays.

The above-described methodology assumes that a fault lies between, rather than within, individual model cells. Locations of faults in the geological model were altered to allow this while retaining unbroken fault traces.

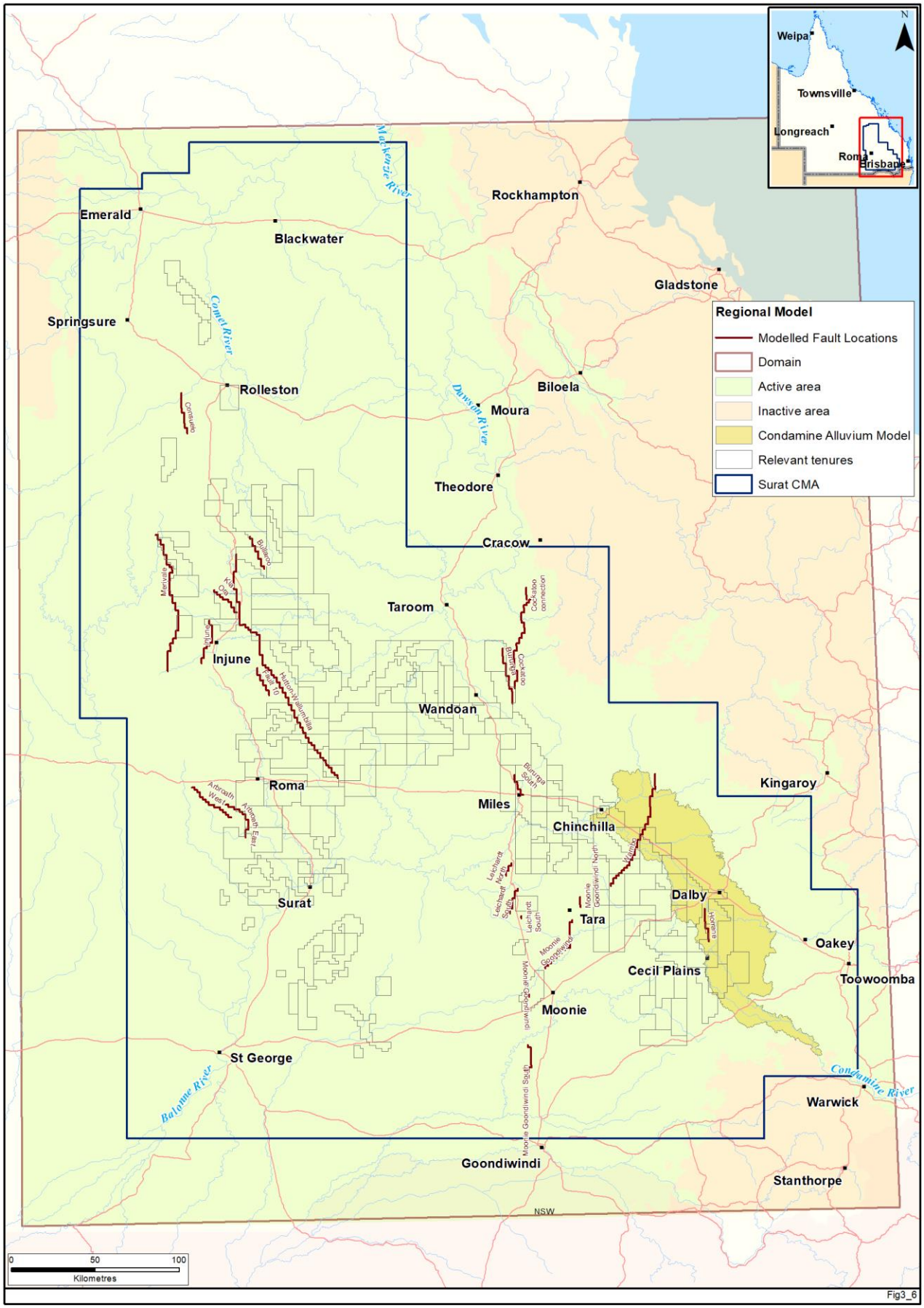

Figure 3-6 Location of mapped regional scale faults included in the UWIR 2019 model

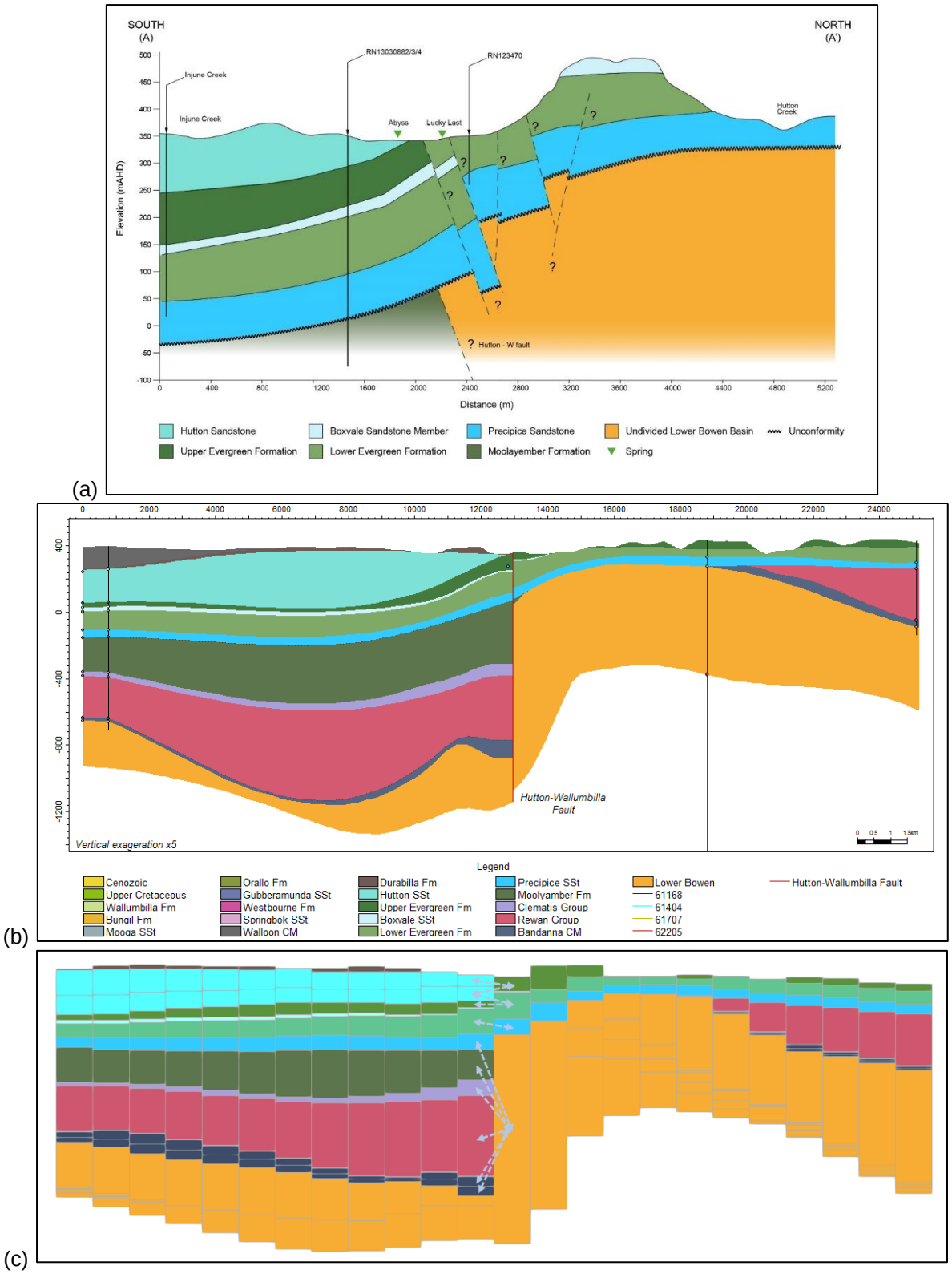

Figure 3-7 (a) Conceptual cross-section, (b) geological model cross-section and (c) numerical model cross-section of the Hutton-Wallumbilla fault close to Lucky Last spring complex

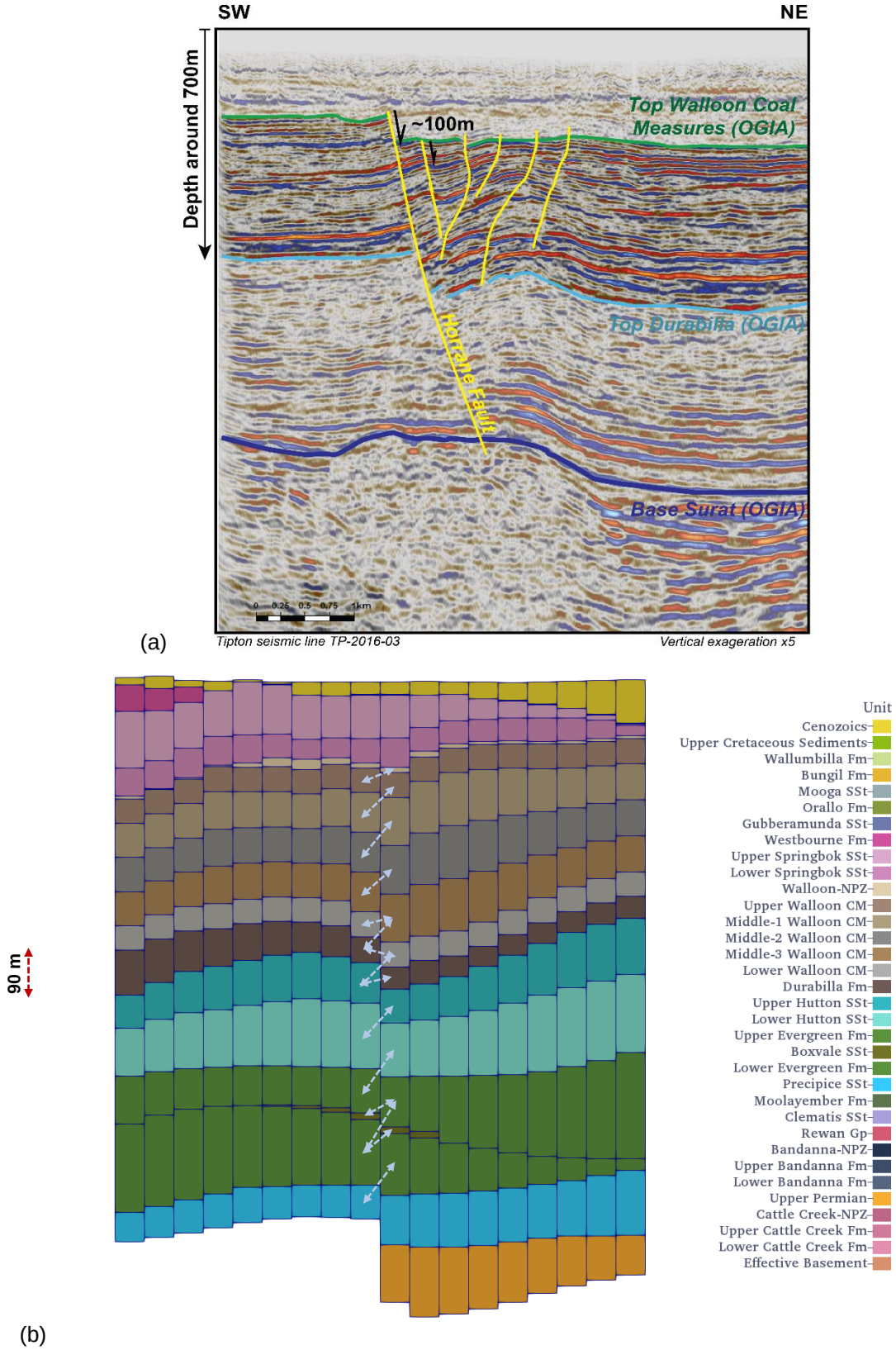

Figure 3-8 (a) Seismic section and (b) numerical model cross-section through the Horrane fault showing MODFLOW-USG non-neighbour connections

3.2.6 MODFLOW layer types

A convertible MODFLOW layer type "5" (specific to the “beta” version of MODFLOW-USG) was assigned to the mobile zone of the following coal-bearing model layers but not extended to their associated non-productive layers:

- Walloon Coal Measures (layers 12–15)
- Bandanna Formation (layers 28–29)
- Cattle Creek Formation (layers 32–33).

This layer type employs the upstream weighting formulation of Niswonger et al. (2011) to calculate flow between neighbouring model cells. Meanwhile relative saturation in dewatered coal measures is calculated using a modified van Genuchten formulation that allows desaturation to commence at pressures that promulgate desorption of gas from coal. Relative permeability is calculated using the Brooks-Corey function expressed as equation 4.26 (section 4.6.3).

A confined MODFLOW layer type “0” was assigned to the remaining model layers. This improves numerical stability and increases execution speed as transmissivity is independent of model-calculated head. It was thereby assumed that the peak-to-peak amplitude of temporal water level responses such as the drawdown and recovery from local pumping when averaged over a regional cell is a relatively small proportion of the cell thickness. Meanwhile, as was discussed in section 2.3.7, modifications to MODFLOW-USG by OGIA allow automatic use of specific yield instead of specific storage for groundwater storage calculations where model layers outcrop.

3.3 Process representation

3.3.1 Surface water–groundwater interaction

Representation of interactions between groundwater and surface water resources represents a significant challenge for any regional groundwater flow model since cell sizes in the 10s of meters or less are typically required to represent the surface water courses and springs. For an area the size of the Surat CMA such small cell sizes would not be practicable, even if a variable model grid was adopted. Furthermore several important recharge and discharge mechanisms operating within the CMA are relatively poorly understood. The majority of the surface water courses in the area, including the Condamine River, are known to ephemeral features which are likely to switch between sources of recharge and discharge depending on antecedent weather conditions and relative groundwater levels (OGIA, 2019a). However, only very limited information on the magnitude of gains or losses from the various water courses in the area is available. Reference to detailed groundwater level records for monitoring points located in outcrop areas also suggests that recharge is limited to relatively infrequent high rainfall events (Kellett et al., 2003) which are often associated with extensive flooding. In areas like the Condamine Alluvium aquifer recharge is likely to occur over an extensive area during such flood events.

Surface water groundwater interactions are represented relatively simply in the UWIR 2019 model, but adopting a conservative risk based approach whereby shallow alluvial systems such as the Condamine River alluvium are represented in the groundwater flow model but the rivers and other surface water features present within these systems are not. Consequently recharge due to flooding events and/or induced leakage from rivers into the underlying shallow alluvial systems are not simulated and where predictions of CSG related impacts on groundwater levels in such systems are likely to be over-predicted.

In the case of the Condamine Alluvium such a local model already exists, outputs from which have been used to improve the representation of recharge in the regional model (section 3.3.1.1). As documented in the UWIR 2019 (OGIA, 2019b) predicted impacts on the Condamine are minor despite the proximity of CSG fields, reflecting the relatively high storage, transmissivity, and incident recharge to this aquifer.

Similarly potential impacts on springs are conservatively predicted in the regional model through reference to predicted drawdown in the source aquifer. Actual impacts on the spring itself will depend on a range of local factors which cannot be accurately represented in a regional groundwater flow model.

Near surface evapotranspirative losses are also not directly represented in the UWIR, rather they are accounted for directly by estimating recharge using a development of the saturated zone chloride mass balance approach used by Kellett et al. (2003). Recharge estimates derived using this approach should theoretically be net of any near surface evapotranspiration and other losses.

3.3.1.1 Recharge

OGIA (2019a) describes the manner in which pre-calibration estimates of recharge were obtained. For all units, apart from the Condamine Alluvium, a two-dimensional array of recharge was obtained through the spatial interpolation of point recharge estimates made on the basis of observed chloride concentrations in groundwater bores. This approach represents an extension of similar work undertaken by Kellett et al. (2003). Whilst the methodology adopted to provide initial estimates of recharge for the UWIR 2019 model is unchanged from the UWIR 2016 model the analysis has been completed using a significantly expanded data set of chloride concentrations and revised aquifer attribution information (based on intersection of bore screens with the revised geological model). Only bores assessed as screening single aquifers are used to estimate recharge.

Groundwater recharge to the Condamine Alluvium was obtained separately from the outputs of a groundwater model that had been built to explore the sustainability of extraction from the Condamine Alluvium. This relatively finely gridded (500 × 500 m) transient model that includes two layers to represent the Condamine Alluvium was initially developed by Klohn Crippen Berger (KCB, 2011) for water resource planning assessments undertaken by the Hydrology Group of the then Queensland Department of Science Information, Technology and Innovation (DSITI). This is referred to herein as the “Condamine Model”. A new version of this model is under development but was not available in time to feature in the UWIR 2019 model. Hence OGIA have continued to use information from the KCB Condamine Model as input to the regional model, although it was first necessary to extend this model such that input recharge values for the Condamine Alluvium were available to the end of the revised transient calibration simulation (i.e. December 2017). This extension of the KCB Condamine Model was also undertaken by KCB based on a revised groundwater extraction dataset provided by Department of Environment and Science (DES). Other than extending the various transient input packages necessary to extend this model no other changes were made. In particular no re-calibration of the model, which was originally calibrated using observed groundwater level data over the period 1980 to 2009, was undertaken. Accordingly some further validation work was undertaken by KCB and OGIA to confirm that the input data files had been correctly updated and that current observed water levels in the Condamine Alluvium are accurately represented in the extended model. Figure 3-9 shows a comparison of current observed and modelled heads extracted from the extended version of the KCB model. As the level of modelled to observed fit at the end of extended model period was

slightly better than that reported during the calibration period then re-calibration was not considered necessary.

Data extracted from this extended model was then used to provide initial recharge estimates within the Condamine footprint for use in the UWIR 2019 model. The approach adopted is unchanged from the UWIR 2016 model, whereby, “long-term” average steady state diffuse recharge and net riverbed leakage between the Condamine River and underlying alluvium extracted from the KCB Condamine Model was summed to produce a total steady state recharge for input to the UWIR regional model. It should be noted that two sets of modelled values for net riverbed leakage were produced prior to computing the long-term average; these were based on either exclusion of extractions for the 1947 steady state or inclusion of extractions for the 1995 steady state period. The cell-by-cell steady state recharge values were then spatially translated to the UWIR 2019 model grid.

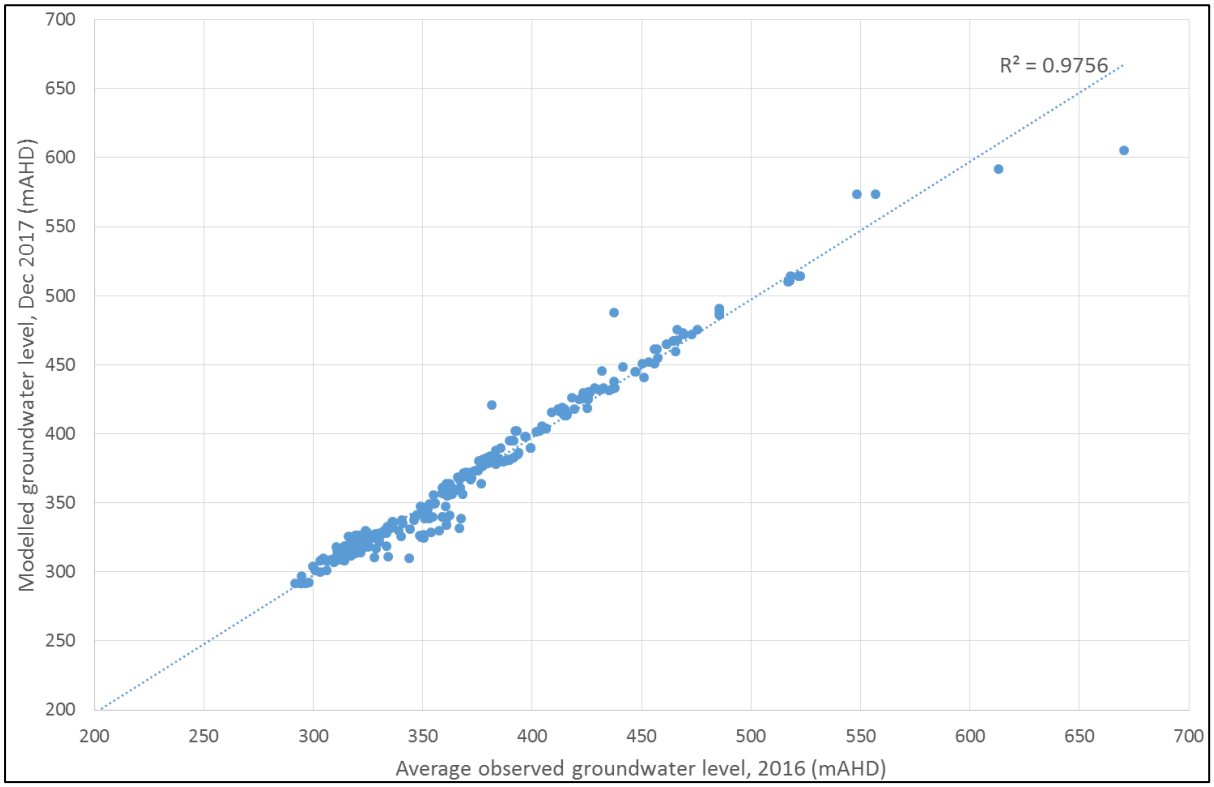

Figure 3-9 Modelled versus observed groundwater levels Condamine Alluvium and tributaries

Figure 3-10 shows the distribution of long-term average estimated recharge over formation outcrop zones used as input to the 1995 steady state simulation. The area and long-term average recharge rate associated with each modelled formation outcrop are provided in Table 3-3.

It is worth noting that errors in estimation of recharge are unlikely to promulgate large errors in predictions of CSG impact by the UWIR 2019 model. This has been demonstrated by a linear analysis undertaken by OGIA on the UWIR 2012 model. It is also an outcome of the fact that a high proportion of recharge is “rejected” by a regional-scale impact assessment model as it is diverted to shallow systems (see section 3.3.1.2).

Table 3-3 Outcrop area and pre-calibration recharge estimates for each modelled formation group

Dominant formation group	Model layer(s)	Modelled outcrop area (km^2)	Average recharge rate (ML/yr)	Average recharge rate (mm/yr)
Condamine Alluvium	1	5,587	19,378 (19,579)	3.5 (3.5)
Non-Condamine Alluvium	1	32,290	93,190	2.9
Main Range Volcanics	1	6,217	46,835	7.5
Other Basalt	1	8,334	50,487	6.1
Cenozoic Sediments	1	65,817	197,670	3.0
Weathered Surat or Bowen	1	1,235	4,284	3.5
Upper Cretaceous	2	11,471	1,180	0.1
Wallumbilla Formation	3	7,562	6,289	0.8
Bungil Formation	4	3,636	5,655	1.6
Mooga Sandstone	5	3,274	6,224	1.9
Orallo Formation	6	4,561	10,977	2.4
Gubberamunda Sandstone	7	2,120	7,216	3.4
Westbourne Formation	8	2,268	3,610	1.6
Springbok Sandstone	9 – 10	4,370	5,705	1.3
Walloon Coal Measures	11 – 16	8,026	10,137	1.3
Durabilla Formation	17	2,210	2,798	1.3
Hutton Sandstone	18 – 19	12,170	39,455	3.2
Evergreen Formation / Boxvale Sandstone	20 – 22	12,746	40,458	3.1
Precipice Sandstone	23	1,231	33,056	26.9
Moolayember Formation	24	4,385	7,275	1.7
Clematis Group	25	3,782	61,556	16.3
Rewan Group	26	4,030	2,093	0.5
Bandanna Formation	27 – 29	704	1,040	1.5
Undifferentiated Bowen Basin Strata	30 and 34	10,251	32,606	3.2
Cattle Creek	31 – 33	NA	NA	NA
Total		**218,275**	**689,174 (689,374)**	**3.2 (3.2)**

Notes:

1. Layer 21 which represents the Boxvale Sandstone and layers 31 to 33 which represents the Cattle Creek Formation are not present at outcrop.
2. Bracketed values refer to 1995 steady state recharge specifically; otherwise all values apply to both the 1947 and 1995 steady state simulations.

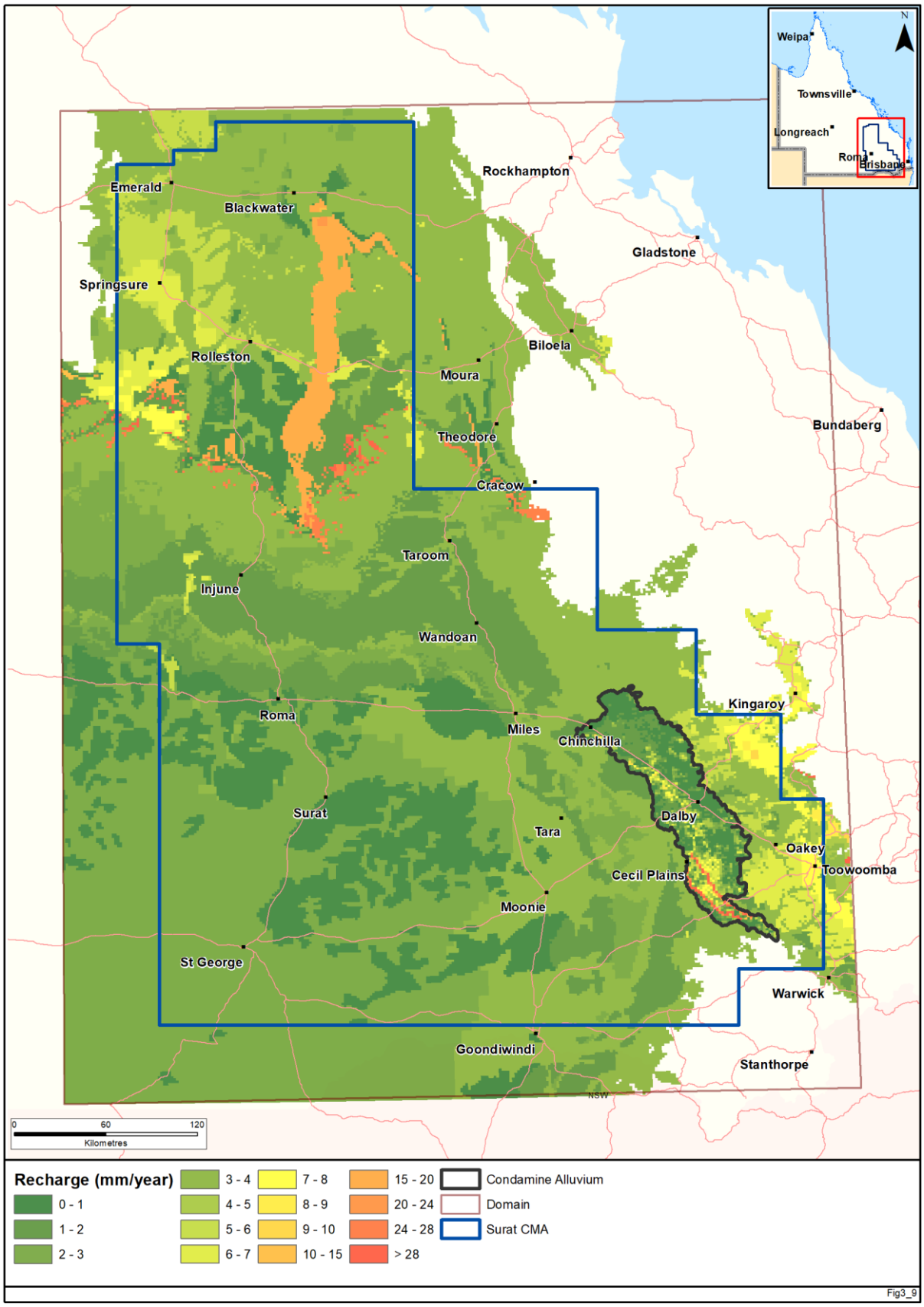

Figure 3-10 Pre-calibration long-term average recharge estimates over modelled formation outcrop areas

For the transient calibration period, estimates of time-varying recharge were required. With the exception of the Condamine Alluvium, these were obtained by means of the PERFECT (Littleboy et al., 1989) simulator; see Appendix D of GHD (2012) for a detailed description of the methodology. In summary, to produce a recharge time series for each of the 24 outcrop recharge zones, cell-by-cell recharge multipliers were calculated for each of zone by taking the ratio of the estimated long-term average steady state recharge for 1995 to a long-term average recharge calculated using PERFECT (approximately 27.5 mm/yr). As noted in (GHD, 2012), only a single long-term average recharge scenario was considered for the transient simulation. Outside of the Condamine area, transient monthly recharge values calculated by PERFECT for the period 1995 to 2017 were scaled by these recharge multipliers to maintain consistency with the long-term average calibrated recharge. For example, a steady state recharge rate to the Mooga Sandstone of 1.9 mm/yr (see Table 3-3) equates to approximately 7% of the PERFECT estimate. Hence, the time series of transient recharge for this formation can be determined by multiplying all elements of the PERFECT recharge time series by 0.07.

From a version of the Condamine Model extended to the end of 2017, model inputs for diffuse recharge and modelled net riverbed leakage (whereby losing conditions represent recharge induced from the river) were summed on a cell-by-cell basis for each month of the transient calibration period and spatially translated to the UWIR 2019 model grid to produce a sequence of monthly recharge inputs for the Condamine Alluvium. It is acknowledged that use of an “enhanced” recharge approach in preference to explicit representation of the Condamine River via the MODFLOW river package does not allow for potential increases in recharge induced from the river over time when net vertical leakage from the Condamine Alluvium increases as a consequence of CSG extractions. However, this approach was deemed acceptable as results from simulations with and without non-CSG extractions in the Condamine Model suggested only a relatively small amount of river leakage was induced. Furthermore, this assumption is conservative given that an over- rather than under-prediction of CSG-related impacts would be produced on this basis.

3.3.1.2 Surficial drainage and recharge rejection

3.3.1.2.1 General

The MODFLOW-USG drain package was used extensively in construction of the UWIR 2019 model. Its use in simulation of CSG extraction was discussed in Chapter 2 and will be further discussed below. However, it also finds extensive use in representation of near-surface conditions. Its use in simulation of near-surficial processes falls into three categories. These are now discussed.

3.3.1.2.2 Condamine Alluvium

The Condamine Alluvium is heavily utilised for groundwater supply. Estimated total groundwater extraction is approximately 70,000 ML/yr (OGIA, 2019b). Nevertheless groundwater extraction from the Condamine Alluvium is not explicitly simulated by the UWIR 2019 model. An implicit representation of Condamine Alluvium water usage is employed instead. This alternative approach was adopted for the following reasons:

- The impacts of pervasive and heterogeneous groundwater extraction that takes place throughout the Condamine Alluvium footprint cannot be reliably simulated using regional model cells of size 1.5 × 1.5 km. Each such cell would contain many extractive wells. Interaction of the groundwater system with the Condamine River would also be difficult or impossible to represent with cells of this size.

- Details of complex pumping regimes that are operative within Condamine Alluvium, and details of the interaction of the Condamine Alluvial aquifer with the Condamine River, are likely to have little bearing on calculations of CSG impact on the Condamine Alluvium.
- Software written by OGIA allows water to be exchanged between the more local-scale Condamine Model and the UWIR 2019 model. Regional impact assessed by the latter model can then be provided to the former model for simulation of local effects of this regional impact (where necessary).

Part of the design philosophy of the UWIR 2019 model therefore rests on an ability to exchange data with the Condamine Model so that advantage can be taken of the more detailed process representations embodied in this model. One outcome of that philosophy is that groundwater extraction in the Condamine Alluvium is represented in a de-facto manner in the UWIR model by assigning a MODFLOW-USG drain to every cell within the Condamine Alluvium footprint. The elevation of the drain within each cell is then set to a level equal to that of the local piezometric surface as calculated by the Condamine Model. Drain conductances are set high enough to present minimal impediment to groundwater escape. Use of drain boundary conditions respects the fact that current Condamine Alluvium water levels are an outcome of a considerable amount of extraction. At the same time, the Condamine Model is able to replicate the considerable decline in groundwater levels which have occurred within the Condamine Alluvium since the 1960s. Average water level declines are approximately 6 m; locally, water level declines of over 25 m have been recorded in areas somewhat removed from the Condamine River (KCB, 2011).

As described in sections 5.4.5.1 and 5.4.5.5, a suite of “observations” was also incorporated into the model calibration process to ensure that modelled groundwater levels – within the model drain cells used to represent the Condamine Alluvium – actually rise to the imposed drainage surface; and that the flows discharging from these cells exceed the amount of groundwater extraction which they are being used to implicitly represent since not all recharge to this area will be extracted.

3.3.1.2.3 Main Range Volcanics

Groundwater is extracted at a rate of about 50,000 ML/yr from the Main Range Volcanics (OGIA, 2019b). As for the Condamine Alluvium, extractive details cannot be simulated using the large cell size of the regional model. The problem of representing details of the phreatic surface within the Main Range Volcanics is exacerbated by the control on water levels that is exerted by details of rugged topography; topographic lows provide ubiquitous locations of groundwater outflow.

To overcome these problems, MODFLOW-USG drains were also emplaced over the footprint of the Main Range Volcanics, with the elevation of each drain being equal to that of the known or interpolated water table. As for the Condamine Alluvium, use of the drain condition respects the fact that the elevation of the water table is determined by removal of water from the system – both through natural points of groundwater escape, such as creeks and gullies, and by pervasive groundwater extraction. As for the Condamine Alluvium (sections 5.4.5.1 and 5.4.5.5), a suite of “observations” was also incorporated into the model calibration process to ensure that modelled groundwater levels – within the model drain cells used to represent the Main Range Volcanics – actually rise to the imposed drainage surface and that flows discharged via this boundary condition exceeds estimated groundwater extraction.

3.3.1.2.4 All other areas

The need for groundwater to find its own points of escape from the groundwater system is not restricted to the Condamine Alluvium and the Main Range Volcanics. In these latter areas, local

pumping presents a significant groundwater loss mechanism. In other areas, water leaves the groundwater system through topographic low points. Some of these are regional, constituting major surface drainage systems. Others are local, comprising small groundwater systems whose details cannot be represented within a large regional model.

In every vertical column of the domain of the UWIR 2019 model, a MODFLOW-USG drain is emplaced in the top cell of that column at a level that is representative of local surface conditions; see section 3.3.1.3 below. Water can thereby emerge from the groundwater model domain wherever it needs to. This may occur where groundwater flow lines converge to a topographic low point. It may also occur as a mechanism for recharge rejection, whereby a portion of recharge waters are directed to shallow groundwater systems that operate at a scale that cannot be represented by the regional model. The conductances assigned to these drains are set at relatively high values such that they present a minimum impediment to the outflow of water.

3.3.1.3 Surface drainage surface specification

For the pre-development or 1947 steady state simulation, the drainage surface (i.e. the collective surface representing all MODFLOW-USG drains) was calculated as the minimum elevation within each model cell of the 1 second digital elevation model (DEM-1S, approximately 30 m resolution). It thus represents the elevation of the lowest point in the landscape within each cell.

For the pre-CSG or 1995 steady state simulation, some adjustments were made to this drainage surface to accommodate extraction from the Condamine Alluvium and Main Range Volcanics in the manner discussed above in section 3.3.1.2.1. The drainage surface within the Condamine Alluvium was calculated through interpolation of calibrated steady state groundwater levels from the Condamine Model to the cell centres of the UWIR 2019 model. These levels are typically well below ground surface, this reflecting the impact of ongoing groundwater extraction for irrigation purposes. The subdued nature of these water levels produces a corresponding net discharge of water from underlying layers of the Walloon Coal Measures to the overlying alluvium. Similarly in order to reflect the influence of long-term extraction from the Main Range Volcanics, the 1995 steady state drainage surface was designed to reflect the ambient regional groundwater table within this unit. This surface was generated by spatial interpolation of observed groundwater levels consistent with this time period to relevant model cell centres.

The hybrid drainage surfaces for the 1947 and 1995 steady state simulations were then "hydraulically corrected" using the ArcGIS *Spatial Analyst* extension to ensure that elevations decrease monotonically in the downstream direction of overland flow paths within each topographic sub-catchment. Further minor modifications were then also required to ensure that the 1947 drainage surface is greater than or equal to the 1995 drainage surface in all model cells and that drain elevations were set no lower than the layer base elevation.

For the historical transient simulation (i.e. the simulation spanning the period 1995 - 2017), the drainage surface remains static at 1995 steady state levels except in the Condamine area. Within this area, the transient drainage surface was set to groundwater levels calculated by the extended Condamine Model (section 3.3.1). When in transient simulation mode, the surficial drains are actually simulated by the MODFLOW river package; this was done as a post-processing convenience as it makes CSG extraction (also accomplished using MODFLOW-USG drains) easily distinguishable from Condamine Alluvium extraction. A MODFLOW-USG river boundary condition emulates a MODFLOW-USG drain boundary condition where the river bed elevation is set equal to the river head elevation.

As was stated above, high values were assigned to all drain conductances in order to incur a minimal head drop as water escapes from the groundwater system. A conductance value of 1,000 m^2/d was chosen for all surficial drain cells under both steady state and transient conditions. This is high enough to allow easy water outflow, but not so high as to instigate numerical instability.

3.3.2 Non-CSG extraction

3.3.2.1 Assimilation of extractive datasets

Non-CSG extraction includes bores in the Surat and Bowen basins from which water is pumped for irrigation, industrial and mining purposes and for stock and domestic supply. It also includes conventional P&G wells which have not yet been decommissioned or converted to water bores. The last of these target the Evergreen Formation and the Precipice Sandstone in the Surat Basin; they include a number of active fields located to the south and east of Roma. The primary formations in the Bowen Basin for conventional P&G activities where water is also extracted are the Showgrounds Sandstone (Clematis Group equivalent) and the Moolayember Formation.

All non-CSG extractions were compiled into MODFLOW-USG well package input datasets for use during the 1995 steady state run and the transient run (1995 - 2017) undertaken for model calibration. Sources of information and processing of data pertaining to non-CSG extraction are reported separately (OGIA, 2019d). In summary, non-CSG extractions associated with bores with a drill date prior to 1995 were included in the 1995 steady state well package input file. For the historical transient simulation, wells were gradually introduced according to information included in the DNRME state groundwater database on the date each bore was drilled and assumed to remain active thereafter unless they have been marked as ‘abandoned and destroyed” in the same database. The spatial distribution of known non-P&G water bores (i.e. excluding conventional P&G and CSG wells) is provided in Figure 3-11.

Estimates of steady state and historical non-CSG extraction (excluding water extracted for stock and domestic and conventional P&G use) were derived from licensed volumetric entitlements supplemented with metered use information, where available, as supplied by the Water Management System of DES. Unfortunately, bores associated with stock and domestic use are unmetered and have no volumetric entitlement so a methodology was implemented for estimating extractive rates in average, dry and wet years based on a range of associated variables (see (OGIA, 2016d) for further details). Estimated rates of non-P&G related extraction from 1900 to the end of 2017, for major water sources, are shown in Figure 3-12.

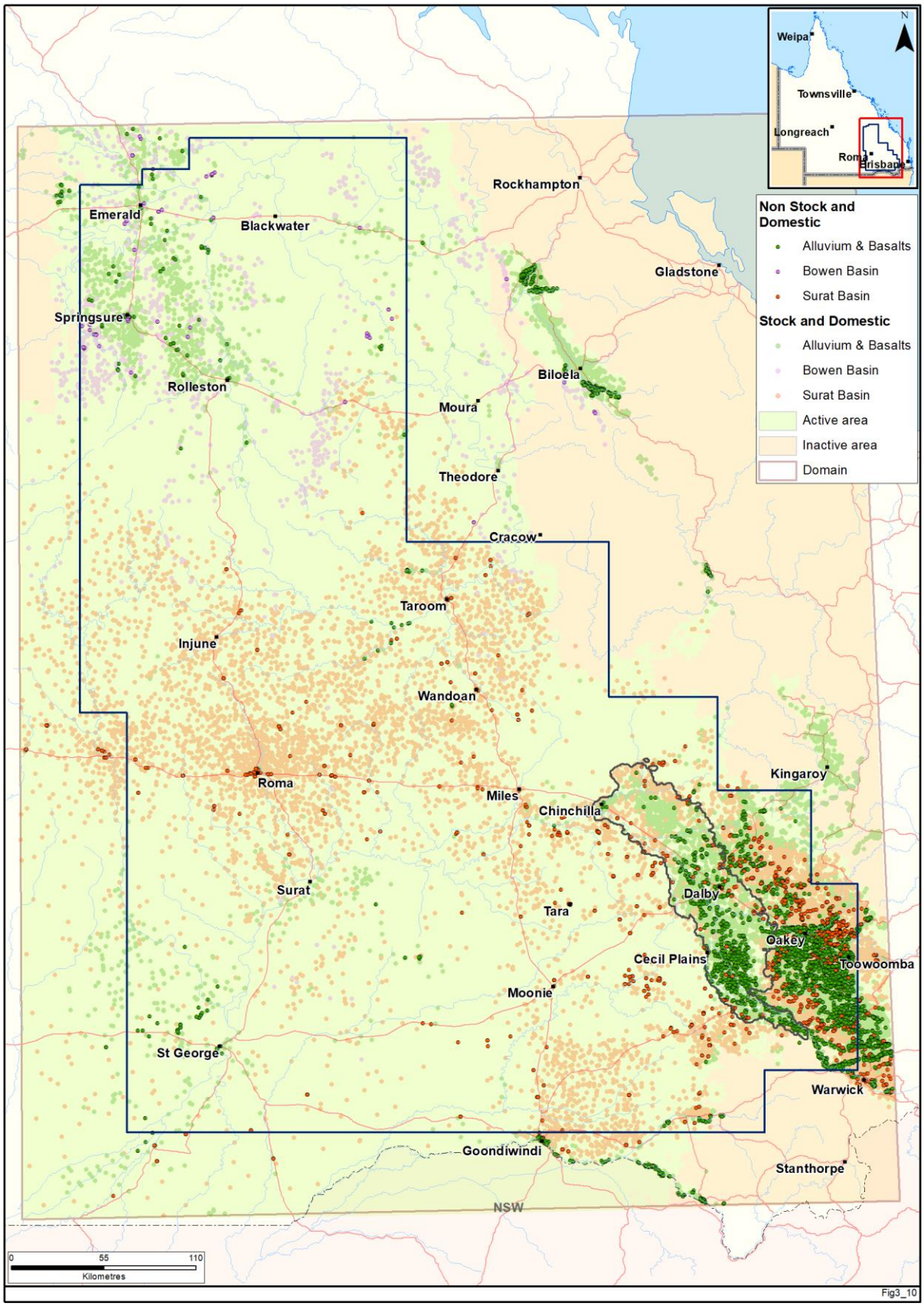

Figure 3-11 Spatial distribution of current registered water supply bores

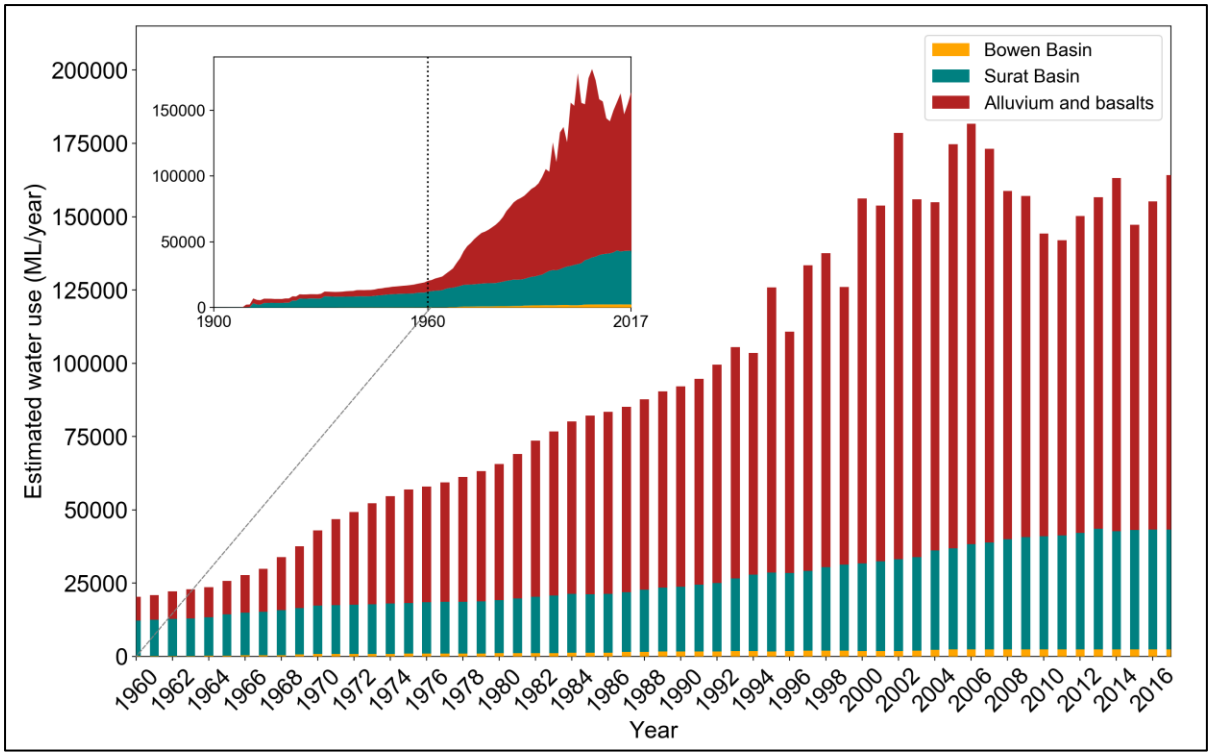

Figure 3-12 Estimated rates of non-P&G water supply extraction for different groundwater sources

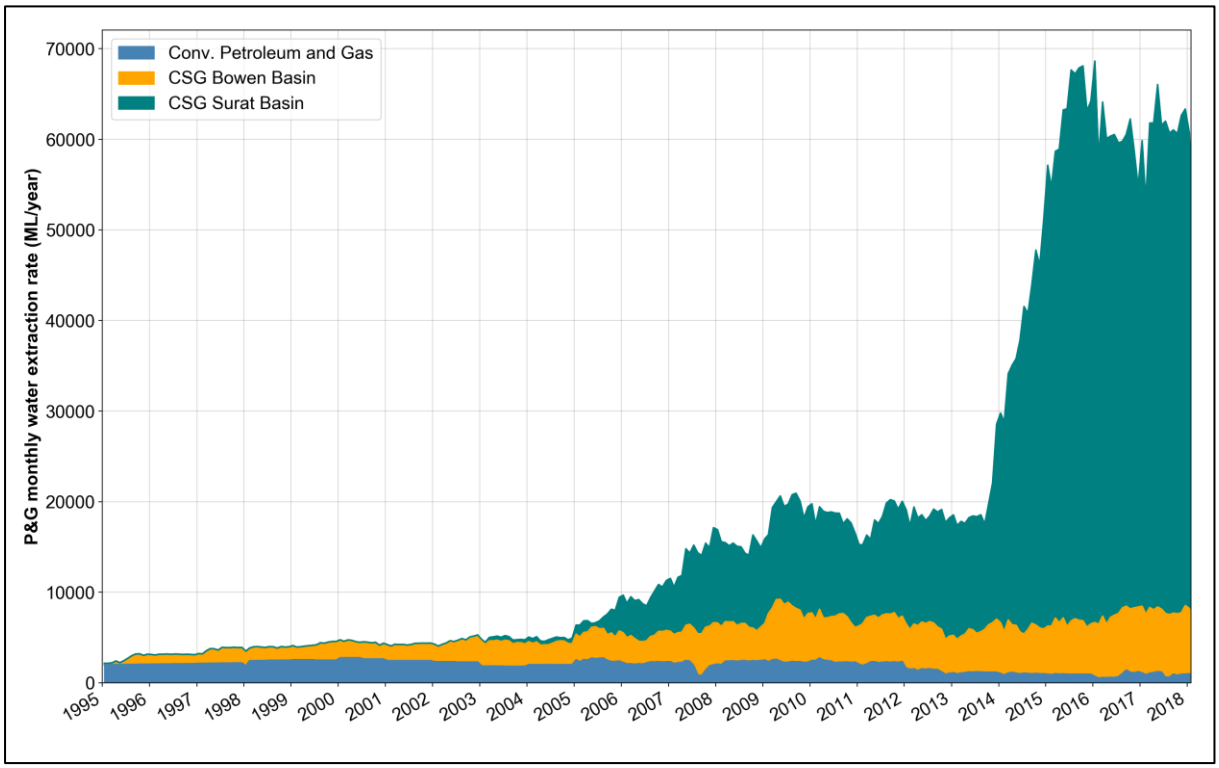

Figure 3-13 Petroleum and gas water extraction from 1995 to 2018

The following aspects of the extractive input datasets used by the model are worthy of note:

- Extractions from the Condamine Alluvium and Main Range Volcanics are not represented explicitly in MODFLOW-USG well package input file for the UWIR 2019 model. Instead, as is

outlined in section 3.3.1.3, they are presented implicitly as drainage surfaces, which are provided through MODFLOW-USG drain and river input files.

- A small amount of extraction totalling around 4500 ML/yr from aquitard units represented in the UWIR 2019 model (namely the Westbourne Formation, Durabilla Formation, upper and lower Evergreen Formation, Moolayember Formation, Rewan Group and Undifferentiated Bowen Basin strata) are also not represented in MODFLOW-USG well files. Their exclusion follows experience gained during development of previous model iterations wherein such extraction precipitated poor model numerical behaviour by generating large drawdowns on account of the generally low permeability of these units.

3.3.2.2 Multiple screened extractions

Simulation of extraction requires that wells that span multiple model layers be considered. These fall into two categories. The first is comprised of wells that are attributed to a formation which is represented by more than one layer in the UWIR 2019 model. Stratigraphic units to which this applies are the Springbok Sandstone, Walloon Coal Measures, Hutton Sandstone, Bandanna Formation and Cattle Creek Formation. The second is comprised of wells whose screens tap multiple stratigraphic units. A database maintained by OGIA which contains well screen information and attributed each well to one or more model layers was utilised for this process.

All multi-layer extractions were subject to transmissivity-weighted flow apportionment taking into account partial penetration of wells, as far as possible based on the data available. Flow apportionment is calculated by a model pre-processor that reads MODFLOW-USG input files; hence it is adjusted as model hydraulic properties are adjusted through the calibration process.

For a bore screened across *N* layers, the adjusted extraction rate in each layer *i* is computed using the following formula:

$$Q_i = \frac{Q_w T_i}{\sum_{i=1}^{N} T_i} \qquad (3.1)$$

where:

Q_i is the pumping rate attributed to an individual cell;

T_i is the transmissivity of an individual cell; and

Q_w is the total well extraction rate.

The individual transmissivity values T_i featured in equation 3.1 are computed as the product of the horizontal hydraulic conductivity of the respective model cell and the minimum of (i) cell thickness, (ii) screen length and (iii) simulated saturated thickness.

3.3.2.3 Well derating

The UWIR 2019 model supports derating of all non-CSG extraction. As was described in section 2.3.2, using functionality added to MODFLOW-USG by OGIA, this supports reduction in extraction necessary for the head in an extraction well to remain above the level of the screen in the well.

Use of the well derating functionality requires that a number of auxiliary variables be specified for each well. These define the well heads at which (i) pump derating is initiated and (ii) pumping ceases. These extra variables are added to standard MODFLOW-USG input files. In fact these input files are

written by model pre-processors developed by OGIA. This enables derating variables to be adjusted as model hydraulic properties are adjusted through the calibration process.

In any cell in which extraction takes place, the difference between the head calculated for the cell and that pertaining to the extraction well can be calculated using the Peaceman equation (Peaceman, 1978). Thus, for any non-CSG extraction well, the elevation at which pump derating is initiated is set to the sum of the cell-to-well correction term calculated using the Peaceman equation and the elevation at which pumping ceases.

The cell-to-well correction term was thereby calculated as follows:

$$s_w = \frac{Q}{2\pi T} \ln\left(\frac{0.208a}{r_w}\right) \quad (3.2)$$

where:

s_w is the cell-to-well correction term

Q is the pumping rate

a is the length of a square cell (or the square root of the product of lengths of a rectangular cell), equating to 1500 m

r_w is the radius of the well, assumed to be 0.1 m

T is the transmissivity of the pumping cell

The latter (i.e. the elevation at which pumping ceases) is set to the elevation of the top of well screen, if this is known, or to the elevation of the top of the uppermost cell from which extraction takes place if no screen information in available. If the uppermost cell from which extraction takes place is the highest cell in a model grid column, the elevation at which pump derating is initiated is set to 25% of the cell thickness above the base of the cell. If the well is assessed as artesian, however, it is set to the elevation of the topographic surface.

3.3.3 CSG extraction

3.3.3.1 General

Simulation of the operation of CSG wells using a MODFLOW-USG “descending drains” methodology by the UWIR 2019 model has been described previously (section 2.3.3). Input files for the MODFLOW-USG drain package are written by model pre-processing software developed by OGIA. The information used by these programs for the writing of these files is now described.

3.3.3.2 Historical CSG well data

Information on CSG wells covering the period January 1995 to December 2017 was obtained from the following sources:

- The locations of existing CSG wells were obtained by querying the Queensland Government QDEX database and validated using similar information provided to OGIA by individual tenure holders.
- Inlet information (i.e. the top and bottom of CSG well screens) for the majority of CSG production wells is provided to OGIA by individual tenure holders.
- Monthly actual water extractions for each CSG well are provided to OGIA by individual tenure holders every six months.

- Typical bottom hole pressure versus time curves were also provided to OGIA by individual tenure holders.

Validation of data directly provided to OGIA was undertaken through comparison with similar information on water extraction volumes and well completions lodged onto the QDEX system. Through comparison of CSG well screen information with stratigraphic picks based on raw geophysical data OGIA has also identified that about 16% of existing CSG wells may be partially completed into the lower parts of the Springbok Sandstone (see section 3.5.2 in (OGIA, 2019a) for more information). The presence of these Springbok Sandstone well completions had not been accounted for in the UWIR 2016 model primarily since the data required to identify these bores was not available to OGIA at the time. The representation of these well screens in UWIR 2019 model therefore represents a key change in the setup compared to the UWIR 2016 model.

3.3.3.3 Historical CSG well emplacement

CSG drains were assigned to cells in which CSG wells operate. In order to account for both vertical and inclined wells, horizontal spatial cell reference was calculated for each CSG well based on the midpoint coordinates of its inlets. Where this information was missing, bore collar coordinates have been used for spatial reference. The model layer attribution process of CSG wells also employed this inlet information. Where inlet information is missing CSG drains are assigned to all layers of the CSG producing formation. This means a maximum of five model layers in the Walloon Coal Measures and a maximum of two model layers in each of the Bandanna and Cattle Creek Formations are candidates for drain cell assignment. A “rule surface” also constrains this default layer assignment in some places of the model area, to account for the manner in which CSG well screens are set in practice. This surface is of particular relevance in areas such as the Condamine Alluvium, where CSG well inlets are not typically placed within 150 m of the ground surface in part to protect the Condamine Alluvium from impact but also since economic quantities of gas are not typically found in coal seams which are within 150 m of the surface.

Figure 3-14 provides the locations of model grid cells with CSG drains assigned to the Walloon Coal Measures, Bandanna Formation and Cattle Creek Formation up to the end of the transient calibration period (i.e. December 2017). Note that a small number of wells are shown outside of current CSG development areas – these pertain to pilot and exploration wells (e.g. the Glenburnie site, located southwest of Cecil Plains).

Figure 3-14 also shows the locations of model grid cells with CSG drains assigned to the lower Springbok Sandstone and the Walloon Coal Measures non-productive zone (i.e. model layers 10 and 11) to represent around 900 existing CSG wells that have been identified as being partially completed into the Springbok Sandstone (OGIA, 2019a).

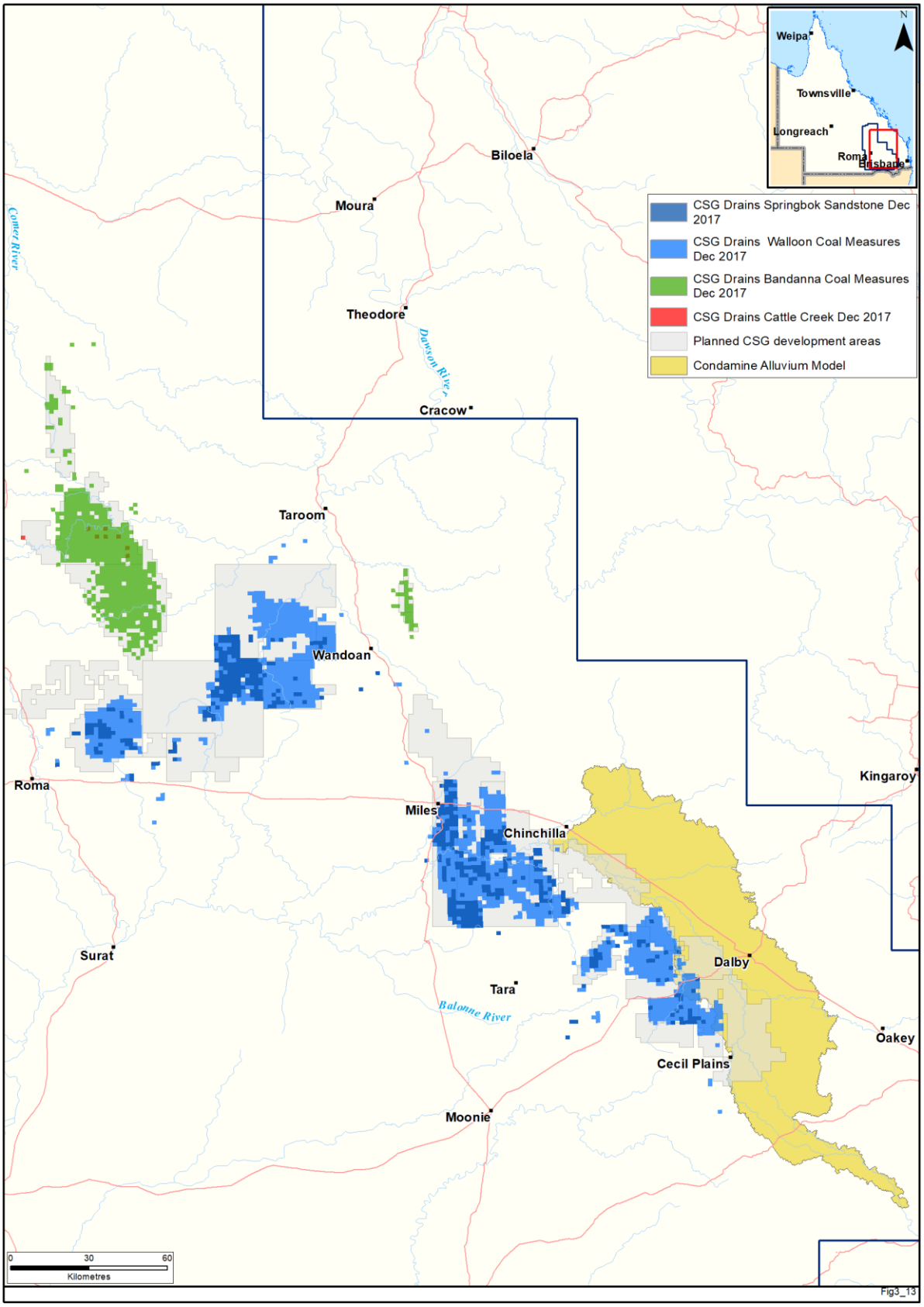

Figure 3-14 Locations of CSG drain cells representing historical CSG extraction in the Walloon Coal Measures, Bandanna Formation and Cattle Creek Formation at the end of the transient calibration period (December 2017)

3.3.3.4 Historical CSG well extraction

Figure 3-15 shows monthly water extraction volumes recorded for a CSG well in the Talinga development area. As for most individual CSG wells, water extraction volumes vary significantly on a month-to-month basis. To simplify representation of CSG well development using descending drains, a minimum water extraction threshold of 0.01 ML/month was defined. If the total monthly water extraction volume for a CSG well falls below this value the well is rendered inactive for regional modelling purposes. Furthermore, CSG well schedules are simplified by keeping wells active/inactive when a well shuts down or is turned on for just a single month. For the Talinga-10 well, this schedule simplification is visualised in Figure 3-15 which shows inactive periods in 2005, 2010 and 2012.

As is described in section 4.6.4, upon commissioning of a CSG well, the CSG drains associated with all model layers that are tapped by the well are initially ascribed an elevation that is equal to the equivalent pressure head at which gas desorption commences. As development of the well takes place, all drains are lowered together at a rate that reflects a notional bottom hole pressure versus time curve ascribed to the well. This curve is based on data supplied by the tenure holder operating the well (see Figure 3-17). Figure 3-16 depicts the temporal evolution (or “descent”) of CSG drain elevations in various model layers that are used to represent the operation of the CSG well featured in Figure 3-15.

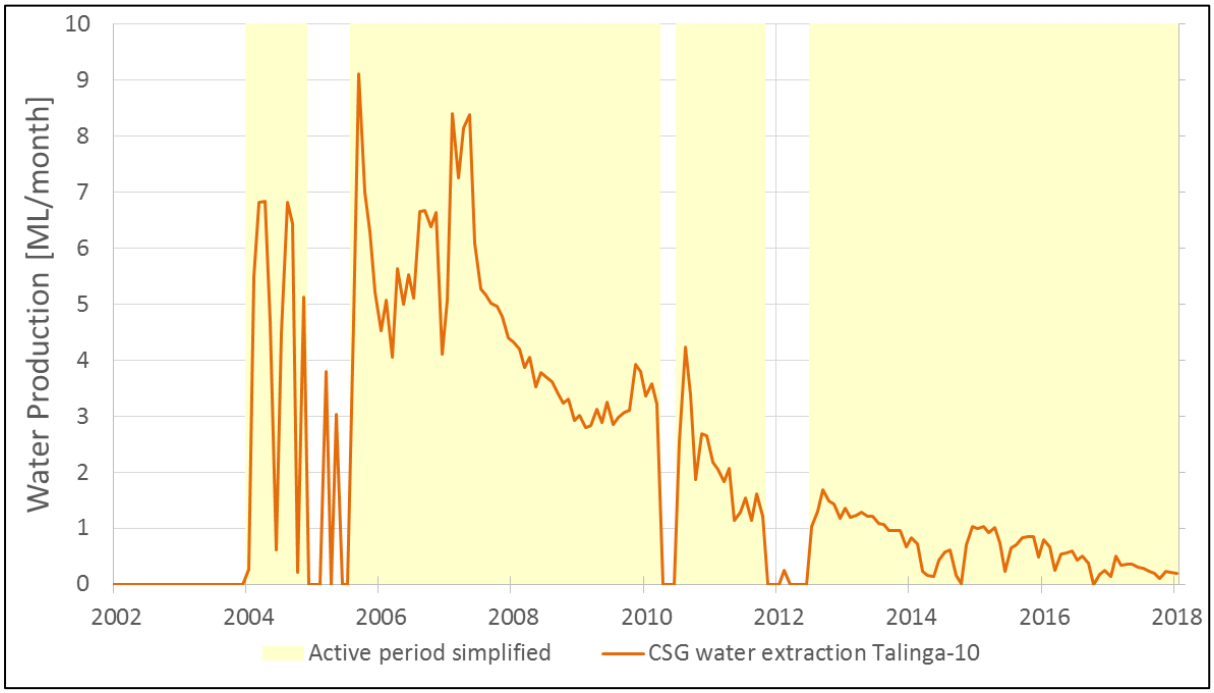

Figure 3-15 Recorded monthly water production volumes for the Talinga-10 CSG well

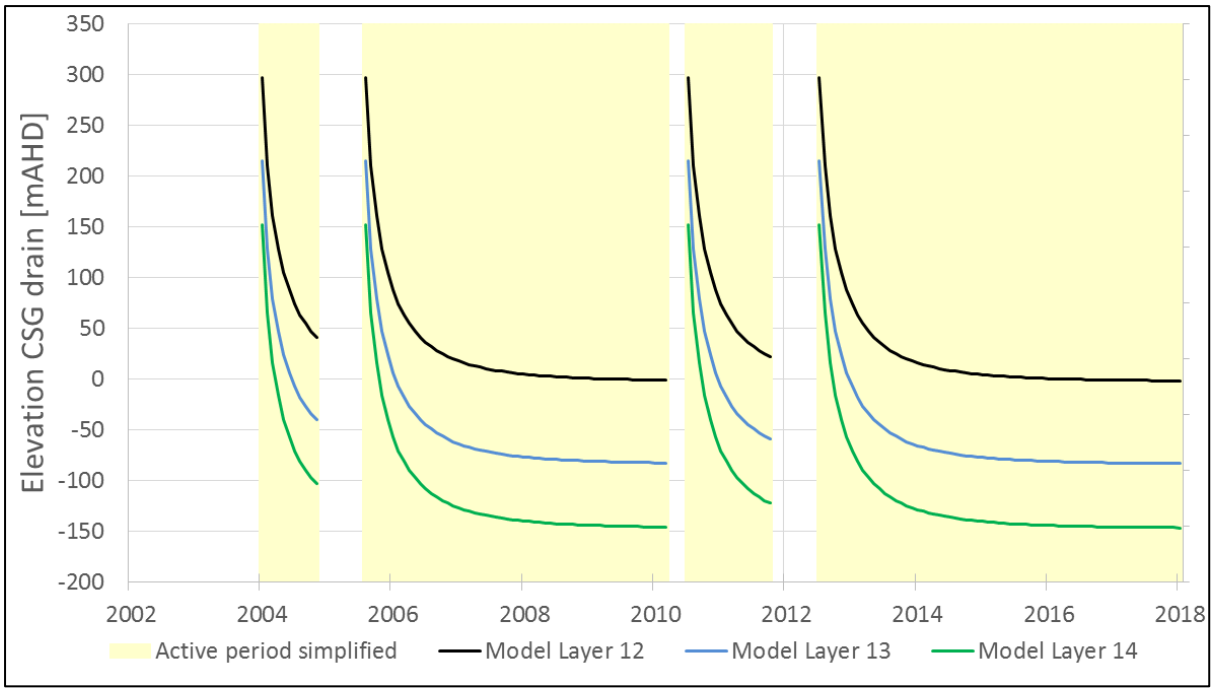

Figure 3-16 CSG drain elevations for three model layers versus time curve for the Talinga-10 CSG well

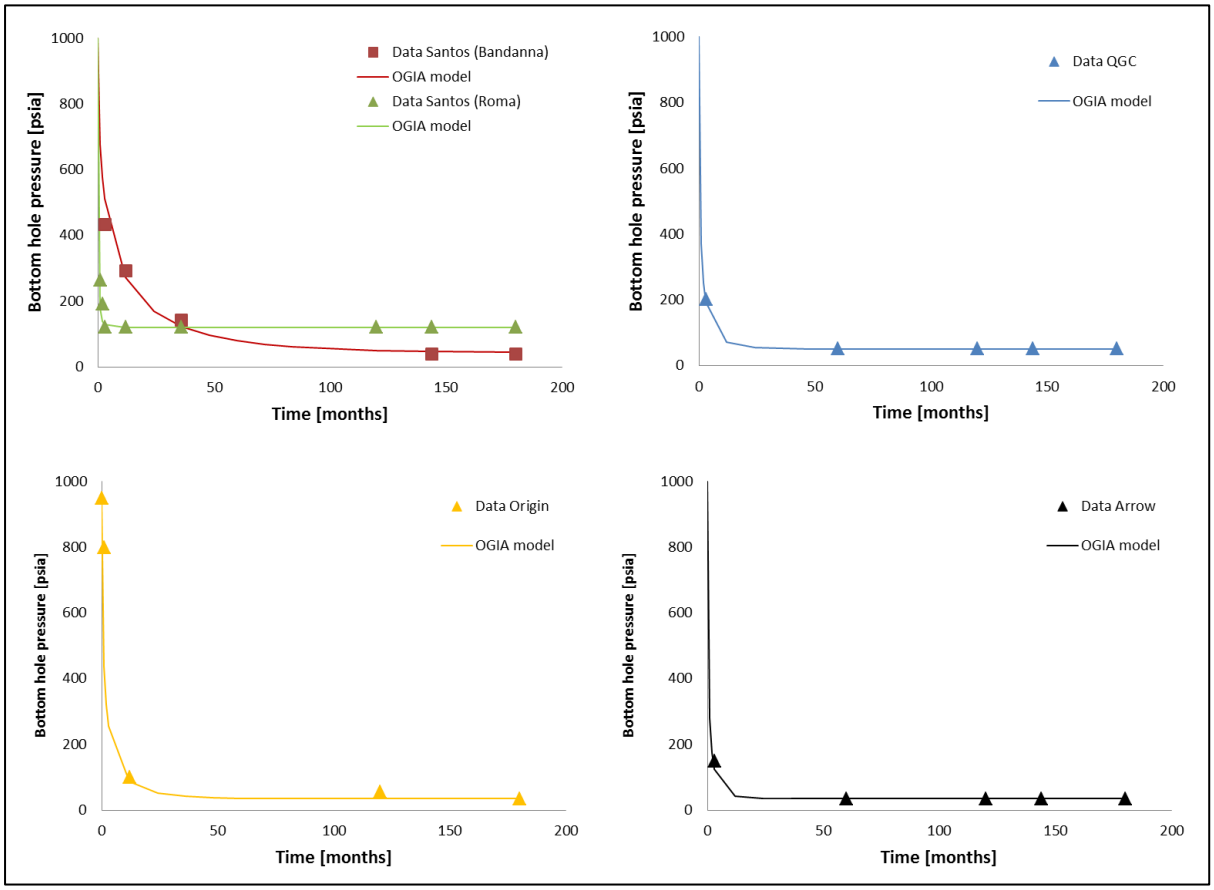

Figure 3-17 Drain descent specifications employed by the UWIR 2019 model; for each CSG operator a specific descent rate and final bottom hole pressure is employed, these being based on information provided by tenure holders.

3.3.3.5 Future CSG well emplacement

Emplacement of future CSG wells in the UWIR 2019 model consists of creating theoretical locations of CSG wells, which are subsequently modified to accommodate the presence of existing wells. This process relies on existing CSG well data and CSG development plans that are provided by each tenure holder. These development plans define the total number of operating CSG wells per development block and the time-period during which the development of the 1.8 by 1.8 km block is active.

Figure 3-18 illustrates the theoretical fill patterns used for emplacement of future CSG wells in gas company development blocks with varying number of production wells. These patterns are modified to accommodate existing wells, as is illustrated in Figure 3-19. Suppose, for example, that a company has reported five future production wells for a development block that already contains three existing CSG wells. The block filling procedure commences by generating five well locations based on the standard five well pattern (Figure 3-19(1)). For each existing well (Figure 3-19(2)), the closest generated well is then removed (Figure 3-19(3)). The five wells that remain (which include the three existing wells, Figure 3-19(4)) constitute the arrangement of production wells for that development block.

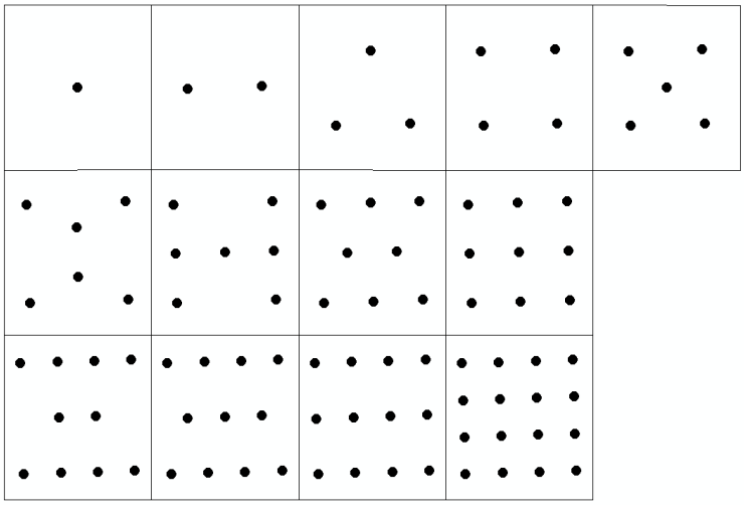

Figure 3-18 Theoretical arrangements of CSG wells in CSG development blocks for different numbers of production wells per block

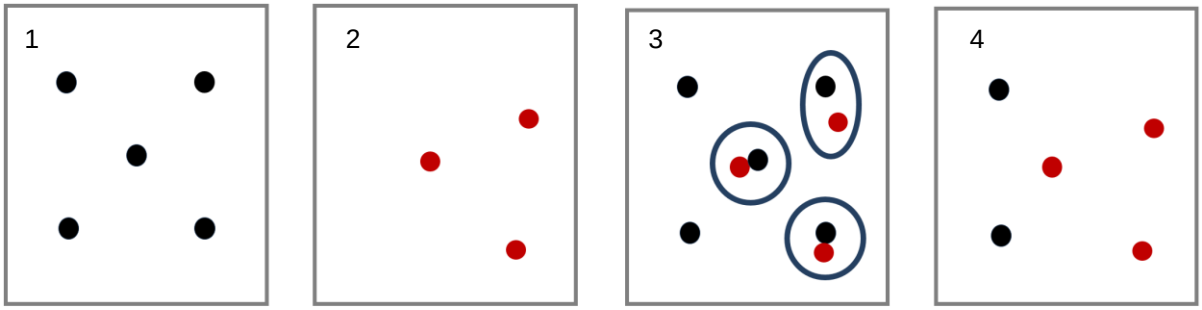

Figure 3-19 Assignment of five wells to a development block that already contains three gas wells; pattern-generated wells (1) and existing wells (2) are combined within the development block (3); excessive new wells are then removed on the basis of proximity to existing wells (4)

Figure 3-20 illustrates future production well infilling for development blocks near Dalby and Cecil Plains. This shows the final arrangement of production wells after merging new and existing wells.

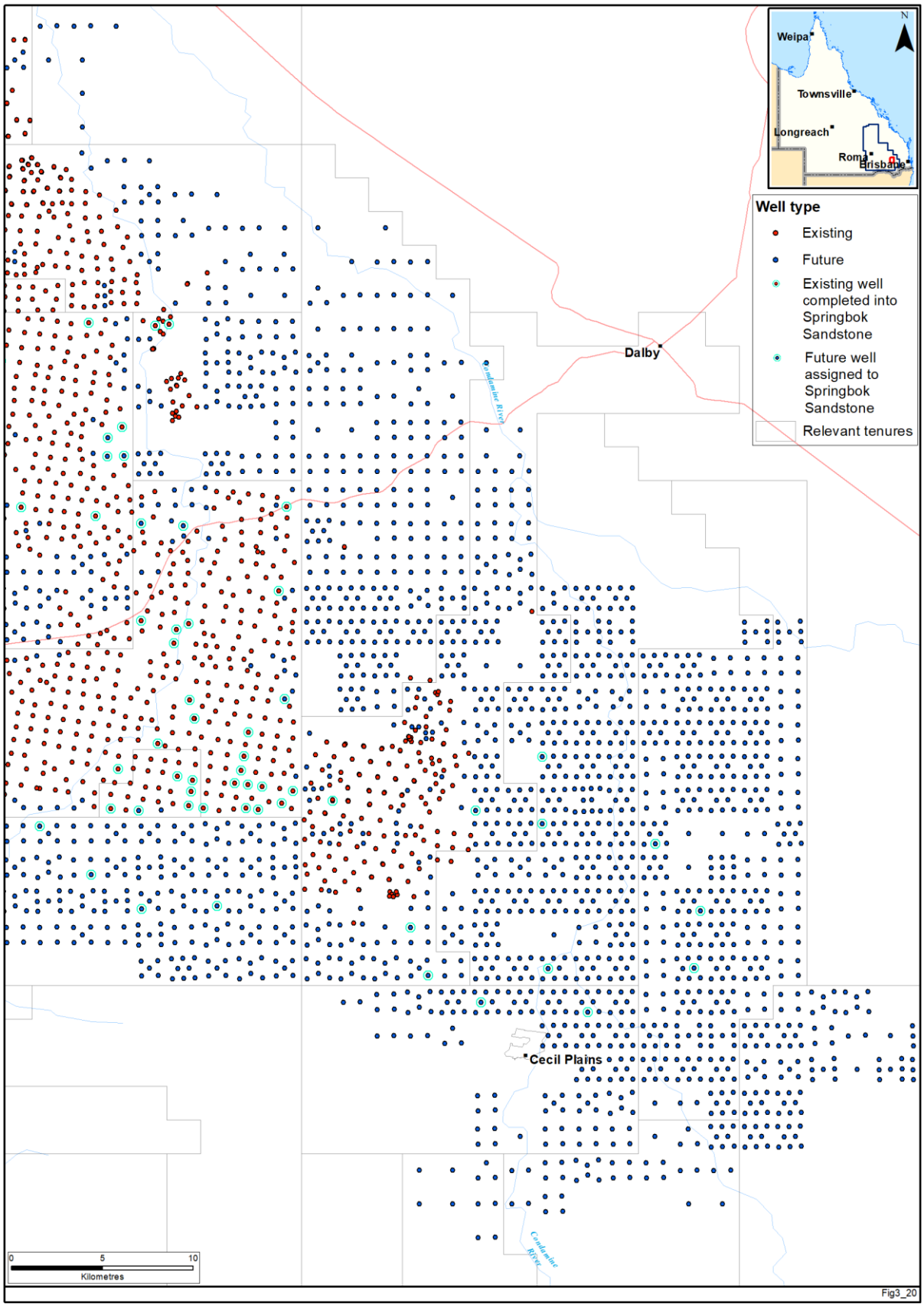

Figure 3-20 Existing CSG production wells infilled with theoretical CSG wells for Arrow Energy Pty Ltd (Arrow) and Queensland Gas Company Pty Ltd (QGC) tenure areas near Dalby and Cecil Plains

3.3.3.6 Future CSG wells attributed to Springbok

As about 16 percent of existing CSG wells are partially completed into the Springbok Sandstone including some recently completed wells, a similar percentage of future CSG wells are defined to be tapping into the Springbok Sandstone. Based on the number of existing CSG wells extending into the Springbok Sandstone, the proportion of future wells is initially specified for each tenure holder and development field. Future CSG wells are then assigned at random as extending into the Springbok until the proportion of future Springbok CSG wells per tenure holder is the same proportion calculated for existing wells. Similarly future Springbok CSG wells are assumed to extend an average thickness into the Springbok as calculated based on data for actual wells. Figure 3-20 shows the location of future CSG wells near Dalby and Cecil Plains that are defined to tap into the Springbok Sandstone.

3.3.3.7 Future CSG well production

Activation of predictive CSG wells relies on the period of operation defined by the company development plans. Maps of production start and end dates based on these development plans for the Walloon Coal Measures and the Bowen Basin coal reservoirs are shown in Figure 3-21 and Figure 3-22, respectively. Once CSG well locations and planned production start and end dates are known, future CSG drains can be attributed to model cells and predictive stress-periods in the same manner as described for historic CSG wells (sections 3.3.3.3 and 3.3.3.4).

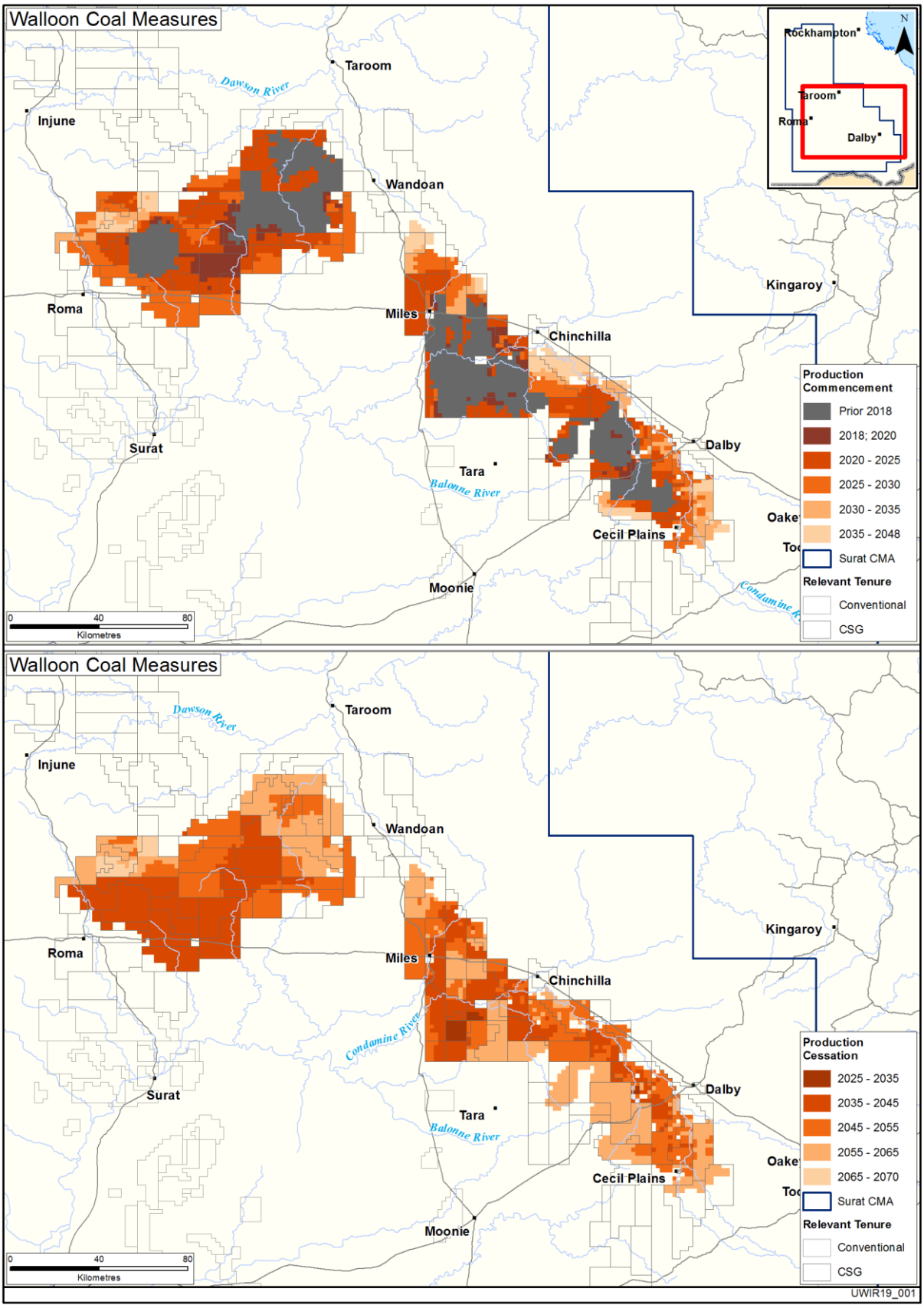

Figure 3-21 Production start and end dates for CSG development areas, Walloon Coal Measures

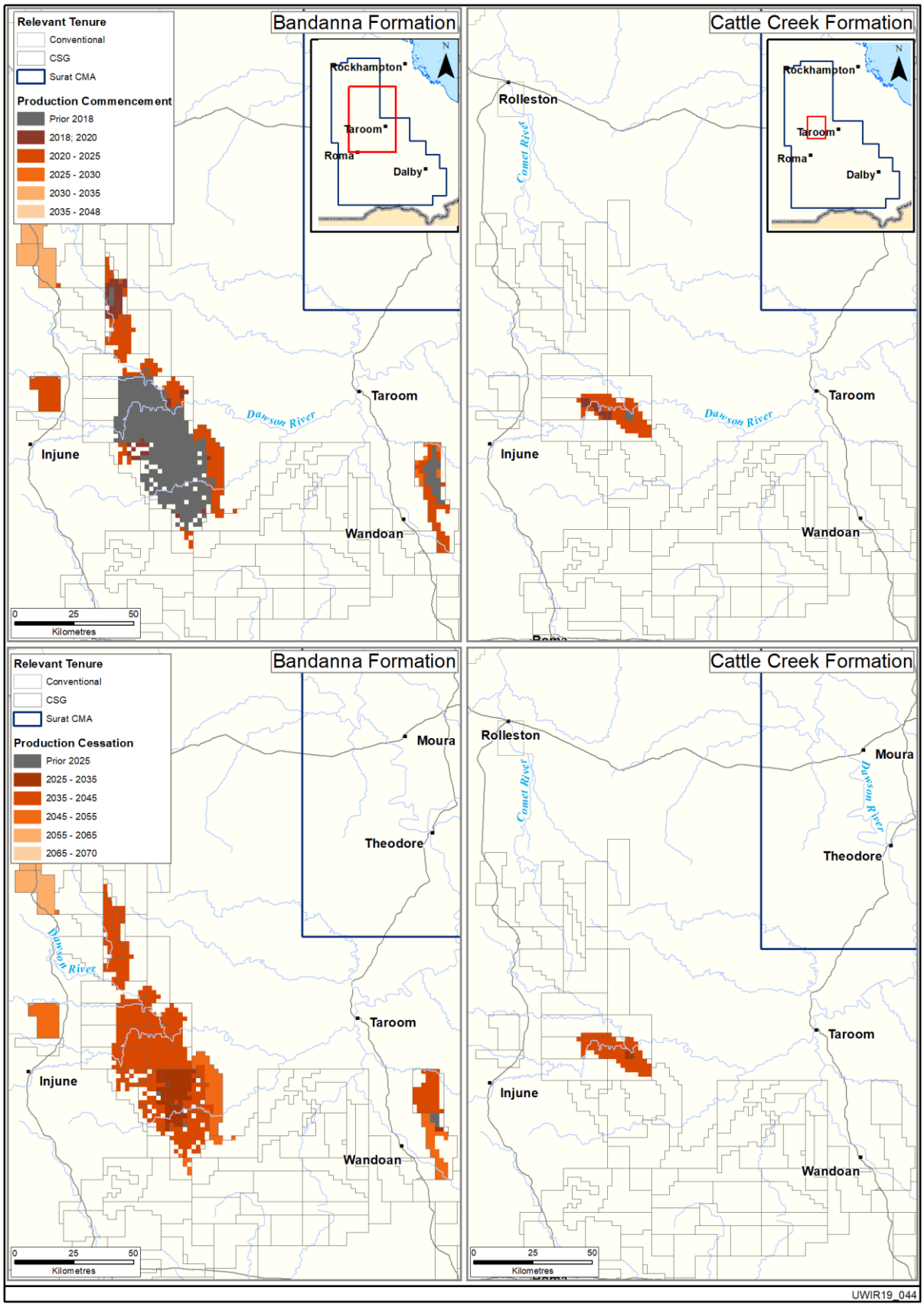

Figure 3-22 Production start and end dates for CSG development areas, Bowen Basin formations

3.3.4 Extraction from conventional petroleum and gas wells

Monthly water production data from each of the conventional petroleum and gas producing wells is reported to OGIA. This is reconciled with monthly production volumes reported in QDEX database. As detailed in UWR 2019, there are an estimated 70 conventional oil and gas production wells in the Surat CMA. Total water production from those wells over time is shown in Figure 3-13.

The conventional P&G industry is in a mature phase in the Surat CMA, with water extraction declining significantly since 2011 to the current level of around 1,000 ML/yr. This also corresponds to declining oil production. The majority of conventional associated water extraction is from the Precipice Sandstone in the Moonie oil field. There is also some minor extraction from the Evergreen Formation and the Clematis Sandstone.

For the purpose of the 1995 steady state simulations, the modelled rates were based on average rates for each conventional well calculated over the available 384-month data period from 1/1/1963 to 31/12/1994. Over the transient calibration period (1995 - 2017), extraction rates attributed to each such well were based on monthly water productions.

3.3.5 Coal mine dewatering

Coal is currently extracted from the Walloon Coal Measures at the following four open cut mining operations within the Surat CMA:

- Commodore (2003 onwards), extracts thermal coal for use in the adjacent Millmeran Power Station
- Cameby Downs (2010 onwards)
- New Acland (2002 onwards) extracts thermal coal from the lower Walloon Coal Measures in the Clarence Moreton Basin
- Kogan Creek (2006 onwards), extracts thermal coal for use in the nearby Kogan Creek Power Station.

Extraction from a further open cut mine at Wilkie Creek took place from 1994 until closure of the operations in 2013.

Each of the pits associated with these operations is relatively shallow (less than 60 m) and the Commodore and New Acland mines are more than 50 km from the nearest CSG fields. However, the Wilkie Creek and Cameby Downs mines are located adjacent to current CSG production areas and hence both CSG and coal mining operations may influence observed groundwater levels in these areas. The UWIR 2019 model therefore includes representation of each of these five open cut operations based on historic mine survey information lodged with the Department of Natural Resources, Mines and Energy. Gravity drainage to each mine pit is simulated through the addition of further MODFLOW-USG drain cells set at the minimum elevation of the surveyed pit shell in each regional model cell. Figure 3-23 shows time series minimum pit shell elevation data extracted from the mine survey data and used as input to the UWIR 2019 model transient simulation As per other surface drainage features a conductance value of 5,000 m^2/d was assigned to all cells used to simulate coal mining operations. This is high enough to allow easy water outflow, but not so high as to instigate numerical instability.

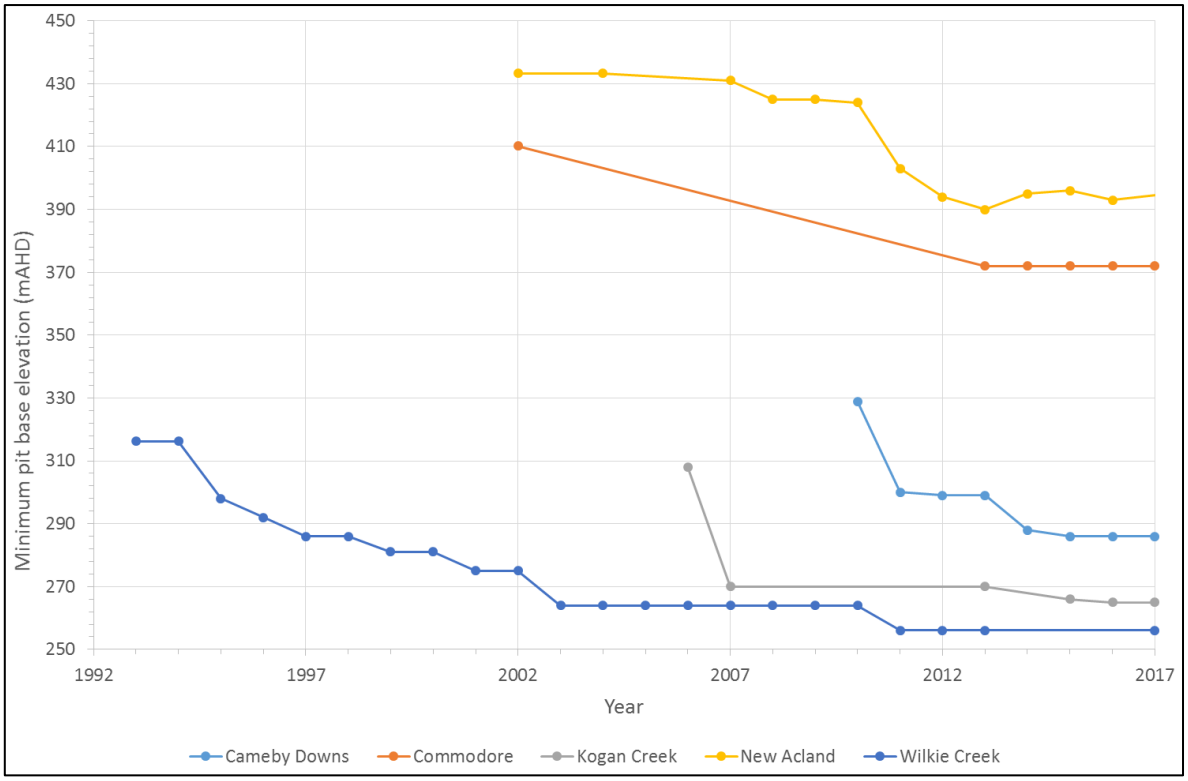

Figure 3-23 Minimum pit base elevation input data, Surat CMA coal mines

3.4 Key model construction assumptions and limitations

Key assumptions and approximations required for construction of the UWIR 2019 model include:

- Model cell sizes are large in lateral extent (1.5 × 1.5 km). One outcome of the large cell size is that shallow, unconfined groundwater systems, and the interaction of these systems with deeper systems, can be simulated only approximately. Another outcome is that multiple CSG extraction wells must often be assigned to the same model cell; this renders simulation of processes that are operative in the immediate vicinities of these wells somewhat approximate.
- Model cell sizes are large in vertical extent. Most stratigraphic layers in the Surat and Bowen basins are represented by only one or two model layers. Vertical head gradients within these layers, and geological details which lead to variations of these gradients, can be represented only approximately. While six model layers are allocated to the Walloon Coal Measures, even this is only sufficient to represent vertical gradients of heads and saturations induced by CSG extraction in an approximate manner.
- The limited vertical grid resolution also affects calculation of CSG impact at sites of interest. For example, evaluation of CSG impact on a particular well which is open to the Springbok Sandstone or Hutton Sandstone can accommodate only to a limited extent the portion of the pertinent formation to which well screens are open. Presumably, impact diminishes with increasing elevation in the Springbok Sandstone and with decreasing elevation in the Hutton Sandstone. Attenuation of impact with vertical separation from the Walloon Coal Measures can only be simulated in an approximate fashion by the existing model.
- The UWIR 2019 model does not simulate flow of gas. Desaturation of coal measures, and hence the dual-phase flow, is approximated using a van Genuchten function in which water saturation is a function of hydraulic pressure alone. This is a simplification of more complex

processes that include desorption of gas from a coal matrix, and then dual-phase flow of gas and water towards CSG extraction wells. Buoyant up-dip movement of gas and associated pressure increases are therefore not represented.

- The cell-to-well conductance (also known as well index in petroleum literature) calculated for CSG drains are based on the Peaceman equation (Peaceman, 1978) which assumes a vertical well. The Peaceman equation is also applied for descending drains that represent inclined and horizontal CSG wells. This is a limitation for representing CSG extraction from the Bandanna Formation, where about 25 per cent of CSG wells are inclined (only 4 per cent of CSG wells in the Walloon Coal Measures are inclined). Cell-to-well conductance calculation for such wells can potentially be improved by solutions provided in (Babu and Odeh, 1989) and (Economides et al., 1996).
- The model does not accommodate buoyant movement of water driven by differences in salinity and temperature, although salinity corrections are applied to observed data before calibration. Salinity differences can be significant between formations. Water temperatures are higher at greater depths.
- The interface between the Walloon Coal Measures and the Condamine Alluvium is represented only approximately. While simulation of vertical head gradients induced by CSG extraction within the Walloon Coal Measures is enhanced by the use of six model layers to represent this unit, in reality, propagation of CSG-induced drawdown is likely to take place along a suite of thin but conductive coal seams whose lateral extents and hydraulic properties are uncertain.
- It is unlikely that the permeability of gas-depleted coal remains the same as its original permeability, due to the effects of matrix shrinkage and geo-mechanical behaviour (Pan and Connell, 2012). The OGIA model does not accommodate for these effects and assumes coal permeability, parameterised by enhanced K in the UWIR 2019 model, is a static property.
- Parameterisation of the western and southern Cauchy boundaries of the model is uncertain. As these boundaries are situated at a considerable distance from sites of CSG extraction, these uncertainties are unlikely to affect predictions of CSG impact to a great extent. Nevertheless, the contributions which these boundaries make to uncertainties in CSG impact prediction is explored in Chapter 7.

The significance or otherwise of a number of the approximations identified above has already been tested as part of the development of the UWIR 2016 model through a comparison of detailed Eclipse simulations and upscaled MODFLOW-USG simulations for the Talinga gas field (OGIA, 2016a).

Comparison of outputs from these two simulations confirmed that the highly upscaled MODFLOW-USG model was able to reasonably replicate:

1. stresses to which overlying and underlying layers are subjected as a result of CSG extraction
2. pressure responses at moderate distances from well fields
3. the effect of gas-filled coal cleats in reducing local relative permeability
4. slowing the lateral progress of pressure reductions away from centres of gas extraction.

On this basis the consequences of upscaling and approximation of dual-phase effects as required by the regional scale of UWIR 2019 model are considered to be acceptable.

4 Initial model parameterisation

4.1 Introduction

4.1.1 In this chapter

This chapter discusses the means by which values were initially assigned to the properties which govern flow of water within and between layers of the UWIR 2019 model. In a groundwater model such as MODFLOW-USG, values for many of these properties must be supplied for every active node (i.e. cell) comprising the model grid; for others they must be supplied only for nodes in certain layers. In both cases they are spatially-distributed properties.

Hydraulic properties on which the present chapter focusses are as follows:

- horizontal hydraulic conductivity
- horizontal-to-vertical hydraulic conductivity anisotropy
- specific storage
- specific yield
- properties which govern the relationship between desaturation and pressure head in coal measures
- properties which govern the relationship between relative permeability and saturation in coal measures
- properties which govern the flow of water from interburden to coal in coal measures from which CSG is extracted
- factors which enhance regional horizontal hydraulic conductivities to account for the flow of water towards CSG extraction wells in coal measure layers.

Values for the first four of these parameter types are required for all model cells. Values for the others are only required for model cells in coal measure layers. In practice, parameters which pertain to desaturation are only of relevance in the vicinity of CSG extraction centres where gas is desorbed. The last of the above list of parameters is only of relevance in model cells from which CSG extraction actually takes place.

The methodology described herein is similar to that developed for parameterisation of the UWIR 2016 model but incorporates a number of improvements. The improved workflow has also now been re-run based on a substantially increased data set comprising an additional 2,456 lithology logs and a revised permeability measurement dataset.

4.1.2 The need for upscaling

As was discussed in Chapter 3 of this document, each layer within the UWIR 2019 model domain represents the entirety, or a considerable proportion, of a discrete stratigraphic unit. An individual model cell can therefore have a vertical thickness of hundreds of metres. A stratigraphic unit, or a portion thereof, that is assigned to an individual model layer, is comprised of a layered sequence of different rock types. Hence, the medium represented by an individual model cell can include layered sequences of sandstones, siltstones, mudstones, shale and coal whose individual hydraulic properties are very different.

As has also been discussed, the horizontal dimensions of each model cell across the model domain are currently 1,500 × 1,500 m. The discretised flow equations which are solved by MODFLOW-USG govern movement of water between these model cells. The hydraulic properties which determine the volume of water which flows between these cells in response to an imposed hydraulic gradient, and the amount of water which can be stored either in pore spaces or elastically within these cells, must therefore pertain to this horizontal scale.

Direct measurements of subsurface hydraulic properties, and inferences of hydraulic properties made on the basis of borehole geophysical data, pertain to scales which are considerably smaller than that of the model cell sizes used by the UWIR 2019 model or most other models. Many of these measurements are associated with restricted vertical intervals and sample the permeability of an individual lithology. Even where hydraulic properties are inferred from pumping tests, the time scales over which water is extracted from a stratigraphic unit are such as to induce flow only within a volume whose lateral extent is considerably smaller than that of a single model cell. In contrast, the hydraulic properties assigned to groundwater model cells must reflect all of the lithologies that these cells contain at a scale that governs horizontal and vertical flow between them. Furthermore, the averaging that is required to represent hydraulic properties at this scale must be done in such a manner that the laws which govern movement of groundwater within a porous medium (namely Darcy's law and conservation of mass) are preserved when applied at the model cell scale. This averaging process is commonly referred to as "upscaling".

The upscaling imperative is not, of course, restricted to groundwater modelling. The need to represent hydraulic properties at the scale of a numerical grid which is considerably coarser than the scale at which heterogeneities exist within a geological medium is common to all modelling of subsurface fluid movement. The literature on upscaling as it pertains to petroleum reservoir modelling is extensive. See, for example, (Dagan et al., 2013; Farmer, 2002; Quental et al., 2012; Wood, 2009), and papers cited therein.

At least three sets of hydraulic properties must be provided for all model layers, these being horizontal hydraulic conductivity, vertical hydraulic conductivity and specific storage; specific yield is also required for coal-bearing units and in outcrop areas of other layers. All of these properties are subject to adjustment through the model calibration process. As will be described in the next chapter, this calibration process is designed to perturb initial parameter values to the minimum extent required to ensure that model outputs match historical measurements of head, water extraction, and other model outputs to which constraints or penalty functions apply. The numerical demands of the calibration process require another upscaling step which supports adjustment of hydraulic properties over areas that comprise hundreds of model cells in some cases through an appropriate model parameterisation device. As will be described in Chapter 5 of this document, pilot points comprise this device (Doherty, 2003).

The process of assigning a hydraulic property to every cell of the model domain (thus satisfying the data input requirements of MODFLOW-USG) thereby becomes a two-step up-scaling process. In the first of these steps hydraulic properties are assimilated from local measurements and assigned to pilot points. In the second step these hydraulic properties are spatially interpolated from the pilot points to all of the nodes that feature in the MODFLOW-USG grid.

The assimilation of pilot-point scale hydraulic properties from local scale permeability measurements is described in section 4.2, which comprises the development of stochastic lithology models and numerical permeameters. More details about the second calibration step are provided in Chapter 5.

4.1.3 The role of initial properties

As was mentioned above, the present chapter describes the assignment of "initial values" to hydraulic properties represented in the UWIR 2019 model. These are then subject to adjustment such that model-calculated heads and flows at certain times and locations within the model domain match their measured counterparts.

The word "parameter" is often used to describe representations of hydraulic properties employed by a model that are adjusted through the calibration process (also known as history-matching). Such adjustment is only possible in a model of the size of the OGIA model if a parameter represents hydraulic properties that are ascribed to many model cells, either through direct association of each cell of the model domain with a particular parameter (e.g. zonal parameterisation), or through use of pilot points as a parameterisation device (where parameter values are interpolated from pilot point locations to the cells of the model grid). Because of the large representative volume of individual parameter values, hydraulic properties which they represent are necessarily upscaled to that volume.

Conceptually, the assignment of values to parameters employed by a model, and the subsequent constraint of parameter values through the history-matching process, is described by Bayes equation. Let the vector **k** represent parameters employed by a model and let $P(\mathbf{k})$ represent the prior probability distribution of these parameters. As a probability distribution, $P(\mathbf{k})$ encapsulates knowledge of these parameters inferred from direct measurements of these properties and subsequent upscaling to the scale associated with each parameter. At the same time, because it is a probability distribution, $P(\mathbf{k})$ represents the fact that actual values of upscaled model properties are not known exactly.

$P(\mathbf{k}|\mathbf{h})$ designates the posterior probability distribution of parameters. This is a probability distribution that is refined, or conditioned, by the necessity for model outputs that are calculated using **k** to respect field measurements of system state that are encapsulated in the vector **h** (heads, fluxes and other components of the calibration dataset) with a level of fit that accommodates the presence of errors in these measurements as well as the presence of numerical errors in corresponding model outputs. The propensity for occurrence of both of these errors is described by another probability distribution, often referred to as the "likelihood function", and designated as $P(\mathbf{h}|\mathbf{k})$. This is related to the "objective function" that is commonly used to describe model-to-measurement misfit. In general, the lower is the objective function, the better is the fit between model outputs and corresponding field measurements of system state, and the higher is the likelihood function.

With this terminology, Bayes equation becomes

$$P(\mathbf{k}|\mathbf{h}) = P(\mathbf{h}|\mathbf{k})P(\mathbf{k}) \tag{4.1}$$

Equation 4.1 makes it plain that the notion of stochasticity should play a fundamental role in parameterisation of a model. The final parameter set employed by a model (i.e. the post-history-matching parameter set) should in fact be described by the posterior parameter probability distribution $P(\mathbf{k}|\mathbf{h})$ derived through constraining the prior parameter probability distribution $P(\mathbf{k})$ by the necessity for pertinent model outputs to match corresponding members of the calibration dataset.

The present chapter describes how a useable prior probability distribution ($P(\mathbf{k})$) was obtained for many parameters employed by the UWIR 2019 model. In particular, it describes how measurements of rock properties, and other lithological information at a variety of scales, was processed in order to obtain estimates of model parameters, together with the uncertainties associated with these estimates. Initial estimates of model parameters provide the starting point for the history matching

process described in Chapter 5. Prior parameter uncertainties are also used in the exploration of post-history-matching parameter and predictive uncertainty described in Chapter 7.

4.2 Hydraulic conductivity: numerical permeameters

4.2.1 General

Figure 3.2 shows the correspondence between layers of the UWIR 2019 numerical groundwater model and stratigraphic units of the Surat and Bowen Basins. Layers 8 to 23 of this model encompass the Westbourne Formation to the Precipice Sandstone, all of these lying within the Surat Basin. Included within this sequence of layers is the primary coal-bearing unit of the Surat Basin, the Walloon Coal Measures. Acquisition of lithological and hydraulic property data within these units has been sufficient to support the development of a stochastic formulation for permeability within the different lithologies which characterise each of them. This stochastic permeability formulation provides the means to generate random realisations of horizontal and vertical permeability for any lithology within any of the above stratigraphic units at any location within the domain of the UWIR 2019 model. At the same time, a stochastic characterisation of lithology was developed. This provides the means to generate stochastic realisations of layered lithological sequences within any of the above stratigraphic units at any location within the domain of the UWIR 2019 model.

The stochastic permeability and lithological models were used in partnership to populate individual elements of a three-dimensional grid of “numerical permeameters” that span the domain of the UWIR 2019 model within the abovementioned stratigraphic units. Detailed numerical representations of each of the stratigraphic units present at the locations of each permeameter were developed and used to estimate formation-scale horizontal and vertical hydraulic conductivity at these locations, and the uncertainties associated therewith.

Figure 4-1 illustrates the overall framework for populating the UWIR UWIR 2019 model with upscaled pre-calibration values of hydraulic conductivity. This framework bears some resemblance to the permeability modelling framework presented by Corvi et al. (1992), and illustrates how stochastic lithology and permeability models are used to populate a set of numerical permeameters from which regional values of hydraulic conductivity for use of the UWIR 2019 model are derived. A summary of this process is provided below in sections 4.2.2 to 4.2.4.

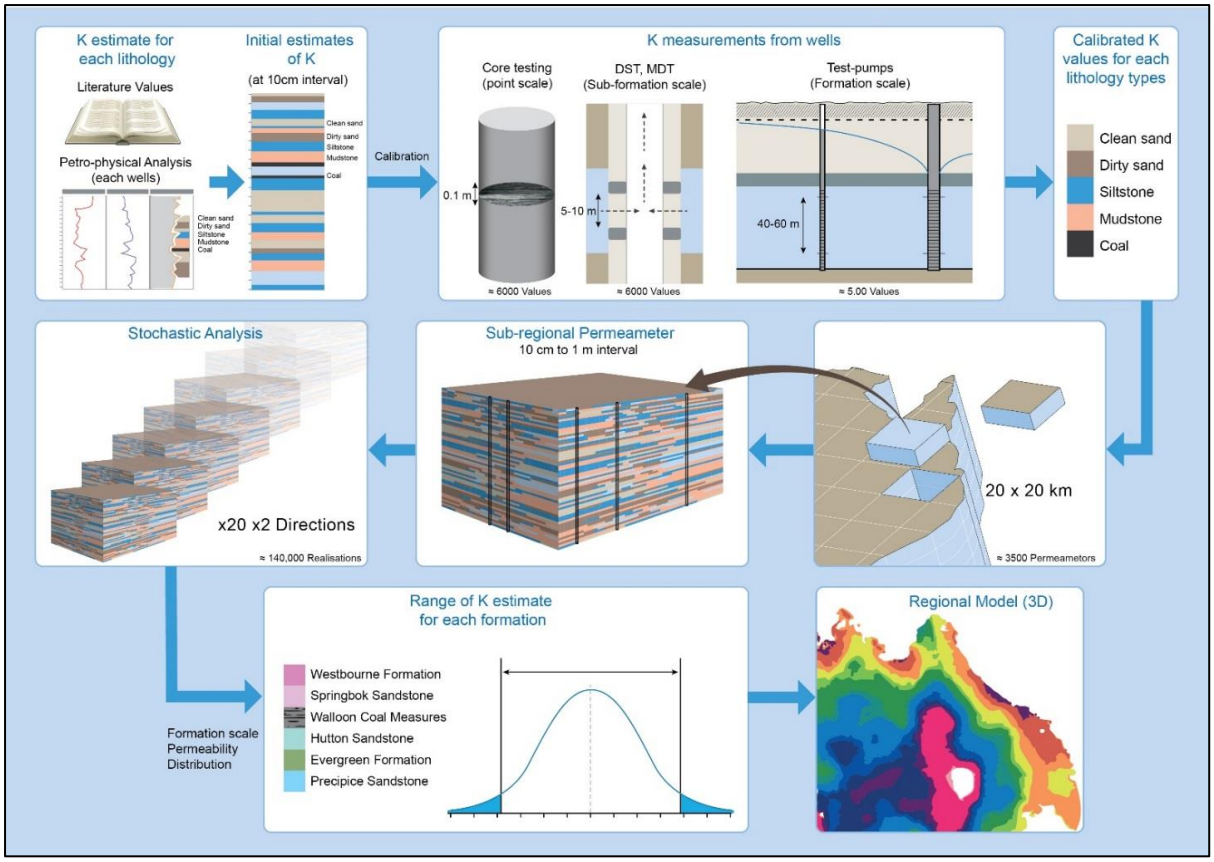

Figure 4-1 Modelling framework used to populate the UWIR 2019 model with prior estimates of hydraulic conductivity.

4.2.2 Stochastic lithology model

At the time of development of the UWIR 2016 model detailed lithological logs were available for some 3,514 bores in the Surat Basin, derived from downhole gamma and density logs run in each bore (see (OGIA, 2019b) for further information). Since this time data for a further 2,456 bores have been processed and hence the current Surat Basin database includes inferred lithologies at intervals of 0.1 m for some 5,970 bores in total. The location of these bores is shown in Figure 4-2.

The lithological classification is based on six different facies, these being:

- clean sandstone
- dirty sandstone
- siltstone
- mudstone
- carbonaceous shale
- coal

As shown in Figure 4-2 the availability of lithological data varies with location; CSG tenure areas are better represented than other areas. Data density diminishes with depth in the vicinity of the Taroom Trough and also varies with stratigraphic unit. The Walloon Coal Measures are better represented than other stratigraphic units, while the Springbok Sandstone is the next best represented unit. For units which underlie the Walloon Coal Measures, representation diminishes with stratigraphic depth

since the majority of CSG wells terminate in the Durabilla Formation immediately below the Walloon Coal Measures.

Geostatistical analysis of lithological juxtaposition, and generation of random layered lithology fields based on the lithology database, was undertaken using the T-PROGS suite of software (Carle, 1999). This suite of programs was supplemented and enhanced by utility programs developed by OGIA. T-PROGS characterises lithological juxtaposition using transition probabilities. Probabilities that describe the transitioning of one lithology to any other lithology are built empirically by processing borehole lithological logs. These empirical transition probabilities then support parameterisation of Markov chain models; the latter are used for generating random realisations of three-dimensional layered lithological sequences with the same geostatistical properties as those that exist in reality. These realisations can be constrained to honour the lithologies encountered in specific boreholes.

While providing a conceptually sound basis for numerical permeameter construction, generation of lithological realisations using T-PROGS was not without its problems. These include the following.

- As stated above, lithological data density varies with location and stratigraphic unit. Local data support for stochastic field generation is therefore lacking in some parts of the UWIR 2019 model domain. Stochastic properties in these areas were therefore inferred from those in other areas where data support is better.
- Within any borehole, the geophysical log processing methodology developed provides lithological data on which to base transition probabilities at a resolution of 0.1 m in the vertical direction. This provides a sound basis for characterisation of local vertical transition probabilities. Unfortunately, transition probabilities (and therefore continuity of individual lithofacie classes) in the horizontal direction are less well known. Estimates of these must therefore rely on expert knowledge. Errors in these estimates may then incur errors in estimates of upscaled hydraulic conductivities.
- Lakes, swamps and meandering rivers constituted the depositional environments in many parts of the Surat Basin. The river environment in particular may promulgate local anisotropy in horizontal transition probabilities; it may also promulgate locally high degrees of lithological continuity that are better characterised by alternative geostatistical descriptors which specifically account for these types of depositional features.
- OGIA has noticed that while T-PROGS honours lithological sequences in boreholes used for conditioning of random lithological realisations, it sometimes fails to honour continuity relationships between these conditioning points and the wider geostatistical domain. (Anecdotal evidence from other T-PROGS users supports this observation.)

Despite these shortcomings, T-PROGS formed the basis for stochastic lithological modelling undertaken by OGIA because of its availability, ease of use, and access to source code. However alternative geostatistical characterisations of Surat Basin lithology are being investigated the use of which has already lead to some revision of the approach to parameterisation of the upper non-productive part of the Walloon Coal Measures (model layer 11, section 4.4.1).

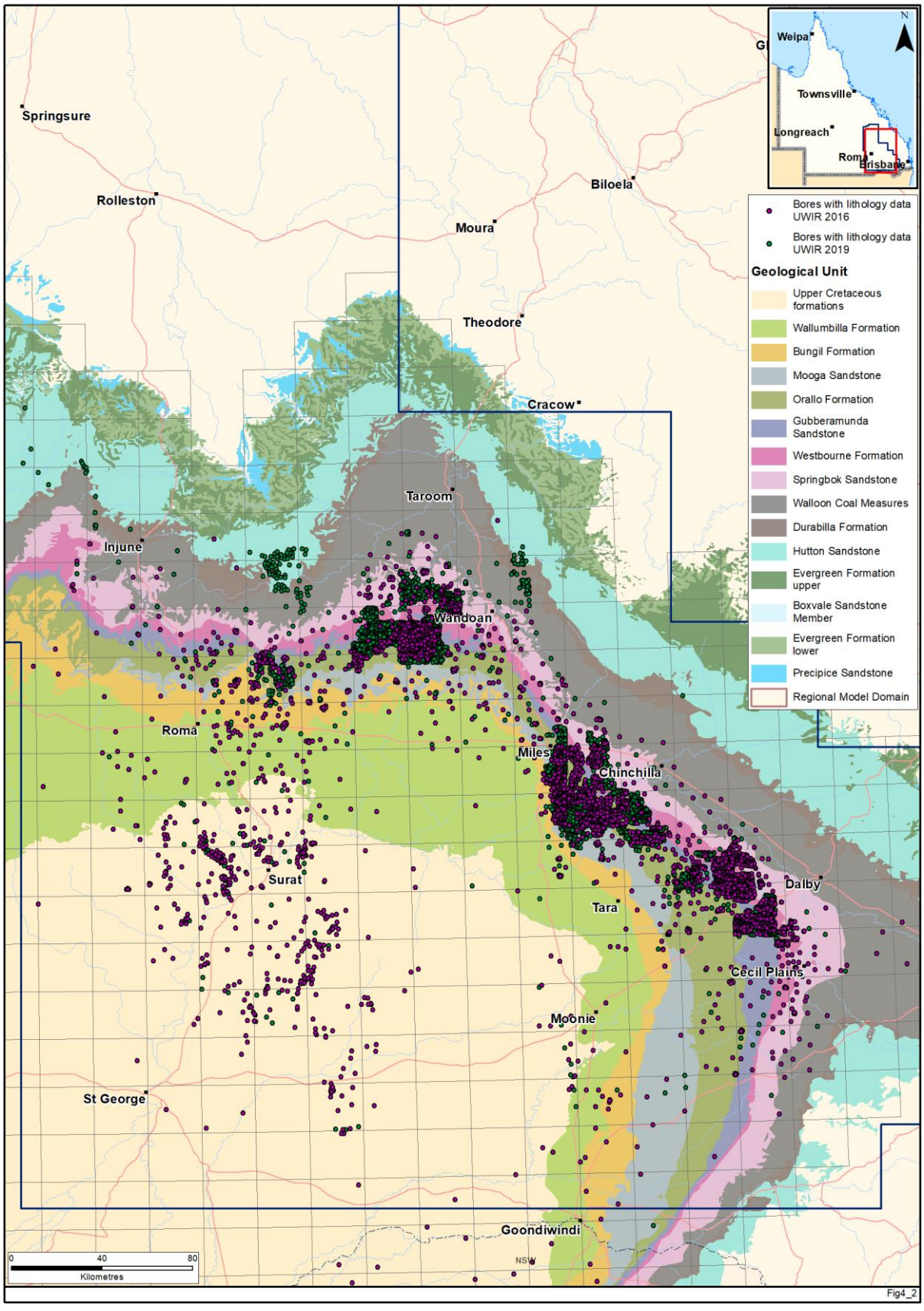

Figure 4-2 Bore-locations with available lithological logs

In summary, T-PROGS-based processing of the lithology database supported stochastic generation of lithofacies realisations (optionally conditioned by local borehole data) in stratigraphic units comprising layers 8 to 23 of the UWIR 2019 model. These realisations were comprised of six lithologies in the Springbok Sandstone and Walloon Coal Measures, and four lithologies in other layers (where carbonaceous shale and coal are typically absent). Separate stochastic processing was undertaken for each stratigraphic unit, so that differences between the characteristics of these units could be maintained.

4.2.3 Stochastic permeability model

4.2.3.1 Dataset

Measurements of horizontal and vertical permeability in stratigraphic units spanned by layers 8 to 23 of the UWIR 2019 model are available over a range of scales. At the time of UWIR 2019 model development (see (OGIA, 2019e)), the permeability dataset for these layers was comprised of the following:

- 6,654 laboratory measurements of horizontal permeability derived from core samples of around 0.1 m in length
- 7,712 drill stem test (DST) measurements associated with test lengths of 2 to 30 m
- 118 pumping tests of many hours duration over screened intervals that are typically greater than 10 m
- 1,448 measurements of vertical permeability, mainly comprising laboratory measurements on cores of around 0.1 m in length.

Assimilation of information that resides in this large, multi-scaled dataset into the UWIR 2019 model presented a challenge. With the possible exception of pumping test data interpretations, most estimates of permeability that comprise this dataset are at a scale that is not directly useable by a regional groundwater model.

The problems associated with use of these data sets are compounded by the fact that the lithologies to which many of the above permeability measurements pertain are not known with a high degree of certainty. In fact, most permeability inferences are likely to be associated with more than one lithology; where this is the case lithological proportions over the sampling interval are unknown. Unfortunately, the problem of lithological attribution cannot be escaped even for core measurements. The vertical locations of most core samples are known only to within about 2 m. Furthermore in some instances there is no associated lithological log available for the hole from which the core was extracted and in others the available lithological logs are not sufficiently detailed to confirm the lithology tested.

Note that hydraulic conductivity (*K*, which is used in most groundwater models) is calculated from permeability (*k)* using the following equation.

$$K = \frac{\rho g}{\mu} k \qquad (4.2)$$

where:

K is hydraulic conductivity [m/day];

ρ is the density of water [kg/m^3];

g is the acceleration due to gravity [m/s^2]; and

μ is the dynamic viscosity of water [kg/(s·m)].

Permeability is an intrinsic quality of a porous medium, whereas hydraulic conductivity also depends on fluid properties. Permeability (rather than hydraulic conductivity) is normally measured in the laboratory and inferred from borehole logs. For the work described in this report, a conversion factor of 1.27E-03 was applied to convert from permeability (k, in mD) to hydraulic conductivity (K, in m/d), i.e. 1 mD equals to 1.27E-03 m/d. This conversion factor assumes a dynamic viscosity of 0.66 kg/(s·m) which is based on viscosity values used in local reservoir simulation models that were made available to OGIA.

4.2.3.2 Stochastic modelling of horizontal permeability

Let k_{ij} depict the horizontal permeability of lithology *i* in stratigraphic unit *j*. The lithology index *i* varies from 1 to 6 (clean sand to coal) in accordance with the lithology types listed above. Stratigraphic units are indexed from 1 to 12, starting at the Westbourne Formation and increasing by 1 with each model layer, except for the middle Walloon Coal Measures where all of layers 13 to 15 of the OGIA model are assigned the same stratigraphic index (more on this below). With the exception of coal (lithological index i=6), it is assumed that k_{ij} can be calculated using the equation provided in Nelson et al. (2013):

$$\log\left(k_{ij}\right)=\log\left(k_{0ij}\right)-\frac{b_{ij}\sqrt{0.0248d}}{2.303}+\varepsilon_{ij} \quad (4.3)$$

where "log" implies base 10 and:

k_{0ij} is the permeability of lithology *i* of stratigraphic unit *j* at zero depth [mD];

b is a fitting parameter [m$^{-1/2}$];

d is depth [m]; and

ε_{ij} is an error term specific to *i* and *j* [mD].

In equation 4.3, characterisation of k_{0ij} as the "permeability at zero depth" follows from substitution of zero for *d* in this equation; the second term then disappears. The term "0.0248d" is an approximation to the effective stress (in kPa) at depth *d*. The decrease of permeability with increasing stress for different lithologies has been measured by CSIRO (Esteban et al., 2015) on the behalf of OGIA (see Figure 4-3). These measurements show the largest reduction in permeability as function of stress for siltstone and mudstone dominated core samples have been used to parameterise the *b* term in the above equation.

For coal (i.e. for *i* equal to 6), the following equation is used in place of equation 4.3.

$$\log\left(k_{ijm}\right)=\log\left(k_{0ij}\right)-\frac{b_{ijm}d}{2.303}+\varepsilon_{ij} \quad (4.4)$$

The "*m*" subscript ascribed to *k* and b in equation 4.4 denotes a subdivision of the model domain into four coal permeability regions defined in the previous OGIA regional conceptualisation report (OGIA, 2016d); see Figure 4-4. As is described in that report, the zonation depicted in this figure is considered to reflect prevailing stresses and the presence of stress-related geological structures. Coal permeabilities appear to be significantly higher in some of these regions than in others and

consequently slightly different rates of reduction in coal permeability with depth also apply. To reflect this, the *b* [m^{-1}] parameter of equation 4.4 is assigned a different value in each of them.

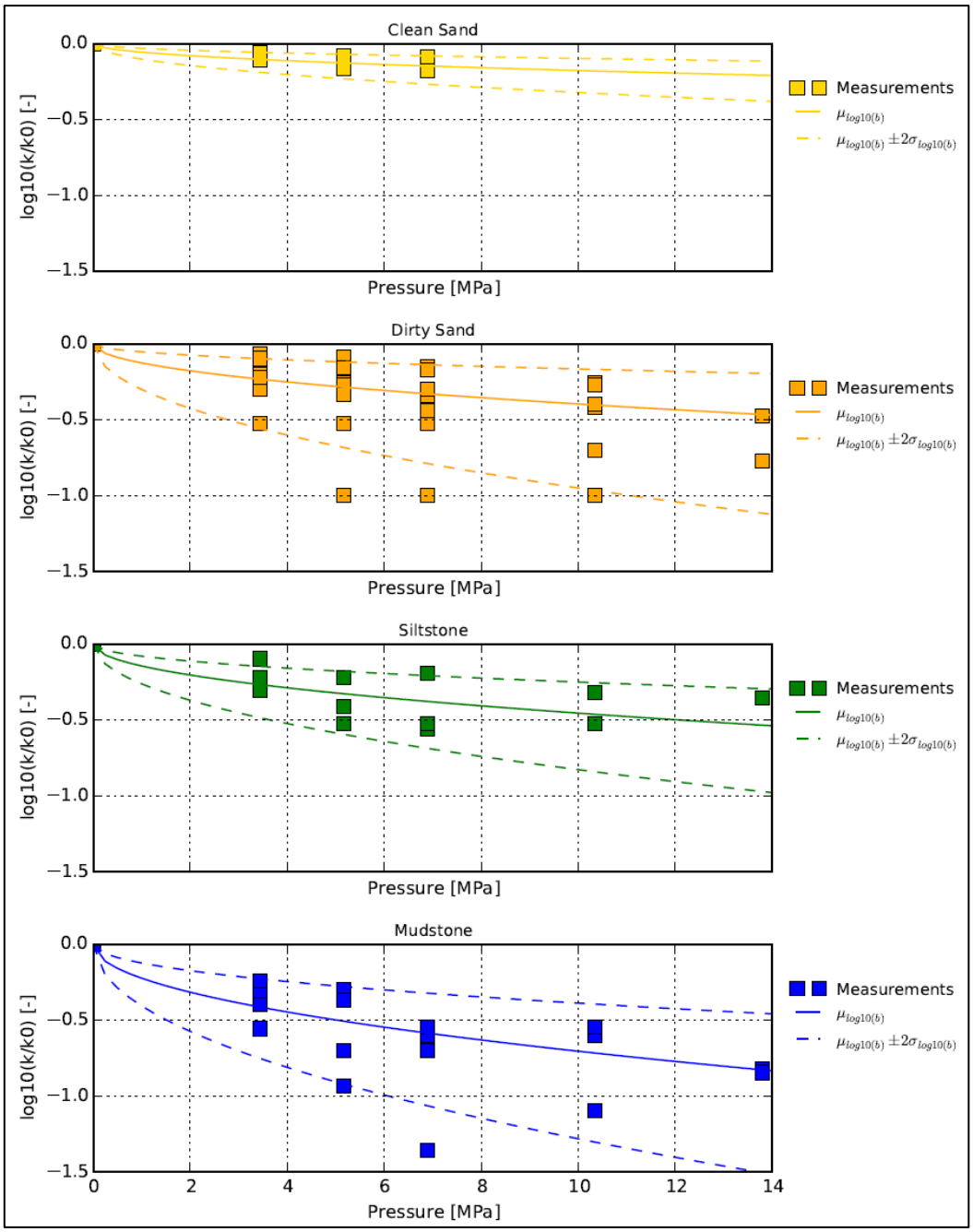

Figure 4-3 Laboratory measurements of permeability for increasing stress levels for different rock-types (Esteban et al., 2015); smooth and dashed lines show a range of applied permeability-stress relationships by Nelson et al. (2013) that are used to parameterise the stochastic permeability model

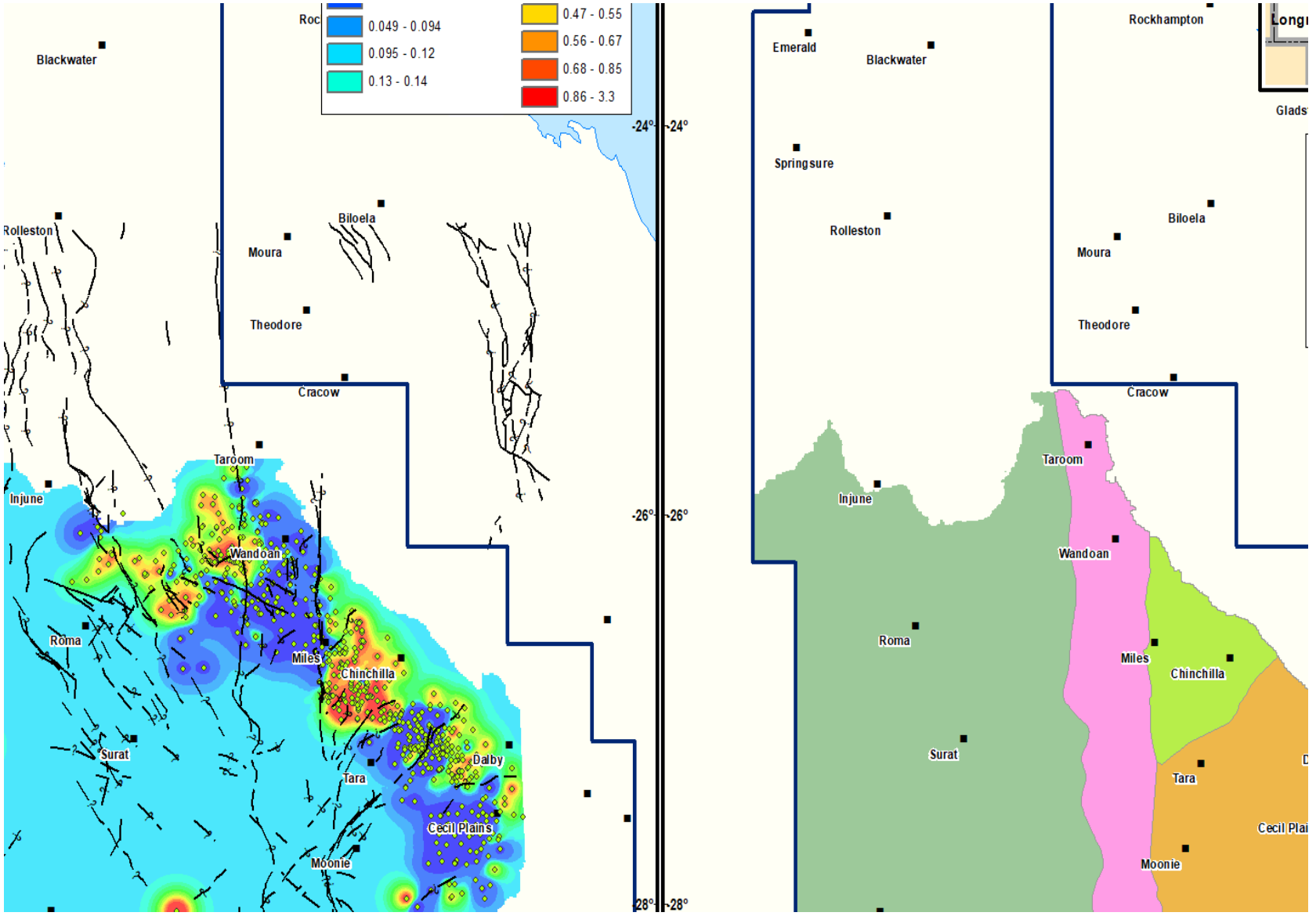

Figure 4-4 Zonation used in defining values for b_{ijm} of equation 4.4

In equations 4.3 and 4.4 k_{0ij}, $b_{ij(m)}$ and ε_{ij} are stochastic variables. k_{0ij}, $b_{ij(m)}$ are assumed to be characterised by a log-normal distribution while ε_{ij} is assumed to be characterised by a normal distribution. Expected values for k_{0ij} and $b_{ij(m)}$ were estimated through a data-matching process described below, while the expected value of ε_{ij} was assumed to be zero. The variances (variance is the square of standard deviation) of the logs of k_{0ij}, $b_{ij(m)}$, and the variance of ε_{ij} were also estimated through data matching.

The error term ε_{ij} featured in equations 4.3 and 4.4 is assumed to show vertical correlation characterised by an exponential decay with distance along a borehole. Hence the covariance of ε_{ij} between two points in a borehole can be symbolised as $C_{ij}(h)$, where h is the vertical separation distance between the two points. Covariance as a function of vertical separation distance is assumed to satisfy the following relationship:

$$C_{ij}(h) = C_{ij}(0)\left[1 - e^{-\frac{3h}{a_{ij}}}\right] \qquad (4.5)$$

where $C_{ij}(0)$ is the covariance at zero separation (i.e. the variance of ε_{ij}), and a_{ij} is the correlation range of the variogram.

4.2.3.3 Parameterisation of horizontal permeability model

To stochastically characterise the permeability ascribed to lithology *i* in stratigraphic unit *j*, the following parameters are required:

- the expected values of $\log(k_{0ij})$ and $b_{ij(m)}$
- the standard deviations of $\log(k_{0ij})$, $b_{ij(m)}$ and ε_{ij}
- the value of a_{ij}.

Standard variogram analysis was used to infer a_{ij}. A combination of expert knowledge, literature review, permeability-stress measurements obtained from CSIRO (see Figure 4-3) and data matching was employed for estimation of the other parameters.

Data matching was undertaken by comparing measurements of permeability with random permeability values generated by the stochastic model described by equations 4.3 to 4.5. However, measured and modelled values for permeability could not be compared on a one-to-one basis because of the random nature of stochastic model outputs. Hence, the data matching process sought to achieve a match between the stochastic characteristics of the observed and simulated permeability datasets, rather than on matching individual measurement values.

The necessity for stochastic matching of observed and modelled permeability datasets was also an outcome of the uncertainty of lithological attribution of the permeability measurements. Stochastic realisations of the locations of observed permeabilities with respect to lithological logs were therefore generated prior to comparing these observations with permeabilities generated by the stochastic model. Thus, for example, each core measurement was randomly ascribed a position on a lithological log within a 2 m interval of its recorded downhole location in order to accommodate uncertainty in the latter. The measured permeability for this core was then compared with weighted averages of stochastically generated permeabilities for the lithologies which are spanned by this interval; weighting reflected lithological proportions prevailing over the depth interval to which the core was ascribed. Similar stochastic positioning was employed when comparing DST and pumping test

observations of horizontal permeability with composite lithological permeabilities generated by the stochastic model; however in these cases arithmetic averaging of stochastic lithology permeabilities took place over a greater bore depth interval. Where a permeability observation (of any scale) was not made in a hole with which a lithological log is associated, the lithological sequence recorded in a random nearby bore was selected for comparison with arithmetically averaged stochastic permeabilities over a similar length of hole.

Figure 4-5 illustrates stochastic matching of measured and modelled core, DST and pumping test horizontal permeabilities for OGIA model layer 10 (i.e. the lower Springbok Sandstone formation). As stated above, an exact match between actual measurements and simulated values is not sought during the calibration process, rather calibration is deemed to have been achieved where the statistics of the measured and simulated populations are similar.

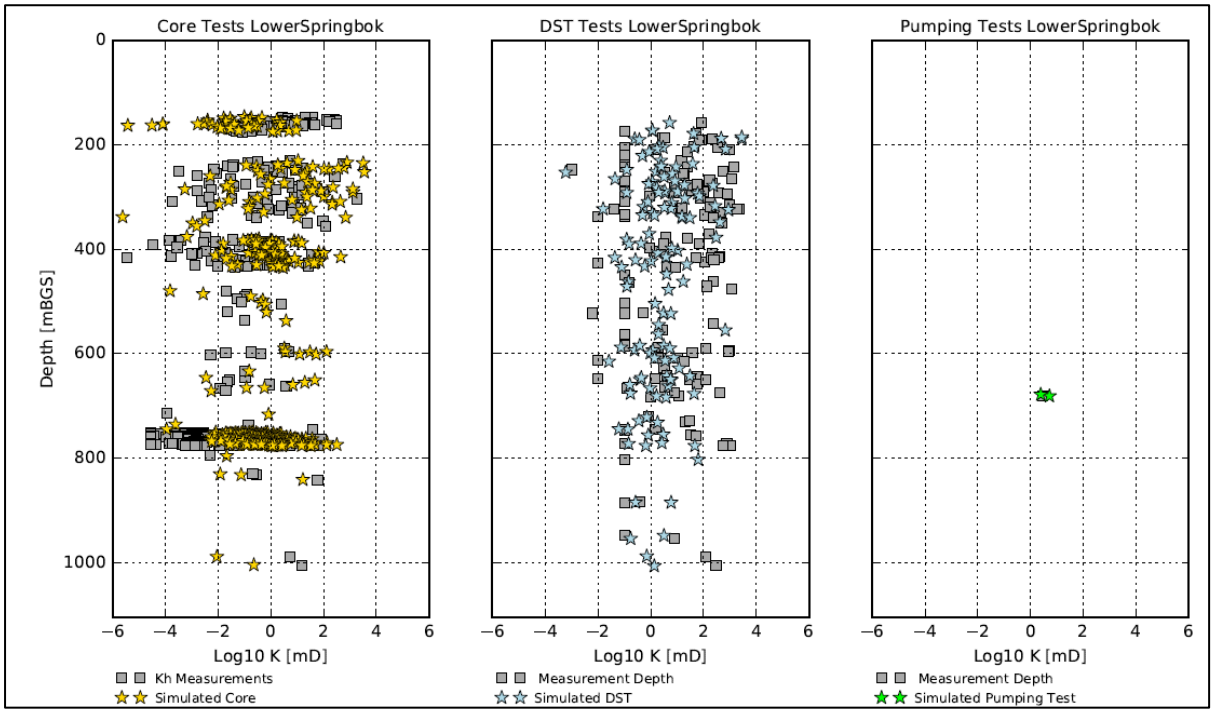

Figure 4-5 Comparison between actual horizontal permeability measurements and simulated horizontal permeability values generated for the lower Springbok Sandstone using the stochastic permeability model for that unit

Adjustment of stochastic model parameters through the data-matching process described above was done manually, this affording maximum use of expert knowledge in assigning values to these parameters. It is hoped that the data-matching process can be automated during any subsequent refinements.

4.2.3.4 Stochastic model of vertical permeability

Once a stochastic value for horizontal permeability k_{ij} is ascribed to lithology i within stratigraphic unit j at a particular location using equations presented in the previous subsection, a value for vertical permeability v_{ij} can be assigned to the same location using the equation

$$v_{ij} = \frac{k_{ij}}{\eta_i} \qquad (4.6)$$

where η_i signifies the horizontal-to-vertical hydraulic anisotropy ratio for lithology type i. In equation 4.6 η is assumed to be independent of stratigraphic unit. For coal, it is assumed to be independent of the zonation depicted in Figure 4-4.

The probability density function ascribed to η_i is the same for all non-coal lithologies; for these lithologies, η_i is sampled from a log-normal probability distribution. For coal, η_i was ascribed a log-normal distribution.

In association with the stochastic horizontal permeability models described by equations 4.3 to 4.5, the probability density functions for η_i were used to simulate core tests of vertical permeability which can be stochastically matched with available measurements. Figure 4-6 shows the stochastic matching of measured and modelled core test vertical permeabilities for layer 18 of the UWIR 2019 model (i.e. the upper Hutton Sandstone formation). Figure 4-7 compares measured and simulated anisotropy for all core tests with measurements of both horizontal and vertical permeability.

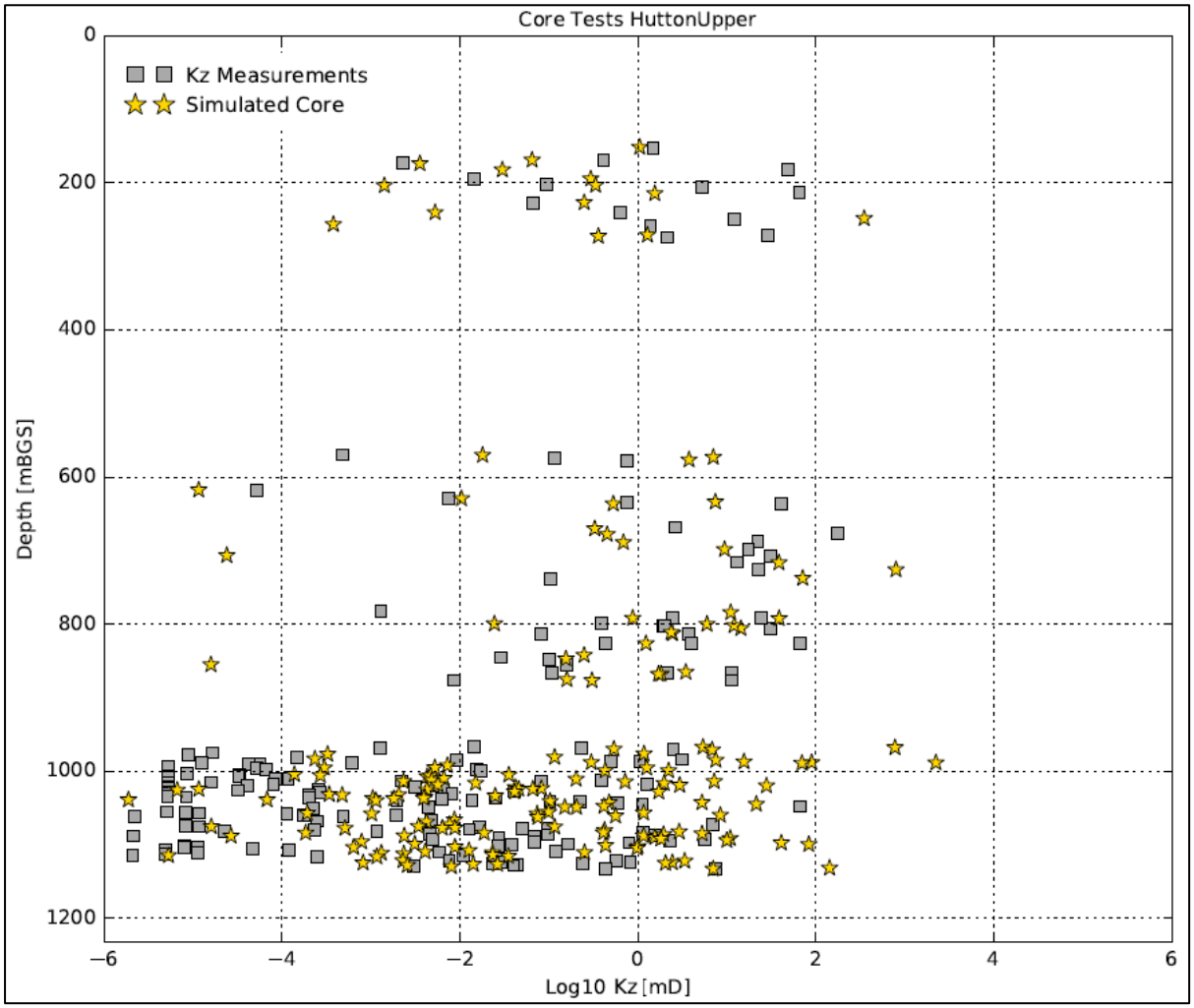

Figure 4-6 Simulated and observed core test vertical permeabilities for the upper Hutton Sandstone

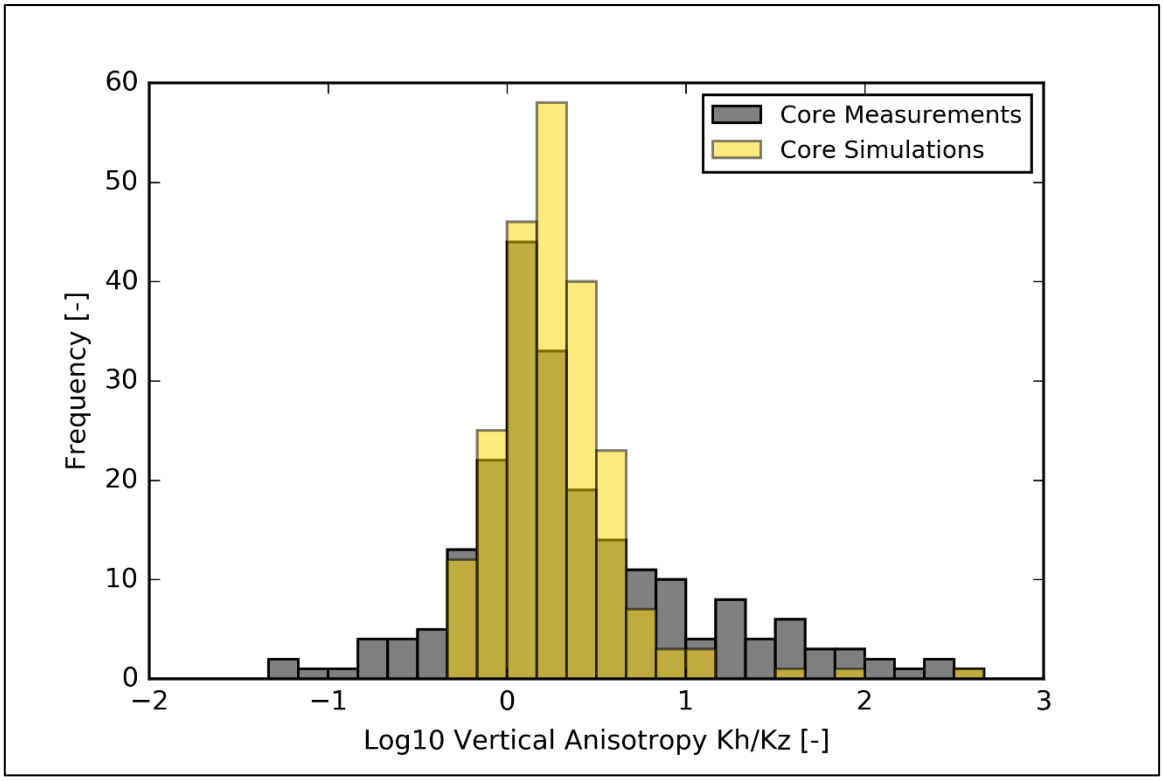

Figure 4-7 Frequency histogram for measured and stochastically generated vertical anisotropies for cores in all Surat stratigraphic units

4.2.4 Numerical permeameters

4.2.4.1 Principle of operation

As was mentioned in section 4.1.2, initial parameterisation of the UWIR 2019 model required an upscaling step that accounts for the fact that permeability measurements at the core, DST or even pumping test scale are not typically directly useable in a regional model, because of:

1) the high level of hydraulic property heterogeneity that prevails at small scales
2) uncertain lithological composition of the intervals sampled in the permeability measurements
3) limited lateral continuity of highly permeable lithology types (e.g. coal), which is likely to reduce the effective regional-scale transmissivity of a formation compared to taking a simple arithmetic average of the permeability of the lithologies present in any well
4) limited lateral continuity of low permeable lithology types (e.g. siltstones), which depending on the disposition of these low permeability strata may allow water to move relatively easily through the strata leading to an increase in the effective formation scale vertical permeability compared to taking a simple harmonic average of the lithologies present in any well.

To address these issues, a large number of numerical permeameters (2,966 in total) are developed, which represent detailed portions of stratigraphic units that are represented in the UWIR 2019 model. Figure 4-8 shows a visualisation of a single numerical permeameter for a portion of the Walloon Coal Measures. For each of these numerical permeameters the complex, local-scale architecture is captured by generating multiple detailed-scale, three-dimensional lithology distributions that are

subsequently populated with hydraulic conductivity properties from the stochastic permeability models described in section 4.2.3. As a final step the numerical permeameters are subjected to horizontal and vertical head gradients, in order to back-calculate effective horizontal and vertical hydraulic conductivity, which are then used to obtain initial values and value ranges for pilot points used to parameterise Kh and Kv in layers 8 to 23 of the UWIR 2019 model. In the following sections the design and usage of the numerical permeameters is described in more detail.

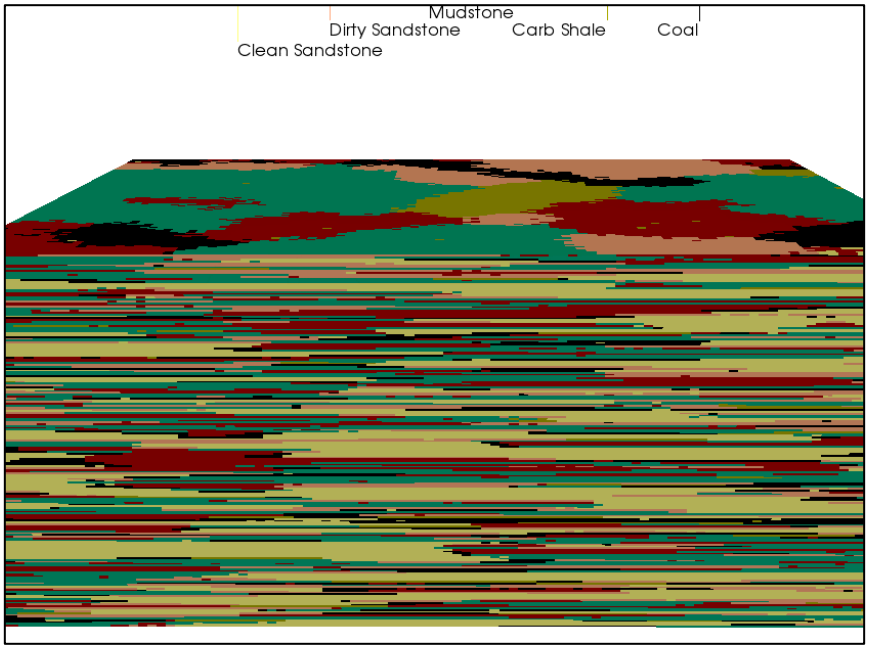

Figure 4-8 Visualisation of a lithology realisation used as input to a numerical permeameter for a portion of the Walloon Coal Measures

4.2.4.2 Numerical permeameter grid

Figure 4-9 displays the numerical permeameter grid, together with the number of numerical permeameters that are developed within each grid 'cell'. Each numerical permeameter is square in plan, 21 km by 21 km in size, and represents a detailed representation of an entire model layer of the UWIR 2019 model, which often corresponds to an entire stratigraphic unit. A maximum of 12 permeameters are created in each location, depending on the extent of stratigraphic units represented by the UWIR 2019 model. Table 4-1 summarises which layers of the UWIR 2019 model are represented by the numerical permeameter grid. Note that for the middle Walloon Coal Measures and Evergreen Formation, single numerical permeameters are used to capture the prior distribution of hydraulic conductivity of multiple model layers.

Table 4-1 Alignment of numerical permeameters with layers in the UWIR 2019 model

Permeameter index	Model layer	Stratigraphic unit(s)
1	8	Westbourne Formation
2	9	upper Springbok Sandstone
3	10	lower Springbok Sandstone
4	11	Walloon Coal Measures non-productive zone
5	12	upper Walloon Coal Measures
6	13,14,15	middle Walloon Coal Measures
7	16	lower Walloon Coal Measures

Permeameter index	Model layer	Stratigraphic unit(s)
8	17	Durabilla Formation
9	18	upper Hutton Sandstone
10	19	lower Hutton Sandstone
11	20,21,22	upper Evergreen Formation, Boxvale Sandstone, lower Evergreen Formation
12	23	Precipice Sandstone

To undertake permeameter calculations, a MODFLOW groundwater model is developed for each permeameter area. Each of these groundwater models employs a structured local grid with horizontal cell dimensions of 200 m by 200 m. The number of layers comprising each of these permeameter-specific models varies between 30 and 357, this being dependent on the local thickness of the regional model layer which the numerical permeameter represents and adopting minimum and maximum permeameter layer thicknesses of 0.1 and 1 m respectively.

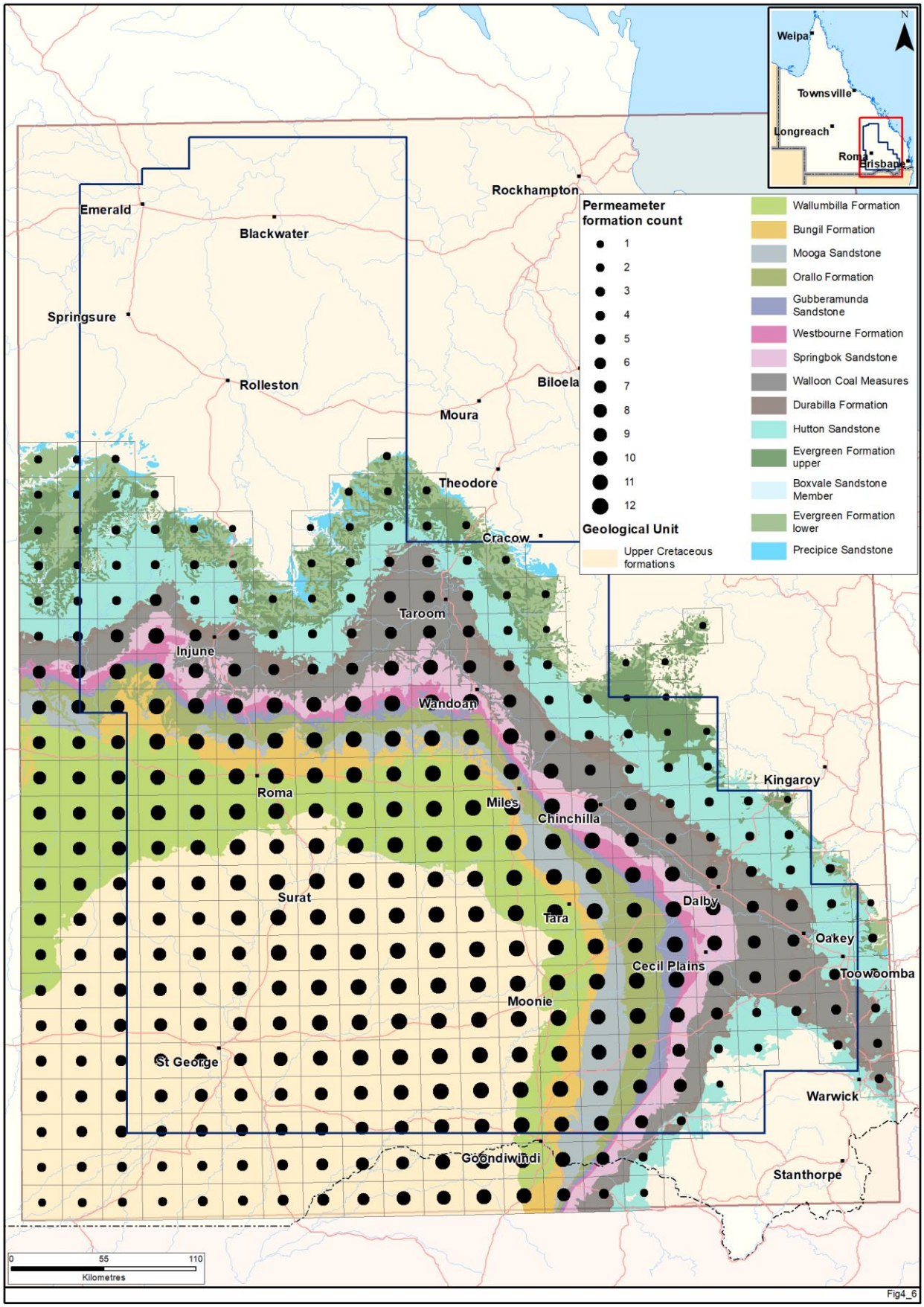

Figure 4-9 Grid of numerical permeameters superimposed on outcrop map of layers 8 to 23 of the UWIR 2019 model

4.2.4.3 Parameterisation

The TSIM utility of the T-PROGS suite (Carle, 1999) was used to populate individual numerical permeameters with three-dimensional lithology distributions; an example of which is displayed in Figure 4-8. Thus each permeameter represents a gridded random realisation of local lithological layering, conditioned, where possible, by lithologies recorded in the lithology bores shown in Figure 4-2. Transition probabilities and lithological proportions which support these realisations were estimated from lithological logs pertaining to the stratigraphic layer which each numerical permeameter represents. If local data density permitted, lithological proportions were calculated using only local lithological logs.

Each of the cells (ranging from 300,000 to 4 million) contained within an individual numerical permeameter represents a single lithology. A random horizontal hydraulic conductivity and vertical hydraulic conductivity were assigned to each cell using the stochastic permeability models described in section 4.2.3. For cells thicker than 0.1 m, some minor upscaling of vertical hydraulic conductivity was implemented to account for vertical permeability variations within a single lithology class.

4.2.4.4 Permeameter calculations

For each numerical permeameter that is parameterised with hydraulic conductivities, an estimate of formation scale horizontal hydraulic conductivity was then obtained by ascribing fixed head conditions to the eastern and western boundaries of the numerical permeameter domain and running its MODFLOW-model to calculate the flux between these two boundaries. An estimate of formation scale vertical hydraulic conductivity was obtained by ascribing fixed head conditions to the upper and lower surfaces of the permeameter model and running the model again to calculate flux between these surfaces. This process was repeated 20 times, using different realisations of cell-based lithology and lithology-based hydraulic conductivity. The median values of upscaled horizontal and vertical hydraulic conductivities, and the standard deviations of these quantities, were thereby calculated.

By repeating this process for all of the 2,966 permeameters comprising the overall grid of numerical permeameters, stochastic characterisation of pilot-point scale horizontal and vertical hydraulic conductivity within layers 8 to 23 of the UWIR 2019 model was achieved. Figure 4-10 shows, for example, the obtained median horizontal hydraulic conductivities and standard deviations of log horizontal hydraulic conductivities based on the numerical permeameters developed for the middle Walloon Coal Measures; these are layers 13 to 15 of the UWIR 2019 model. Figure 4-11 does the same for vertical hydraulic conductivities. In these figures some permeameters are depicted as being of “type A”. These are permeameters for which enough local borehole information exists to condition the stochastic lithology fields, and compute local transition probabilities and lithological proportions for stochastic lithology generation with TSIM.

As can be judged from the above description, the numerical burden of numerical-permeameter-based upscaling is high, requiring a total of 59,320 lithology realisations (generated using the TSIM utility from the T-PROGS suite) and 118,640 MODFLOW runs. These simulations take approximately a week of computational time on the DES high performance cluster which comprises more than 500 cores. Despite this high computational burden, the numerical returns are considerable. The process yielded estimates of the median values of upscaled horizontal and vertical hydraulic conductivity at 2,966 locations within the model domain, together with the range of values that these upscaled properties may take, this expressing their prior uncertainties.

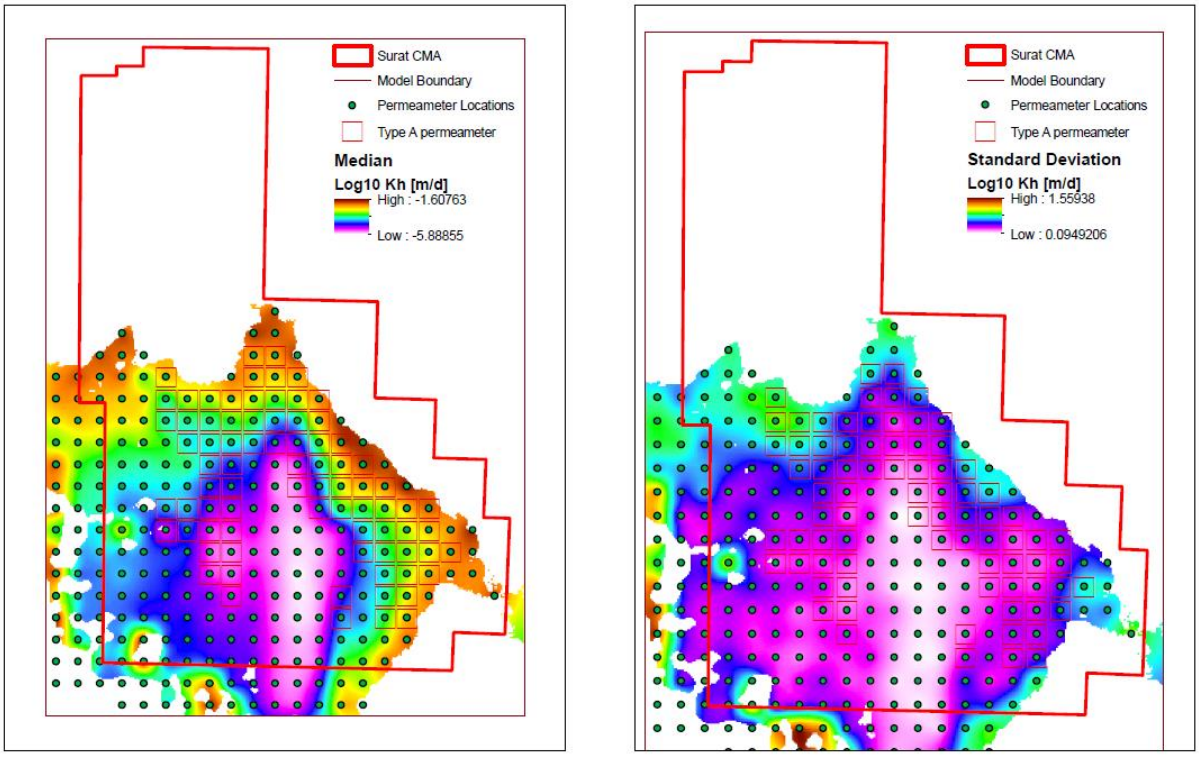

Figure 4-10 Median (left) and standard deviation (right) of permeameter-calculated log (to base 10) upscaled horizontal hydraulic conductivity in the middle Walloon Coal Measures (model layers 13 to 15)

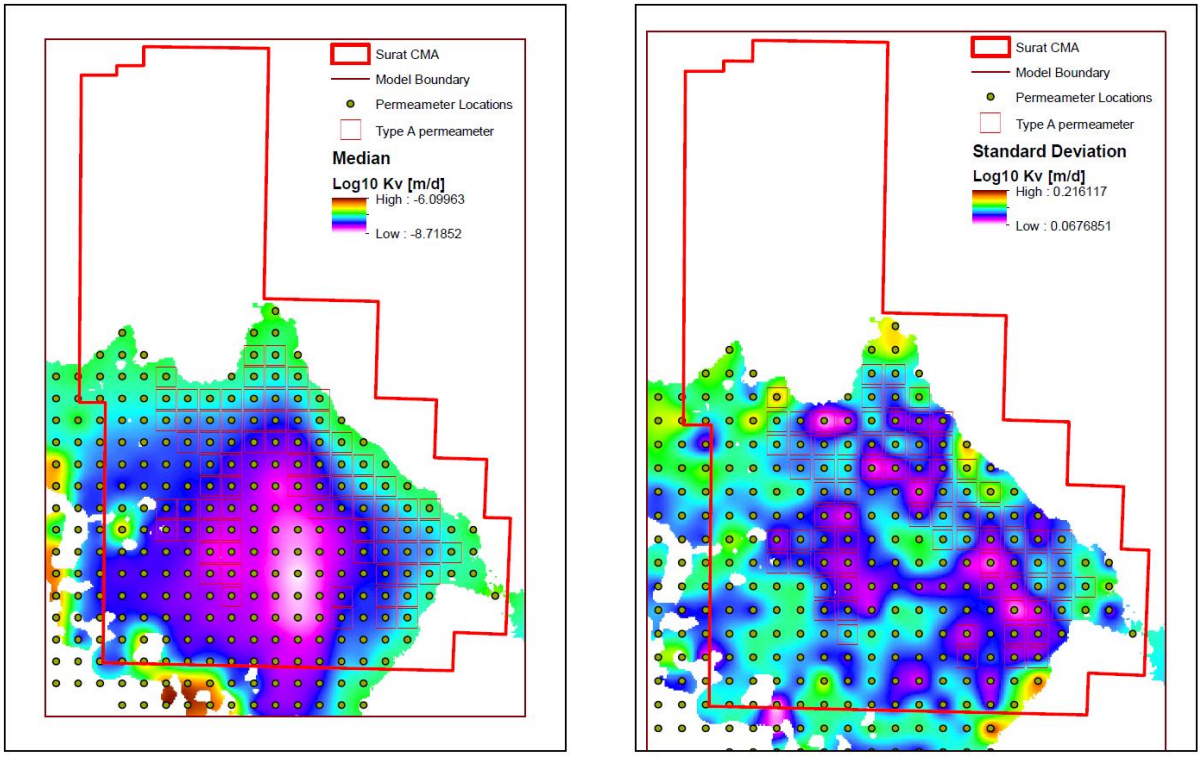

Figure 4-11 Median (left) and standard deviation (right) of permeameter-calculated log (to base 10) upscaled vertical hydraulic conductivity in the middle Walloon Coal Measures (model layers 13 to 15)

4.2.4.5 Some outcomes

As has already been mentioned (section 4.1) and discussed in more detail in section 5.5, pilot points comprised the primary parameterisation device used for adjustment of UWIR 2019 model hydraulic conductivities through the calibration process; pilot point values are interpolated to the MODFLOW-USG grid using the PLPROC utility (John Doherty, 2018). Initial values for pilot point hydraulic conductivities were calculated from median hydraulic conductivities obtained from numerical permeameters. For the UWIR 2019 model, Kh and Kv pilot points in layer 8 to 23 were positioned at the centre of each numerical permeameter grid to allow direct sampling of the numerical permeameter results with no further interpolation therefore required. Vertical hydraulic conductivity anisotropy was also parameterised using pilot points. Initial values ascribed to pilot points were similarly sampled from the numerical permeameters by calculating the ratio of median vertical hydraulic conductivity to the median upscaled horizontal hydraulic conductivity.

In addition to assigning initial pilot point values for Kh and Kv in model layers 8 to 23, data sets generated as part of the numerical permeameters based workflow were also used to define:

- calibration parameter bounds for Kh and Kv in layers 8 to 23
- fault downscaling factors (see section 2.5)
- prior uncertainty bounds for Kh and Kv in layers 8 to 23 (see Chapter 7)
- specific storage values in layers 8 to 23 (see section 4.5.2.2)
- coal thickness values as part of initial parameterisation of DDFTR (see equation 4.16 in section 4.6.2).

4.2.4.6 Comparison with 2016 numerical permeameter results

A comparison of 2019 numerical permeameter results with results used for the UWIR 2016 model is shown in Figure 4-12. Generally, estimated hydraulic conductivities are lower. This is predominantly due to the inclusion of permeability depth relationships for non-coal lithologies based on laboratory tests undertaken by CSIRO (Figure 4-3). The rate of decline in permeability with depth suggested by these results is greater than that assumed in 2016 resulting in lower permeability values at depth.

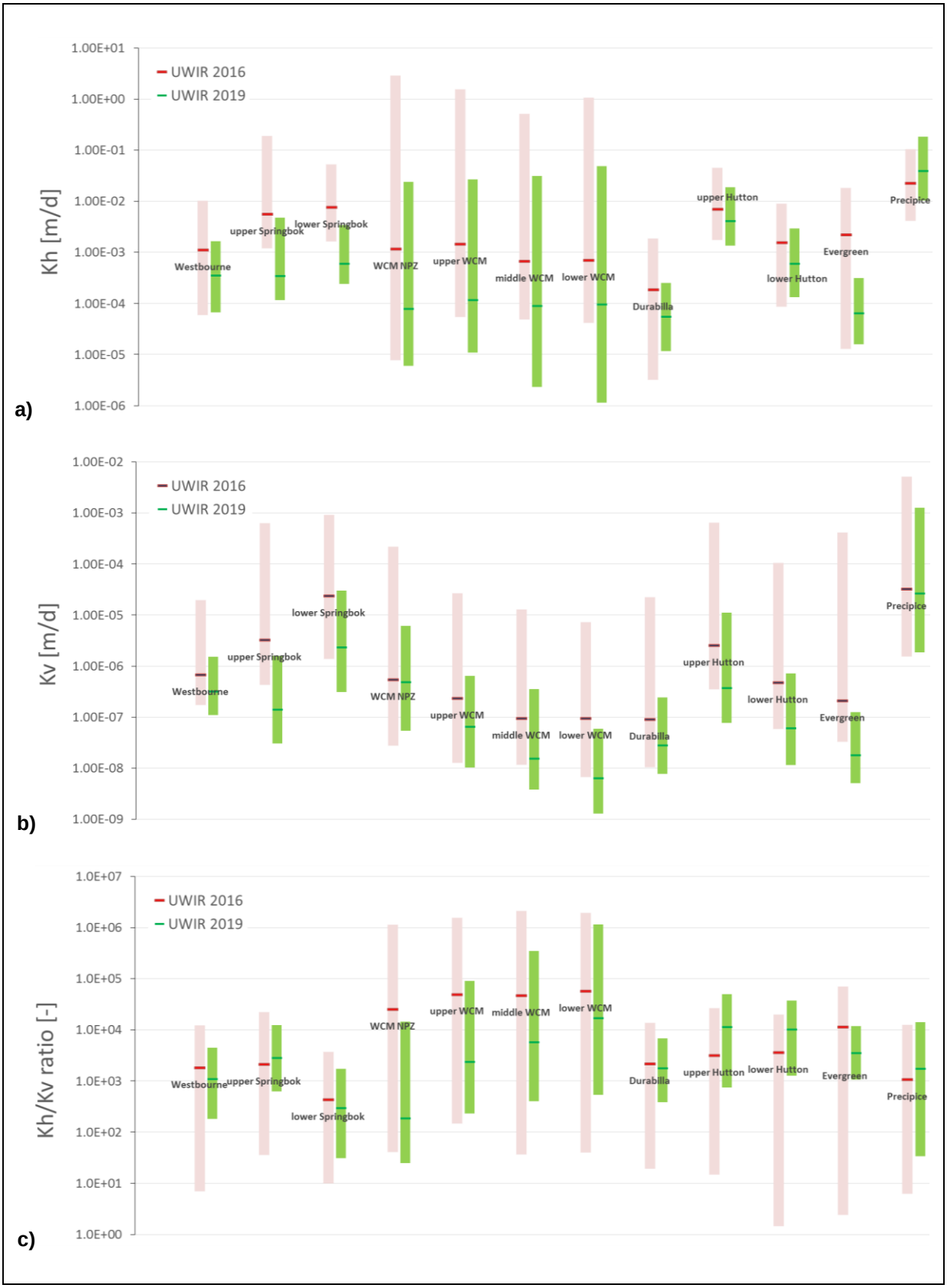

Figure 4-12 Comparison of 2016 (OGIA, 2016a) and 2019 numerical permeameter results for (a) Kh, (b) Kv and (c) Kh:Kv ratio

4.3 Hydraulic conductivity: non-permeameter layers

Assignment of initial values of hydraulic conductivity to non-permeameter layers of the UWIR 2019 model (i.e. layers 1 to 7 and layers 24 to 34) was supported by processing of measured hydraulic conductivities and permeabilities in pertinent layers, supplemented where necessary by adoption of values used in previous models as described below in sections 4.3.1 to 4.3.3.

4.3.1 Condamine transition zone

Hydrogeological characterisation of the Condamine Alluvium includes representation of a "transition zone" at its base. In the UWIR 2019 model (as per the previous version) this unit is parameterised using a spatially variable vertical resistance term; spatial interpolation of resistance is somewhat simpler to implement than separate spatial interpolation of vertical hydraulic conductivity and thickness of this unit. Note that vertical resistance is defined herein as the thickness of a layer divided by its vertical hydraulic conductivity.

The layer-property-flow (LPF) package of MODFLOW-USG does not allow direct assignment of vertical resistance to either a discrete model layer or to a quasi-three-dimensional confining layer. So in order to support parameterisation of vertical resistance of the Condamine Transition Zone, a uniform thickness of 1 m was excised from the base of the Condamine Alluvium represented by the first layer of the UWIR 2019 model; this was then assigned to the second model layer. At any location within the UWIR 2019 model where the transition zone is known to exist, an equivalent layer 2 vertical hydraulic conductivity k_v' can then be calculated using the following equation:

$$k_v' = \frac{b_t}{R} \qquad b_t > 0 \tag{4.10}$$

In equation 4.10 b_t is the estimated thickness of material comprising the transition zone and R is the vertical resistance. Figure 4-13 depicts the transition zone thickness adopted for use in equation 4.10 (OGIA, 2016c). For layer 2 cells where the transition zone is assessed as absent, the cell is initially assigned the same vertical hydraulic conductivity as that in layer 1 immediately above it, this representing the Condamine Alluvium, although this is allowed to vary during the subsequent model calibration (section 5.5.1.8).

Transition zone resistances are parameterised using pilot points in the UWIR 2019 model. Initial pilot point resistances were calculated by first calculating vertical resistances on a cell-by-cell basis using equation 4.10 together with estimated transition zone thicknesses depicted in Figure 4-13 and a uniform vertical hydraulic conductivity of 10^{-6} m/d in areas where the transition zone is present (this being the average vertical hydraulic conductivity for the transition zone estimated by detailed investigations at two test sites (OGIA, 2016a)). Least-squares interpolation was then undertaken to pilot point locations using the PPSAMP utility.

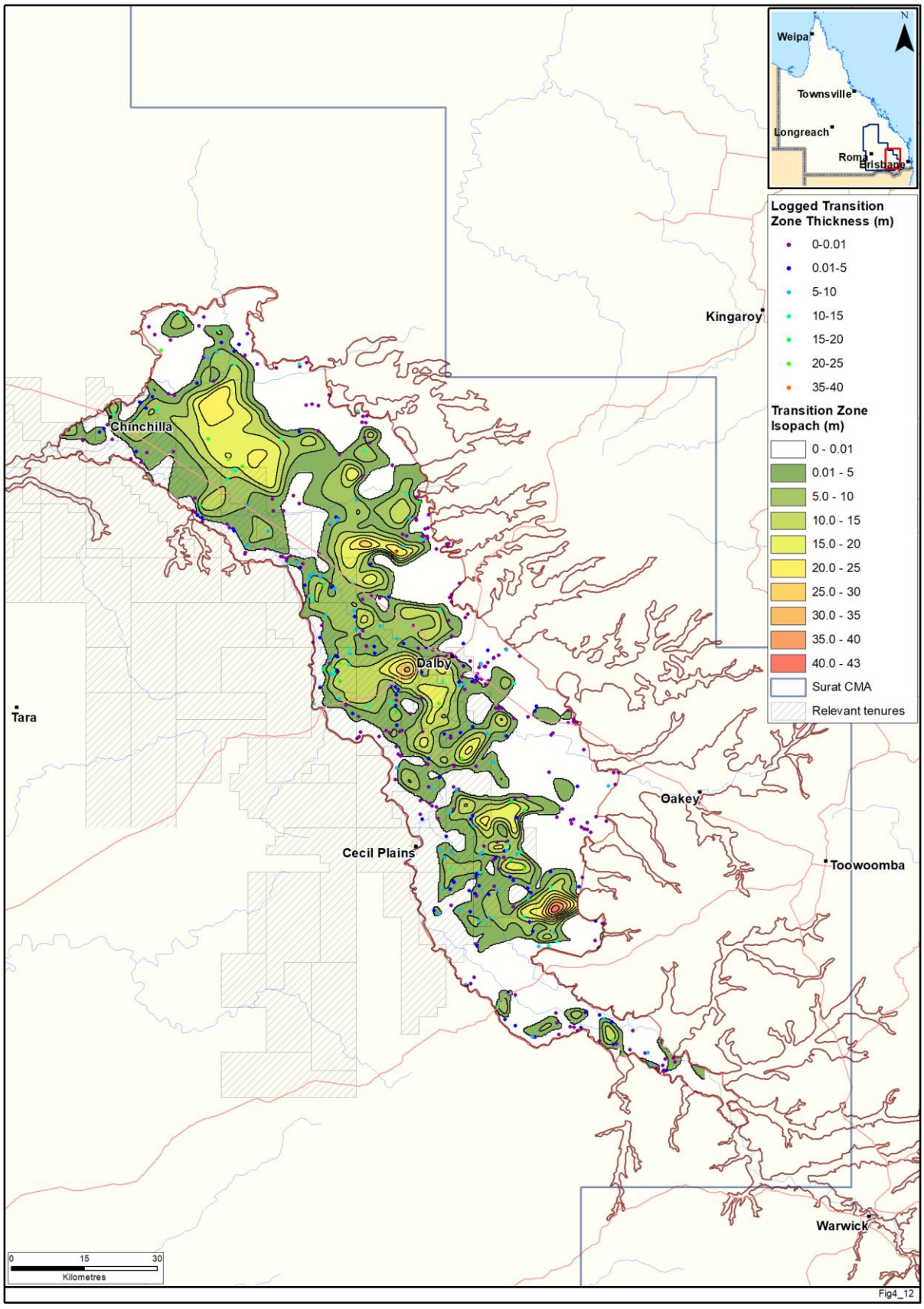

Figure 4-13 Thickness of the undifferentiated clay (transition zone) between the Condamine Alluvium and the Walloon Coal Measures

4.3.2 Boxvale Sandstone

As mentioned previously the UWIR 2019 model includes an additional two layers to allow representation of the Boxvale Sandstone which forms part of the Evergreen Formation. As shown in Appendix B1, Figure B1-21 the thickness of the Boxvale Sandstone is quite variable but tends to be relatively thick towards the north west of the area and thin or even absent within many CSG production areas. Accordingly relatively few measurements of the permeability of this unit are available. No DSTs have been attributed to this unit although data are available for around 500 laboratory core samples. Data from these tests suggest a median horizontal hydraulic conductivity of 1.3E-04 m/d, around six times higher than the median of core test results for the Evergreen Formation. Initial horizontal hydraulic conductivity arrays for the Boxvale Sandstone (model layer 21) were therefore calculated by multiplying estimates for the Evergreen Formation (based on outputs from the numerical permeameter workflow, section 4.2.4.6) by a factor of six. Vertical anisotropy for the Boxvale Sandstone was assumed to be the same as for the Evergreen Formation.

4.3.3 Other units

The following equation was employed to estimate formation scale permeability of layer *j* at depth *d*, where *j* ranges from 1 to 32 but excludes layer 1 (surficial layers comprised of alluvium and basalt) and layers 8 to 23 (numerical permeameter layers). This is the same as equation 4.3 used in the stochastic permeability modelling part of the numerical permeameter workflow (section 4.2.3.2), but without the stochastic ε term used to express small scale variability.

$$\log\left(k_j\right) = \log\left(k_{0j}\right) - \frac{b_j\sqrt{0.0248d}}{2.303} \qquad (4.7)$$

where:

- d is depth of burial;
- k_{0j} is the permeability at zero depth for stratigraphic unit j; and
- b is a fitting parameter estimated as 0.3325 based on laboratory CSIRO test results and assuming average proportions of lithofacies derived from the entire lithology data set (which suggests on average 20% clean sandstone, 29% dirty sandstone, 33% siltstone and 51% mudstone).

In applying equation 4.7 to parameterisation of a particular cell of the UWIR 2019 model, *d* is computed as the distance from the cell midpoint to the top of the uppermost model cell in the same vertical column.

In parameterising a particular layer of the UWIR 2019 model, equation 4.7 was first employed to calculate either horizontal or vertical permeability, the former if the layer is categorised as being primarily an aquifer, and the latter if it is categorised as being primarily an aquitard; see Figure 3-2 for layer classification details. Note that given the high vertical anisotropy values modelled in each layer and the alternating sequence of aquifers and aquitards present in the area the vertical permeability of an aquifer layer generally has little effect on any model outputs of interest. Similarly, model predictions are also generally insensitive to the horizontal permeability of aquitard layers since the vertical permeability dominates. Permeability was then converted to hydraulic conductivity using equation 4.2. The hydraulic conductivity in the other direction was then calculated through division or multiplication by a layer-specific value of vertical anisotropy. Values of k_0 and vertical anisotropy used for initial parameterisation of pertinent model layers are listed in Table 4-2.

Table 4-2 Values for K_0 (hydraulic conductivity) and vertical anisotropy used in initial parameterisation of non-permeameter layers of the UWIR 2019 model

Model layer	Stratigraphic unit(s)	Parameter type (K_h or K_v)	K_0 (m/d)	Vertical anisotropy
2	Upper Cretaceous / Cenozoic Sediments	K_v	7.6E-05	1000
3	Wallumbilla Formation	K_h	6.0E-02	2797
4	Bungil Formation	K_h	3.5E-02	2797
5	Mooga Sandstone	K_h	2.5E-01	2797
6	Orallo Formation	K_v	1.5E-04	2797
7	Gubberamunda Sandstone	K_h	7.1E-01	2797
24	Moolayember Formation	K_v	1.8E-06	3517
25	Clematis Sandstone	K_h	1.3E-02	3517
26	Rewan Group	K_v	6.8E-07	3517
27–29	Bandanna Formation	K_h	5.7E-03	3517
30	Undifferentiated Lower Bowen Basin strata	K_v	2.0E-07	3517
31–33	Cattle Creek Formation	K_h	5.7E-03	3517
34	Undifferentiated Lower Bowen Basin strata	K_v	2.0E-07	3517

Initial values of anisotropy provided in Table 4-2 were based on the median value obtained from numerical permeameter calculations for either the upper Springbok Sandstone or Evergreen Formation; these units were considered proxies for the Surat Basin layers and Bowen Basin layers respectively.

After assignment of horizontal or vertical hydraulic conductivity values to every cell within a particular aquifer or aquitard layer of the UWIR 2019 model grid, horizontal/vertical hydraulic conductivity values where then calculated for pilot points assigned to these layers through spatial least-squares interpolation, achieved once again using the PPSAMP utility. Vertical anisotropy for these non-permeameter layers remained a layer-wide parameter and therefore did not require interpolation to a pilot point field.

For surficial formations such as the non-Condamine alluvium, Main Range Volcanics and Basalt outcrops which comprise layer 1 of the UWIR 2019 model a relationship between hydraulic conductivity and depth is not required. Initial parameterisation of these units therefore comprised the assignment of a single value of horizontal hydraulic conductivity to each such unit. In non-Condamine alluvial areas pilot points were assigned uniform values of 18 m/d. In both the Main Range Volcanics and Basalt outcrop areas pilot points were assigned initial values of 0.11 m/d. These initial values were derived from the mean of the calibrated horizontal hydraulic conductivity in layer 2 of the Condamine Alluvium model (KCB, 2011) and the mean of the calibrated horizontal hydraulic conductivity for the Main Range Volcanics in the UWIR 2012 model (GHD, 2012) respectively.

Layer-wide vertical anisotropies of 7 and 250 were adopted for computation of vertical hydraulic conductivity for non-Condamine alluvials and Main Range Volcanics respectively based on previous UWIR model calibration results.

For those parts of layer 1 which correspond to the Condamine Alluvium, initial values of hydraulic conductivity were obtained through interpolation of calibrated values from the cell centres of the Condamine Alluvium Model to pilot points within the Condamine footprint of the UWIR 2019 model.

4.4 Hydraulic conductivity: further adjustments

In two cases initial parameters derived from numerical permeameter calculations were adjusted as described below in sections 4.4.1 and 4.4.2 prior to their use as input to the UWIR 2019 groundwater flow model.

4.4.1 Walloon Coal Measures non-productive zone (layer 11)

The non-productive part of the Walloon Coal Measures as represented in the UWIR 2019 is a relatively thin (less than 10 m) zone sitting between the uppermost screens in CSG production wells and the top of the Walloon Coal Measures (see Figure B1-11, Appendix B1). As such whilst numerical permeameter calculations have been undertaken for this layer (as described in section 4.2) the upscaling problem for this model layer is less acute since the difference between the vertical scale of the available measurements and the model layer thickness is somewhat smaller than for other layers. Furthermore as discussed in section 4.1.2 since the numerical permeameter workflow generates estimates of hydraulic conductivity on a 21 × 21 km grid which are used to generate initial values at pilot points then this methodology also leads to additional upscaling in the horizontal direction. Analysis of the available lithological data confirmed significant variability in the composition of this zone. In particular a number of areas where the lithology comprised almost 100% sandstone were identified based on the input data set. However, these features were often not well represented in the numerical permeameter outputs since they pertain to scales significantly less than the scale of the permeameters and associated pilot points.

In order to further improve initial parameterisation of the hydraulic conductivity of this key layer a revised workflow was therefore developed and applied to all current and proposed CSG production areas in the Walloon Coal Measures. Outside of these areas initial hydraulic conductivity values remain based on the numerical permeameter calculations described in section 4.2 since the revised approach is computationally expensive and is reliant on lithology data which is limited outside and CSG production areas. Fortunately the importance of this layer in predicting the vertical transmission of CSG impacts is also limited in areas outside of areas where de-pressurisation actually occurs.

Within current and proposed CSG production areas rather than generate geological realisations for each 21 × 21 km permeameter block using TPROGS a single detailed model of the entire thickness of the Walloon Coal Measures non-productive zone has been generated in Petrel. The lithological input data set used to develop this model was the same as used as input to TPROGS. As per the numerical permeameter workflow 20 different realisations of the lithology were also developed. Each of these lithological realisations was populated using permeability values derived using an Artificial Neural Network (ANN) based workflow which was conditioned using all of the hydraulic conductivity measurements available within the Petrel model domain. Formation scale horizontal and vertical hydraulic conductivity values for each 250 × 250 m model cell in the Petrel model were then calculated by taking the arithmetic or harmonic mean of all of the 0.1 m-thick Petrel model layers present. This was then repeated for each of the 20 available realisations and the median value for each cell upscaled onto the 1500 × 1500 m grid of the UWIR 2019 model. This partial coverage grid was then merged with numerical permeameter results outside of current and proposed CSG production areas to generate full coverage input grids for numerical modelling purposes. The resulting

median vertical hydraulic conductivity values used to for initial parameterisation are shown in Figure 4-14. Initial horizontal hydraulic conductivity values are shown in Figure D1-10, Appendix D1. The 5th and 95th percentiles of the 20 estimates available for each cell were also calculated to define upper and lower likely limits for this layer for subsequent model calibration and uncertainty analysis purposes.

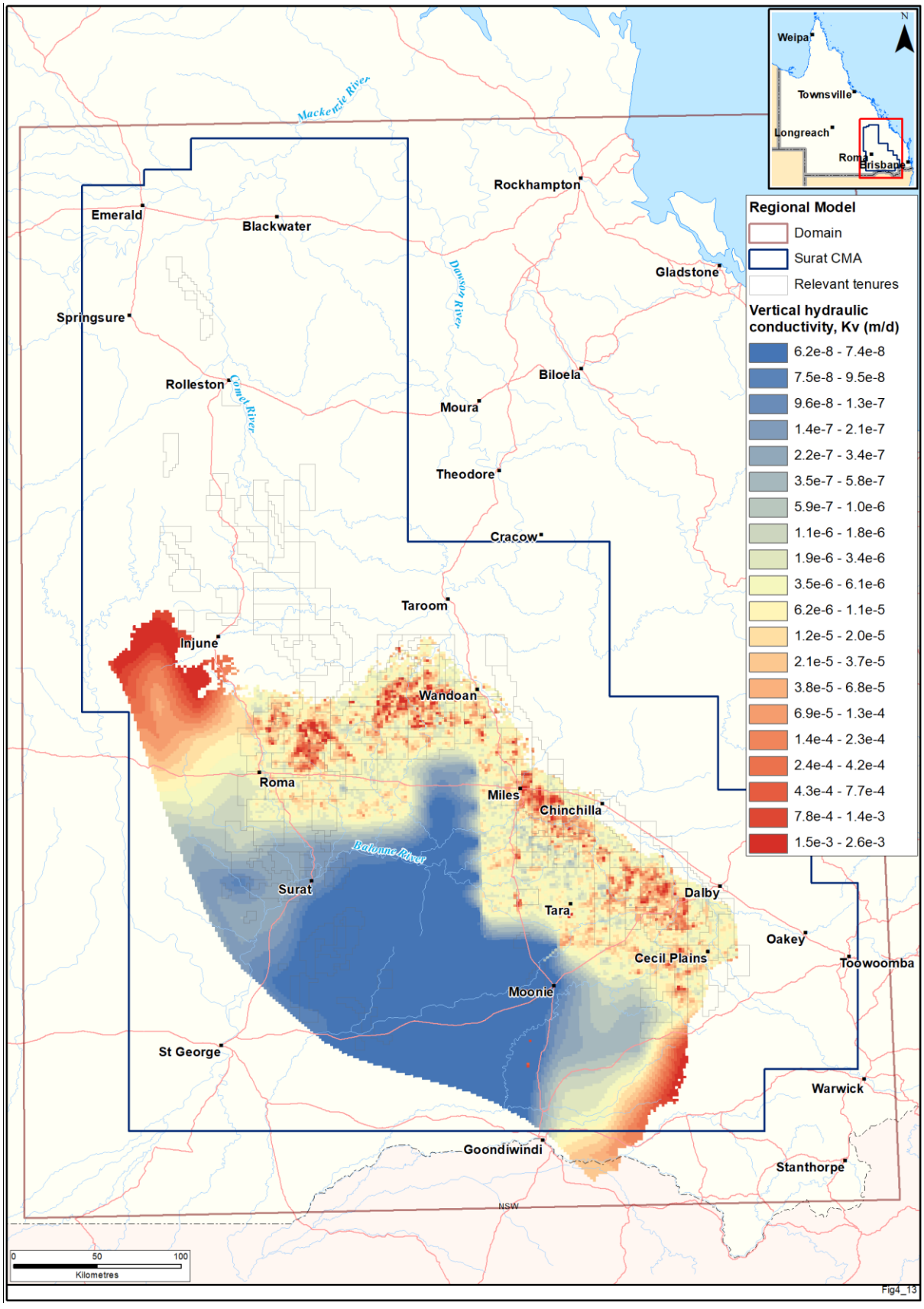

Figure 4-14 Initial vertical hydraulic conductivity parameterisation, Walloon Coal Measures non-productive zone (model layer 11)

4.4.2 Precipice Sandstone

Since early 2015 Origin has been re-injecting substantial quantities of treated water into the Precipice Sandstone at two sites near the Spring Gully and Ready Creek gas fields. Groundwater level monitoring data for the Precipice Sandstone suggests measurable increases in levels at locations tens of kilometres away from these sites. Re-calibration of the UWIR model based on these observed increases suggested a substantially higher horizontal hydraulic conductivity values than previously estimated at the time of the UWIR (OGIA, 2016a). A similar calibration exercise undertaken by the University of Queensland (Hayes et al., 2019) reached a similar conclusion suggesting that horizontal hydraulic conductivities of in excess of 100 m/d were required in some areas to match the observed re-injection responses. As shown in Figure 4-12a whilst output from the 2019 numerical permeameter workflow suggest higher horizontal hydraulic conductivity values for the Precipice Sandstone than previously calculated the upper bound value from permeameter calculations is around 0.2 m/d (i.e. around 2-3 orders of magnitude less than estimated by UQ).

Reference to pumping test results included in the State groundwater database for bores which solely intersect the Precipice Sandstone suggest values ranging from 0.4 to 32.3 m/d which therefore also suggest that the numerical permeameter workflow may be underestimating the permeability of this aquifer. The majority of this pumping test data is, however, not used to constrain numerical permeameter results since it is of variable quality and since the aquifer tested has been inferred by intersecting basic bore construction information with OGIAs geological model.

This cause of the apparent tendency for the numerical permeameter workflow to under-estimate the permeability of the Precipice Sandstone is not known at this stage. Possible explanations include that the primary permeability of the Precipice Sandstone is being substantially increased by secondary permeability associated with faults and fracturing of the sandstone blocks which dominate this formation. Such features are nor represented in the numerical permeameter calculations which take account only of permeability derived from primary porosity. Preliminary analysis of a number of borehole image logs undertaken by OGIA suggests relatively high incidences of fracturing in the Precipice Sandstone, compared to other units present in the area, which tends to support this hypothesis.

Given the evidence that the numerical permeameter outputs represent an under-estimate of the actual horizontal hydraulic conductivity, and rather than rely solely on the calibration to adjust these values, initial parameters for Precipice Sandstone were instead revised prior to their use for model calibration. The revision process involved direct comparison of initial horizontal hydraulic conductivity estimates derived from the numerical permeameter workflow with all of the available measurements for this unit. At locations where this comparison suggest that the measured hydraulic conductivity exceeded the initial permeameter estimated value then the latter were increased using a multiplier. This process therefore increased the estimated horizontal hydraulic conductivity values only in areas where there is some evidence from actual measurements that it may be too low. The resulting revised initial horizontal hydraulic grid is presented in Figure D1-23, Appendix D1 and varies from around 0.01 to 30 m/d. Comparison of this range of values with the permeameter outputs shown in Figure 4-12 confirms that the minimum values are largely unchanged but the maximum value has increased by around two orders of magnitude.

4.4.3 Upper bound hydraulic conductivity values for other aquifers

Based on the findings summarised above for the Precipice Sandstone (section 4.4.2) upper bound horizontal hydraulic conductivity values for other major aquifers used during calibration were also

increased, where necessary, from the upper bound values resulting from numerical permeameter or other calculations. This adjustment affected upper bound horizontal hydraulic conductivity values for the Hutton Sandstone (layers 18 and 19), Boxvale Sandstone (layer 21) and Clematis Sandstone (layer 25) which were all increased to 10 m/d.

4.5 Storage parameters

4.5.1 General

In a confined groundwater system such as the GAB water is stored within the aquifer pore spaces themselves but also as elastic (or confined) storage. In a groundwater flow model the former storage component is parameterised using specific yield (Sy) which is defined as the amount of water released from pores and fractures per unit area per unit fall in the water table. The value assigned to specific yield can be no greater than that assigned to the porosity of the porous medium since a proportion of water in the pore space will remain trapped even then the aquifer block is fully drained. Elastic or confined storage is parameterised using specific storage (Ss). This is defined as the volume of water released per unit volume of saturated subsurface material per unit fall in head.

Upscaling of storage parameters is more straightforward than upscaling of hydraulic conductivities as they are not tensors. Total storage can be estimated by averaging over a volume that is representative of the desired scale. Numerical permeameters calculations are therefore not required for this operation, but as described below in section 4.5.2.2 the same three-dimensional lithological distributions that were developed as part of the permeameter workflow can be used.

As for hydraulic conductivity, the desired outcome of the upscaling process is a suite of expected upscaled values for storage parameters that are usable by the UWIR 2019 model. Ideally, the uncertainties associated with these upscaled values should also emerge from the upscaling process.

4.5.2 Specific storage

4.5.2.1 Equations

The specific storage S_s of a porous medium can be calculated using the following equation.

$$S_s = \rho_w g[\alpha + n\beta] \quad (4.11)$$

where:

ρ_w is the density of water [$kg.m^{-3}$];

g is the gravitational constant [$m.s^{-2}$];

α is the bulk rock compressibility [Pa^{-1} or $m^2.N^{-1}$];

n is the porosity of the medium [-]; and

β is the compressibility of water [Pa^{-1} or $m^2.N^{-1}$].

Compressibility of coal is often calculated as:

$$\alpha = nc \quad (4.12)$$

where c is the coal cleat compressibility [Pa^{-1} or $m^2.N^{-1}$]. For coal, equation 4.11 then becomes

$$S_s = \rho_w gn[c + \beta] \quad (4.13)$$

In these equations α, c and n are stochastic quantities as their values at any point in the subsurface cannot be known with certainty. Random realisations of these quantities are generated from

appropriate probability distributions (see below); random realisations of S_s can then be generating by employing these random realisations of α, c and n in equations 4.11 and 4.13. The expected value and standard deviation of S_s can then be calculated by appropriate processing of these realisations.

ρ_w is a function of temperature, which is in turn a function of depth of burial. β is assumed to be constant. Neither of these are stochastic quantities.

Equations 4.11 and 4.13 omit a point error term (the ε term of equations 4.3 and 4.4). This term is assumed to be lost in the volume integration process through which upscaled estimates of storage coefficient are obtained from point estimates. Equations 4.11 and 4.13 are therefore assumed to be directly applicable to the scale at which estimates of specific storage are required by the UWIR 2019 model.

4.5.2.2 Numerical permeameter layers

As has been discussed in previous sections of this chapter, lithological information is available from interpretation of geophysical logs taken in bores which intersect stratigraphic units corresponding to layers 8 to 23 of the UWIR 2019 model (see Figure 4-2). Proportions of clean sandstone, dirty sandstone, siltstone, mudstone, carbonaceous shale and coal for each model can be inferred from these logs. The certainty with which these inferences can be made, decreases with distance to the nearest logged bore. Lithological proportions are therefore stochastic quantities whose uncertainties are highest where bore density is least.

In permeameter layers, where lithological proportions can be estimated, equation 4.11 is applied to individual non-coal lithologies while equation 4.13 is applied to coal. The total, upscaled, specific storage for a particular stratigraphic layer can then be calculated by adding the specific storage for all the present lithology classes, using:

$$S_s = \sum_{i=1}^{N} S_{si} p_i \qquad (4.14)$$

where:

- S_{si} is the specific storage attributed to lithology i;
- p_i is the proportion of lithology i; and
- N is the number of lithologies (6 in the Springbok Sandstone and Walloon Coal Measures and 4 elsewhere).

At any location within a particular layer of the UWIR 2019 model where upscaled estimates of S_s are required, realisations of lithological proportions, p_i, were first generated and adjusted where necessary to ensure that they add up to 1. Equations 4.11 and 4.13 were then employed to calculate S_{si} for each lithology at that location. As stated above, each such S_{si} calculation relies on random sampling of appropriate probability distributions for α and n for each lithology. A realisation of S_s for the entire stratigraphic layer can then be generated using equation 4.14. This process was repeated many times in order to calculate an expected value for upscaled S_s at each location, together with the standard deviation of upscaled S_s.

The stochastic model of bulk compressibility (α in equation 4.11) is based on a limited number of rock compressibility tests undertaken on core samples from the Surat CMA, which are shown in Figure 4-15. As shown in Figure 4-15 these test results suggest a tendency for rock compressibility to

decrease with depth. Based on which the following equation was adopted to estimate α in non-coal lithologies in all layers:

$$\alpha_i = \alpha_{ref} e^{b_{\alpha,i}(d-d_{ref})} \quad (4.15)$$

where:

d is depth of burial [m];

d_{ref} is an appropriately chosen (non-stochastic) reference depth [m];

α_{ref} is an appropriately chosen bulk compressibility (non-stochastic) at the chosen reference depth [Pa^{-1}]; and

$b_{\alpha,i}$ is a stochastic quantity described by an appropriately defined log-normal distribution.

Values for d_{ref} and α_{ref} are defined as 3,000 m and 1.0E-11 Pa^{-1}, respectively (based on the convergence point shown in Figure 4-15). Parameters which govern the distributions of α are specific to each lithology but do not vary with stratigraphic unit. These are based on the limited available data shown in Figure 4-15 together with information gleaned from international literature (Fitts, 2013; Freeze and Cherry, 1979). Coal cleat compressibility *c* employed in equations 4.12 and 4.13 was assumed to be depth-invariant but stochastic, also described by a log-normal distribution. Parameterisation of this distribution was also based on limited data, supplemented by information from the literature (Seidle, 2011) and available reservoir characterisation studies (Moore et al., 2013; QGC, 2014a).

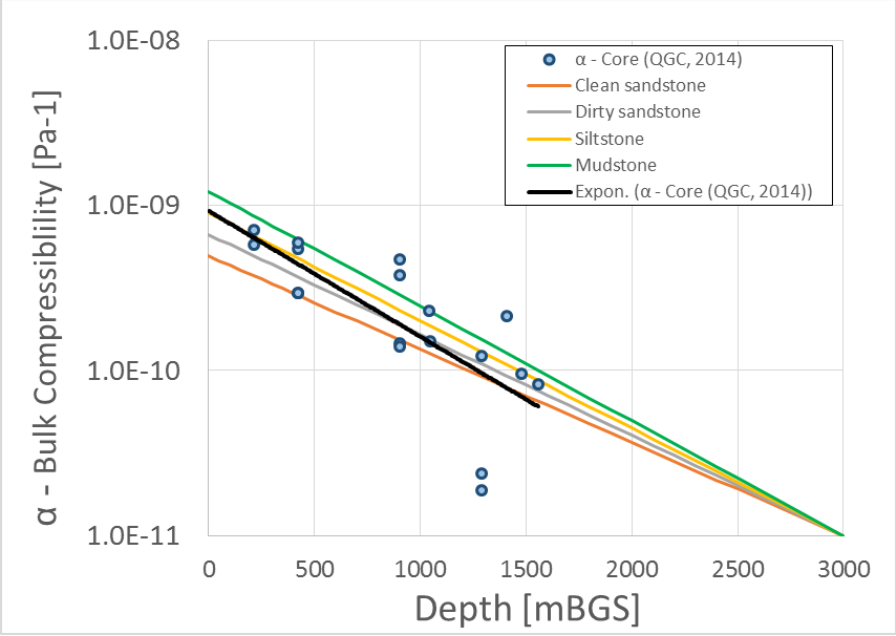

Figure 4-15 Bulk compressibility data and depth-relationships used for computing S_s in model layers 8 to 23

Equations 4.11 and 4.13 require values for lithology-specific porosities n_i. As stated above, n_i is a stochastic quantity and assumes the following depth-relationship:

$$n_i = n_{0,i} e^{b_{n,i}(d)} \quad (4.16)$$

where:

d is depth of burial [m];

$n_{0,i}$ is the porosity at surface (i.e. no overburden) ; and

$b_{n,i}$ is a stochastic quantity described by an appropriately defined log-normal distribution.

The stochastic depth-relationships for n have been defined based on downhole porosities and lithologies previously estimated by Weatherford (Weatherford, 2014) and in the international literature; see e.g. (Dong et al., 2010; Sclater and Christie, 1980). Statistical distributions for coal and carbonaceous shale porosities were assumed to be invariant with stratigraphic unit; a mean and standard deviation was assigned to each of these based on literature and expert knowledge (Moore et al., 2013; QGC, 2014b; Seidle, 2011).

In parameterising the UWIR 2019 model, the above S_s calculations were made at pilot point locations. As has already been discussed, the grid-based storage parameters required by the model itself are then obtained by interpolation from pilot points to the model grid. Equation 4.13 is also applied directly to pilot points to estimate initial S_s values for the mobile domain of Walloon Coal Measure layers (i.e. layers 12 to 16 of the UWIR 2019 model), using a coal compressibility (c) of 5.13E-08 Pa^{-1} and a coal porosity (n) of 1%.

As an illustrative example, Figure 4-16 and Figure 4-17 show the median and standard deviation of S_s values for the interburden and coal material for the middle Walloon Coal Measures (layers 13 to 15) that are obtained with the calculations described above.

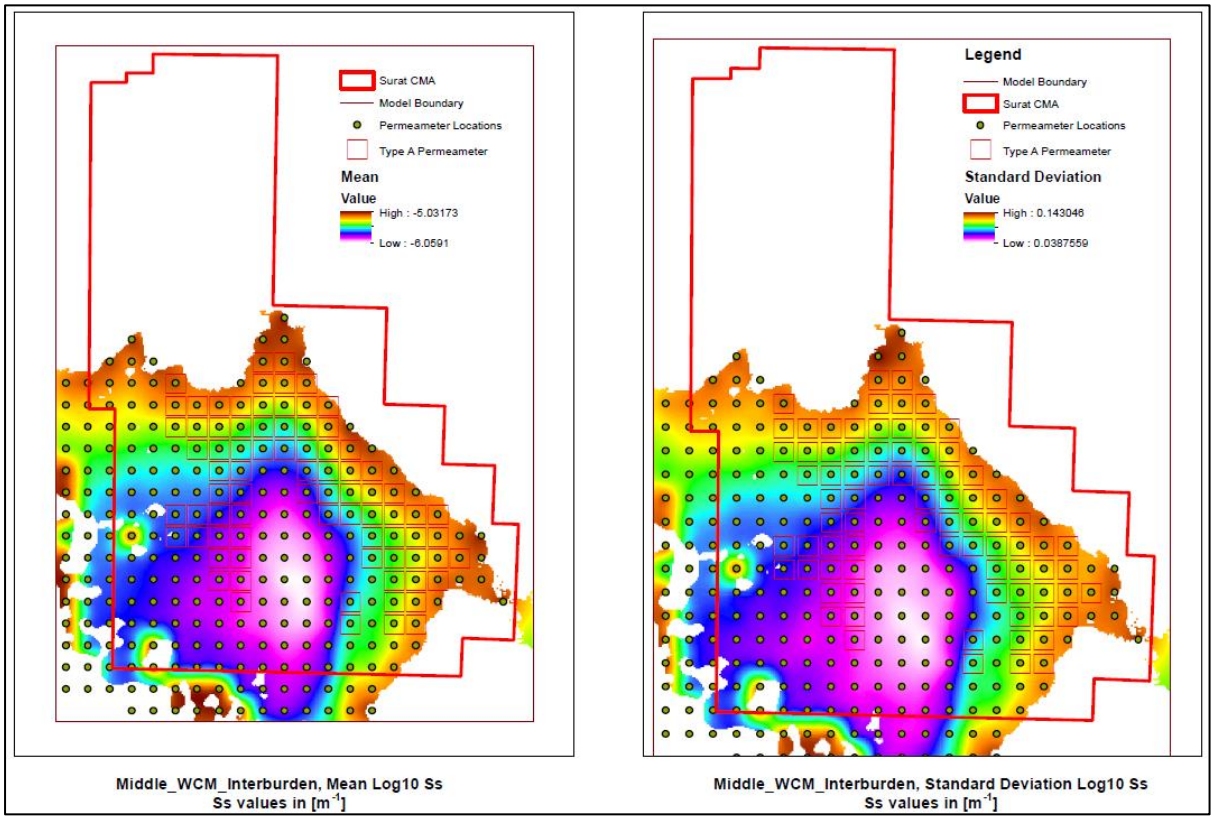

Figure 4-16 Median (left) and standard deviation (right) of permeameter-based interburden Ss for the middle Walloon Coal Measures (model layers 13 to 15)

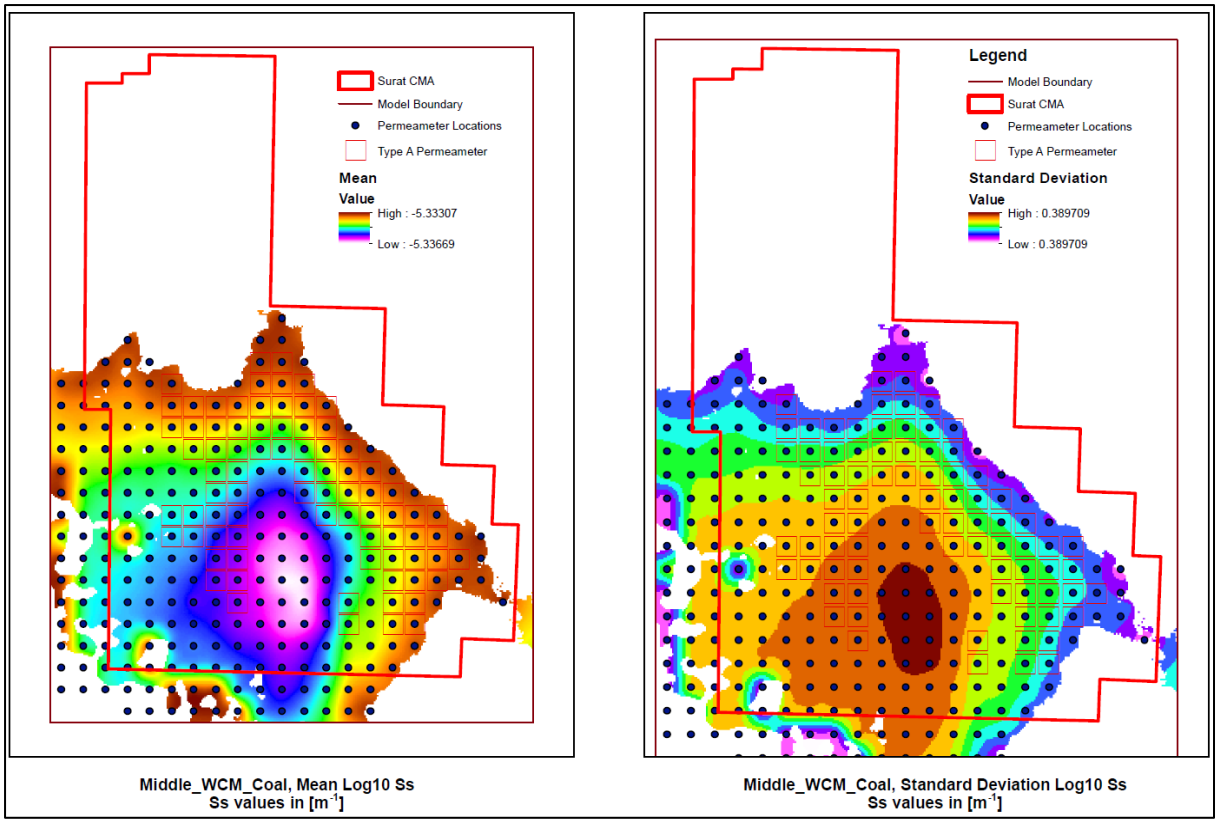

Figure 4-17 Median (left) and standard deviation (right) of permeameter-based coal Ss for the middle Walloon Coal Measures (model layers 13 to 15)

4.5.2.3 Non-permeameter layers

S_s in layers 1 to 7 and layers 24 to 34 is not parameterised with pilot points (with the exception of the Bandanna Formation and Cattle Creek Formation). For these layers, equation 4.11 was instead used to calculate initial S_s values for each model cell assuming a single depth-relationship for sandstone, α calculated using equation 4.15 (d_{ref} of 3,000 m, α_{ref} of 1.0E-11 and b of -0.0014) and n calculated using equation 4.16 (n_0 of 0.2 and b of -0.09).

Initial S_s values for the mobile domain (i.e. coal) of the Bandanna Formation (layers 28 and 29) and Cattle Creek Formation (layers 32 and 33) are assigned by applying equation 4.13 directly to pilot points. Input to equation 4.13 assumed the same parameters as were used for the Walloon Coal Measures. S_s for the immobile domain in these layers is defined based on the permeameter calculations for the lower Walloon Coal Measures.

4.5.3 Specific yield

Specific yield plays two different roles in the UWIR 2019 model. Firstly, it replaces specific storage as the parameter which governs storage of water where stratigraphic layers outcrop. (Alterations made to MODFLOW-USG source code by OGIA facilitate this replacement without the need to declare a layer is “unconfined”, this reducing the propensity for numerical instability in outcrop areas.) Secondly it provides the principle mechanism for release of water from coal layers where the latter desaturate because of displacement of water by desorbed gas.

Values of specific yield for use by coal-bearing formations are assigned directly to pilot points dispersed over the aerial extent of pertinent model layers for this purpose. More specifically, as is discussed in the following chapter, a set of pilot points are deployed in each of the upper, middle and

lower subdivisions of the Walloon Coal Measures, and in the upper and lower subdivisions of the Bandanna and Cattle Creek Formations.

Expected values of specific yield ascribed to the Condamine Alluvium were obtained through interpolation to the locations of pilot points from grid cells of the Condamine Alluvium model (KCB, 2011). A uniform expected value of 1.4% was ascribed to all surficial alluvial material represented in the UWIR 2019 model, based on the average of the calibrated values for the Condamine Alluvium model. A value of 1% was ascribed to all other outcropping material, this including the Main Range Volcanics, all layers of the Surat Basin and all layers of the Bowen Basin. Where coal measures outcrop, both the mobile and immobile domains were assigned this preferred value. Single specific yield values applied to all outcrop cells in each layer were also adjusted during model calibration.

4.5.4 Summary of initial storage properties

Table 4-3 provides a summary of storage properties used to parameterise the UWIR 2019 model prior to model calibration. Values for specific storage (S_s) are based on a range of depth relationships inferred from literature and rock compressibility measurements, and calculations using the lithological distributions that are used for the numerical permeameters as described above in section 4.5.2. An upper bound S_s value of 1.3E-5 was also applied based on the results of recent research (Rau et al., 2018). As described in section 4.5.3 and summarised in Table 4-3 initial values for specific yield were largely based on previous UWIR and Condamine Alluvium modelling results (OGIA, 2016a) and (KCB, 2011).

Table 4-3 Initial storage parameters used for the UWIR 2019 model

Unit	Layer	Value Source(s)	Ss [m^{-1}]	Sy [-]
Cenozoic Formations (incl. Condamine Alluvium)	1	Condamine Model (KCB, 2011)	Not applicable	0.001 - 0.1
Upper Cretaceous Formations to Gubberamunda Sandstone	2 to 7	Depth-relationship	1.4E-06 to 7.4E-06	0.01
Westbourne Formation	8	Permeameter	1.5E-06 to 1.0E-05	0.01
Springbok Sandstone	9 and 10	Permeameter	1.3E-06 to 8.8E-06	0.01
Walloon Coal Measures - Coal	11 to 16	Literature	4.9E-06	0.01
Walloon Coal Measures - Interburden	11 to 16	Permeameter	1.6E-07 to 9.06E-06	0.01
Durabilla Formation	17	Permeameter	7.8E-07 to 9.9E-06	0.01
Hutton Sandstone	18 and 19	Permeameter	7.1E-07 to 1.0E-05	0.01
Evergreen and Boxvale Formation	20 to 22	Permeameter	6.3E-07 to 9.7E-06	0.01
Precipice Sandstone	23	Permeameter	7.6E-07 to 7.0E-06	0.01
Moolayember Formation to Rewan Group	24 to 26	Depth-relationship	3.6E-07 to 7.3E-06	0.01
Bandanna Formation - Coal	27 to 29	Literature	4.9E-06	0.01
Bandanna Formation - Interburden	27 to 29	Based on Walloon Coal Measure parameters	3.0E-07 to 9.1E-06	0.01

Unit	Layer	Value Source(s)	Ss [m^{-1}]	Sy [-]
Lower Bowen 1	30	Depth-relationship	2.5E-07 to 7.3E-06	0.01
Cattle Creek Formation - Coal	31 to 33	Literature	4.9E-06	0.01
Cattle Creek Formation - interburden	31 to 33	Based on Walloon Coal Measure parameters	6.1E-07 to 9.06E-06	0.01
Lower Bowen 2	34	Depth-relationship	4.7E-07 to 6.4E-06	0.01

4.6 Extra parameters required for coal measure layers

4.6.1 General

Coal measures from which gas is extracted are represented in the UWIR 2019 model as dual porosity media (section 2.2.4). In this formulation water is allocated to two domains. In MODFLOW-USG parlance these are referred to as the “mobile” and “immobile” domains. As gas extraction commences, drawdown propagates rapidly along thin, horizontally-disposed coal seams; these comprise the mobile domain. Meanwhile drawdown propagates in the vertical direction through interburden material (i.e. non-coal material) on either side of these seams; collectively, interburden comprises the immobile domain. Water flows from interburden to the nearest coal seam in response to the local vertical hydraulic gradient.

As pressure is reduced in coal seams, gas is desorbed. The UWIR 2019 model does not simulate desorption and flow of gas. Rather, as a proxy for increasing gas saturation of the coal cleat network, it simulates desaturation of water under the assumption of a monotonic relationship between pressure head and water saturation. This monotonic relationship is described by a modified van Genuchten function. (Note that this van Genuchten relationship has little to do with desaturation of soils under atmospheric pressure, this being the regime to which the van Genuchten relationship is most commonly applied.) As gas is desorbed and coal cleats fill with gas, water emerges from both elastic and pore storage within the mobile domain to flow towards extraction wells. However it is released only from elastic storage within the immobile domain since the interburden generally remains saturated since its vertical permeability is substantially lower than the horizontal permeability of the adjacent coal seams. Meanwhile as desaturation of the mobile domain (i.e. the coal) progresses, relative water permeability of this domain decreases; the relationship between relative permeability and water saturation is described by a Brooks-Corey function.

As is discussed in sections 2.3.3 and 3.3.3, gas wells are simulated as fixed-pressure boundary conditions using the MODFLOW-USG drain package. The head attributed to each well-emulating drain changes over time until a user-specified long-term head is established; this head is determined by the bottom hole pressure under which the gas well operates. The conductance ascribed to each drain replicates that encountered by water as it flows radially towards the gas well. This is calculated using the Peaceman equation (Peaceman, 1978), and is a function of local relative hydraulic conductivity. In contrast to the “regional hydraulic conductivity” ascribed to the mobile domain (this being estimated using numerical permeameters), the local hydraulic conductivity that governs flow of water to a well is determined by the amount and permeability of coal that is connected to that well. This local coal permeability is substantially greater than the hydraulic conductivity of the regional mobile domain since the latter takes account of the limited lateral connectivity of coal seams. It is this local coal permeability that must be used in calculation of drain conductance. As is described in

section 2.3.4, alterations made to the MODFLOW-USG source code allow calculation of CSG well drain conductance internally using “enhanced cell hydraulic conductivities” supplied by the user. This conductance is reduced with saturated water content of the cell in which the CSG well is emplaced using the same Brooks-Corey formulation as that which is used for reduction of regional mobile domain relative hydraulic conductivity.

The parameters required by the above processes, and the initial values provided to these parameters, are now discussed.

4.6.2 Dual porosity parameters

The UWIR 2019 model represents any stratigraphic layer from which gas is extracted as a dual porosity medium. These are layers 12 to 16 (Walloon Coal Measures), 28 to 29 (Bandanna Formation) and 32 to 33 (Cattle Creek Formation). A multi-layer representation of coal measures allows simulation of vertical head gradients between them; this is important as hydraulic head drawdowns induced by gas extraction are greater in lower parts of a coal measure sequence than in upper parts. Near an extraction well the vertical hydraulic gradient approaches unity, this being an outcome of the near-zero vertical pressure gradient which prevails within a coal seam gas well.

Hydraulic conductivity and storage properties are ascribed to the mobile domain of a dual porosity medium in accordance with normal MODFLOW-USG layer property input protocols. In the UWIR 2019 model both specific storage and specific yield must be supplied; the requirement for the latter reflects the fact that coal measures desaturate in response to gas extraction.

As has been extensively discussed in section 4.2, in Walloon Coal Measure layers initial values for the upscaled hydraulic conductivity of the mobile domain were calculated using numerical permeameters. Horizontal hydraulic conductivities obtained in this way reflect the discontinuous nature of coal seams; they are lower than the hydraulic conductivity of coal itself. Vertical hydraulic conductivities reflect that of interburden, but allow for some vertical connectivity of more conductive lithologies.

The specific storage and specific yield assigned to the mobile domain are those pertaining to coal. The former were calculated using equation 4.13 for all coal measure layers; the latter were assigned an initial value of 1%.

Parameterisation of a dual domain medium also requires that the following additional hydraulic properties be assigned to each MODFLOW-USG cell:

- mobile domain fraction
- specific storage of the immobile domain
- dual domain transfer rate (DDFTR).

Note that, as stated above, the specific yield of the immobile domain is not required in the UWIR 2019 model as this domain is assumed to remain completely water-saturated.

The mobile domain fraction is equivalent to the percentage of coal in the pertinent model layer which are inferred from available lithological logs. In the Walloon Coal Measures the percentage of coal varies from less than 1 to around 20% (mean 8.5%). The proportion of coal in the Bandanna Formation is typically somewhat higher and varies from less than 5 % to values over 30% in some cases although the mean is only around 14% (OGIA, 2019b). Insufficient data is currently available to

derive meaningful statistics on coal proportions in the Cattle Creek Formation, which was instead assigned a uniform value equivalent to the mean coal proportion in the Bandanna Formation.

The specific storage of the immobile domain can be calculated using equation 4.11 (section 4.5.2). Within the Walloon Coal Measures values of upscaled specific storage were averaged over stochastic realisations which were generated using the methodology described in section 4.5.2.2.

DDFTR (units of $m^{-1}d^{-1}$) is the proportionality constant governing flow from the immobile domain to the mobile domain per unit volume of dual domain material, per unit head difference between the two domains. For an entire model cell, the flow transfer rate must be multiplied by the volume V_c of the cell. Based on MODFLOW-USG documentation provided by Panday et al. (2017), this total cell water transfer rate can be calculated using the following formula:

$$V_c \times DDFTR = \frac{m k_v A_c}{t} \quad (4.16)$$

where, for a medium in which the mobile domain is represented by coal and the immobile domain is represented by interburden:

- m is the number of “blocks” of interburden within a model cell [-];
- k_v is the average vertical hydraulic conductivity of interburden material within each block [md^{-1}];
- A_c is the area of the coal/interburden interface within each block [m^2]; and
- t is the distance from the centre of a coal seam to the centre of an interburden block [m].

The disposition of coal and interburden within a model layer of total thickness D is schematised in Figure 4-18. Based on equation 4.16 and the conceptual model in Figure 4-18, OGIA has developed an analytical approximation to calculate DDFTR for each regional model cell based on local coal proportion (net-to-gross), coal seam thickness and vertical interburden permeability. The derivation of this analytical approximation is presented below.

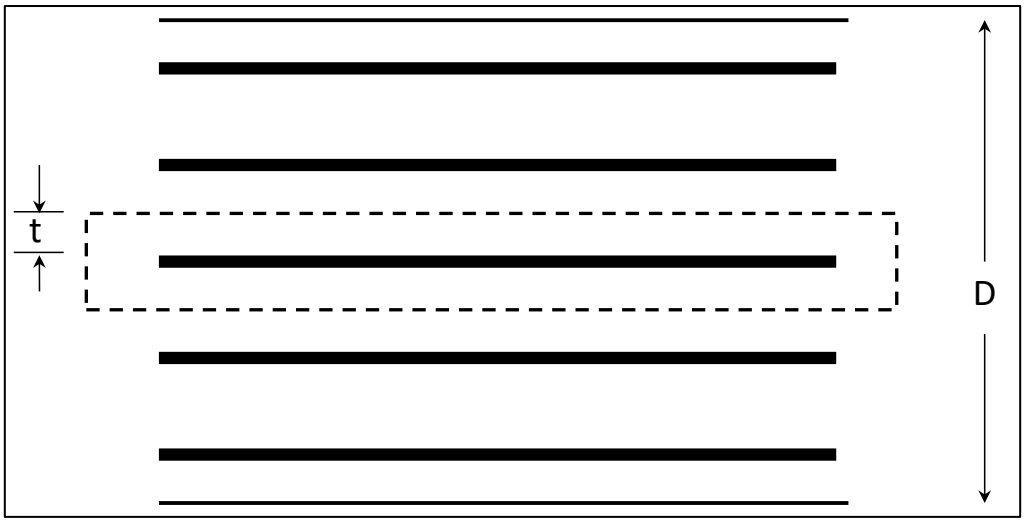

Figure 4-18 Coal (dark layers) and interburden within a model layer whose total thickness is D; a “block” of interburden surrounding a coal seam is defined by dashed boundaries

Because coal has an upper and lower surface exposed to interburden, A_c of equation 4.16 becomes:

$$A_c = 2A \tag{4.17}$$

where A is the area of a cell. Equation 4.16 then becomes:

$$V_c \times DDFTR = \frac{2mk_vA}{t} \tag{4.18}$$

m can be calculated as the total thickness of coal within a model layer divided by the mean thickness of a coal seam. If the latter is denoted by L_c then:

$$m = \frac{Dp_c}{L_c} \tag{4.19}$$

where p_c is the proportion of coal.

t in Figure 4-18 is equal to half the total thickness of the coal measure layer divided by the number of blocks. Thus:

$$t = \frac{D}{2m} \tag{4.20}$$

From equation 4.19 this becomes:

$$t = \frac{L_c}{2p_c} \tag{4.21}$$

k_v is equivalent to the harmonic average of all lithologies that are encountered on a traverse between the centre of an interburden block and the centre of a coal seam. Thus:

$$\frac{1}{k_v} = \frac{\sum \frac{p_i}{k_{vi}}}{\sum p_i} = \sum \frac{p_i}{k_{vi}} \tag{4.22}$$

where the summation in equation 4.22 takes place over coal and non-coal facies. From equation 4.22:

$$k_v = \frac{1}{\sum \frac{p_i}{k_{vi}}} \tag{4.23}$$

By substituting equations 4.19, 4.21 and 4.23 into 4.18 we obtain:

$$V_c \times DDFTR = \frac{4DAp_c^2}{L_c^2 \sum \frac{p_i}{k_{vi}}} \tag{4.24}$$

Dividing both sides of this equation by V_c we obtain:

$$DDFTR = \frac{4p_c^2}{L_c^2 \sum \frac{p_i}{k_{vi}}} \tag{4.25}$$

Table 4-4 summarises the values that are assigned to p_c, L_c and k_{vi} to calculate initial values for DDFTR for the dual porosity layers in the UWIR 2019 model. In the Walloon Coal Measures and

Bandanna Formation, lithology proportions (p_i) and coal thickness values (L_c) can be estimated from available lithology logs. For the Walloon Coal Measures, values for k_{vi} can be estimated using the stochastic permeability model discussed in section 4.2.3; see equations 4.3 and 4.4. For the Cattle Creek Formation and Bandanna Formation k_{vi} values are based on a depth relationship inferred from the permeameter results for the lower Walloon Coal Measures. As discussed previously only very limited data is currently available on coal proportions in the Cattle Creek Formation and uniform values for L_c and p_c have instead been assumed based on average properties for the Bandanna Formation.

Using the values summarised in Table 4-4 estimates of DDFTR can therefore be made for all the dual porosity layers in the UWIR 2019 model. Initial values calculated in this manner vary between a minimum of 9.0E-13 $m^{-1}d^{-1}$ and a maximum of 3.0E-07 $m^{-1}d^{-1}$ with an average value of 2.6E-09. Outcrop cells are ascribed a DDFTR value of 1.0E-02 $m^{-1}d^{-1}$, this being large enough to ensure a minimal delay between mobile domain head reduction and release of water from interburden storage in these areas.

Table 4-4 Summary of properties used to calculate initial values of DDFTR

Model layer	Stratigraphic unit(s)	Coal proportion, p_c [%]	Mean coal thickness, L_c [m]	Average vertical hydraulic conductivity interburden, K_{vi} [m/d]
12	Upper Walloon Coal Measures	3.7 – 33.8	0.3 – 0.9	2.7e-9 – 1.9e-06
13-15	Middle Walloon Coal Measures	2.9 – 18.4	0.3 – 0.4	1.4e-9 – 5.5e-07
16	Lower Walloon Coal Measures	2.9 – 39.9	0.3 – 0.7	7.5e-10 – 2.7e-08
28-29	Bandanna Formation	2.9 – 47.9	0.5 – 7.0	6.8e-12 – 9.3e-09
32-33	Cattle Creek Formation	14	1.6	3.3e-10 – 9.3e-09

4.6.3 Parameters governing coal desaturation

MODFLOW-USG allows cells to undergo water desaturation using a modified form of the van Genuchten equation to calculate water saturation S_w as a function of pressure head h. S_w and h are thereby related through the following equation.

$$S_e = \frac{S_w - S_{wr}}{1 - S_{wr}} = \left[1 + \{\alpha(h_b - h)\}^{\beta}\right]^{-\gamma} \quad \text{for } (h_b - h) > 0 \qquad (4.26a)$$

$$S_e = 1 \quad \text{for } (h_b - h) \leq 0 \qquad (4.26b)$$

where:

S_e is effective saturation [-];

S_{wr} is residual water saturation [-];

α and β are fitting parameters [1/m] and [-];

h is pressure head calculated for a cell [m];

h_b is the bubble point pressure head [m] below which desaturation commences; and

γ is calculated as $1 - 1/\beta$

MODFLOW-USG calculates relative permeability for the water-phase, k_{rw}, from effective saturation using the Brooks-Corey formulation:

$$k_{rw} = S_e^n \quad (4.27)$$

Herckenrath et al. (2015) show that with careful selection of α and β, pressure heads calculated by MODFLOW-USG can closely emulate those calculated by a two-phase reservoir simulator such as ECLIPSE where both of these models are endowed with the same S_{wr} parameter, the same Brooks-Corey exponent n, and where h_b is equal to the saturation pressure at which, according to the ECLIPSE Langmuir isotherm, gas desorption commences. Where a gas reservoir is comprised of a single horizontal coal seam, pressure heads calculated by MODFLOW-USG are asymptotically accurate. Under more complex subsurface circumstances, very good replication of ECLIPSE-calculated pressures by MODFLOW-USG-calculated heads (after conversion to pressure) can be achieved by matching the van Genuchten relationship to a scatterplot of ECLIPSE-calculated saturations and pressures.

Based on the previous modelling work (OGIA, 2016a), values of 1.0E-02 and 2.1 were employed for α and β in all coal measure layers represented in the UWIR 2019 model. These values were obtained by approximate fitting of a van Genuchten curve to saturation vs pressure scatterplots obtained from a number of ECLIPSE models. These included an ECLIPSE model constructed by OGIA for the Talinga area, as well as a number of ECLIPSE reservoir models developed by gas companies. A value of 0.2 was employed as the initial value for S_{wr} throughout the model domain.

The bubble point pressure head (h_b) was estimated initially as the immersion depth of a model cell, based on pressure heads obtained from the 1995 – steady-state simulation which are subsequently lowered by 5 to 80 meters depending on the depth of the CSG reservoir. This lowering is applied in order to avoid model cells to be initialised at maximum gas saturation pressure and coal desaturation would begin at the smallest amount of drawdown. This approach was supported by an estimation of van Genuchten parameters and comparing its estimated water saturation-pressure head relationship with simulated outputs from an Eclipse reservoir model for the Tipton development field (Arrow Energy, 2015); see Figure 4-19. As shown in Figure 4-19 the parameterisation of the modified van Genuchten relationship was slightly revised compared to the 2016 groundwater model, as the latter yielded relative low levels of water saturation for deeper coal seams. Bubble point pressure heads were capped based on gas saturation pressures associated with Langmuir isotherms commonly used in gas company reservoir modelling. For the Walloon Coal Measures and Bandanna/Cattle Creek Formation, these adopted maximum values were 833 m and 1,009 m, respectively.

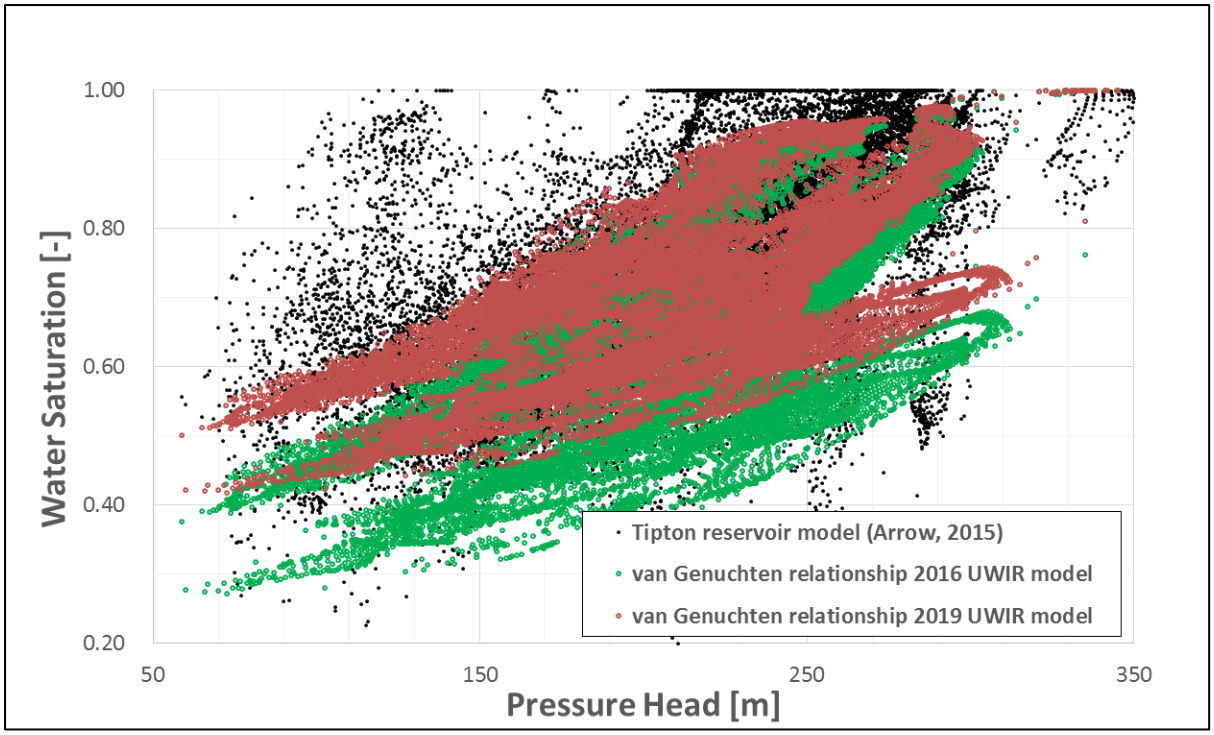

Figure 4-19 Desaturation curves based on the modified van Genuchten equation employed by the UWIR 2019 model and UWIR 2016 model; the saturation vs. pressure scatterplot on which these curves are superimposed was generated using outputs provided by an ECLIPSE model of the Tipton field (Arrow Energy, 2015)

Based on previous modelling work (OGIA, 2016a) an initial value of 4.6 was employed throughout the model domain for the Brooks-Corey exponent *n* appearing in equation 4.27. Values used in gas company reservoir models more commonly lie in a lower range between 1.9 and 4.3. However, the dimension of model cells used in company reservoir models which often only represent individual wellfields are typically much smaller than the 1.5 × 1.5 km grid blocks used in the UWIR 2019 model. Desaturation of the larger blocks in the regional model therefore requires a higher Brooks-Corey exponent resulting in a more aggressive relative permeability curve to better match expected saturation profiles with distance from CSG wells.

4.6.4 Enhanced horizontal hydraulic conductivities

As has already been discussed in section 2.3.3, coal seam gas wells are simulated using a "descending drain" methodology wherein a MODFLOW-USG drain boundary condition is assigned to each CSG well within each layer in which the CSG well operates. These drains "descend" as their elevations are gradually reduced to simulate the achievement of a final bottom hole pressure within each gas well.

In the absence of actual screen information then all productive coal units within a coal measure sequence are assumed to be tapped by an individual CSG well, although in most cases wells are assigned to one for more coal bearing layers based on screen information provided by CSG companies to OGIA. A maximum of five model layers can be tapped by a single well in the Walloon Coal Measures; up to two layers can be tapped in the Bandanna Formation and the Cattle Creek Formation.

Suppose that a CSG well is in contact with all five layers of the productive Walloon Coal Measures represented in the UWIR 2019 model. Then five drain boundary conditions are assigned to that well. As explained in section 3.3.3.4 the elevation assigned to these drains descend together from a pressure head of 690 m (equivalent to 1,000 psia) according to the curves depicted in Figure 3-17. The drain elevations are layer-specific. The descent for a drain that is associated with the uppermost layer of the Walloon Coal Measures stops when the drain reaches the top of the well screen (or the top of the model layer if well screen information is missing), plus an elevation equivalent to the predefined final bottom hole pressure of the well. This final bottom hole pressure is usually between 35 and 120 psia (equivalent to 14 m and 74 m of water head). After the drain associated with the uppermost extractive layer has ceased its descent the drains associated with other layers continue their descent. Each drain ceases its descent at an elevation equal to the midpoint of the respective layer plus the final bottom hole pressure. However the lowermost drain ceases its descent at an elevation equal to the bottom of the CSG well screen (or the bottom of the productive Walloon Coal Measures if well screen information is missing), plus the head equivalent of the final bottom hole pressure.

As has already been discussed, a CSG well presents to the groundwater regime a cylindrical seepage face along which the pressure is relatively constant. Hence, the seepage head is equal to the elevation within the CSG well. The conductance ascribed to each drain simulates the cylindrical flow path of water towards the well. From the Peaceman-equation (Peaceman, 1978) this can be calculated as:

$$C_d = \frac{2\pi K_h k_{rw} D}{\ln\left(\frac{0.208l}{r_w}\right)} \tag{4.28}$$

where:

- K_h is the local horizontal hydraulic conductivity of the rock with which the well is in contact when this rock is fully saturated with water;
- k_{rw} is the relative permeability for the water-phase (see equation 4.27);
- D is the thickness of the layer penetrated by the well;
- l is the horizontal length of a side of a square model cell; and
- r_w is the radius of the CSG extraction well.

In applying equation 4.28, the water saturation state of the cell tapped by the well is taken into account by adjusting hydraulic conductivity using equation 4.27.

In many coal measure sequences, coal occurs as thin discontinuous seams. In the Walloon Coal Measures connectivity of coal seams rarely extends over distances of greater than a few kilometres (Ryan et al., 2012). This has a profound effect on upscaled hydraulic conductivities assigned to model layers that represent all or part of a coal measure sequence wherein coal is normally the dominant contributor to hydraulic conductivity. Numerical permeameter results show that this local-scale coal hydraulic conductivity can be more than a factor 100 higher when compared to the permeameter-scale hydraulic conductivity that accounts for the lateral discontinuity of coal seams.

It is important to note that K_h appearing in equation 4.28 is not the regional hydraulic conductivity assigned to a coal measure layer. Rather it is the local hydraulic conductivity of coal measures that

are connected to a CSG well. The latter conductivity can be approximated as the thickness-weighted arithmetic mean of lithology-scale hydraulic conductivities intersected by the well. Because of the low hydraulic conductivities of interburden, i.e. non-coal, material, this is generally dominated by the hydraulic conductivity of coal seams intersected by the well. In the remaining part of this document, we will refer to this local well-scale hydraulic conductivity as “enhanced hydraulic conductivity”.

The modified version of MODFLOW-USG employed by the UWIR 2019 model reads an array of enhanced hydraulic conductivities so that it can employ equation 4.28 to calculate drain conductances. The values provided for these hydraulic conductivities can have a considerable effect on model-calculated heads in and around cells that are subject to CSG extraction. As will be discussed in later chapters of this report, these heads, and functions of these heads, are featured in the model calibration process. As a consequence, hydraulic conductivities used by equation 4.28 constitute a spatially varying parameter field that can be varied through the calibration (or history matching) process.

For layers of the OGIA model which represent the Walloon Coal Measures, local initial values for the “enhanced hydraulic conductivities” used by equation 4.28 were based permeability-depth relationships inferred from available DSTs. Different depth relationships were used for the zones shown in Figure 4-4. For the Bandanna Formation, enhanced hydraulic conductivities were based on a combination of coal permeability maps from various tenure holders, interpolated DST results and permeability-depth relationship inferred from the available DSTs (see Figure 4-20). For the Cattle Creek Formation, the permeability-depth relationship of the Bandanna Formation was used, as only limited DSTs were available for this formation.

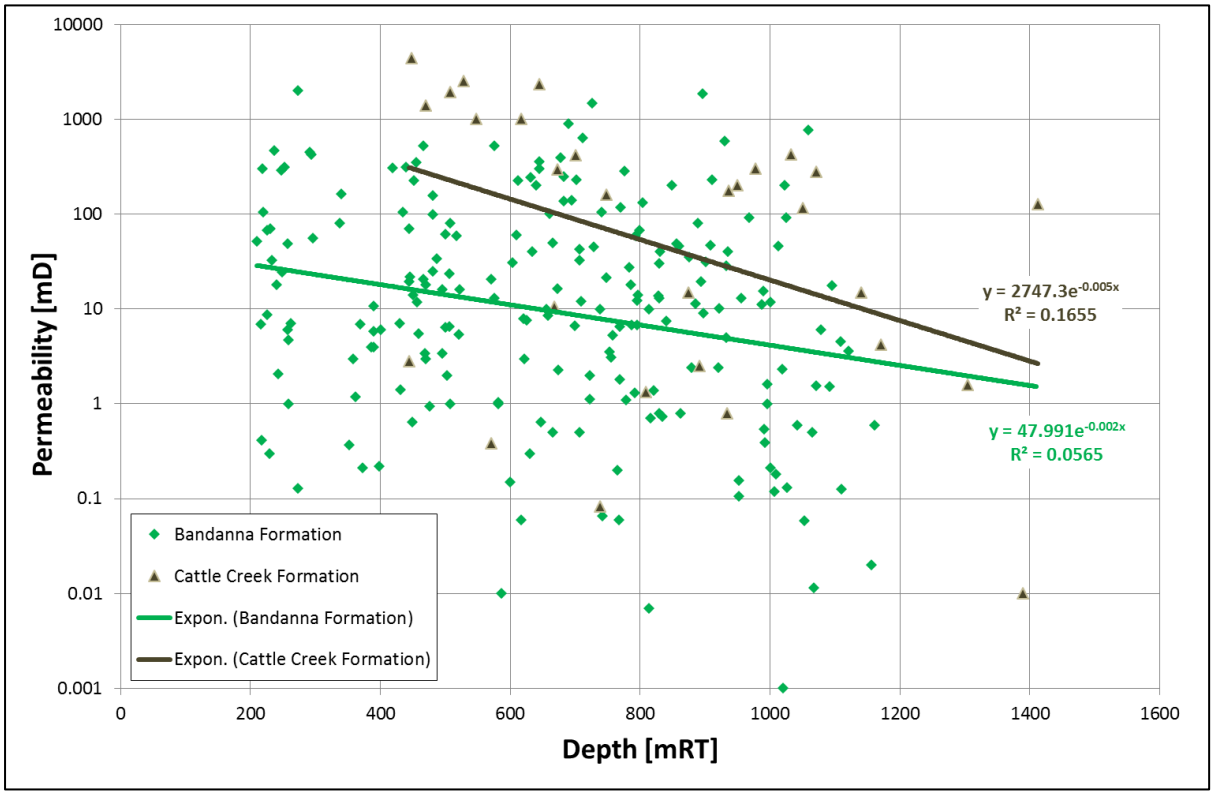

Figure 4-20 Permeability depth-relationship for the Bandanna Formation and Cattle Creek Formation

4.7 Key parameterisation assumptions and limitations

Like the model itself, parameterisation of the domain of the UWIR 2019 model is regional in nature and therefore approximate. Aspects of parameterisation of the UWIR 2019 regional model that are likely to have most influence on predictions of CSG impact made by this model are listed below:

- Hydraulic properties of rocks that are measureable in the laboratory or in the field must be upscaled before they can be ascribed to model layers whose vertical extent is such that many different facies are represented within a single layer. As is described in Chapter 4 of this document, for model layers within the Surat Basin that include the Walloon Coal Measures and neighbouring stratigraphic units, upscaling for the UWIR 2019 regional model was predominantly implemented using numerical permeameters. This process yields initial estimates of upscaled hydraulic conductivity which can then be adjusted through subsequent calibration of the model. These estimates are sensitive to assumptions regarding lateral continuity of conductive lithologies such as coal, and resistive lithologies such as shale. Errors in assumptions of lithological continuity which support generation of stochastic realisations of lithological sequences required to populate numerical permeameters may then lead to errors in estimates of upscaled hydraulic conductivities. Similarly, preferential flow paths that, in the horizontal direction may represent channelized alluvial deposits, and in the vertical direction may represent local faulting, may also induce errors in local upscaled hydraulic conductivities, although these do get adjusted through the model calibration process.
- The stochastic permeability model used for generation of hydraulic properties for lithologies represented in numerical permeameters attempts to assimilate measurements made at multiple scales into a single, coherent stochastic framework. As stated above, this approach to model parameterisation is far more advanced than that which is commonly employed in regional models. However, parameterisation of the stochastic relationships embodied in the permeability model has only been undertaken manually to date.
- Upscaling of parameters in layers for which permeameter calculations have not been carried out is presently approximate and somewhat subjective. If and when more data becomes available then it may be possible to expand the stochastic permeability model and permeameter grid to include other layers and/or areas including the Bandanna Formation in the Bowen Basin.
- Pilot points form the parameterisation device through which regional, upscaled model parameters are adjusted so that model outputs match observations which comprise the calibration dataset. These are typically arranged on a 21 × 21 km grid; however their emplacement density is greater than this in some parts of the model domain and the number of pilot points has been significantly increased compared to the UWIR 2016 model. Ideally, greater spatial density of pilot points will be preferable. However, solution of the inverse problem of model calibration would become numerically intractable under these circumstances, even with the high performance computing resources available to OGIA, because of the large number of parameters which would thereby require estimation. An outcome of this large pilot point spacing is that information emerging from direct measurements of system properties on the one hand, and information that is resident within the calibration dataset on the other hand, must be assigned to parameterisation receptacles which are necessarily regional in nature. This is an issue that besets regional modelling in general.

- Some parameters employed by the UWIR 2019 model, particularly those that pertain to desaturation in the vicinity of CSG extraction centres, are abstract in nature. This is because they describe “hydraulic properties” that pertain to processes that the model simulates in an approximate manner that is not in strict accordance with the way that these processes operate in the real world. These properties cannot therefore be measured; nor can they be subjected to standard upscaling procedures. They can only be inferred through processing of reservoir model outputs, and through calibration of the regional model. Note however that despite their abstract nature, the contributions that these parameters make to uncertainties of model predictions can be assessed through linear and nonlinear uncertainty analysis.
- Although initial hydraulic conductivity values have been generated using a robust numerical permeameter based workflow (section 4.2) the uncertainties associated with hydraulic properties of all types assigned to all model layers are expected to remain relatively high since they can theoretically vary across several orders of magnitude. The ranges of these uncertainties have been explored as part of the numerical permeameter methodology discussed in this report and formally assessed as part of an uncertainty analysis. These uncertainty ranges will have been reduced in some areas through model calibration. However, considerable uncertainty is likely to remain as an outcome of calibration data paucity and of uncertainties associated with measurements comprising this dataset. This is discussed further in Chapter 7.

5 Model calibration

5.1 In this chapter

The present chapter describes calibration of the groundwater flow model whose construction details are provided in Chapters 2 and 3. In doing so, it describes how the values of model parameters discussed in Chapter 4 were adjusted in order for model outputs to match observed behaviour of the groundwater system simulated by the UWIR 2019 model over time periods prior to the present. In other disciplines, model calibration is therefore also known as history matching.

One of the major improvements of the UWIR 2019 model is the inclusion of a large amount of additional transient head data for CSG reservoirs and key aquifers into the model calibration process. Description of this data and how it is included in this process is describe further in section 5.4.6.

This chapter begins with some reflections on model calibration in general, as well as the benefits to be gained through a highly parameterised approach using pilot-points and Tikhonov-regularisation (Doherty, 2003). Next, the following topics are addressed:

- the simulation stages used in the calibration process
- the types of observations that comprised the calibration dataset for each of these simulation stages
- the model parameters that were adjusted in order to achieve a suitable fit between model outputs and members of the calibration dataset
- the calibration results, showing a comparison of field measurements comprising the calibration dataset and their modelled counterparts after the parameter adjustment process
- the values of parameters resulting from the calibration process.

5.2 Calibration methodology

Model calibration was implemented using the PEST suite of software (Doherty, 2016a, 2016b). PEST is model-independent and is supported by a comprehensive suite of utility programs. The numerical burden of model calibration is accommodated by undertaking model runs in parallel using different cores on the same computer, different computers within a network, and/or different nodes on a high-performance computing platform.

As is described in many texts (such as (Aster et al., 2005; Doherty, 2015; Menke, 1984)), model calibration constitutes an “inverse problem” in which parameters are adjusted until an acceptable fit is achieved between model outputs and corresponding measurements of system state. The parameter field obtained through this process is not to be viewed as correct. However, through proper formulation of the inverse problem, a parameter field of “minimised potential incorrectness” (or “minimised error variance” to use mathematical terminology) can be obtained. Of the infinite number of parameter fields which can be found to match a given calibration dataset, this is the parameter field that occupies a central position in parameter space with respect to these other parameter fields. By making its potential for wrongness symmetrical, that potential is thereby minimised.

Once the parameter field of minimised error variance has been obtained through model calibration, alternative calibration-constrained parameter fields can then also be generated using methodologies such as the null space Monte Carlo method described by Tonkin and Doherty (2009) and supported

by PEST. By making predictions using all of these alternative parameter fields, post-calibration predictive uncertainty can be explored.

As will be described in the following sections of this chapter, calibration of the UWIR 2019 model required adjustment of 14,016 parameters on the basis of 63,542 observations comprising the calibration dataset. The calibration dataset does not support unique estimation of these parameters. Hence, the inverse problem of model calibration can be mathematically characterised as “ill-posed”. Uniqueness is obtained, however, through seeking the parameter set that allows the model to fit the calibration dataset to an acceptable level (see below), while departing from pre-calibration parameter values to only the minimum extent required to achieve this fit. Because pre-calibration parameter values are the products of expert knowledge, or the outcomes of more complex expressions of expert knowledge forthcoming from processes such as numerical permeameter upscaling, the parameter field obtained in this way can claim a status of minimised error variance.

Calibration of the UWIR 2019 model was achieved through highly parameterised inversion using pilot points in which uniqueness is obtained through enforcement of “Tikhonov constraints” (Doherty, 2003). In the present case, these were comprised of a suite of additional, user-specified, “observations” (formulated as “prior information” equations) declaring equality of parameters to their initial values. Rules for departure from these values were encapsulated in parameter covariance matrices that suggested, for spatial parameters based on pilot points, collective rather than individual deviations from initial values.

While highly parameterised inversion is computer-intensive, it offers many benefits. A pronounced benefit is that it offers far greater flexibility to the inversion process than alternative means of seeking parameter uniqueness, such as adjustment of a parsimonious set of parameters that are few enough in number for their estimation to constitute a well-posed inverse problem. The inverse problem solver is thus free to alter the values of those parameters whose adjustment realises the mutual goals of a good fit with the calibration dataset on the one hand, and minimised error variance on the other hand, in the most effective manner. A full discussion of the benefits of numerical regularisation and the disadvantages of manual regularisation can be found in Doherty (2015).

In practice, numerical solution of an inverse problem is achieved through minimisation of an objective function. Where Tikhonov regularisation is implemented, this objective function can be subdivided into two components, namely that based on the observation dataset (referred to in PEST parlance as the “measurement objective function”) and that based on departures of parameter values from their initial values (referred to as the “regularisation objective function”). PEST adjusts the weight on the latter component of the objective function so that the former can be lowered to a value that a modeller deems to constitute a good fit between model outputs and field measurements. Where the term “objective function” is employed herein, it refers only to the measurement objective function.

The level of fit that should be sought between model outputs and corresponding field measurements depends on the reliability of those measurements, and on the credibility of the model. Numerical simulation on a regional scale of processes that occur at a much smaller scale can only be approximate. The level of approximation is exacerbated by the fact that historical system stresses (for example, rates of groundwater extraction prior to CSG extraction) are only approximately known. Doherty and Christensen (2011) and White et al. (2014) show that, even though highly parameterised inversion can promulgate very good fits between model outputs and field measurements, there is a strong case for eschewing a good fit where a model’s ability to simulate details of environmental processes is compromised. Failure to do so may lead to bias in estimated parameters, and to bias in

predictions which are sensitive to them. This is particularly true for predictions which depend jointly on some parameters that are uniquely estimable through the calibration process and some that are not. Predictions required by the UWIR 2019 model are of this type.

It is important to note that failure to achieve a good fit between model outputs and members of the calibration dataset should not be construed as grounds for invalidation of a model. As is stated above, parameters of even a “perfectly calibrated” model are not correct; the best that they can claim is a status of minimised error variance. Post-calibration parameter and predictive uncertainties can be explored once a parameter field of minimised error variance has been obtained. The looser the fit between model outputs and field measurements, the greater will be the uncertainties that are ascribed to some parameters through this process. The uncertainties of some predictions will also rise with a greater tolerance of calibration misfit. The range of uncertainties thereby exposed will accommodate misfits incurred through the calibration process. On the other hand, bias incurred through over-fitting is not quantifiable. Hence, a calibration philosophy that views under-fitting as preferable to one that pursues over-fitting has been adopted for the calibration process documented herein.

Doherty and Welter (2010) and White et al. (2014) show that formulation of an appropriate multi-component objective function whose value is minimised through the inversion process can often mitigate the propensity for bias in parameters estimated for a numerical model. Each component of this function would involve different types of observations and/or the same observations processed in ways that extract information pertinent to different parameters. Each component of this objective function should be weighted in such a way as to render it “visible” in the overall objective function. As is discussed in section 5.4 below, this path was followed in calibrating the UWIR 2019 model.

5.3 The calibration simulation stages

5.3.1 General

MODFLOW-USG allows the intermixing of steady state and transient stress periods in a single model run. This facilitates calibration under both of these conditions. Estimation of parameters using a calibration dataset that includes measurements taken under both steady state and transient conditions offers the advantage that heads throughout a model domain calculated under steady state conditions can then serve as initial heads for an ensuing model run in which transient conditions are simulated. It also reduces the propensity for non-uniqueness of estimation of conductance parameters because they are less susceptible to post-calibration correlation with storage parameters.

Calibration of the UWIR 2019 model was based on a three-stage model run. The first two stages were steady state while the third was transient. Some parameters are shared between stages while others are specific to certain stages. All were estimated concurrently. These three simulation stages are now described.

5.3.2 First steady state stage, 1947 pre-development

The first simulation stage pertains to steady state conditions which existed prior to the commencement of any groundwater extraction from the Surat CMA.

The main purpose of this stage was to allow inclusion in the calibration dataset of a suite of head measurements which are not the outcome of an extraction regime whose pumping details are uncertain. Unfortunately, all measurements of groundwater head within the domain of the UWIR 2019 model postdate the commencement of water extraction from stratigraphic units featured in this model. However, some early measurements of groundwater head are nevertheless relatively unaffected by

pumping. A review of entries in the DNRME Queensland groundwater database reveals that fewer than 10% of extraction bores drilled within the area covered by the CMA were operative prior to 1947. Hence, groundwater head measurements prior to this date were considered for inclusion in the observation dataset that pertains to this first steady state simulation stage. During this pre-development period, water is introduced to the groundwater system only through recharge and is lost from the system only through outflow boundary conditions.

In order to verify the appropriateness of individual head measurements included in this first component of the calibration dataset, these measurements were subjected to a quality assurance protocol discussed in section 5.4.3 in which their steady state credentials were tested. Measurements which failed this test were removed from the calibration dataset.

This first pre-development steady state simulation stage is hereafter referred to as the "1947 steady state simulation".

5.3.3 Second steady state stage, 1995 pre-CSG development

A steady state simulation of hydraulic conditions which existed prior to the commencement of CSG extraction from the Surat and Bowen basins within the CMA in 1995 comprised the second simulation stage. This simulation stage served two purposes, these being as follows:

- it allowed inclusion in the calibration dataset of a further set of observations which were presumed to reflect steady state conditions prior to the commencement of CSG extraction in 1995
- heads calculated through this simulation stage served as initial heads for the ensuing transient model stage.

During this second steady state simulation stage, extraction from stratigraphic units represented in the UWIR 2019 model is that which was occurring in 1995 (as far as this can be inferred from uncertain pumping records and related data). Flow within the regional groundwater system is assumed to be in equilibrium with this extraction. While this is unlikely to be the case throughout the system, heads in many boreholes show only minor long-term trends at this time. Furthermore, the same methodology as used to test the steady state credentials of head measurements used for the calibration of the 1947 steady state simulation (section 5.4.4) was employed to exclude borehole water level measurements from the calibration dataset if they were construed to deviate too far from steady state conditions.

This second pre-CSG development steady state simulation stage is hereafter referred to as the "1995 steady state simulation".

5.3.4 Transient stage, 1995 to 2017

The third stage of the overall model run employed in the calibration process comprised a transient simulation representing the post-CSG development period from January 1995 to December 2017. It simulates the response of the groundwater system to increasing levels of CSG extraction.

Use of this simulation stage in the overall model run used for calibration of the UWIR 2019 model allows inclusion in the calibration dataset of measurements that reflect the influence of CSG extraction. It also allows inclusion in the calibration dataset of synthetic observations, generated by detailed reservoir models and developed using ECLIPSE, that can "train" the UWIR 2019 model to replicate processes that are operative near gas extraction points, despite the fact that gas extraction

is simulated using a single phase simulator. Values for parameters which govern operation of these processes, together with parameters that are associated with elastic and inelastic storage, can be inferred from these constituents of the overall calibration dataset.

This third, post-CSG development, transient simulation stage is hereafter referred to as the “transient simulation”.

5.4 The calibration dataset

5.4.1 General

The model calibration dataset used for the UWIR 2019 model has been significantly extended since the development of the UWIR 2016 model. Monitored groundwater heads comprise an important component of this dataset. Groundwater heads did not, however, comprise the only component of the calibration dataset. Other components, such as groundwater water extraction rates and available reservoir modelling information, are described in following subsections, together with details of the simulation stage with which they are associated.

5.4.2 Preliminary screening of groundwater head data

The total database with head monitoring information that OGIA considered for model calibration comprises head data for over 42,000 monitoring locations. This dataset was subjected to correction for temperature and density and quality assurance processes that are described in more detail in the previous OGIA regional conceptualisation report (OGIA, 2016d).

As a first pass, the following processing steps were undertaken to select head measurements to feature in the model calibration dataset:

- Groundwater heads in surficial model cells associated with alluvium (except for the Condamine Alluvium) or outcropping Cretaceous age units were removed from the calibration dataset if they are more than 20 meters below the modelled ground surface. It is considered that these observations are most likely representing local aquifer responses due to surficial pumping which are not represented in the UWIR 2019 model.
- For each of the simulation stages, attribution of head measurements to model layers was conducted using a combination of company monitoring information and intersection with the 2019 OGIA regional geology model. For monitoring locations which tap multiple model layers the observations are assigned to a dominant single layer based on the length of screen in each model layer multiplied by the pre-calibrated hydraulic conductivity.
- Data consistency and flagging of anomalous head data was also undertaken based on a spatial analyses using interpolated potentiometric maps and plots of topographic elevation versus observed heads. For monitoring locations with time series data a visual inspection of each hydrograph was undertaken and anomalous values removed from the data set as appropriate. Proposed observation targets for the three simulation stages were also compared to ensure internal consistency i.e. at locations with targets in more than one calibration stage that:
    - observed target heads used in the 1947 simulation were greater than or equal to the observed head in 1995 steady state simulation; and
    - target heads in the 1995 steady state simulation were greater than or equal to observed targets used during the transient calibration 1995 to 2017 stage

- Where multiple monitoring points are located in a single cell in the regional model then average heads were calculated for use in the 1947 and 1995 steady-state calibration stages. Where this occurred in the candidate transient calibration data set then the most reliable data set (section 5.4.7.2) was adopted.

Prior to their use in the final calibration dataset, candidate head measurements were also excluded based on the following comparisons with the model structure. Head measurements were excluded where they:

- apply to surficial layers and exceed model-assigned drain elevations by more than 10 m; this is based on the premise that such observations reflect shallow (potentially perched) local groundwater systems rather than those associated with the deeper systems that are simulated by the UWIR 2019 model
- fall below the base of a model cell with which it is associated
- all outside the active model area or are located in model cells with a modelled thickness of less than 1 m
- are attributed to the following aquitard layers: layer 8 (Westbourne Formation), layer 18 (Durabilla Formation), layer 20 (upper Evergreen Formation), layer 22 (lower Evergreen Formation), layer 24 (Moolayember Formation) and layer 26 (Rewan Formation) as previously discussed in section 3.3.2.1.

5.4.3 Testing the steady state assumption

As discussed previously in section 5.3, two steady-state stages were included in the overall simulation used for calibration of the UWIR 2019 model. In each of these simulation stages, equilibrium conditions are assumed to prevail. This implies that model calibration data pertaining to the steady-state simulation stages need to reflect equilibrium conditions for the following two periods:

- 1947, before there was any significant groundwater extraction from areas within the Surat CMA
- 1995, before there was any significant CSG extraction from areas within the Surat CMA.

In order to assess the extent to which the steady-state head observations are affected by non-equilibrium groundwater flow, a transient model run and two steady state model test runs were undertaken. These runs are used to generate synthetic observations of head at the same sites and times as those which were candidates for inclusion in the 1947 and 1995 components of the calibration dataset. The transient run, comprised of 1,140 monthly stress periods, spanned the period January 1900 to December 1995. It was parameterised with initial parameter values derived using methodologies discussed in Chapter 4 of this document. Beginning with no extraction (reflected by a steady state initial stress period), pumping was gradually introduced to the model during the course of the simulation. Extraction bores were activated at the time of their drilling as recorded in the DNRME Queensland groundwater database.

The two steady state runs employed the same parameters as the transient run (i.e. initial parameter values). One of these featured no pumping while the other featured 1995 pumping; as such they employed the same stresses as those used during the first and second steady state stages of the overall UWIR model calibration run. Equilibrium heads under both 1947 and 1995 steady state conditions were calculated for monitoring points which were candidates for inclusion in the UWIR model calibration dataset. These were compared with their transient counterparts. In the discussion

that follows, the difference between a steady state head and its transient counterpart is referred to as "*ΔH*" for brevity. Where *ΔH* is small, observations are considered to reflect steady-state ("equilibrium") conditions.

For around 90% of the candidate observations for the 1947 steady state model *ΔH*s fell in the range 0 to 1.0 m. On this basis, the entire 1947 observation head dataset was used in the UWIR 2019 model calibration dataset. However, about 60% of 1995 steady state head observation showed *ΔH*s exceeding 1.0 m. This suggests that a large proportion of the 1995 observation head dataset does not reflect steady state conditions. To use this part of the observation dataset for calibrating the UWIR model a different observation weighting scheme was implemented that does not require an assumption of equilibrium conditions; this is described in Section 5.4.5.2

5.4.4 1947 steady state simulation

5.4.4.1 Observed heads

Preliminary processing of head observations in the manner described in section 5.4.2 above reduced the number of observed heads for the 1947 steady state simulation from around 1,100 points to a total of 587. The distribution of these observations among stratigraphic units represented in the UWIR 2019 model is summarised in Table 5-1. The spatial distribution of observations within these units is provided in Appendix C1. As shown in Table 5-1 and Appendix C1 the head data set available for calibration of the 1947 steady state simulation is relatively limited. In particular the majority of the data for most units are limited to areas close to outcrop. Other than for the Gubberamunda Sandstone (model layer 7, see Appendix C1, Figure C1-7) observed head data in deeper parts of the basin during this early stage of development are extremely limited.

Table 5-1 1947 and 1995 steady state groundwater level observations by stratigraphic unit

Stratigraphic unit(s)	Model layer number	Number of observations 1947	Number of observations 1995
Cenozoic aged units (excluding Condamine and MRV)	1	150	1,027
Upper Cretaceous	2	23	93
Wallumbilla Formation	3	29	79
Bungil Formation	4	38	160
Mooga Sandstone	5	83	430
Orallo Formation	6	77	396
Gubberamunda Sandstone	7	51	346
Westbourne Formation	8	0	0
Upper Springbok Sandstone	9	4	81
Lower Springbok Sandstone	10	1	32
Walloon Coal Measures non-productive zone	11	1	5
Upper Walloon Coal Measures	12	8	148
Middle Walloon Coal Measures	13-15	21	283
Lower Walloon Coal Measures	16	10	183
Durabilla Formation	17	0	0
Upper Hutton Sandstone	18	57	949
Lower Hutton Sandstone	19	8	273
Upper Evergreen Formation	20	0	0
Boxvale Sandstone	21	0	29
Evergreen Formation	22	0	0
Precipice Sandstone	23	13	201
Moolayember Formation	24	0	0
Clematis Sandstone	25	1	99

Stratigraphic unit(s)	Model layer number	Number of observations 1947	Number of observations 1995
Rewan Group	26	0	0
Bandanna Formation non-productive zone	27	0	0
Upper Bandanna Formation	28	0	19
Lower Bandanna Formation	29	0	8
Undifferentiated Bowen Basin strata	30	12	149
Cattle Creek Formation non-productive zone	31	0	0
Upper Cattle Creek Formation	32	0	1
Lower Cattle Creek Formation	33	0	0
Undifferentiated Bowen Basin strata	34	0	108
Total		**587**	**5,099**

5.4.4.2 Parallel flow to western general head boundary

Groundwater is conceptualised as flowing parallel to the GHB located along the westernmost extent of the model domain; see section 3.2.4.2 for details. Heads along this boundary are adjustable through the calibration process; as will be discussed below, they are parameterised using pilot points emplaced at 9 km intervals.

In order to ensure estimation of boundary heads which respect the concept of flow parallel to this boundary, a suite of observations specifying zero head gradient perpendicular to the boundary were introduced to the calibration dataset. This was done by extracting model-calculated heads at a series of cell midpoints offset from boundary pilot points by four cell centres (i.e. 6 km). Differences between these heads, and heads at the boundary directly opposite, were “observed” to be zero. This component of the observation dataset was only applied during the 1947 steady state simulation stage. Hence, inflow to the model domain induced by post 1947 pumping is not precluded.

Zero gradient observations were introduced to the layers listed in Table 5-2. These are the same layers as those in which the GHB boundary conditions themselves are featured. The total number of zero gradient observations is 308. See Appendix C2 for their locations.

Table 5-2 Paired horizontal head difference observations by stratigraphic unit for the 1947 steady state simulation

Stratigraphic unit	Model layer	Number of observations
Bungil Formation	4	34
Mooga Sandstone	5	35
Gubberamunda Sandstone	7	36
Upper Springbok Sandstone	9	32
Lower Springbok Sandstone	10	32
Upper Walloon Coal Measures	12	5
Middle 1 Walloon Coal Measures	13	8
Middle 2 Walloon Coal Measures	14	12
Middle 3 Walloon Coal Measures	15	23
Lower Walloon Coal Measures	16	34
Upper Hutton Sandstone	18	23
Lower Hutton Sandstone	19	23
Boxvale Sandstone	21	3
Precipice Sandstone	23	8
Total		**308**

5.4.5 1995 steady state simulation

5.4.5.1 Heads – Condamine Alluvium and Main Range Volcanics

As noted in section 3.3.1.3, 1995 steady state heads experienced in the Condamine Alluvium and Main Range Volcanics were obtained from the Condamine Alluvium Model (KCB, 2011) in the former case, and through spatial interpolation of observed water levels in the latter case. These were then ascribed directly to MODFLOW-USG drains assigned to all model cells which comprise this part of the model domain.

In order to ensure that water levels within these cells actually rise to the drainage surface, these heads were also introduced to the calibration dataset as observations. Heads cannot rise above the drainage surface due to the action of the drains. This resulted in 278 head observations for the Condamine Alluvium footprint of the UWIR 2019 model and 386 head observations for the footprint of the Main Range Volcanics. See Appendix C3 for locations of these calibration targets.

5.4.5.2 Heads – other stratigraphic units

Following processing of groundwater head data in the manner described in section 5.4.2, a total of 5,099 measurements were available for use in the calibration dataset in conjunction with the 1995 steady state simulation. Their disposition with respect to model layers and stratigraphic units is listed in Table 5-1.

Values of ΔH (see section 5.4.3) computed for each head observation were used to identify those observations for which the departure from the steady state assumption was likely to be greatest. The ΔH values of greater than 5 m were assumed to be significant.

Observations for which ΔH exceeded this threshold were placed into a "penalty" group. Asymmetric residual calculation was employed for each member of this group, where a residual is the value of an observation minus its model-calculated counterpart. The asymmetric residual was designed to forgive model-calculated heads which are less than their observed counterparts but to penalise those which are above their observed counterparts. This acknowledges the fact that steady state water levels (as computed by the model) will be lower than transient water levels (which are observed) in a context where steady state conditions in response to gradually increasing groundwater extraction have not yet been achieved.

Let h_0 denote the observed head for a member of the penalty group. Let h_m denote the model-generated counterpart to this observation. A zero residual is calculated if h_m is between h_0 and $h_0 - \Delta H$. Hence, if h_o is 300 mAHD and ΔH is 10 m, then model-to-measurement misfit is deemed to be zero if the simulated head falls in the range 290 to 300 mAHD. Where h_m is less than ($h_o - \Delta H$), the residual (r) is calculated as

$$r = -[h_m - (h_o - \Delta H)] \quad (5.1)$$

Alternatively, if h_m is greater than h_0 then the residual is calculated in the conventional way, i.e. as ($h_o - h_m$)..

Water level observations for which the ΔH value is less than 5 m were placed into the "traditional" group. Residuals were calculated in the usual way for members of this group, that is as ($h_o - h_m$).

Table 5-3 lists the number of observations belonging to each of the traditional and penalty groups within each model layer. Appendix C4 and Appendix C5 show the locations of these partitioned observations for the traditional and penalty groups respectively.

Table 5-3 Partitioning of groundwater water level observations used in conjunction with the 1995 steady state simulation into traditional and penalty groups

Stratigraphic unit(s)	Model layer number	Number of traditional observations	Number of penalty observations
Cenozoic aged units (excluding Condamine and MRV)	1	970	57
Upper Cretaceous	2	91	2
Wallumbilla Formation	3	79	0
Bungil Formation	4	103	57
Mooga Sandstone	5	261	169
Orallo Formation	6	270	126
Gubberamunda Sandstone	7	243	103
Westbourne Formation	8	0	0
Upper Springbok Sandstone	9	25	56
Lower Springbok Sandstone	10	10	22
Walloon Coal Measures non-productive zone	11	2	3
Upper Walloon Coal Measures	12	69	79
Middle Walloon Coal Measures	13-15	43	240
Lower Walloon Coal Measures	16	62	121
Durabilla Formation	17	0	0
Upper Hutton Sandstone	18	343	606
Lower Hutton Sandstone	19	49	224
Upper Evergreen Formation	20	0	0
Boxvale Sandstone	21	5	24
Lower Evergreen Formation	22	0	0
Precipice Sandstone	23	21	180
Moolayember Formation	24	0	0
Clematis Sandstone	25	47	52
Rewan Group	26	0	0
Bandanna Formation non-productive zone	27	0	0
Upper Bandanna Formation	28	17	2
Lower Bandanna Formation	29	6	2
Undifferentiated Bowen Basin strata	30	148	1
Cattle Creek Formation non-productive zone	31	0	0
Upper Cattle Creek Formation	32	1	0
Lower Cattle Creek Formation	33	0	0
Undifferentiated Bowen Basin strata	34	108	0
Total		**2,973**	**2,126**

5.4.5.3 Vertical inter-aquifer head differences

As highlighted by White et al. (2014) where observed differences between heads in different layers are directly compared with differences between the model-calculated counterparts to these heads, this can promulgate better estimates of the vertical resistance of the aquitard that separates these layers than would be the case if heads alone comprised the calibration dataset. This acknowledges the fact that numerical models, despite their defects as simulators of real-world behaviour, can often calculate differences (both temporal and spatial) with greater integrity than they can calculate the actual values of these quantities.

The dataset used in partnership with the 1995 steady state simulation was expanded to include head differences between the Condamine Alluvium and underlying Surat Basin layers, and between the Main Range Volcanics and underlying Surat Basin layers. These differences were taken at locations where 1995 observations were available from bores which tap Surat Basin units. In each case, the Condamine Alluvium or Main Range Volcanics head was set equal to the drainage surface elevation

at the same horizontal location as the partnered Surat Basin observation. The elevation of the drainage surface is calculated from the Condamine Model within the Condamine Alluvium footprint, and from spatial interpolation between measurement points in the Main Range Volcanics footprint.

1995 data availability was such that further head difference observations could be formulated for Surat Basin layers at a number of locations within the domain of the UWIR 2019 model. For all observations of this type, the difference was calculated by subtracting head in the lower aquifer from the head in the upper aquifer.

In total, 260 vertical head difference observations were added to the 1995 component of the calibration dataset, the locations of which are shown in Appendix C6. These comprised the following:

- 96 differences between head in the Condamine Alluvium (layer 1) and that in an underlying Surat Basin layer (layers 12 to 16)
- 164 differences between head in the Main Range Volcanics (layer 1) and a head in an underlying Surat Basin layer (layers 12 to 19).

5.4.5.4 Condamine water flux exchange

Water balance studies undertaken by KCB (2011) suggest that groundwater inflow to the Condamine Alluvium from all adjacent and underlying strata is about 16,200 m^3/d (5,913 ML/yr). This was included as an observation in the component of the calibration dataset that complements the 1995 steady state simulation, however, the effect of this target was 'softened' somewhat by allowing modelled fluxes to increase to 10,000 ML/yr before any residuals are calculated (i.e. any penalties are incurred during the calibration), reflecting that this is an estimate based on conceptual calculations and may therefore subject to error.

5.4.5.5 "Extractive" drain flow in the Condamine Alluvium and Main Range Volcanics

As explained in section 3.3.1.2.1 groundwater extractions are not explicitly simulated, either in the Condamine Alluvium footprint of the UWIR 2019 model or in the Main Range Volcanics footprint of the model. Instead groundwater levels within these areas are prevented from rising above estimated 1995 levels using a suite of MODFLOW-USG drain boundary conditions which collectively form a drainage surface over these areas. This surface typically lies at some distance below the ground surface. At the same time, as is explained above, the calibration process penalises heads which are below the level of this drainage surface.

To complete characterisation of extraction-induced water levels in these areas, penalty functions were introduced to the 1995 component of the calibration dataset to ensure that loss of water through these drainage surfaces equals or exceeds 90% of extraction that is assessed as occurring from these areas. The residual is zero for each of these observations if these conditions are met. Use of a figure of 90% rather than 100% accommodates the fact that pumping rates were increasing in 1995 and that new equilibrium water levels may not have yet been established at this time. A single drain flow target was considered sufficient for the Condamine Alluvium. However, because of topographic variability in areas associated with the Main Range Volcanics and because of the large spatial variability of extraction which prevails in these areas, 14 zones were introduced to its footprint in the UWIR 2019 model, with a penalty function associated with each. These zones, which are based on hydrological basin delineation, are depicted in Figure 5-1. Table 5-4 provides details of these components of the 1995 steady state calibration dataset.

Table 5-4 Drainage "extractive" flow targets belonging to the 1995 steady state component of the calibration dataset

Zone	Minimum flow target (ML/yr)
Condamine Alluvium - Total	**31,183**
Main Range Volcanics - 1	2,828
Main Range Volcanics - 2	3,392
Main Range Volcanics - 3	7,613
Main Range Volcanics - 4	18
Main Range Volcanics - 5	24,258
Main Range Volcanics - 6	3,358
Main Range Volcanics – 7	6,495
Main Range Volcanics – 8	1
Main Range Volcanics – 9	18
Main Range Volcanics – 10	1,960
Main Range Volcanics – 11	2,955
Main Range Volcanics – 12	117
Main Range Volcanics – 13	1
Main Range Volcanics – 14	1
Main Range Volcanics - Total	**53,016**

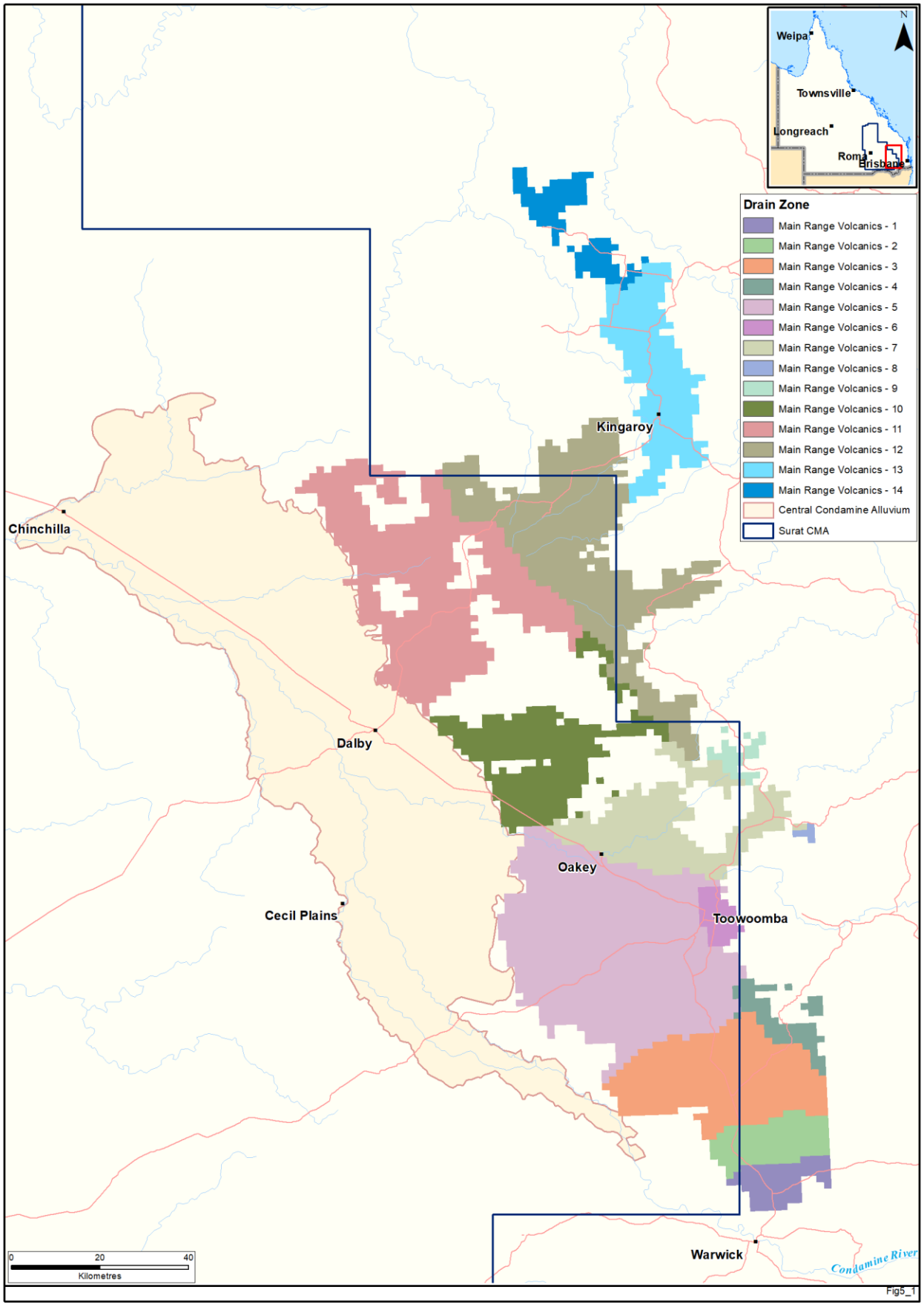

Figure 5-1 "Extractive" drain zones generated from hydrological basin delineation for the Main Range Volcanics

5.4.6 1995-2017 transient simulation

Observations comprising the transient component of the overall calibration dataset are now discussed. These include actual measurements, together with expert knowledge-based specifications of system behaviour that ensure good performance of those facets of the UWIR 2019 model that simulate extraction of water from CSG wells.

5.4.6.1 Non-CSG groundwater extraction

As is discussed in section 3.3.2, simulation of groundwater extraction for purposes other than CSG production in the UWIR 2019 model is undertaken using the MODFLOW-USG well package. Each well is set up to extract water at its metered rate or a proportion of its estimated "licensed" or full entitlement rate. Extraction rates assigned to conventional P&G are based on metered information. However, for all groundwater extraction wells this rate is automatically reduced (also referred to as "derating)" if the head in the well falls below a user-specified level – either the screen level or the top of the cell in which the well is emplaced.

To prevent unrealistic derating of extraction (resulting from underestimation of local hydraulic conductivity), the transient calibration dataset was supplemented to include time series of estimated actual non-CSG extraction from each of the main aquifers in the area (see Table 5-5). Note that further refinements to water use estimate where made as presented in the UWIR 2019. For each of these aquifers, a non-zero residual is calculated if the total modelled extraction falls below 80% of the estimated actual extraction. For the Walloon Coal Measures a threshold of 50% was used. The computed residual is then equal to the extraction deficit below this value. Table 5-5 shows the target extraction at the end of the transient simulation period.

Table 5-5 Estimated actual and targeted non-CSG groundwater extraction featured in the transient simulation dataset, December 2017

Stratigraphic unit / model layer	Estimated actual extraction (ML/yr)	Targeted extraction (ML/yr)
Gubberamunda Sandstone (Layer 7)	6,458	5,167
Springbok Sandstone (Layers 8 and 9)	544	436
Walloon Coal Measures (Layers 11 to 16)	3,921	1,961
Hutton Sandstone (Layers 18 and 19)	15,512	12,410
Boxvale Sandstone (Layer 21)	151	121
Precipice Sandstone (Layer 23)	6,052	4,841
Clematis Sandstone (Layer 25)	664	531
Total	33,304	25,466

5.4.6.2 Measured CSG water extraction rates

CSG water extraction data featured in the transient component of the calibration dataset includes the following:

- total monthly CSG co-produced water from the 20 individual CSG development areas listed in Table 5-6 and shown in Figure 5-2 and the total CSG co-produced water outside these main development areas (since a small number of wells outside of currently active CSG areas also extraction a small amount of water for pilot testing and other purposes)
- totals of the aforementioned monthly CSG co-produced water according to their sources (Walloon Coal Measures, the Bandanna Formation and the Cattle Creek Formation).

In total this observation dataset currently comprises 6,624 observed monthly water extraction targets relating to 6,641 CSG wells spanning the entire transient calibration period from January 1995 to December 2017.

Table 5-6 CSG development areas for which monthly water production volumes feature in the transient calibration dataset

Development area	Target coal formation	Company
Alfredson	Walloon Coal Measures	Origin
Arcadia Gas Field	Bandanna Formation	Santos Ltd (Santos)
Central Development Area	Walloon Coal Measures	QGC
Combabula	Walloon Coal Measures	Origin
Condabri	Walloon Coal Measures	Origin
Daandine	Walloon Coal Measures	Arrow
Development Area 2	Walloon Coal Measures	Arrow
Development Area 5	Walloon Coal Measures	Arrow
Development Area 8	Walloon Coal Measures	Arrow
Fairview Gas Field	Bandanna and Cattle Creek Formations	Santos
Kogan North	Walloon Coal Measures	Arrow
Northern Development Area	Walloon Coal Measures	QGC
Peat	Bandanna Formation	Origin
Roma Gas Field	Walloon Coal Measures	Santos
Scotia Gas Field	Bandanna Formation	Santos
Southern Development Area	Walloon Coal Measures	QGC
Spring Gully	Bandanna Formation	Origin
Talinga / Orana	Walloon Coal Measures	Origin
Tipton	Walloon Coal Measures	Arrow
Western Surat Gas Project	Walloon Coal Measures	Senex

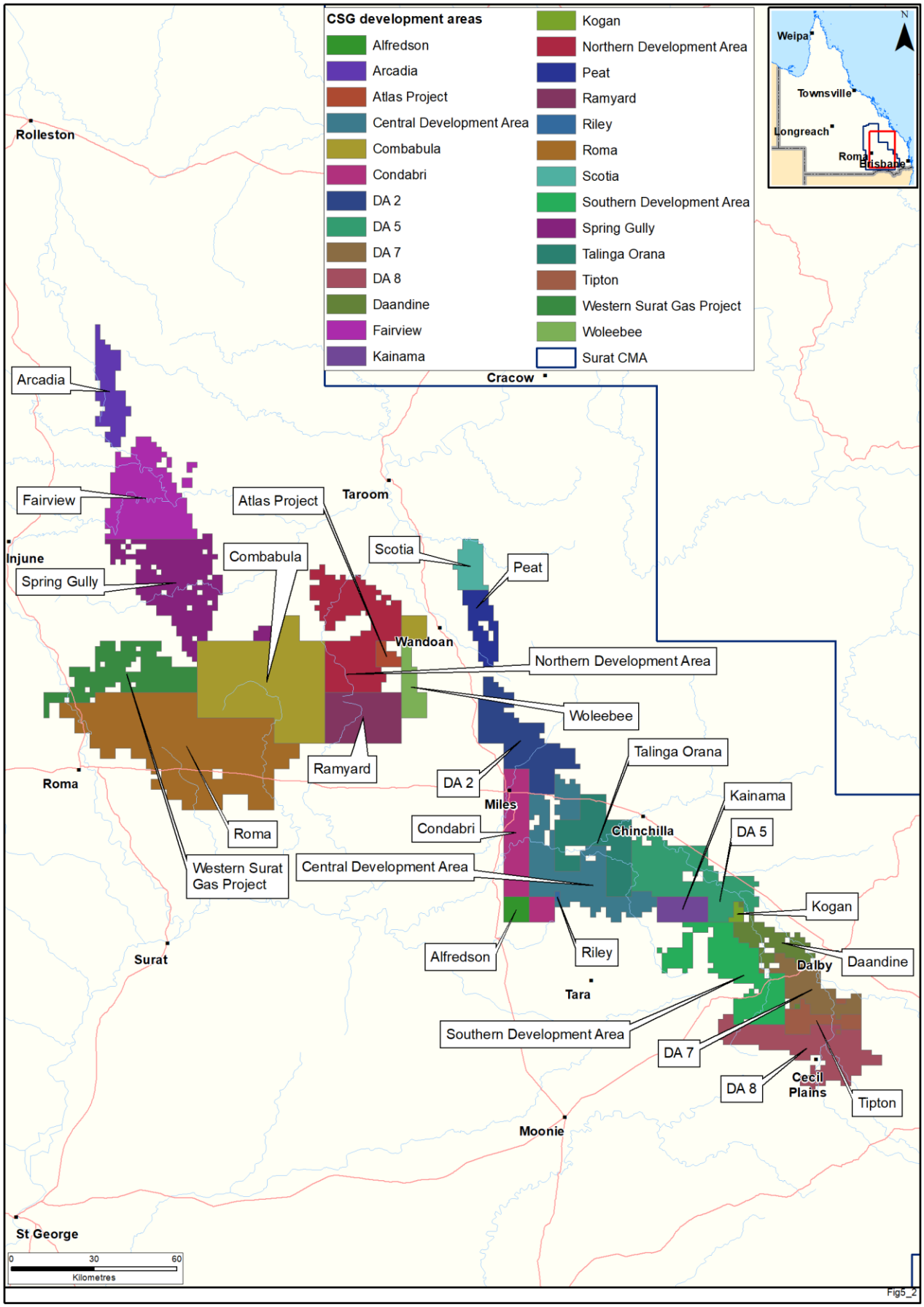

Figure 5-2 Location of CSG development areas in the Surat and Bowen basins

5.4.6.3 Transient head elevation observations

Transient head observations in key units form a substantial part of the 2019 transient calibration dataset. In addition to the preliminary screening process described in section 5.4.2, the following criteria were applied to further select monitoring locations for inclusion in the transient calibration dataset:

- time series with records between 1995 and 2017
- a minimum of 3 head measurement records
- at least on year of data
- attributed to one of the following formations: Springbok Sandstone (layers 9 and 10), Walloon Coal Measures (layers 12-16), Hutton Sandstone (layers 18 and 19), Precipice Sandstone (layer 23) and Bandanna Coal Measures (layers 28 and 29).

The resulting dataset was subsequently resampled to monthly values (Figure 5-3) to match the monthly stress period lengths used in the simulation. This yielded a total of 17,539 head observations at 470 monitoring points. These observations are distributed over the various model layers as outlined in Table 5-7 and shown spatially in Appendix C7.

As shown in Table 5-7 some 214 out of 470 monitoring points are located in the Walloon Coal Measures, the majority of which are located within or near active CSG development areas. The coverage of monitoring points within current and planned CSG productions areas in the Springbok Sandstone, Walloon Coal Measures and Hutton Sandstone is generally relatively good. However, monitoring in outcrop areas of the Hutton Sandstone is relatively sparse (Appendix C7, Figure C7-7), since these areas are some distance from CSG production areas. As shown in Figure C7-2 (Appendix C7) there are also relatively few monitoring points in the lower Springbok Sandstone within current production areas, especially in the area north east of Roma and south west of Chinchilla.

For model calibration purposes data for the transient observation points listed in Table 5-7 have been further subdivided into the following groups:

- Observed heads in the Walloon Coal Measures are subdivided into head observations that fall within and outside active CSG production areas (Appendix C7, Figures C7-3, C7-4 and C7-5). This subdivision has been made to amplify the visibility of more subtle head trends observed outside active CSG production areas in the model calibration process (see also section 5.4.7.6 which discusses observation weighting).
- Observed heads in the Precipice Sandstone are subdivided into observations that show a response to reinjection in the Spring Gully and Reedy Creek area and sites further away that do not (Appendix C7, Figure C7-8).
- Observed heads at a number of key monitoring sites referenced in the UWIR 2019 (OGIA, 2019b) are also grouped together again to ensure that the have a relatively high visibility in the model calibration process.

Table 5-7 Transient head elevation observation locations by stratigraphic unit

Stratigraphic unit(s)	Model layer	Number of observations
Upper Springbok Sandstone	9	30
Lower Springbok Sandstone	10	23
Upper Walloon Coal Measures	12	53
Middle Walloon Coal Measures	13-15	108
Lower Walloon Coal Measures	16	56
Upper Hutton Sandstone	18	78
Lower Hutton Sandstone	19	27
Precipice Sandstone	23	83
Bandanna Formation	28-29	12
Total		**470**

5.4.6.4 Transient head change observations

The large number of observed head elevation measurements described in the previous section represents a valuable resource for characterising the temporal evolution of heads throughout the Surat CMA. However, Doherty and Welter (Doherty and Welter, 2010) highlight that a calibration dataset must capture the key aspects of available information that are important to describe the system behaviour of interest. In the case of the UWIR 2019 model, temporal head changes (rather than absolute head elevations) in major aquifers and CSG reservoirs are particularly important since they may be indicative of actual CSG related impacts which OGIA are required to predict. As an additional measure to ensure that these observed head changes are highly visible in the calibration time-series of monthly temporal head changes were calculated for the same monitoring locations shown in Appendix C7 and listed in Table 5-7.

Temporal head differences were calculated using the first head observation at each monitoring point as reference head (Figure 5-3). This generated a further 17,069 temporal head change observations relating to the 470 monitoring locations with transient head data for use in the model calibration. These observations were split into the same groups used for the head elevation observations.

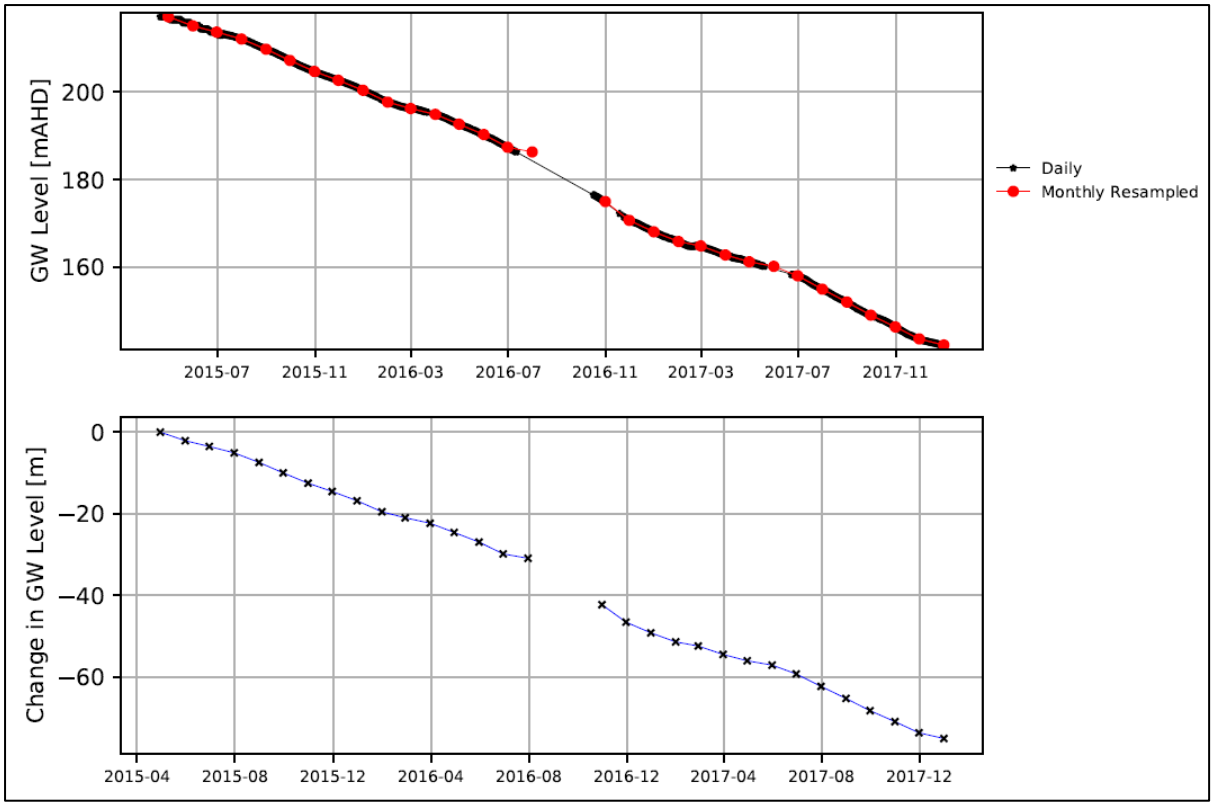

Figure 5-3 Example of monthly resampled heads and temporal head changes inferred transient head observations for the lower Walloon Coal Measures monitoring point RN 160710A

5.4.6.5 Transient vertical head difference observations

Based on the observed head data, a dataset of interlayer vertical head differences has also been generated and added to the transient calibration dataset. As discussed in Doherty and Hunt (2010) this can be an important type of information to estimate vertical hydraulic conductivities. In the UWIR 2019 model the vertical hydraulic conductivity of the following key aquitard layers play a particularly important role in the transmission of CSG impacts:

- transition zone between the Condamine Alluvium and Walloon Coal Measures (layer 2)
- Westbourne Formation (layer 8)
- Walloon Coal Measures non-productive zone (or upper aquitard) (layer 11)
- Durabilla Formation (layer 17).

Observed vertical head differences to constrain the vertical hydraulic conductivity of these layers are based on pairs of monitoring points that are situated above and below the afore-mentioned aquitard layers and within 1 km of each other (in most cases, however, the selected observation points are within 100 m of each other). An example is shown in Figure 5-4, which shows observed vertical head differences used to estimate the vertical hydraulic conductivity of the Durabilla Formation based on monitoring points in the lower Walloon Coal Measures (layer 16) and upper Hutton Sandstone (layer 18). Vertical head difference observations are also used to estimate the vertical hydraulic conductivity of the various Walloon Coal Measures (layers 12 to 16) and Hutton Sandstone (layers 18 and 19). For these layers, pairs of monitoring points are based on monitoring points slotted in different vertical sections of the same formation.

A total of 55 pairs of monitoring points are used to generate time-series of observed intra- and inter-formation head differences, constituting a dataset of 1,824 monthly average head difference observations that are added to the transient calibration dataset. These observations are subdivided into six groups as shown in Table 5-8. The locations of the monitoring locations which feature in each of these six groups are shown in Figure C8-1 to C8-6 (Appendix C8).

Table 5-8 Transient vertical head difference observations by stratigraphic unit pair

Stratigraphic unit pair	Targeted parameter	Upper model layer	Lower model layer	Number of observation locations
Condamine Alluvium – Springbok Sandstone or Walloon Coal Measures	Kv Condamine transition zone (layer 2)	1	10,12,13,14,16	8
Gubberamunda Sandstone – Upper Springbok Sandstone	Kv Westbourne Formation (layer 8)	7	9	5
Lower Springbok Sandstone – Upper Walloon Coal Measures	Kv Walloon non-productive zone (layer 11)	10	12	8
Upper – Middle or Lower Walloon Coal Measures	Kv Walloon Coal Measures (layers 12 to 16)	12	13,14,15,16	22
Lower Walloon Coal Measures - Upper Hutton Sandstone	Kv Durabilla Formation (layer 17)	16	18	9
Upper - Lower Hutton Sandstone	Kv Hutton Sandstone (layers 18 and 19)	18	19	3
Total				**55**

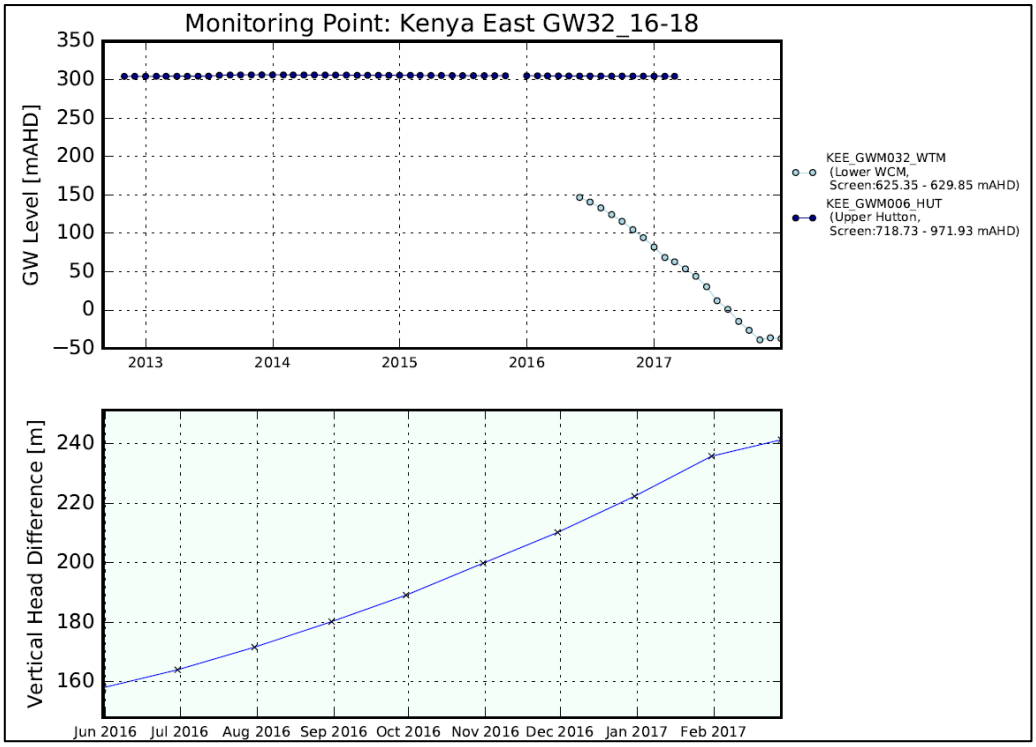

Figure 5-4 Example of monthly resampled vertical head difference observations between the upper Hutton Sandstone and Walloon Coal Measures based on transient head data for monitoring point pair KEE_GWM032_WTM and KEE_GWM006_HUT

5.4.6.6 CSG water re-injection rates & reinjection head-target

Two groups of observations related to re-injection to the Precipice Sandstone were also included in the transient calibration dataset. These were observed monthly re-injection volumes and heads in re-injection wells.

Re-injection to the Precipice Sandstone occurs at two APLNG aquifer injection facilities close to the Spring Gully and Reedy Creek gas fields, the locations of which are shown in Figure C7-8 (Appendix C7). Time-series of measured monthly reinjected water volumes used for model calibration are shown in Figure 5-5. Individual observation groups are used for each of the two reinjection sites, comprising a total of 69 observations.

A third observation group was also created to provide a head target for the Spring Gully reinjection site. Observed groundwater levels at both sites remain below ground level during re-injection. This was not well matched at the Spring Gully during early test runs of the model and hence a head penalty was introduced to limit simulated heads to no more than 10 m above ground surface. This penalty is asymmetric and only returns a residual when the simulated head at the Spring Gully reinjection facility is more than this 10-m threshold.

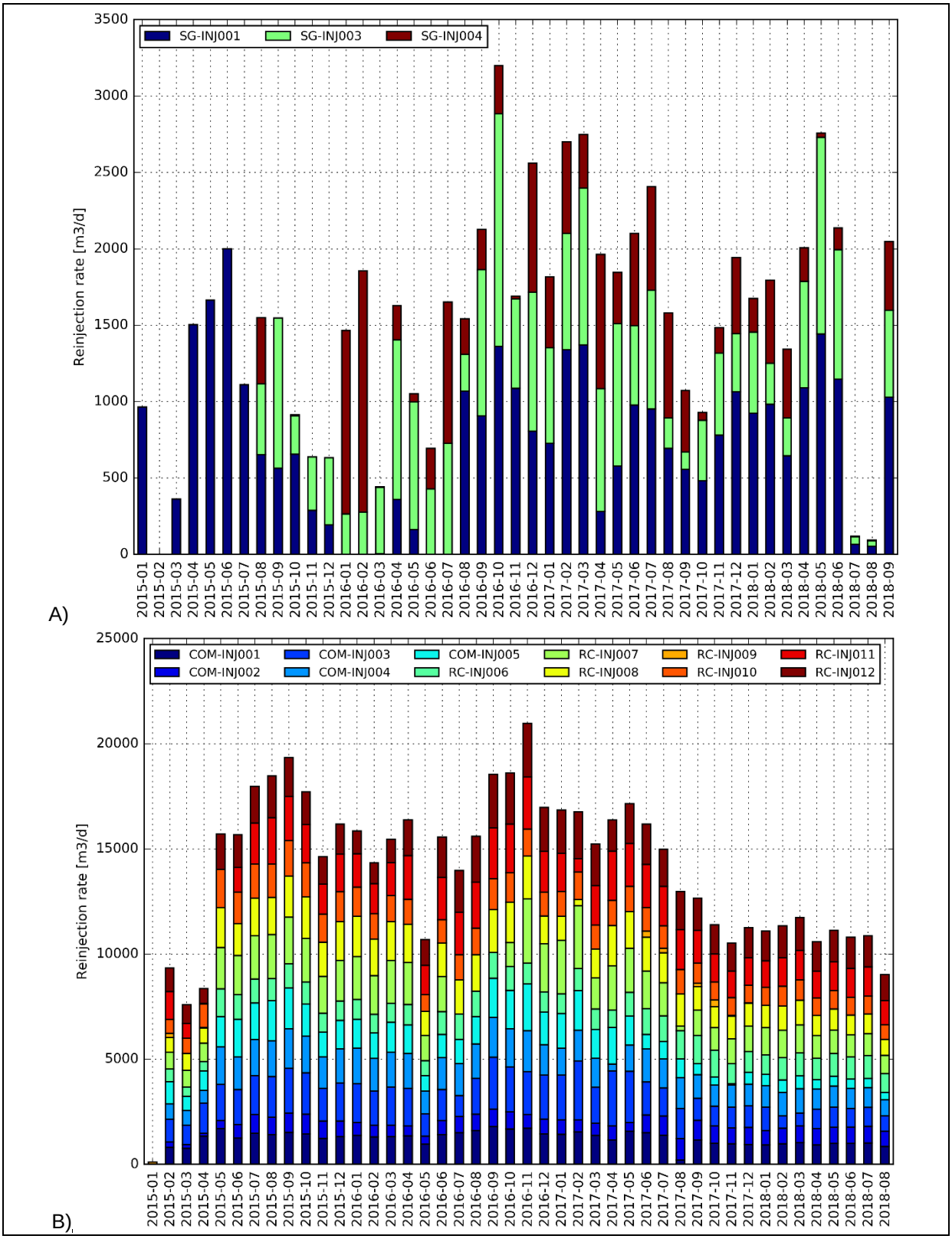

Figure 5-5 Monthly time-series of reinjected water for A) Spring Gully and B) Reedy Creek; data up to December 2017 is used for model calibration

5.4.6.7 Vertical head differences in coal-bearing units

As is discussed in section 2.3.3, groundwater heads in the vicinities of CSG production wells are expected to develop vertical gradients over time that approach 1:1. Furthermore, the head in coal

seams are expected to approach the elevation of the coal in the near-well region. This is an outcome of the fact that the rate of water extraction from a gas well diminishes over time; hence the fluid in the wells and the coal seams becomes dominated by gas. The time-asymptotic approach of near-well heads in coal seams to their elevation is supported by detailed dual-phase modelling work undertaken by OGIA; see Figure 5-6. Further outcomes of this modelling work displayed in Figure 5-7 suggest that near-well vertical head gradients of between 0.7 and 0.9 can be expected after several years of CSG production. These conclusions have been corroborated by gas company reservoir modelling results which show similar outcomes.

"Observations" of vertical head differences which respect this gradient in areas subject to extended periods of active CSG extraction were introduced to the transient calibration dataset. Let dh_o represent a vertical head difference observation. For a vertical column of model cells containing one or more extraction wells which have been operating for at least five years, the observed value of dh_o is calculated using the equation:

$$dh_0 = dh/dz\ (z_{w\_top} - z_{w\_bot}) \qquad (5.2)$$

where:

- dh/dz is the expected vertical head gradient as determined from representative dual-phase reservoir simulations; a value of 0.7 is adopted;
- z_{w_top} is the highest well screen elevation within the uppermost model layer in which active wells are screened; and
- z_{w_bot} is the lowest well screen elevation in the lowermost model layer in which active wells are screened.

This was undertaken for pertinent model layers and cells in both the Walloon Coal Measures and Bandanna Formation. Historical CSG extractions from the Cattle Creek Formation have occurred over a period less than the five year minimum duration adopted for inclusion of these vertical head difference targets.

A total of 399 vertical head difference calibration targets were calculated in this way. This represents one target for each vertical column of model cells from which gas is extracted from more than one model layer for more than five years. The 189 vertical head difference observations pertaining to the Walloon Coal Measures ranged in value from 54 to 316 m. The remaining 210 observations pertaining to the Bandanna Formation, ranged in value between 7 and 119 m.

These vertical head differences were incorporated into the calibration process using a one-sided penalty function; only model-calculated vertical head differences which are less than the target vertical head difference incur a residual, and hence contribute to the overall objective function whose task it is for PEST to minimise.

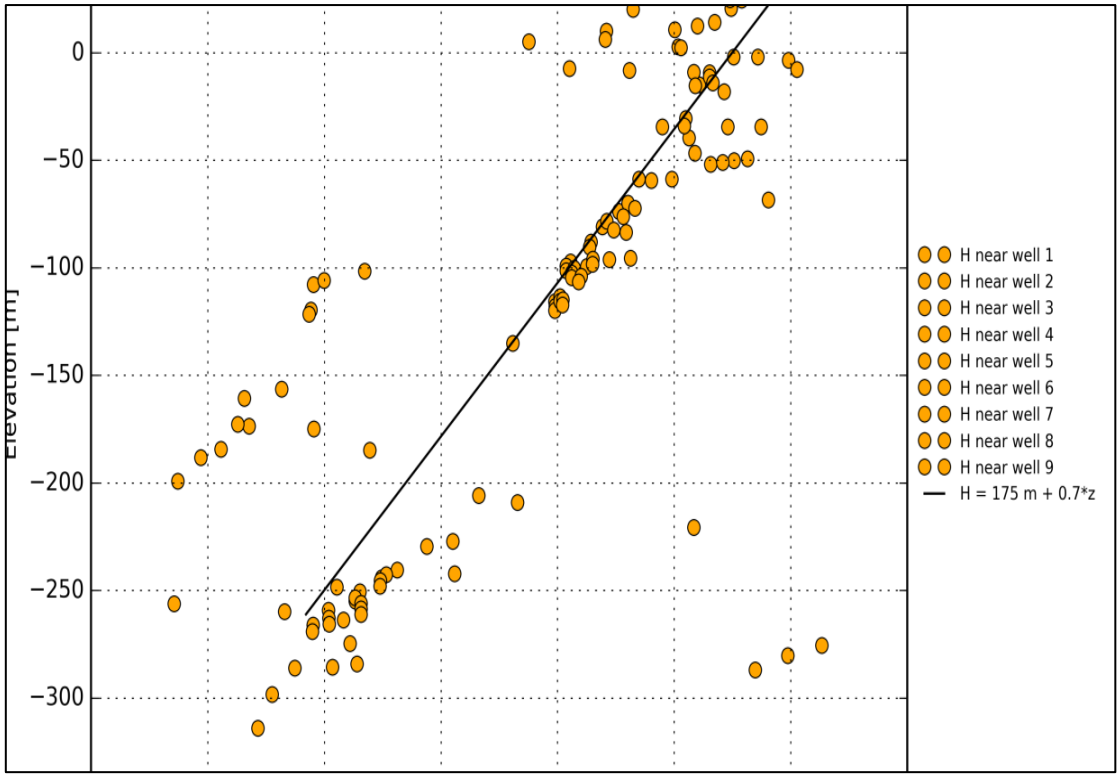

Figure 5-6 Heads in a CSG reservoir near a selection of nine extraction wells after 25 years of CSG production; heads were calculated by OGIA using a detailed reservoir model; the black line depicts a vertical head gradient (dH/dz) of 0.7

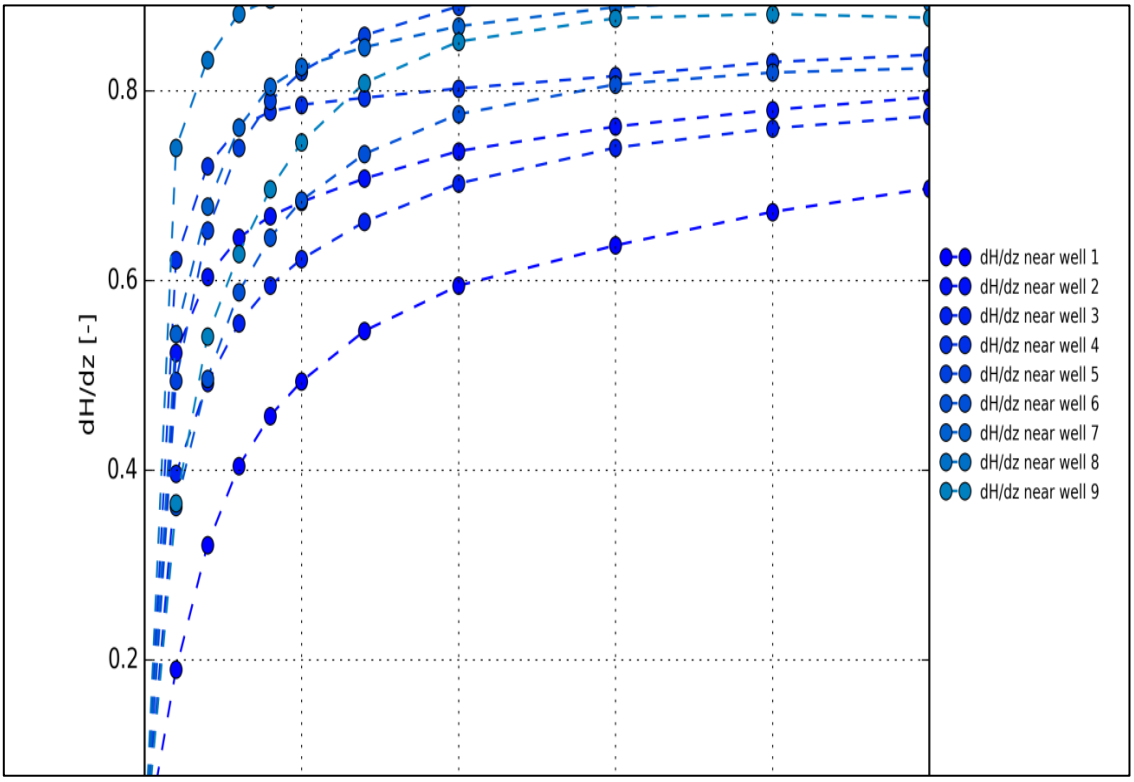

Figure 5-7 Vertical head gradient (dH/dz) in a CSG reservoir near a selection of nine CSG wells as function of CSG production time; results were obtained from detailed reservoir modelling undertaken by OGIA

5.4.6.8 Water saturation in coal-bearing units

A suite of anticipated water saturation “observations” were also included in the transient calibration dataset. These were also based on the outcomes of representative detailed dual-phase flow modelling undertaken by OGIA referred to in the previous section. In the example provided in Figure 5-8 near-well water saturation after 25 years of gas extraction, varies between 0.2 and 0.9. Figure 5-9 plots vertically averaged water saturation against time of CSG production for the same model. In this example, water saturation approaches a high-time asymptote of around 0.6.

Based on these and other examples (including the outcomes of gas company reservoir modelling), a water saturation value of 0.7 was used as a calibration target for cells in the UWIR 2019 model that contain CSG wells which have been active for five years or more. A total of 1,402 such saturation observations were included in the component of the calibration dataset associated with the transient simulation. These comprised 973 observations in the Walloon Coal Measures and 430 observations in the Bandanna Formation. No observations were included for the Cattle Creek Formation as none of the CSG wells currently extracting from this formation have been operational for more than five years.

Similar to the vertical head differences discussed in the previous section, water saturation targets contributed to the total objective function as a suite of one-sided penalties; only model-simulated water saturations that are greater than the target water saturation of 0.7 incur a residual.

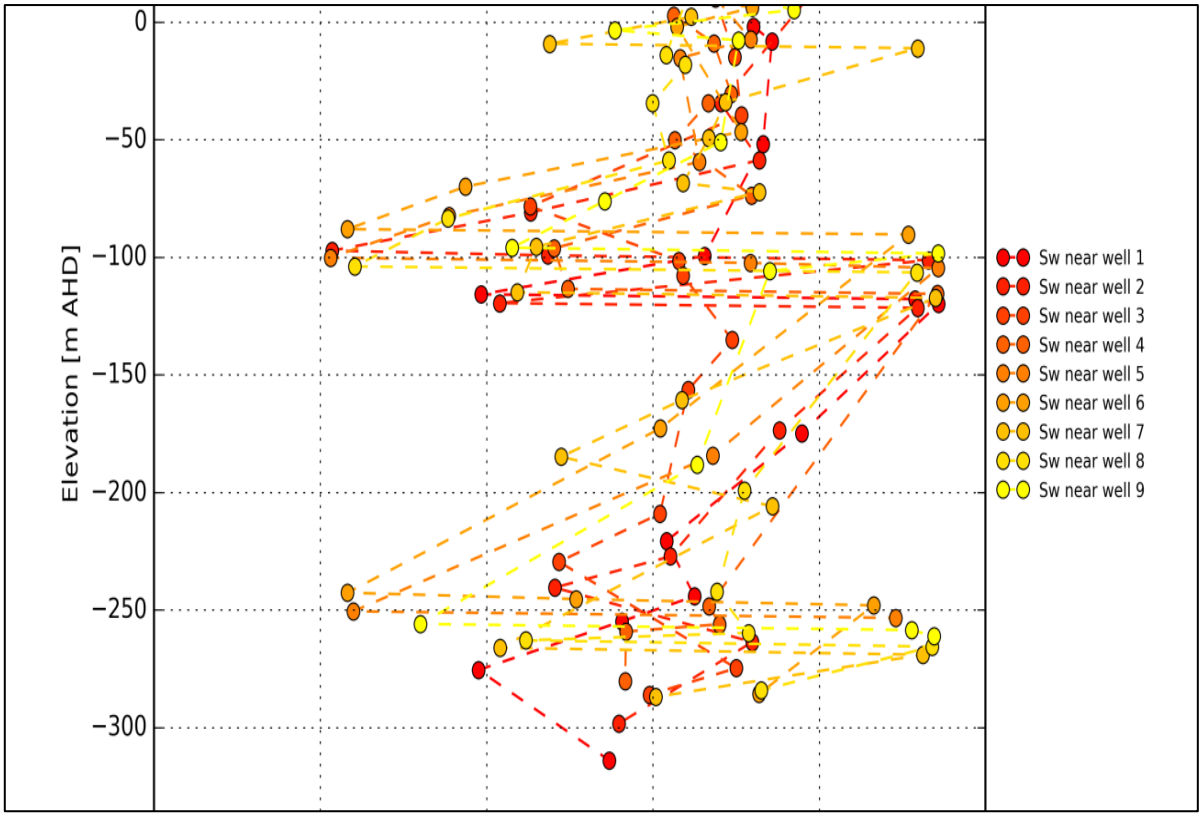

Figure 5-8 Modelled reservoir water saturation near nine CSG extraction wells after 25 years of CSG production; results were obtained from detailed reservoir modelling undertaken by OGIA

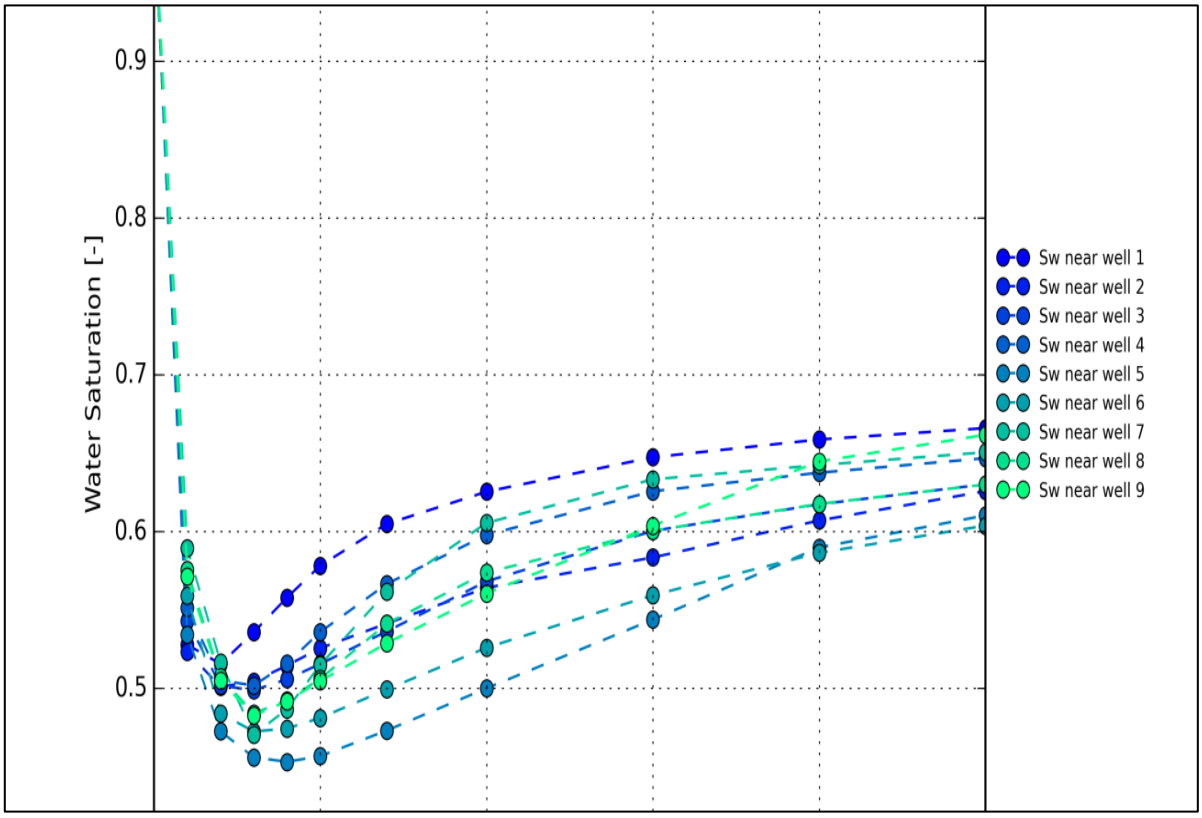

Figure 5-9 Modelled average water saturation near nine CSG extraction wells as function of CSG production time; results were obtained from detailed reservoir modelling undertaken by OGIA

5.4.6.9 Eclipse Modelling Results for the Walloon Coal Measures - QGC

Further 'observations' were also added to the transient simulation component of the observation dataset based on the outcomes of reservoir simulations undertaken by QGC. Simulation results comprised annual heads and water saturations for the Walloon Coal Measures at a 250 m spatial resolution for the period January 2010 to January 2016. The spatial extent of these simulation results encompass QGC's Central and Southern Development Area and represent the Walloon Coal Measures using 14 model layers.

Figure 5-10 and Figure 5-11 show snapshots of this data and display modelled head and water saturation for the lower Walloon Coal Measures in January 2016. These simulation results were attributed to individual cells of the UWIR 2019 model through averaging over reservoir model cells contained within each 1.5 × 1.5 km cell of the UWIR 2019 model.

A total of 11,044 transient calibration targets were inferred from the reservoir simulation information provided by QGC, comprising 4,693 heads, 4,693 water saturation targets and 1,658 vertical head differences.

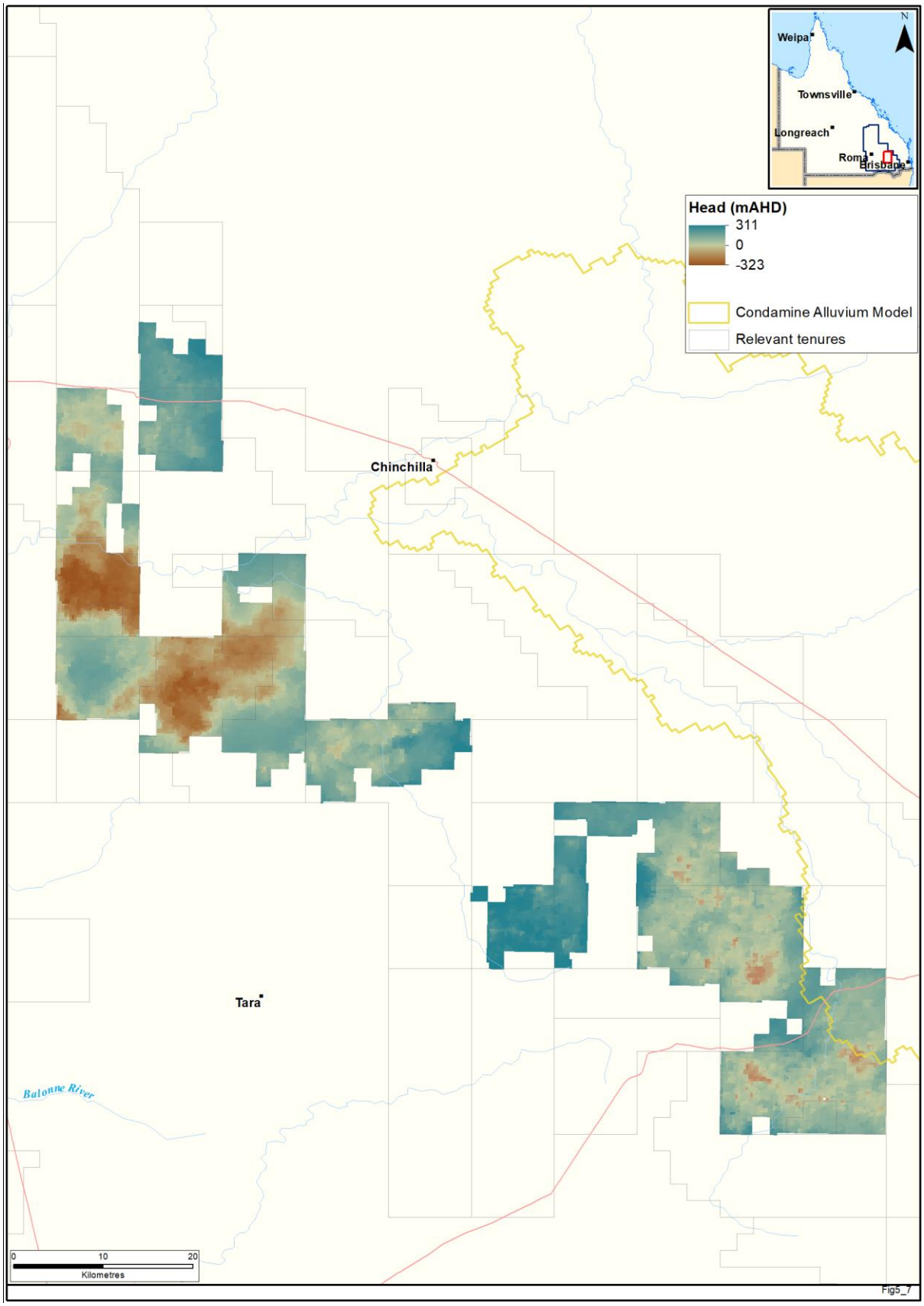

Figure 5-10 Reservoir model head output for the lower Walloon Coal Measures, January 2016

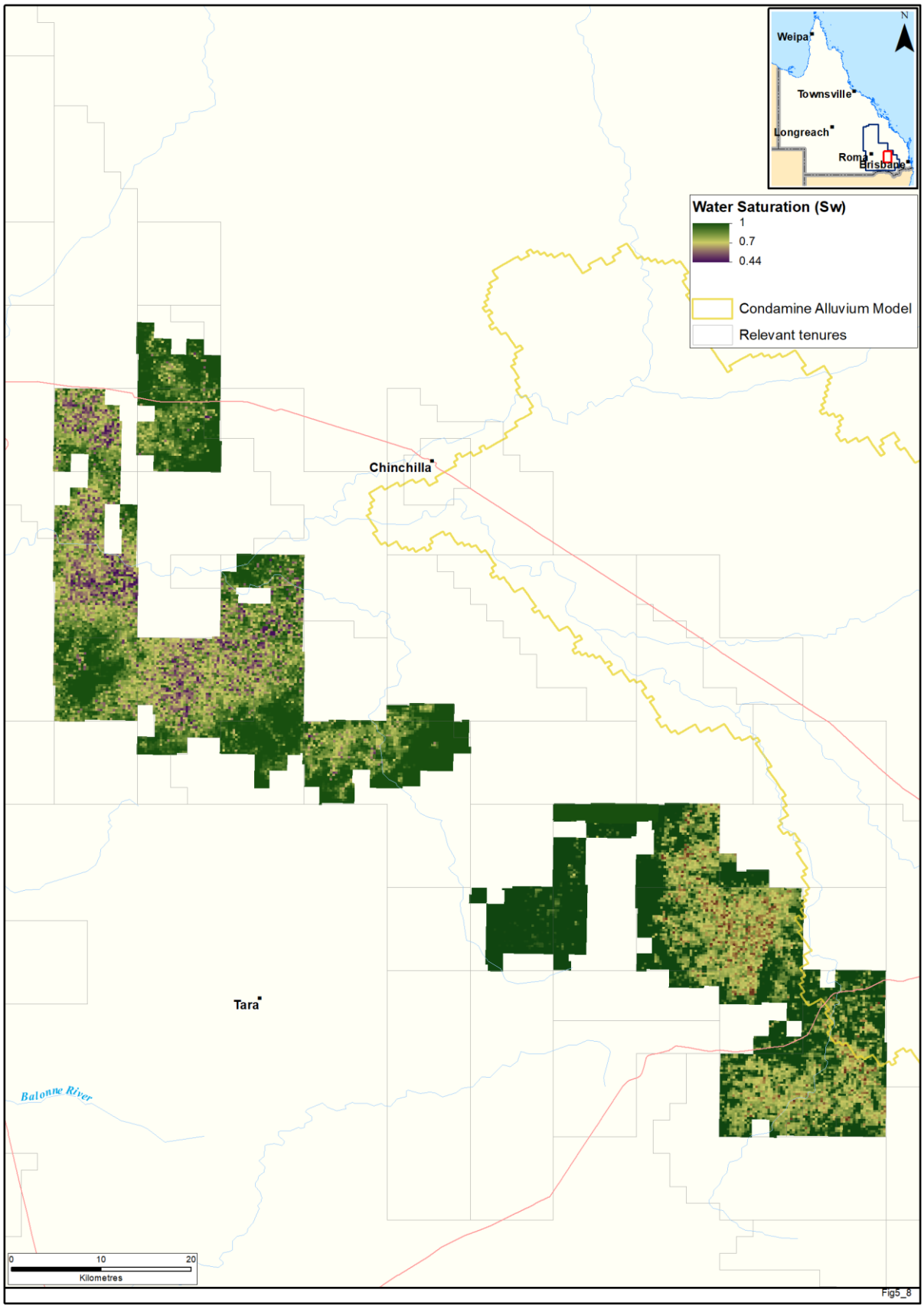

Figure 5-11 Reservoir model water saturation (Sw) output for the lower Walloon Coal Measures, January 2016

5.4.7 Observation weighting strategy

5.4.7.1 General

The objective function used by PEST in calibration of a model is formulated as the sum of weighted squared differences (i.e. residuals) between observations and their model-generated counterparts. Where an inverse problem is well-posed, minimisation of this objective function leads to solution of the inverse problem of model calibration. Where it is ill-posed, the component of the objective function that includes the calibration dataset (i.e. the "measurement objective function" in PEST parlance) should be lowered to a value that is "reasonable", subject to constraints exerted by another objective function component (the "regularisation objective function") which embodies Tikhonov constraints that enforce parameter reasonableness. In either case, achievement of a solution to the inverse problem which is of minimised error variance requires that weights associated with observations be inversely proportional to the standard deviations of noise associated with those observations, and that the constant of proportionality be the same for all observations.

In practice, in most instances of groundwater model calibration, measurement noise is only partially responsible for model-to-measurement misfit. This is particularly the case for large regional models such as the UWIR 2019 model. A larger contributor to model-to-measurement misfit is the fact that a regional groundwater model, like any environmental model, can only simulate the details of groundwater flow (including its response to CSG extraction) in an approximate manner. This is reflected in the inability of most regional models to fit all aspects of a calibration dataset to within a level determined by noise associated with field and other measurements without the need for at least some of its parameters to adopt spurious values as a consequence of achieving this level of fit. The phenomenon that is responsible for this higher level of model-to-measurement misfit is often termed "structural noise". It refers to imperfections that accompany model-generated quantities that are an outcome of the approximate nature of the model as a simulator of real-world processes.

From their study of the origins and ramifications of structural noise, Doherty and Welter (2010) and White et al. (2014) concluded that unless the calibration process reflects its presence, structural noise can inflict unquantifiable bias on model parameters, and on predictions that are sensitive to these parameters. Ideally, as is discussed by Cooley and Christensen (2006), a weighting strategy should be adopted that reflects the sum of measurement and structural noise. However, this is not possible in practice because of the indeterminate statistical character of structural noise, and because the covariance matrix of structural noise (even if it could be determined) is highly correlated and quite probably singular.

Doherty and Welter (2010) and White et al. (2014) demonstrate, however, that alternative, more heuristic, and more easily implemented weighting strategies can be just as effective in accommodating the effects of structural noise on the calibration process. The advice that they provide was adopted for setting weights used by the UWIR 2019 model. It can be summarised as follows:

- Formulate a multi-component objective function. This objective function should include raw measurements, as well as measurements that are processed (often by differencing) in a way that grants some immunity from structural noise. The total calibration dataset should then be subdivided into different observation groups. If possible, this subdivision should be such that each measurement group informs different suites of parameters and/or is pertinent to different aspects of a system's behaviour.

- Within each observation group, ensure that relative observation weighting reflects relative observation credibility. Lack of observation credibility can be an outcome of measurement and/or structural noise. In general, the weight ascribed to each observation should be inversely proportional to the standard deviation of noise/error that may afflict that observation.
- Ensure that, at the beginning of the inversion process, the (measurement) objective function is not dominated by any observation group, and that no observation group is "invisible" to the total objective function because it is dominated by other groups. An easy way to achieve this is to adjust inter-group weighting (while maintaining intra-group weighting relativity based on observation credibility) such that the contribution of each observation group to the total objective function at the beginning of the inversion process is approximately equal.

Relative weighting applied to observation groups which are comprised of heads and head differences is now addressed in sections 5.4.7.2 to 5.4.7.5. This will be followed by a brief discussion in section 5.4.7.6 of weighting strategies adopted for observations related to coal-bearing units for the transient calibration stage. The total composition of the calibration dataset is then reviewed in section 5.4.7.7.

5.4.7.2 Reliability of monitoring facilities

Head measurements employed in the 1947 and 1995 steady state and transient components of the calibration dataset are each assigned an observation weight that is based on a reliability index assigned to each monitoring facility. (This was not applied to the 1995 steady state water level targets ascribed to the Condamine and Main Range Volcanics for the maintenance of drain elevation levels; the relative weightings of these targets were set to unity). This index was calculated by OGIA and reflects the fidelity of head measurements associated with each facility, which depends on factors such as the facility construction type, confidence in its attribution to a stratigraphic unit and the quality of its head measurement records.

Weights ascribed to the head observations in the calibration dataset rely on a classification of the monitoring points according to the overall percentile rank of its reliability index. The percentile rank for each monitoring point defines the percentage of monitoring points that have an equal or lower reliability index. For the purpose of observation weight assignment, percentile ranks were subdivided into 20 classes (see Table 5-9). The reliability of a head observation decreases with increasing percentile rank. Hence, a linear weighting scheme by Stillwell et al. (1981) was adopted, using:

$$w_r = \frac{(n+1-r)}{n} \tag{5.3}$$

where:

w_r is the reliability weight for an observation;

r is the class index of the percentile rank for an observation; and

n is the number of classes.

Table 5-9 provides the weighting scheme employed for percentile rankings of the bore reliability index.

Table 5-9 Linear weighting scheme for percentile rankings of the bore reliability index

Percentile rank	Rank class	Linear weighting
0	1	1.000
0.1	2	0.950
:	:	:
1	20	0.050

5.4.7.3 Degree of departure from steady state

As described in section 5.4.3, a series of calculations were carried out in order to assess whether groundwater head observations used in the 1947 and 1995 steady state simulations are likely to reflect steady state conditions. This process returned a *ΔH* estimate for each head measurement comprising the calibration dataset defining the difference between steady state and transient simulated heads for 1947 and 1995. Groundwater head observations were subsequently divided into penalty and traditional groups accordingly.

Each observation, regardless of the sub-group to which it was assigned, was also weighted according to its associated *ΔH*. Similar to the calculation of weights based on monitoring point reliability, 15 rank classes were adopted after inspection of the probability distribution for steady-state discrepancies, where a higher rank class pertains to head measurements that are less reflective of steady-state conditions. The weight associated with each class was calculated using equation 5.3. The outcomes are listed in Table 5-10.

Table 5-10 Linear weighting scheme for steady state discrepancy

Steady state discrepancy (m)	Rank class	Linear weighting
0	1	1.000
0.5	2	0.933
1.0	3	0.867
1.5	4	0.800
2.0	5	0.733
2.5	6	0.667
3.0	7	0.600
3.5	8	0.533
4.0	9	0.467
4.5	10	0.400
5.0	11	0.333
7.5	12	0.267
10.0	13	0.200
25.0	14	0.133
50.0	15	0.067

5.4.7.4 Measurements in outcrop areas

In addition to the weight assignment of head measurements based on monitoring point reliability and steady-state, lower weights were also assigned to head observations within outcrop areas. This recognises the fact that these measurements are more informative of shallow groundwater processes that are not well-simulated by the UWIR 2019 model. Weights for outcrop observations were reduced by a factor 10.

5.4.7.5 Final combined weight

Final weights were assigned to each water level observation pertaining to the 1947 and 1995 steady state and the transient simulation by combining the three weighting components described in the preceding sections using the following equation.

$$w_t = \frac{(w_r + w_s)}{2\omega}$$

(5.4)

where:

w_t is the total weight for an observation;

w_r is the reliability weight for an observation (see section 5.4.7.1);

w_s is the steady state discrepancy weight for an observation (see section 5.4.7.3); and

ω is the outcrop index of an observation , this being 10 for outcrop and 1 for non-outcrop (see section 5.4.7.4);

Weight statistics for observation datasets ascribed to the 1947 and 1995 steady state and transient simulations are listed in Table 5-11. The higher mean and median estimated weight values for the 1947 steady state simulation reflect the generally lower degree of departure from steady state for members of this group.

Table 5-11 Statistics of observation weights for the steady state observation components following application of equation 5.7

Calibration period	Total weight, w_t			
	Min	Max	Mean	Median
1947 steady state (pre-development)	0.053	1.0	0.48	0.56
1995 steady state (pre-CSG)	0.014	1.0	0.36	0.35
1995 to 2017 transient simulation	0.006	1.0	0.51	0.40

Observations of vertical steady state head difference discussed in section 5.4.5.3 were also weighted according to their reliability score using equation 5.3. All observations belonging to other steady state groups were ascribed a relative weight of 1.0.

All observations comprising other observation groups assigned to the transient simulation were given a weight of 1.0, except where relative intra-group weighting was calculated using an approach specific to an observation group in ways discussed in the next section.

5.4.7.6 Observation weights in coal-bearing units for transient calibration

Two observation groups for coal-bearing units employed in the transient calibration utilised different relative weights for observations within the group. These groups were CSG water production and vertical head differences.

In formulating the CSG water production component of the objective function, relative weights assigned to these observations were inversely proportional to the volumes themselves. Since this can lead to very high relative weights being associated with low flow volumes thresholds of 50 ML/yr for formation-scale water production and 20 ML/yr for water production in individual development areas were also applied such that weights of 1 were applied to all flows below these values.

Similarly for the observation group pertaining to vertical head differences in the coal-bearing units, relative weights were calculated under the assumption that errors in "observed" vertical head differences are proportional to the differences themselves. The following equation was employed:

$$\frac{1}{w} = \varepsilon_{\mathrm{dH/dz}} \cdot (\mathrm{z_{w\_top}} - \mathrm{z_{w\_bot}}) \qquad (5.5)\ \frac{1}{\mathrm{w_i}} = \varepsilon_{\mathrm{dH/dz}} \cdot (\mathrm{z_{w\_top}}\text{-}\mathrm{z_{w\_bot}})$$

where:

w is the relative weight associated with a particular head difference; and

$\varepsilon_{dh/dz}$ is an error term.

Values for $\varepsilon_{dh/dz}$ are assumed to be 0.05 for the Walloon Coal Measures and 0.1 for the Bandanna Formation. A larger error term is assumed for the Bandanna Formation than for the Walloon Coal Measures as no detailed reservoir simulations were available to OGIA for this formation.

5.4.7.7 Weighting data of different types

Observations comprising the entirety of the calibration dataset were divided into the 138 observation groups as specified in Table 5-12. Group subdivision is based on observation type and the simulation with which the observations are associated. For head observations, groups are further divided according to the model layers to which the observations pertain. Observation weights were the same for all measurements within each observation group except where previously noted.

Table 5-12 Number of observation groups for each observation type

Observation type	Simulation	Number of observation groups
Groundwater heads (section 5.4.4.1)	1947 steady state	18
Parallel flow to western GHB (section 5.4.4.2)	1947 steady state	14
Groundwater heads - Traditional group (section 5.4.5.2)	1995 steady state	24
Groundwater heads - Penalty group (section 5.4.5.2)	1995 steady state	20
Groundwater heads – Condamine (section 5.4.5.1)	1995 steady state	1
Groundwater heads - Main Range Volcanics (section 5.4.5.1)	1995 steady state	1
Vertical head differences (section 5.4.5.3)	1995 steady state	2
Condamine water flux exchange (section 5.4.5.4)	1995 steady state	1
Net "extraction" – Condamine (section 5.4.5.5)	1995 steady state	1
Net "extraction" - Main Range Volcanics (section 5.4.5.5)	1995 steady state	1
CSG water extraction rates (section 5.4.6.2)	Transient	4
CSG water re-injection rates (section 5.4.6.6)	Transient	3
Non-CSG water extraction rates (section 5.4.6.1)	Transient	7

Observation type	Simulation	Number of observation groups
Vertical head differences (section 5.4.6.5)	Transient	6
Predicted water saturation and vertical head differences in coal-bearing units (section 5.4.6.8)	Transient	3
Predicted reservoir pressures (section 5.4.6.9)	Transient	4
Groundwater heads (section 5.4.6.3)	Transient	14
Groundwater head change (section 5.4.6.4)	Transient	14
Total		**138**

Prior to the commencement of the calibration process, a weight multiplier was applied to each observation group such that the contribution made to the total measurement objective function by each group was the same. This provides equal visibility to the different observation groups that are likely informative of different parameter types employed by the UWIR 2019 model.

5.5 Parameterisation devices

In most cases calibration has been undertaken using pilot points at the primary calibration device, as described below in section 5.5.1 such that modelled parameters can be endowed with spatial variability. In other cases, in particular layers which are highly unlikely to be affected by P&G activities and for which there is generally only very limited data, zonal or layer wide parameters are defined as outlined in section 5.5.2.

5.5.1 Pilot point parameters

5.5.1.1 General

Pilot points allow representation of hydraulic property variability at a spatial density that is sufficiently high for realisation of the benefits offered by a highly-parameterised regularised inversion process. Values of pertinent hydraulic property values are estimated at the user-defined locations of these points. Hydraulic property values are then assigned to the cells comprising the model grid through spatial interpolation from those points. A more detailed description of this parameterisation device in groundwater model calibration is provided in Doherty (2003).

5.5.1.2 Advantages of using many pilot points

In calibration of a spatial model, a high level of parameterisation has the benefit of introducing heterogeneity to a model domain at locations where its existence can be inferred from the calibration dataset. At the same time, use of Tikhonov regularisation suppresses the emergence of heterogeneity at those locations where its existence cannot be justified on the basis of the calibration dataset. If properly applied, Tikhonov regularisation also constrains heterogeneity to emerge in ways that are geologically plausible.

A highly parameterised and appropriately regularised approach to inversion therefore supports the estimation of parameter fields that reflect, as much as possible, the information content of the calibration dataset in geologically meaningful ways. This, in turn, assists the process in achieving a solution to the inverse problem of model calibration that approaches that of minimum error variance. As stated in section 5.2 however, the estimated parameter field will therefore constitute a simplified representation of the true, but unknown, hydraulic property field that prevails in the real world. The use of many parameters supports exploration of other parameterisation possibilities that, on the one hand, allow the model to fit the calibration dataset, and on the other hand express geologically

realistic, but inestimable, heterogeneity. This can be achieved using methods such as the null space Monte Carlo method supported by PEST.

5.5.1.3 Parameter types

As was discussed in preceding sections, calibration of the UWIR 2019 model was effected by matching model outputs generated over three simulation stages to corresponding field measurements and “penalty observations” which collectively comprised the calibration dataset. Two of these simulation stages were steady state while the third was transient. The “model” as run by PEST comprised all of these simulations. Many parameters were estimated collectively on the basis of these three simulations. The following parameters, employed in both the steady state and transient simulations, were represented using pilot points:

- horizontal and vertical hydraulic conductivity (section 5.5.1.5)
- vertical anisotropy (Condamine Alluvium and permeameter layers, section 5.5.1.6)
- horizontal hydraulic conductivity multipliers for the Condamine Alluvium and other surficial units (section 5.5.1.7)
- vertical "resistance" multipliers for the transition zone (section 5.5.1.8)
- vertical hydraulic conductivity multipliers for the Walloon Coal Measures non-productive zone
- heads assigned to the GHB conditions along the western limit of the model and conductances assigned to GHB conditions along the southern limit of the model (section 5.5.1.9)

The following parameters, employed only in the transient simulation, were also represented using pilot points:

- specific storage, coal cleat compressibility and porosity (section 5.5.1.10)
- Brooks-Corey relative permeability parameters (CSG reservoir layers only, section 5.5.1.11)
- “enhanced hydraulic conductivity” used for the CSG drain conductance calculation (CSG reservoir and lower Springbok layers, section 5.5.1.12)

5.5.1.4 Pilot point interpolation

Values for head and conductance at GHB-specific pilot points were linearly interpolated to cells along the western and southern boundaries of the UWIR 2019 model domain to which these boundary conditions were assigned using OGIA-developed software. Values for hydraulic properties of all other types associated with pilot points were spatially interpolated to the model grid using the PLPROC parameter list processor developed by Doherty (2018). Interpolation was effected using the *inverse multi-quadratic* radial basis function with a value for "epsilon" calculated as the reciprocal of 0.8 times the distance between each pilot point and its nearest neighbour.

The radial basis function interpolation process was applied to the logs of hydraulic properties rather than to their native values. All pilot points were positioned at model cell centres. The spatial distribution of pilot points associated with each layer of the UWIR 2019 model was sufficient to ensure full coverage of that layer. The same applied to pilot points associated with GHB conditions.

5.5.1.5 Hydraulic conductivity pilot points

For permeameter layers in the Surat Basin, as well as coal-bearing layers within the Bowen Basin, both horizontal hydraulic conductivity and vertical anisotropy were parameterised using pilot points; the values of these pilot point parameters were adjusted through the calibration process. The vertical

hydraulic conductivity associated with a cell was calculated from its horizontal hydraulic conductivity through division by its vertical anisotropy field; the latter was configured to have a lower bound of 1.0.

A less parameter-intensive approach to calibration was adopted for the remaining model layers. If groundwater flow in a model layer is primarily horizontal as an outcome of its high hydraulic conductivity relative to overlying and underlying layers, then it is considered to be "aquifer-dominant". Layers with low vertical conductivity are denoted as "aquitard dominant", as their primary hydrogeological role is to restrict movement of water between aquifer dominant layers.

Pilot points were used to parameterise horizontal hydraulic conductivity in aquifer-dominant layers, and vertical hydraulic conductivity in aquitard dominant layers. In both cases, the non-dominant hydraulic conductivity was calculated from the dominant hydraulic conductivity using a uniform layer-wide value of vertical anisotropy ratio. This latter, layer-specific parameter was adjusted during the calibration process wherein it was constrained to adopt a value greater than 1. Layer designations as aquifer-dominant or aquitard-dominant are provided in Table 5-13.

Table 5-13 "Aquifer-dominant" (K_h) or "aquitard-dominant" (K_v) designation of non-coal-bearing and non-permeameter model layers

Stratigraphic unit(s)	Model layer	Dominant K type
Non-Condamine Alluvium	1	K_h
Main Range Volcanics	1	K_h
Other Basalt	1	K_h
Cenozoic Sediments	1	K_h
Weathered Surat or Bowen	1	K_h
Upper Cretaceous	2	K_v
Wallumbilla Formation	3	K_h
Bungil Formation	4	K_h
Mooga Sandstone	5	K_h
Orallo Formation	6	K_v
Gubberamunda Sandstone	7	K_h
Moolayember Formation	24	K_v
Clematis Sandstone	25	K_h
Rewan Group	26	K_v
Undifferentiated Bowen Basin strata	30	K_v
Undifferentiated Bowen Basin strata	34	K_v

Most of the pilot points used for parameterisation of the UWIR 2019 model were emplaced on a 21 km grid (note: pilot point spacing was 30 km for the UWIR 2016 model). This achieved a coverage that is satisfactorily dense while remaining numerically manageable. However pilot points ascribed to the surficial units comprising model layer 1 (excluding the Condamine Alluvium) were more closely spaced at 15 km due to the highly variable spatial extents of these stratigraphic units.

Separate suites of pilot points were generally used for parameterisation of each coal measure layer. These are layers 11 to 16 (Walloon Coal Measures), layers 28 and 29 (Bandanna Formation) and layers 32 and 33 (Cattle Creek Formation). However, the three model layers comprising the middle Walloon Coal Measures were assumed to be vertically homogeneous; a single set of pilot points was therefore required for each of the horizontal and vertical hydraulic conductivities of these three layers.

The locations of pilot points used to represent horizontal and vertical hydraulic conductivity in applicable model layers are shown in Appendix D1 and Appendix D2 respectively.

Initial (i.e. pre-calibration) values of horizontal hydraulic conductivity and vertical anisotropy at pilot point locations in permeameter layers (i.e. layers 8 to 23 of the UWIR 2019 model but excluding the Boxvale Sandstone layer 21) were populated directly using the median of the 20 numerical permeameter test results available at each location (section 4.2). For layers where additional pilot points have been added at a spacing of less than 21 km, initial values were derived from least squares interpolation from the permeameter grid to the locations of each pilot point.

In non-permeameter layers initial values of horizontal or vertical hydraulic conductivity (depending on whether the layer is aquifer or aquitard dominant) were calculated in the manner described in section 4.3.

Parameters adjusted by PEST during calibration of the UWIR 2019 model were constrained to lie between appropriate upper and lower bounds. For permeameter layers, upper and lower bounds for pilot point horizontal hydraulic conductivities were typically obtained through spatial interpolation of highest and lowest realisations of upscaled hydraulic conductivity throughout the numerical permeameter grid to the locations of pilot points. As discussed in section 4.4.3 upper bound horizontal hydraulic conductivity values for the Hutton Sandstone (layers 18 and 19), Boxvale Sandstone (layer 25) and Clematis Sandstone (layer 25) were increased to 10 m/d. The upper bound horizontal hydraulic conductivity values for the Precipice Sandstone was increased to 100 m/d (section 4.4.2), since there is evidence that the numerical permeameter derived upper bounds for these major aquifers may be too low.

The bounds applied to horizontal hydraulic conductivity in non-permeameter, non-coal-bearing layers were derived from core and DST results, as well as from previous modelling investigations. They were also informed by bounds determined using numerical permeameters in geologically similar layers. Further information on the upper and lower parameter bounds and how these were derived for individual layers is provided in Table E1-1 and Table E1-2 (Appendix E1).

5.5.1.6 Vertical anisotropy pilot points

To provide the parameterisation flexibility necessary for fitting the multitude of observation targets which directly or indirectly pertain to the Condamine Alluvium, vertical anisotropy of the Condamine Alluvium (as well as horizontal hydraulic conductivity multipliers described in section 5.5.1.7) was parameterised using 88 pilot points disposed on a uniform 9 km grid; see Appendix D3 for their locations. Initial values of vertical anisotropy were set to 1.0 for consistency with the Condamine Model. Vertical anisotropy values were constrained to lie between 1 and 100. Meanwhile vertical hydraulic conductivities calculated by dividing horizontal hydraulic conductivity by vertical anisotropy were limited to the range provided in Table E1-2 of Appendix E1.

For permeameter layers in the Walloon Coal Measures, as well as coal-bearing layers in the Bowen Basin, the same set of pilot points that were used for parameterisation of hydraulic conductivity (see Appendix D1) were also used for parameterisation of vertical anisotropy. In permeameter layers, initial values of vertical anisotropy were obtained through least-squares interpolation from the permeameter grid. For the Bandanna and Cattle Creek formations, values were obtained in the manner described in section 4.3.3.

In permeameter layers, upper and lower bounds for pilot point vertical anisotropies were obtained through direct sampling or least-squares interpolation of maximum and minimum realisations of permeameter vertical anisotropies to pilot point locations. In the Bandanna and Cattle Creek formations a range of 10 to 8,432 was imposed on pilot point vertical anisotropies. See Table 5-14 for

the estimable range of pilot point vertical anisotropy for pertinent model layers. After interpolation of pilot point vertical anisotropies to the model grid (implemented using the PLPROC utility, as described above), vertical hydraulic conductivity is calculated on a cell-by-cell basis by dividing horizontal hydraulic conductivity by vertical hydraulic conductivity. The cell-by-cell bounds imposed on thus-calculated vertical hydraulic conductivities are provided in Table E1-2 of Appendix E1.

Table 5-14 Upper and lower parameter bounds imposed on pilot point vertical anisotropies during the calibration process

Stratigraphic unit	Model layer	Lower bound for vertical anisotropy	Upper bound for vertical anisotropy
Condamine Alluvium	1	1	100
Westbourne Formation	8	183	3,369
Upper Springbok Sandstone	9	624	9,550
Lower Springbok Sandstone	10	31	1,455
Walloon Coal Measures non-productive zone	11	10	7,300
Upper Walloon Coal Measures	12	229	88,955
Middle 1 Walloon Coal Measures	13	406	343,564
Middle 2 Walloon Coal Measures	14	406	343,564
Middle 3 Walloon Coal Measures	15	406	343,564
Lower Walloon Coal Measures	16	532	1,138,803
Durabilla Formation	17	200	5,061
Upper Hutton Sandstone	18	741	38,994
Lower Hutton Sandstone	19	1268	27,797
Upper Evergreen Formation	20	253	8,432
Boxvale Sandstone	21	1068	8,432
Lower Evergreen Formation	22	253	8,432
Precipice Sandstone	23	34	12,363
Bandanna Formation non-productive zone	27	10	8,432
Upper Bandanna Formation	28	10	8,432
Lower Bandanna Formation	29	10	8,432
Cattle Creek Formation non-productive zone	31	10	8,432
Upper Cattle Creek Formation	32	10	8,432
Lower Cattle Creek Formation	33	10	8,432

5.5.1.7 Hydraulic conductivity multiplier pilot points, Condamine Alluvium

As has been described in section 4.3.3, initial values for horizontal hydraulic conductivity of the Condamine Alluvium employed by the UWIR 2019 model were transferred directly to the UWIR model grid from that of the Condamine Model. These values were then subject to calibration adjustment through multiplication by a cell-based multiplier field derived from PLPROC interpolation to the grid of the UWIR 2019 model from a set of 88 pilot points arranged on a regular 9 km grid over the footprint of the Condamine Alluvium (see Appendix D3). Initial values for pilot point multiplier parameters were uniformly 1.0. Lower and upper bounds of 0.01 and 10.0 were imposed on pilot point multipliers. Post-multiplication cell-by-cell horizontal hydraulic conductivities were constrained to lie in the range provided in Table E1-1 of Appendix E1.

5.5.1.8 Transition zone resistance pilot points, Condamine Alluvium

As described in section 4.3.1, the transition zone at the base of the Condamine Alluvium was parameterised using spatially variable resistance. Resistance values were ascribed to 88 pilot points arranged on a regular 9 km grid over the footprint of the Condamine Alluvium; see Appendix D3. Initial values of vertical resistance were attributed to pilot points in the manner described in section 4.3.1. In

areas where the transition zone exists, cell-by-cell resistances interpolated by PLPROC from pilot points are used to calculate cell-by-cell vertical hydraulic conductivities using equation 4.10. Alternatively, where the transition zone is absent, a cell in the transition zone layer of the UWIR 2019 model is assigned the same vertical (and horizontal) hydraulic conductivity value as that associated with the Condamine Alluvium cell immediately above it. Recognising that the extent and thickness of the transition zone is somewhat uncertain the hydraulic properties of cells in areas where the transition zone is absent are allowed to vary during model calibration within the same specified bounds in the same way as the rest of the transition zone.

5.5.1.9 General head boundary pilot point specifications

The western and southern GHBs of the UWIR 2019 model were parameterised using pilot points located along the first column and last row respectively of the model at a uniform spacing of 9 km. GHB pilot points, like the GHBs themselves, were placed only in aquifer-dominant and/or coal-bearing model layers. The disposition of pilot points was consistent for each layer, subject to the lateral extent of each unit represented therein. A total of 353 pilot point parameters were estimated for the western GHB and a total of 274 pilot point parameters were estimated for the southern GHB. The GHB pilot point locations are shown in Appendix D4.

Each pilot point associated with the western GHB was assigned a head value representing a notional groundwater level at some distance to the west of the boundary itself. These heads were based on those calculated by the UWIR 2012 model along its western boundary. Conductance values assigned to these GHBs were not adjusted from those calculated using the methodology described in section 3.2.4.2.

Pilot point conductances for the southern GHB were also estimated through the calibration process. An initial value of 1.0E-3 m^2/d were assigned to all of these, as an outcome of an initial calibration exercise based on the 1947 steady state component of the calibration dataset. Bounds imposed on estimated GHB conductances during the calibration process were effectively infinite.

5.5.1.10 Storage pilot points

Pilot points were also used to parameterise specific storage in the following stratigraphic units:

- Westbourne Formation (layer 8),
- Springbok Sandstone (layers 9 and 10)
- Walloon non-productive zone (layer 11)
- Durabilla Formation (layer 17)
- Hutton Sandstone (layers 18 and 19)
- Precipice Sandstone (layer 23).

In comparison to the parameterisation of hydraulic conductivity, a lower density of pilot points was applied for specific storage parameters, using a spacing of 21 kilometres. Initial values and ranges of these pilot points are based on the stochastic storage calculations analysis described in section 4.5.2.2.

Storage properties for the mobile domain of Walloon Coal Measures layers also make reference to pilot points for two sub-parameters, namely coal cleat compressibility and coal porosity for the mobile domain of Walloon Coal Measure layers from which CSG extraction takes place. Coal porosity determines the specific yield of the mobile domain and its specific storage is calculated using equation 4.13. The lower and upper bounds imposed on coal cleat compressibility were 2.90E-09 to 3.63E-07 $m^2.N^{-1}$ while those imposed on porosity were 0.1% to 5% respectively.

Similarly tor the Bandanna Formation pilot points were used to parameterise coal porosity, whereas a layer-wide multiplier was used to estimate its specific storage. Storage property parameterisation for the Cattle Creek Formation included estimation of layer-wide coal porosity and specific storage multiplier.

Similar layer-wide specific storage multipliers were estimated for all other model layers and applied to preserve the depth relationship of the initial parameter values (see section 4.5.2.3). Specific storage multipliers were assigned a range of 0.1 to 10. All specific storage values were subject to an upper bound of 1.3E-5 m^{-1} (Rau et al., 2018).

5.5.1.11 Brooks-Corey parameter pilot points

Pilot points were also used for parameterisation of the Brooks-Corey relative permeability relationship for the Walloon Coal Measures and Bandanna Formation. More specifically, the exponent *n* in equation 4.27 was estimated, which determines the rate of decrease of hydraulic conductivity with decreasing water saturation in a model cell. As noted previously in section 4.6.3 initial values of the Brooks-Corey exponent *n* were set based on previous modelling results at the upper range of values employed in various gas company reservoir models. Parameter bounds of 1 and 8.5 were adopted for calibration. Where the lower bound value results in a linear relationship between relative permeability and the upper bound being the maximum value that could be accommodated without serious degradation of model run-time performance. For the Cattle Creek Formation a single layer-wide value of *n* was estimated, adopting these same bounds during calibration.

5.5.1.12 Enhanced hydraulic conductivity pilot points

In addition to regional-scale hydraulic conductivity, “enhanced hydraulic conductivity” is estimated to compute CSG drain conductances using equation 4.28. As described in section 4.6.4, this parameter represents the local hydraulic conductivity of coal measures that are connected to a CSG well. As discussed previously initial values for this parameter are based on permeability-depth relationships inferred from available DSTs. Pilot point based multipliers were used to estimate enhanced hydraulic conductivity in the Walloon Coal Measures and Bandanna Formation. Multiplier values were allowed to range from 1.0E-03 to 1.0E+03 during calibration. Layer wide multipliers were estimated for the Cattle Creek Formation.

5.5.2 Zonal and layer-specific parameters

5.5.2.1 Parameter types

Parameter types that are either layer-wide or specified using zones of piecewise constancy are as follows:

- vertical anisotropy non permeameter layers (section 5.5.2.2)
- recharge multipliers (section 5.5.2.3)
- width of fault cores and associated damage zones (section 5.5.2.4)
- a DDFTR-to-Kv-adjustment-factor (section 0)
- Brooks-Corey parameters and enhanced hydraulic conductivity for the Cattle Creek Formation (section 0).

5.5.2.2 Vertical anisotropy non-permeameter layers

As previously discussed, non-permeameter layers were assigned a single layer-wide value of vertical anisotropy. The non-dominant hydraulic conductivity was computed from the dominant hydraulic conductivity on a cell-by-cell basis using this single, layer-specific value of vertical anisotropy. Meanwhile the dominant hydraulic conductivity was parameterised using pilot points.

Initial values for layer-wide vertical anisotropy for non-permeameter layers were listed previously in Table 4-2. Bounds on layer-wide vertical anisotropies imposed during the calibration process are given in Table 5-15. The upper bound of 100 for the non-Condamine Alluvium encapsulates the calibrated vertical anisotropy of 97 employed by the UWIR 2012 model. The upper bound of 500 for the Main Range Volcanics and other basalts accommodates the layered sequencing of high-permeability weathered units and low-permeability fresher units that comprise this single model layer. Upper bounds for the remaining layers broadly reflect the range of anisotropy values calculated for the Upper Springbok and Evergreen units using numerical permeameters; these units were taken as proxies for non-permeameter Surat Basin layers and Bowen Basin layers respectively.

Table 5-15 Upper and lower bounds for vertical anisotropy ratios employed in the calibration process.

Stratigraphic unit(s)	Model layer	Lower bound for vertical anisotropy	Upper bound for vertical anisotropy
Non-Condamine Alluvium	1	1	100
Main Range Volcanics	1	1	500
Other Basalt	1	1	500
Cenozoic Sediments	1	10	10,000
Weathered Surat or Bowen	1	10	10,000
Upper Cretaceous	2	10	10,000
Wallumbilla Formation	3	10	10,000
Bungil Formation	4	10	10,000
Mooga Sandstone	5	10	10,000
Orallo Formation	6	10	10,000
Gubberamunda Sandstone	7	10	10,000
Moolayember Formation	24	10	8,432
Clematis Sandstone	25	10	8,432
Rewan Group	26	10	8,432
Undifferentiated Bowen Basin strata	30	10	8,432
Undifferentiated Bowen Basin strata	34	10	8,432

5.5.2.3 Recharge multipliers

The manner in which estimates of average recharge over the outcrop areas of different stratigraphic units were obtained is described in section 3.3.1. Recharge shows spatial variation over the area of each outcropping unit because of variation in long-term average rainfall over each such outcrop zone. However, the “leaching fraction”, that is, the ratio of recharge to rainfall, is constant over each zone. In order to support adjustment of recharge during the model calibration process, a spatially invariant multiplier was applied to recharge over each outcrop zone. Its initial value was set to 1.0. Lower and upper bounds for most of these zone-specific multipliers were set to 0.1 and 2.0 respectively.

A smaller adjustment range was allowed for the recharge multiplier applied to the Condamine Alluvium, this reflecting its inheritance from the Condamine Alluvium model (KCB, 2011) model. Recharge multipliers for other alluvia were provided with a lower bound of 0.5 to prevent estimation of

unrealistically low recharge values. An upper bound of 3.3 was imposed on the recharge multiplier for the Main Range Volcanics; this allowed recharge to be as high as 25 mm/yr in accordance with estimates provided by the Murray Darling Basin Authority (MDBA) Basin Plan for this unit.

Pre-calibration rates of steady state recharge over stratigraphic unit outcrop zone are provided in Table 3-3. Lower and upper bounds for the 24 zonal recharge multipliers associated with each zone are listed in Table 5-16.

Table 5-16 Bounds for zonal multipliers of steady state recharge employed in the calibration process

Formation outcrop	Model layer(s)	Recharge zone number	Lower bound for recharge multiplier	Upper bound for recharge multiplier
Condamine Alluvium	1	3	0.9	1.1
Non-Condamine Alluvium	1	5	0.5	2.0
Main Range Volcanics	1	4	0.1	3.3
Other Basalt	1	1	0.1	3.3
Cenozoic Sediments	1	2	0.1	2.0
Weathered Surat or Basalt	1	6	0.1	2.0
Upper Cretaceous	2	7	0.1	2.0
Wallumbilla Formation	3	8	0.1	2.0
Bungil Formation	4	9	0.1	2.0
Mooga Sandstone	5	10	0.1	2.0
Orallo Formation	6	11	0.1	2.0
Gubberamunda Sandstone	7	12	0.1	2.0
Westbourne Formation	8	13	0.1	2.0
Springbok Sandstone	9 – 10	14	0.1	2.0
Walloon Coal Measures	11 – 16	15	0.1	2.0
Durabilla Formation	17	16	0.1	2.0
Hutton Sandstone	18 – 19	17	0.1	2.0
Evergreen Formation	20 and 22	18	0.1	2.0
Boxvale Sandstone	21	NA	NA	NA
Precipice Sandstone	23	19	0.1	2.0
Moolayember Formation	24	20	0.1	2.0
Clematis Sandstone	25	21	0.1	2.0
Rewan Group	26	22	0.1	2.0
Bandanna Formation	27 – 29	23	0.1	2.0
Undifferentiated lower Bowen Basin strata	30 and 34	24	0.1	2.0
Cattle Creek Formation	31 – 33	NA	NA	NA

Note:
Layers 21, 31 to 33 which represent the Boxvale Sandstone and the Cattle Creek Formation are not present at outcrop.

Additional regularisation constraints were applied to recharge multipliers as they were adjusted during the calibration process such that the following relationships between steady state recharge rates in different zones were preferred:

- recharge to the Westbourne Formation outcrop was less than that applied to the adjacent outcrop areas of the Gubberamunda Sandstone and Springbok Sandstone
- recharge to the outcrop of the Durabilla Formation was less than that applied to the Walloon Coal Measures and the Hutton Sandstone

- recharge to the Evergreen Formation was less than that to the adjacent Hutton and Precipice sandstones
- recharge to the Moolayember Formation was less than recharge to the adjacent Precipice and Clematis sandstones
- recharge to the Rewan Group was less than recharge to the adjacent Clematis Sandstone and Bandanna Formation.

As was explained in section 3.3.1, recharge time series applied to different outcrop zones during the transient simulation are normalised so that their average values are in accordance with steady state estimates of recharge for the same zones.

5.5.2.4 Fault specifications

As discussed previously in section 2.5, layer displacement and the allied modification of inter- and intra-layer connections along the fault planes are not the only mechanisms by which faults may influence regional groundwater flow patterns. The potential for enhanced cross-fault resistance arising from the smearing of fault-entrained material and enhanced vertical conductivity within the damage zone adjacent to the fault have also been incorporated.

The initial fault widths were set to a maximum of 2 m for the most laterally extensive fault (the Hutton-Wallumbilla, Figure 3-6) and reduced linearly to 0.5 m for the shortest modelled fault (Leichhardt - South). The associated damage zone for each fault was initially set as four times its fault width. No variation of these properties was assumed along the fault. Table 5-17 summarises the initial fault core and damage zones widths for each fault represented in the regional model.

During calibration, the lower bounds ascribed to each fault core width and damage zone width were set such that each fault could, if necessary to fit the observation dataset, be parameterised such that was no increase in lateral cross-fault resistance or enhancement of vertical hydraulic conductivity was introduced, over and above the effects of the modelled layer displacements. Conversely, the maximum allowable widths of the fault core and damage zones were assumed to be 10 m and 20 m respectively. Thus, a total of 44 parameters (22 fault widths and 22 damage zone widths) were included in the calibration process for regionally represented faults.

Table 5-17 Initial values of regional fault parameters which are calibrated in the UWIR 2019 model

Fault	Initial fault core width (m)	Initial damage zone width (m)
Horrane	0.71	2.86
Wallumbilla	2.00	8.00
Bullaroo	0.71	2.86
"Fault 10"	0.68	2.73
Injune	0.78	3.12
Merivale	1.40	5.59
Arbroath - West	0.75	2.99
Consuelo	0.76	3.05
Burunga - South	0.86	3.45
Wambo	1.23	4.9
Leichardt - Central	0.66	2.66

Fault	Initial fault core width (m)	Initial damage zone width (m)
Cockatoo	1.16	4.64
Arbroath - East	0.76	3.02
Leichhardt - North	0.58	2.33
Leichhardt - South	0.52	2.07
Kia Ora	0.67	2.69
Miles	0.64	2.56
Moonie Goondiwindi (s1)	0.83	3.32
Moonie Goondiwindi (s3)	0.55	2.2
Moonie Goondiwindi (s5)	0.71	2.86
Moonie North Fault	0.57	2.26
Cockatoo-Connection	0.58	2.33

5.5.2.5 Extra parameters required for coal measure layers

The transient calibration involved the estimation of a range of parameters that were integral to modelling the following processes which operate within coal-bearing strata:

- dual porosity formulation for differing hydraulic responses of coal seams and interburden material
- water desaturation in response to reduction in pressure as a proxy for dual-phase flow

Brooks-Corey exponents and enhanced hydraulic conductivity are estimated using pilot points for the Walloon Coal Measures and Bandanna Formation, see section 5.5.1.11 and section 5.5.1.12. A layer wide parameterisation approach was used to estimate both properties for the Cattle Creek Formation.

A layer-wide and zonal parameterisation was used to estimate the “dual domain flow transfer rate” or DDFTR. DDFTR is closely related to the upscaled vertical hydraulic conductivity of a coal measure layer (see equation 4.25); the latter being an adjustable parameter during the calibration process. To reflect this fact, a derived property calculated as the ratio of DDFTR to upscaled vertical hydraulic conductivity, was assigned to every pertinent coal measure cell within the domain of the UWIR 2019 model based on the initial values of DDFTR and vertical hydraulic conductivity. Another new parameter was then defined for adjustment of this property during the calibration process. This being the factor by which the initial cell-based DDFTR to upscaled vertical hydraulic conductivity ratio should be multiplied in calculating DDFTR from upscaled *kv* as the latter is adjusted through the calibration process. A value of 1.0 maintains this initial ratio. This new parameter is referred to as the “DDFTR-to-kv-adjustment-factor”.

A single, formation-wide DDFTR-to-kv-adjustment-factor was assigned to each of the upper, middle and lower Walloon Coal Measures layers. A single formation-wide DDFTR-to-kv-adjustment-factor was employed for each of the upper and lower Cattle Creek layers. For the upper and lower Bandanna Formation layers a pair of DDFTR-to-kv-adjustment-factors were employed, one pertaining to each side of the Taroom Trough. Allowable values for calibration purposes ranged from 1.0E-04 to 1.0E+04 for all coal measure layers. Note that the DDFTR value of 1.0E-02 $m^{-1}d^{-1}$ ascribed to outcrop areas was not adjusted in the calibration process.

5.6 Regularisation constraints

Calibration of the UWIR 2019 model was implemented using PEST. During this process, parameters declared as adjustable were estimated on the basis of the calibration dataset. As has already been discussed in section 5.2, model calibration constitutes an ill-posed inverse problem for which a unique solution of minimised error variance is sought. Uniqueness is achieved through the introduction of regularisation to the inverse problem solution process.

Two types of regularisation were employed in calibration of the UWIR 2019 model:

1. Subspace methods, as embodied in the LSQR solver, (Paige and Saunders 1982a, 1982b). These employ an iterative inversion technique that is widely used in geophysical data analysis. Its operation is similar to that of truncated singular value decomposition in that it separates parameter space into two orthogonal subspaces, namely the solution and null spaces. It then calculates a solution parameter set that eschews null space departures from the starting parameter set.
2. Tikhonov regularisation. This operates by seeking a solution to the inverse problem in which parameters, or functions of parameters, depart to the minimum extent possible from a user-defined preferred condition. To the extent that departures must occur in order for model outputs to fit the calibration dataset, these departures are constrained to occur in ways that are geologically plausible.

PEST implements Tikhonov regularisation by adjusting weight factors applied to sets of observations or prior information equations in which parameter constraints are defined. These weight factors are similar to Lagrange multipliers used in the solution of a constrained minimisation problem. For regularised inversion, the constrained minimisation problem is that of minimising the “regularisation objective function” subject to the constraint that the “measurement objective function” attains a user-specified value. The lower the measurement objective function, the better is the fit between model outcomes and field measurements. See Doherty (2015c) for details.

Tikhonov constraints employed in calibration of the UWIR 2019 model were as follows:

- A difference of zero was sought between the GHB conductance ascribed to each pertinent pilot point and that ascribed to its neighbour (both vertically and horizontally) along the southern model boundary of the model domain. This effectively limits spatial variation of GHB conductance to only that required to achieve calibration of the model.
- A difference of zero was sought between values of the following parameter types ascribed to neighbouring model layers:
    - the DDFTR-to-kv-adjustment-factor that governs the flow of water from interburden to coal seams during depressurisation of the latter (see section 4.6.2)
    - the Brooks-Corey exponent *n* that defines the relationship between relative permeability and water saturation (see section 4.6.3)
    - factors by which regional drain conductivities are multiplied to represent enhanced values of hydraulic conductivity in the vicinity of CSG extraction wells (see section 4.6.4).
- An inter-layer vertical difference of zero was sought between coal cleat compressibility and coal cleat porosity parameters associated with pertinent pilot points.

- All remaining parameters were assigned preferred values from which minimum departures were sought during calibration of the UWIR 2019 model. In all cases, preferred values were the same as initial values.

Covariance matrices were employed instead of weights when ascribing preferred values to all pilot points except for those representing GHB conductances. Regularisation constraints for GHB conductances were of the preferred-zero-difference type. The covariance matrix in each case embodied spatial correlation over a distance equal to about twice that between each pilot point and its nearest neighbour. Thus, to the extent that departures from preferred parameter values were required for model outputs to fit the calibration dataset, regularisation tends to smooth these departures over a number of neighbouring pilot points rather than ascribed them to individual points.

PEST allows a user to set a target measurement objective function. It will not seek a better fit than this. However, during calibrating of the UWIR 2019 model, the optimum target measurement objective function was not known in advance. Hence, PEST was instructed to minimise this function over successive iterations of the inversion process.

5.7 Singular value decomposition (SVD)

PEST uses a gradient-search algorithm which requires the computation of a Jacobian matrix in which parameter sensitives are stored. This Jacobian matrix is generated by running the model once or more for each parameter and updating the parameter values to better match simulation outputs with its observed counterparts. The sequence of computing a Jacobian matrix and updating model parameters is done in an iterative fashion as part of a model calibration exercise. With a total number of 14,016 parameters and transient model runtimes of up to 2.5 hours, the computational burden associated with calibrating the UWIR 2019 model is very large. For the calibration of the UWIR 2016 model this computational burden was reduced by splitting parameters into two groups depending on whether or not the parameter values are likely to be sensitive to observations used in the transient calibration stage. Parameters located close to transient observations were therefore included a group that required only steady-state simulations and a parameter group that required both steady-state and transient simulations (OGIA, 2016a). However, since this sub-division of parameters was undertaken based solely on their location then there is a risk that some parameters which are relatively sensitive to transient observations will have been excluded. Initially this same approach was adopted for calibration of the UWIR 2019 model. However, in an effort to improve some aspects of the calibration, all estimable parameters were included in both the dual steady-state and transient stages; numerical tractability of the inverse problem was accomplished through implementation of singular value decomposition (SVD).

SVD reduces the dimensionality of the inverse problem by splitting the parameter space into two subspaces referred to as the “null space” and the “calibration solution space”, which is spanned by pairs of orthogonal unit vectors. The unit vectors which span the calibration solution space represent combinations of parameters that are estimable on the basis of the current calibration dataset. In PEST parlance these estimable parameter combinations are referred to as “super parameters”.

As part of the calibration process of the UWIR 2019 model, SVD was applied to an initial Jacobian matrix which contained sensitivities for all estimable parameters. Creation of this initial Jacobian matrix required perturbing all 14,016 parameters and running all three calibration simulation stages. SVD on this initial Jacobian matrix yielded a number of 2,000 “super parameters”, which are

subsequently used to speed up subsequent iterations of Jacobian matrix calculation and parameter updating.

When model parameters are changed, the SVD process should ideally be repeated. To account for this, but still make use of the reduced computational burden associated with an SVD-assisted calibration of the UWIR 2019 model, SVD was repeated after each three cycles of Jacobian computation and parameter updating.

5.8 Calibration results

5.8.1 Introduction

A summary of the observations involved in the calibration process are provided in Table F1-1 and Table F1-2 of Appendix F and of parameters which are estimable based on these observations in Table F2-1 to Table F2-2. These tables contain salient information on the quantity of the various observations/parameters and the calibration simulation stage(s) in which they were applied. Calibration results relating to the version of the UWIR 2019 model which was used to generate the impact predictions described in the UWIR 2019 are provided in Appendix G. The following sections include a brief commentary on the calibration results presented in this appendix.

5.8.2 Steady state heads

5.8.2.1 General

Explanatory notes for figures summarising steady state head calibration results are as follows:

- Given that the influence of faults on steady state heads is of interest, the traces of major structural faults represented in the model have been superimposed on contour maps of calibrated heads. These plots also feature a standardised head scale for clarity of comparison between layers.
- Pilot point locations have been superimposed on spatial contour maps for horizontal and vertical hydraulic conductivity to better understand any artefacts resulting from spatial interpolation.
- Head residuals are defined as observed minus modelled values of steady state head.
- Scatter plots of modelled versus measured heads feature four classes that represent equal subdivisions of observation weights between 0 and 1.0 to emphasise the preferential fitting of higher quality information in most instances. The values of root mean square (RMS) error and scaled root mean square (SRMS) error are also annotated on these figures. The RMS statistic is calculated as follows:

$$RMS = \sqrt{\frac{1}{n}\sum_{i=1}^{n}\left(w_i\left(y_i - x_i\right)\right)^2} \qquad (5.6)$$

where:

x_i is the *i*'th term of the modelled time series;

y_i is the *i*'th term of the observed time series;

w_i. is the weight of observation *i;* and

n is the number of data points.

This statistic is also known as the fit standard error and the standard error of the regression. It is an estimate of the standard deviation of the random component in the data. An ideal fit is indicated by an RMS of 0. It is most accurate for approximately normally distributed data since it is a mean-based function.

The scaling of RMS reduces the impact of different ranges of data used during model calibration and produces a better comparison of results across different simulations. The scaled RMS (SRMS) as a percentage is calculated as follows:

$$SRMS = \frac{100RMS}{\Delta y}\% \quad (5.7)$$

where:

Δy is the range of the observed values for the entire time period of the evaluation.

SRMS ranges from 0–100%; MDBC (2001) suggests a value of less than 5% is preferable. Two different values for each of these statistics have been calculated, the first excludes the relative weights assigned to the observations (i.e. all weights equal to 1.0) and the second includes the observation weights (weights between 0 and 1.0), which is signified as RMS(w) and SRMS(w) on these plots.

5.8.2.2 1947 steady state simulation

Calibrated steady state head contours for the 1947 steady state simulation in each model layer are provided as Appendix G1.

Scatter plots of modelled versus measured heads in model layers for which observations are available are shown in Appendix G2.

Maps showing the spatial distribution of modelled head residuals in each model layer for which observations exist are provided as Appendix G3.

These outputs suggest a generally satisfactory agreement between observed and modelled groundwater levels given that a significant proportion of observation data available for this period were (i) of relatively low reliability and (ii) located in outcrop areas, with attendant reductions in observation weights. Furthermore, it should be acknowledged that observation data available for this part of the calibration process was scarce in key units such as the Springbok Sandstone, Walloon Coal Measures and Hutton Sandstone.

In most layers the SRMS errors reported for the 1947 steady state simulation in Appendix G2 are lower than those achieved during calibration of the UWIR 2016 model (OGIA, 2016c). However, data for the Gubberamunda Sandstone (Figure G2-7 and Figure G3-7) suggests a relatively poor fit especially towards the western and southern model boundaries. As shown in these figures the model typically over-estimates observed heads in these areas. One possible explanation being that observed pressures had already been affected by groundwater extraction in these areas leading to lower pressures than those simulated in the 1947 steady simulation which assumes zero extraction.

5.8.2.3 1995 steady state simulation

Calibrated steady state head contours for the 1995 steady state simulation in each model layer are provided as Appendix G4. The effect of the Moonie conventional P&G field which has been extracting from the Precipice and Evergreen at rates of up to 2 ML/d since the 1960s can be seen in the area west Moonie (Figure G4-23), although consistent with the significantly increased modelled horizontal hydraulic conductivity of the Precipice Sandstone (section 4.4.2) the impacts of this extraction are substantially less than predicted in 2016 (OGIA, 2016c).

The calibration of groundwater levels in the Condamine Alluvium and Main Range Volcanics are represented by scatter plots of observed versus modelled heads in Figure G5-1 and G5-2 of Appendix G5 respectively. These plots indicate only relatively minor under-prediction of the head targets that represent the ambient water table elevation in these areas. As intended, the 1995 steady state water levels are thereby maintained at, or just below, the imposed drainage surface.

Calibration results for heads in other modelled units are partitioned into traditional and penalty observation groups. Modelled versus measured scatter plots for each model layer of interest with respect to the traditional observation group are provided as Appendix G6. Maps showing the spatial distribution of these modelled head residuals are provided as Appendix G7.

Scatter plots of modelled versus measured steady state heads for the penalty observation group are provided as Appendix G8. Maps showing the distribution of modelled head residuals for the penalty observation group are provided as Appendix G9.

Head targets attributed to the traditional observation group (on the basis of only minor departures between simulated equilibrium heads under 1995 conditions and their transient simulated counterparts as described in section 5.4.5.2) fitted symmetrically on either side of the 1:1 line. Post-calibration, this is exemplified by the modelled versus measured scatter plot for heads in the upper Hutton Sandstone shown in Figure G6-14 of Appendix G6 where a close fit is achieved with minimal bias and a low SRMS and weighted SRMS(w) of 4.7% and 0.6% respectively.

Scatter plots for the penalty observation group included in Appendix G7 show a similar level of fit to that achieved for the traditional group reflecting that a better fit to this data was deliberately sought in the UWIR 2019 model calibration than in 2016. A relatively poor match was achieved in the UWIR 2016 model calibration to data within current CSG production areas leading to unrealistically low starting heads in the Walloon Coal Measures in many areas. Reference to Figures G9-11 to G9-16 in Appendix G9 suggests that this systematic bias towards under-prediction of heads outside of outcrop area which was present in the UWIR 2016 model calibration has been substantially reduced. Scaled RMS statistics for the upper Hutton Sandstone penalty group (which suggest a SRMS and weighted SRMS of 4.9 % and 1.8% respectively Figure G9-16, Appendix G9) are therefore similar to those for the traditional group mentioned above.

5.8.3 Parallel flow to western general head boundary

For the 1947 steady state simulation, a relatively close match was achieved between paired head difference observations of zero representing parallel flow to the western GHB and their modelled equivalents. The RMS statistic for each relevant stratigraphic unit is provided in Table 5-18.

Table 5-18 Measure of fit between paired horizontal head difference observations of zero and the modelled equivalent, by stratigraphic unit

Stratigraphic unit	Model layer	RMS (m)
Bungil Formation	4	1.71
Mooga Sandstone	5	0.97
Gubberamunda Sandstone	7	0.35
Upper Springbok Sandstone	9	0.65
Lower Springbok Sandstone	10	0.85
Upper Walloon Coal Measures	12	3.83
Middle 1 Walloon Coal Measures	13	2.01
Middle 2 Walloon Coal Measures	14	1.52
Middle 3 Walloon Coal Measures	15	1.11
Lower Walloon Coal Measures	16	0.56
Upper Hutton Sandstone	18	3.19
Lower Hutton Sandstone	19	2.20
Boxvale Sandstone	21	11.91
Precipice Sandstone	23	5.00

5.8.4 Vertical inter-aquifer head differences

Scatter plots of modelled versus measured vertical head differences for the 1995 steady state simulation for the Condamine Alluvium, Main Range Volcanics and the combined data sets respectively are shown in Figure G10-1 to Figure G10-3 of Appendix G10. The corresponding RMS statistic varies from approximately 18 m to 21 m, which is comparatively high in relation to the other observation types. Once relative weights are considered however, the RMS(w) statistic ranges between around 3 m and 16 m, with the best level of fit evident for the Main Range Volcanics. The level of fit achieved for this observation group is somewhat lower than achieved for the 2016 calibration. The reasons for this degradation are not known at this stage but may be related to the substantially increased volume and types of transient calibration data used to calibrate the UWIR 2019 model. Whilst as discussed in section 5.2 the use multiple observation types is seen as technically preferable it does inevitably lead to some competition between different observation groups and the degradation of the degree of fit that can be achieved in some cases.

5.8.5 Non-CSG extractions

Figure G11-1 in Appendix G11 shows a comparison of estimated actual and modelled total non-CSG water extraction and confirms that the targeted total non-CSG extraction from the main aquifers of interest listed in Table 5-5 are close to being achieved. Hence modelled extraction in most layers is close to 80% of the estimated actual volume. As shown Figure G11-1 at the end of the transient calibration period total modelled extraction from the Springbok Sandstone, Walloon Coal Measures, Hutton Sandstone, Boxvale Sandstone, Precipice Sandstone and Clematis Sandstone is around 21,000 ML/yr, compared to an estimated actual extraction rate of around 33,300 ML/yr and a target rate of 25,500 ML/yr. Modelled extraction is therefore around 63% of estimated actual or 82% of the target. Whilst this represents a substantial improvement on early calibration runs it is an area where further improvement could be sought during future model re-calibration exercises. In particular modelled extraction from the Hutton Sandstone at the end of December 2017 is around 8,994 ML/yr, compared to an estimated actual take from this aquifer of 15,512 ML/yr and this may be a partial explanation for the lack of trend in modelled hydrographs for the Hutton Sandstone highlighted below in section 5.8.9.

The difficulties encountered with achieving a match to this observation emphasise the need for calibration be undertaken through comparison with both head and flux observations as previously identified by Doherty and Welter (2010).

5.8.6 Condamine water flux exchange

For the 1995 steady state simulation, the modelled total groundwater inflow to the Condamine Alluvium from adjacent and underlying strata post-calibration was 10,219 ML/yr i.e. only marginally exceeding the target range outlined in section 5.4.5.4.

5.8.7 "Extractive" drain flow in the Condamine Alluvium

A comparison of the minimum "extractive" drain flow targets with their modelled equivalents for the Condamine Alluvium and 14 hydrologic zones in the Main Range Volcanics, is provided in Table 5-19 for the 1995 steady state period. For all areas in the Main Range Volcanics except Zone 6, which is 47% below the minimum flow target, the penalty function used to ensure that loss of water through drains equals or exceeds 90% of the extraction that is considered as occurring from these areas was satisfied. Modelled drain flow that significantly exceeded the minimum flow target implies that the contribution from recharge which is rejected or diverted to shallow systems via drains in such areas is notable. In the Condamine Alluvium, the modelled flow was only 16% below the minimum flow target.

Table 5-19 Minimum "extractive" drain flow target and modelled "extractive" drain flow

Zone	Minimum flow target (ML/yr)	Modelled flow (ML/yr)
Condamine Alluvium	31,183	26,189
Main Range Volcanics - 1	2,828	2,960
Main Range Volcanics - 2	3,392	4,448
Main Range Volcanics - 3	7,613	13,851
Main Range Volcanics - 4	18	4,356
Main Range Volcanics - 5	24,258	30,038
Main Range Volcanics - 6	3,358	1,773
Main Range Volcanics - 7	6,495	11,647
Main Range Volcanics – 8	1	302
Main Range Volcanics – 9	18	1,270
Main Range Volcanics – 10	1,960	7,491
Main Range Volcanics – 11	2,955	18,998
Main Range Volcanics – 12	117	26,658
Main Range Volcanics – 13	1	12,000
Main Range Volcanics – 14	1	4,539

5.8.8 CSG water extraction time series

As described in section 3.3.3 predicted pressures in CSG wells (rather than extraction) forms a key input to the UWIR model. Consequently comparisons of actual and modelled CSG water extraction are a key metric of model performance.

Plots of modelled and observed CSG water production for all development areas shown in Figure 5-2 are supplied in Appendix G12. As shown in Figure G12-1 a good match to total CSG water extraction from the Walloon Coal Measures is achieved. The level of fit is somewhat better than achieved in the UWIR 2016 model calibration. The previous model tended to over-estimate extraction during the period of rapidly increasing extraction in 2014. The current model simulates this period much more accurately and also shows a good match to the more recent period during which extraction has

fluctuated between around 50,000 and 60,000 ML/yr. As shown in Figures G12-2 to G12-16 a reasonable match is also achieved between modelled and actual CSG water extraction in many individual development areas in the Walloon Coal Measures although there is some variability in the degree of fit as would be expected.

As shown in Figure G12-17 a reasonable match to total water extraction from the Bandanna Formation is also achieved although again the degree of fit in individual development areas is variable (Figures G12-2 to G12-16). Extraction from CSG fields to the west of the Bowen Basin (Arcadia, Fairview and Spring Gully) tend to the over-estimated, whilst those towards the east of the basin (Peat and Scotia) are underestimated. A generally poorer fit to extraction from the Bandanna Formation is expected to some extent since the volume of geological and hydrogeological data available for model construction and calibration in the Bowen Basin is substantially less than for the Walloon Coal Measures. In particular the lithology of the Bandanna Formation and other surrounding units in the Bowen Basin is relatively poorly understood compared to the Surat Basin strata.

The small amount of current extraction from the Cattle Creek is also relatively well matched by the UWIR 2019 model (Figure G12-23).

5.8.9 Head time series

Scatter plots showing comparisons of observed and modelled head time series for different transient calibration groups are provided in Appendix G14. Scaled RMS errors by formation are also provided in Table 5-20. Links to individual modelled and observed hydrographs for each transient monitoring location are provided in Appendix G15.

Table 5-20 Scaled RMS Errors by formation, transient calibration

Formation	Model layers	Number of observation target locations	Scaled RMS, heads (m)	Scaled RMS error, heads (%)	Scaled RMS error, head change (%)
Springbok Sandstone	9-10	53	12.3	11.0	17.9
Walloon Coal Measures	12-16	217	36.3	6.3	6.5
Hutton Sandstone	18-19	105	12.1	3.9	13.1
Precipice Sandstone	23	83	17.6	5.9	4.1
Bandanna Formation	27-29	12	71.2	18.0	14.8

Overall as summarised in Table 5-20 and in Appendix G14 relatively good matches (SRMS errors of less than 10%) are achieved to both observed heads and temporal head changes in the Walloon Coal Measures and Precipice Sandstone.

The model is therefore generally able to replicate observed drawdowns in the Walloon Coal Measures in and around current CSG production areas. One example from the Daandine field is shown in Figure 5-12. This is a particularly valuable data set as it provides a long time series of observed pressures in a field which has been operational since 2005 and confirms background pre-development heads as well as heads during operation of the field. As shown in Figure 5-12 the model is able to replicate the rapid observed drawdown of around 220 which occurred until mid-2017 and the relatively static heads which have been observed since.

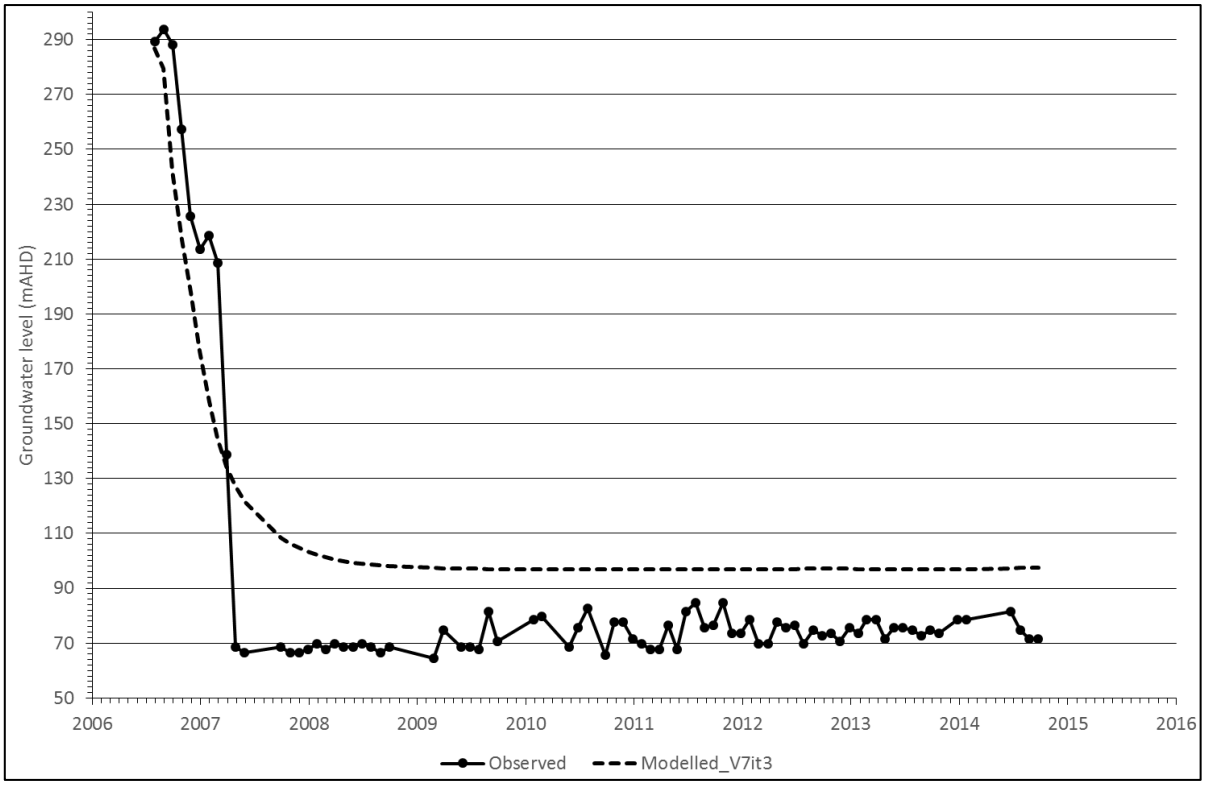

Figure 5-12 Comparison of observed and modelled heads, Daandine 11 middle Walloon Coal Measures (layer 14)

The model is also generally able to match head increases in and around the Precipice re-injection sites relatively well. One example is provided in Figure 5-13 which shows a comparison of observed and modelled heads at the Reedy Creek Precipice re-injection site.

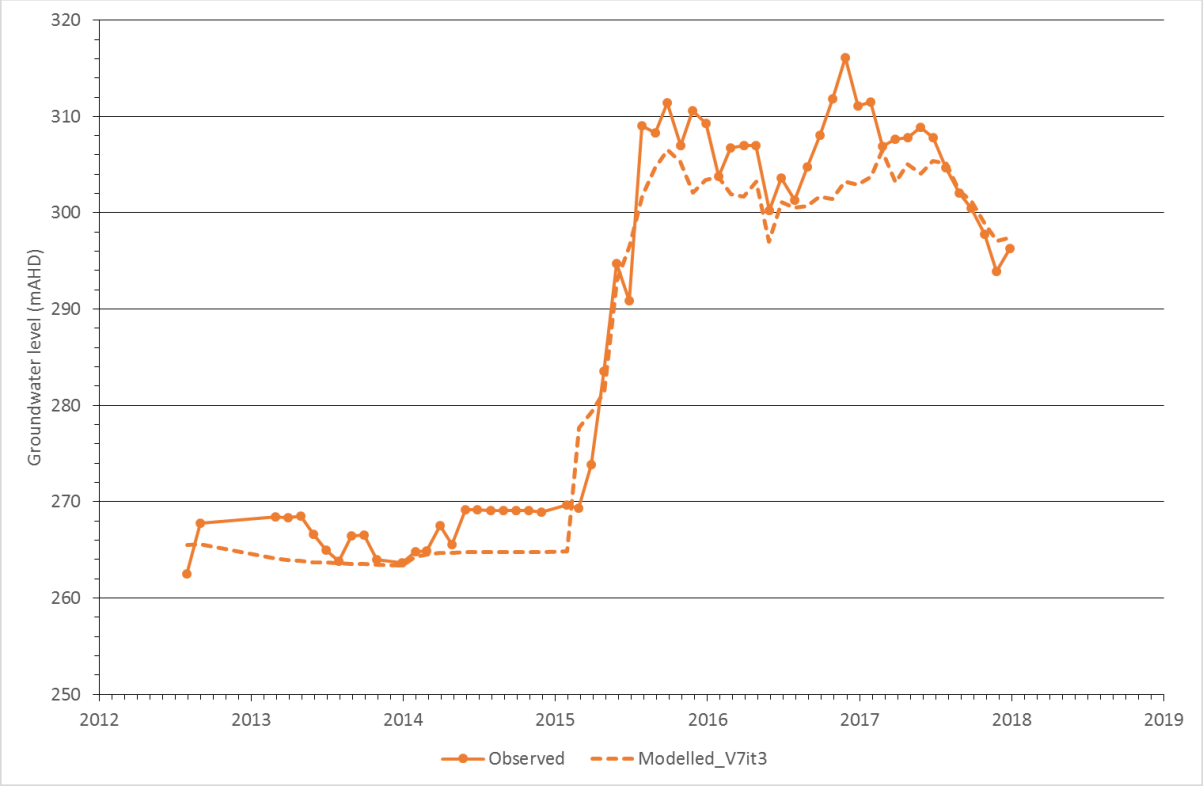

Figure 5-13 Comparison of observed and modelled heads, Reedy Creek INJ2 Precipice Sandstone (RN160964A)

As summarised in Table 5-20 and in Appendix G14 head elevations in the Hutton Sandstone are also relatively well matched but the model generally achieves a lower level of fit to observed head changes in this aquifer. One example of this is shown in Figure 5-14 which shows a comparison of observed and modelled heads in the upper Hutton Sandstone in the vicinity of the Talinga CSG field. Previous investigations undertaken at this site (OGIA 2019a) have concluded that the observed drawdown at this site are likely to be related to non-CSG extraction from the Hutton Sandstone itself rather than CSG extraction from the overlying Walloon Coal Measures. Consistent with this assessment predictions made using the UWIR 2019 model described herein (section 7.4.2) also suggest no significant CSG impact at this location. However, as shown in Figure 5-14 the model generally under-estimates observed rates of groundwater level declines at a number of locations in the Hutton Sandstone. The cause of this under-estimation is not known at this stage but may be related to under-estimation of non-CSG extraction and/or over-estimation of the lateral connectivity of aquifer material within the Hutton Sandstone. However, in the context of CS impact assessment, the model is able to replicate the observed head elevations in both the Walloon Coal Measures and the Hutton Sandstone and hence the head difference at this location (Appendix G16) and so should be capable of accurately simulating interaction between these two formations.

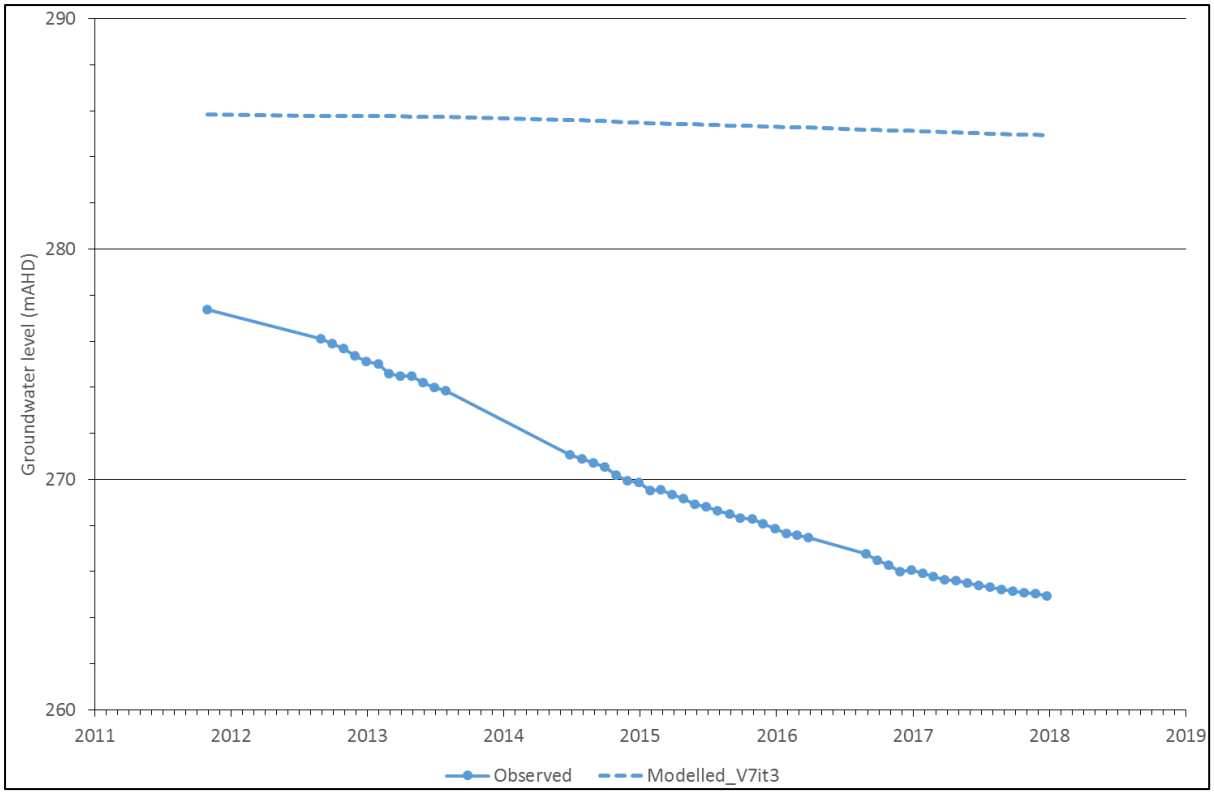

Figure 5-14 Comparison of observed and modelled heads, Talinga MB3-H upper Hutton Sandstone (RN160634A)

Both heads and temporal changes in heads are less well matched in the Springbok Sandstone and Bandanna Formation, SRMS errors for these formations fall in the range 11 to 18%. To some extent the larger SRMS errors for these units reflect the relatively small calibration dataset available for these two strata. Monitoring of groundwater levels in the Springbok Sandstone has also proved relatively difficult and much the of available data is marked by gradually rising or falling water levels which the regional model finds difficult to match in many cases. However, a very good fit is achieved to observed heads in the Springbok Sandstone at Kenya East (Figure 5-15). This is a key monitoring bore which is discussed in the 2016 and UWIR 2019s (OGIA 2016d; and OGIA 2019b) and which shows clear CSG impacts from late 2014 onwards which the model is able to replicate.

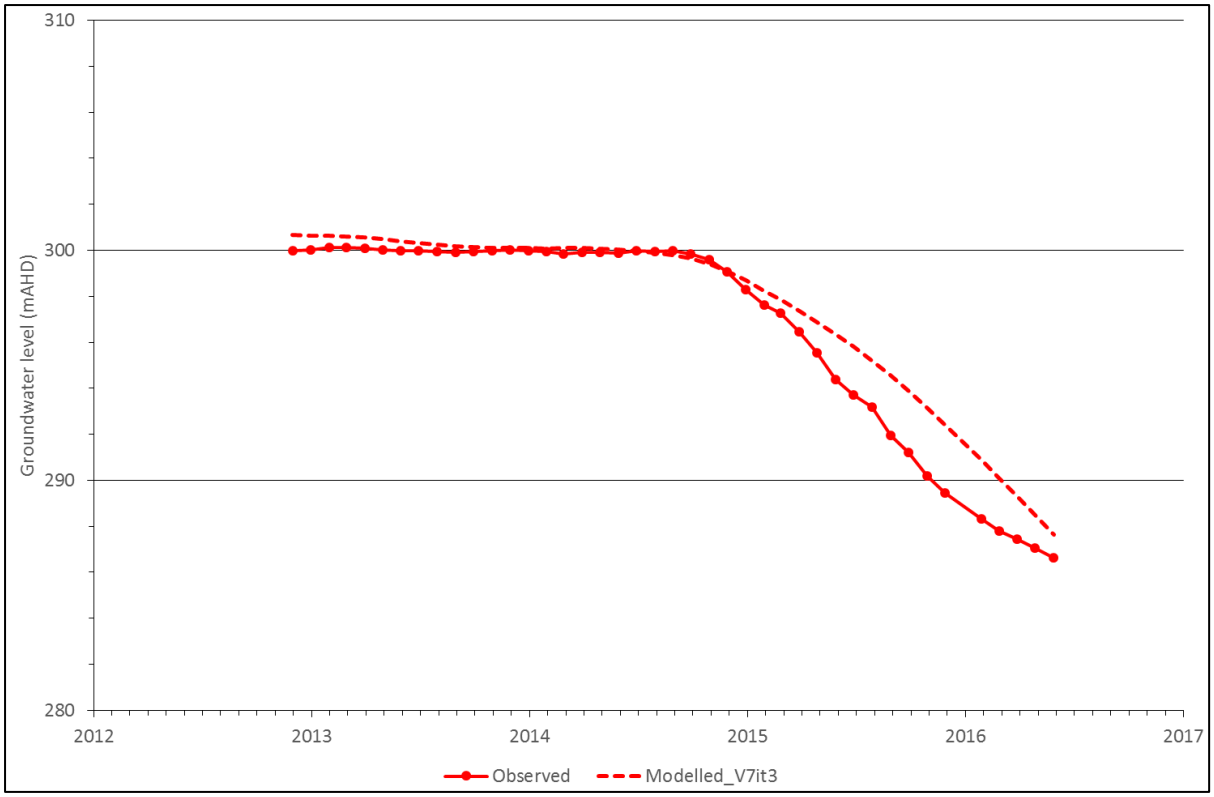

Figure 5-15 Comparison of observed and modelled heads, Kenya East lower Springbok Sandstone (RN160525A)

5.8.10 Vertical head difference time series

As discussed in section 5.4.6.5 observed transient head differences at 55 locations are also included in the transient calibration data set. These are sites where data are available for: adjacent aquifer layers; or aquifers above and below aquitards.

A download link to a pdf file including all individual modelled and observed hydrographs for all 55 locations is provided in Appendix G16. Maps of the locations of these observation points are shown Figure C8-1 to C8-6 in a8

Note that since the Condamine model, from which modelled heads are extracted to populate layer 1 of the Surat CMA model within the Condamine footprint, does not typically simulate sub-yearly fluctuations in water levels then observed fluctuations at sites like Daleglade cannot be accurately matched in the model. For these sites then the best that can be achieved in the regional model is a good match between average observed and modelled head differences.

In general observed vertical head differences are relatively well matched by the model:

- within the Walloon Coal Measures, which suggests that the vertical hydraulic conductivity of the various Walloons layers (12 to 16) is relatively well calibrated
- between the Walloon Coal Measures and the Hutton Sandstone, which suggests that the vertical hydraulic conductivity of the Durabilla Formation (layer 17) is relatively well calibrated
- between the Condamine Alluvium and underlying GAB units, which suggests that the hydraulic conductivity of the Condamine Transition Zone (layer 2) is relatively well calibrated.

However, observed vertical head difference are less well matched by the model:

- within the Hutton Sandstone, which suggests that the vertical hydraulic conductivity of layers 18 and 19 is relatively poorly calibrated
- between the Springbok Sandstone and the Walloon Coal Measures, which suggests that the vertical hydraulic conductivity of the Walloon Coal Measures NPZ (layer 11) is relatively poorly calibrated
- between the Gubberamunda Sandstone and the Springbok Sandstone, which suggests that the vertical hydraulic conductivity of the intervening Westbourne Formation (layer 7) is relatively poorly calibrated.

5.8.11 Water saturation, vertical head difference and reservoir pressure in coal-bearing units

As discussed previously in sections 5.4.6.6, 5.4.6.8 and 5.4.6.9 a suite of calibration 'observations' relating to water saturation, vertical head differences and reservoir pressure in coal reservoirs have been extracted from reservoir models developed by OGIA and the CSG companies. This data has been to supplement groundwater level and CSG water extraction observations within current CSG production areas only and predominantly assists with calibrating parameters which govern CSG water extraction from coal bearing layers.

Scatter plots showing modelled versus "observed" vertical head differences (the latter based on detailed OGIA reservoir modelling described in section 5.4.6.7) are shown in Figures G17-1 and G17-2 of Appendix G17 for the Walloon Coal Measures and Bandanna Formation respectively. These indicate that the UWIR 2019 model is able to match these targets at 84 per cent of the locations within the Bandanna Formation and at 54 per cent of the locations within the Walloon Coal Measures. This fit is substantially better than that achieved in the UWIR 2016 model (OGIA 2016c).

Similar plots showing modelled water saturations in the Walloon Coal Measures and Bandanna Formation after 5 years production are shown in Figure G18-1 and G18-2. In this case saturations of less than 0.7 are expected. Again almost all modelled cells within the Bandanna Formation achieve this target as do 77 per cent of cells in the Walloon Coal Measures. As per the head differences discussed above this level of fit is substantially better than that achieved in the UWIR 2016 model (OGIA 2016c).

Modelled heads, vertical head differences and water saturation within current QGC fields in the Walloon Coal Measures have also been compared to 'observations' from reservoir models developed by QGC. Observed vs modelled scatter plots showing the results of these comparisons are included in Appendix G19, G20 and G21 respectively. It is clear that this data has influenced the calibration and that the UWIR 2019 model is generally able to match average behaviours since the data generally plots parallel to the 1:1 line. However, the values are relatively widely scattered around the 1:1 line reflecting that, as would be expected, the UWIR model is not always able to match outputs from reservoir models, as these models fully represent dual-phase flow processes associated with CSG-extraction and tend to include much higher levels of geological detail. Furthermore, detailed matching of this information is not intended as it does not represent actual observed data.

5.9 Calibrated model parameters

5.9.1 Horizontal hydraulic conductivity

Calibrated horizontal hydraulic conductivity values for all model layers are presented in Appendix H1 and summarised in Table H2-2 in Appendix H2. As shown in Table H2-2, despite the relatively narrow range of values adopted during calibration, and excluding Cenozoic aged units represented in model layer 1, the upper and lower bounds were typically only reached in a small proportion of model cells. Over 10% of cells in the non-permeameter model layers representing the Wallumbilla, Bungil and Orallo formations attained values at the upper bound suggesting that the actual hydraulic conductivity of these formations may be somewhat higher than modelled. Conversely only a very small percentage of model cells in layers 8 to 23 for which permeameter calculations have been undertaken are at either the upper or lower bounds. This suggests that the permeameter based methodology is a reasonable predictor of formation scale horizontal hydraulic conductivity in the majority of the stratigraphic units modelled.

Also of note around 16% of cells representing the Walloon Coal Measures non-productive zone (layer 11) are also at either the upper or lower bounds. As described in section 4.4.1 this layer was subject to further detailed calculations to improve representation of this key unit. However, as shown in Figure H1-11 these particularly high and low values occur in the central part of the CMA and towards the extreme south east and north west in areas where there is no proposed CSG extraction and little or no available data to calibrate the model. Model predictions are therefore considered unlikely to be affected by parameters being at bounds at these locations.

Figure 5-16 shows a comparison of median horizontal hydraulic conductivity values resulting from calibration of the 2016 and UWIR 2019 models. As shown in Figure 5-16 median horizontal hydraulic conductivity values the Springbok Sandstone and Walloon Coal Measure layers are generally lower than previously calibrated. Conversely median values for the Hutton Sandstone and Precipice Sandstone aquifers are higher than previously estimated. The relatively large shift in the Precipice Sandstone is predominantly a result of re-calibration of the model using observed groundwater level responses to re-injection at Reedy Creek and Spring Gully.

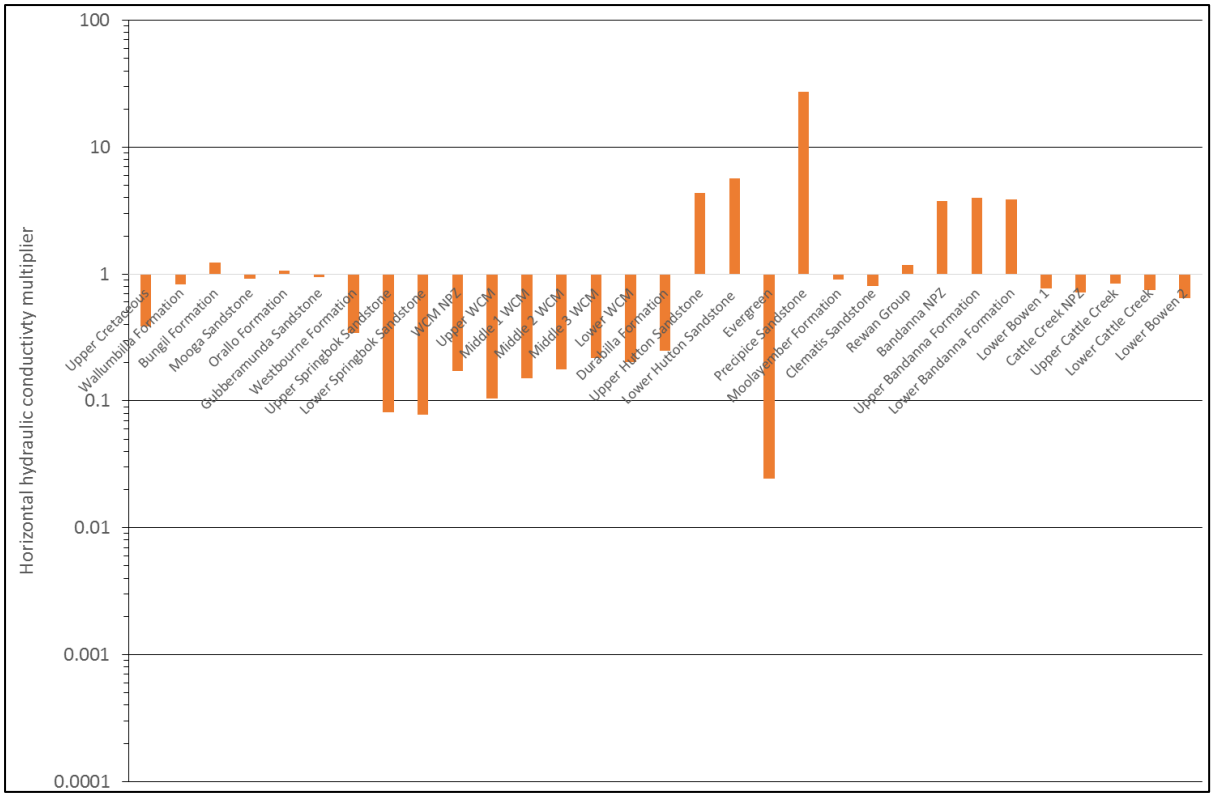

Figure 5-16 Comparison of median calibrated horizontal hydraulic conductivity 2016 and UWIR 2019 models

5.9.2 Vertical hydraulic conductivity

Calibrated vertical hydraulic conductivity values for all model layers are presented in Appendix H3 and summarised in Table H2-2. Unlike the horizontal hydraulic conductivity results described above a number of model layers are characterised by calibrated vertical hydraulic conductivity values which are at upper bounds. This includes a number of permeameter layers including the Springbok Sandstone, Walloon Coal Measures, Hutton Sandstone and Precipice Sandstone. This implies that the model may currently be under-estimating the vertical hydraulic conductivity of these units in some parts of the model. This is particularly true for the lower Hutton Sandstone (layer 19) where as shown in Figure H3-19 large parts of the model domain are at the adopted upper bound Kv value of 1e-06 m/d. Importantly, however, only a small proportion of cells in the overlying Durabilla Formation (layer 17) are at either upper or lower bounds. There is no suggestion therefore that Kv in this key layer affecting propagation of CSG impact from the Walloon Coal Measures is being under-estimated.

Reference to Table H2-2 also suggests that Kv in a relatively large proportion of cells in the Walloon Coal Measures non-productive zone (layer 11) are at the adopted lower bound. As discussed previously in relation to Kh (section 5.9.1) and as shown in Figure H3-11 these cells are located towards the centre of the Surat Basin in areas where there is no proposed CSG extraction.

Figure 5-17 shows a comparison of median vertical hydraulic conductivity values resulting from calibration of the 2016 and UWIR 2019 models. As shown in Figure 5-17 median vertical hydraulic conductivity values are predominantly lower than previously estimated. In part this reflects the generally lower initial values for vertical hydraulic conductivity which were output from the numerical permeameter workflow (section 4.2.4.6). Median values for some layers have, however, increased including the Walloon Coal Measures non-productive zone (layer 11), which has increased based on

the more detailed modelling of the lithology of this layer described in section 4.4.1. As discussed above, in relation to the horizontal hydraulic conductivity, the median vertical hydraulic conductivity of the Precipice Sandstone has also increased substantially based on re-calibration to groundwater levels affected by re-injection.

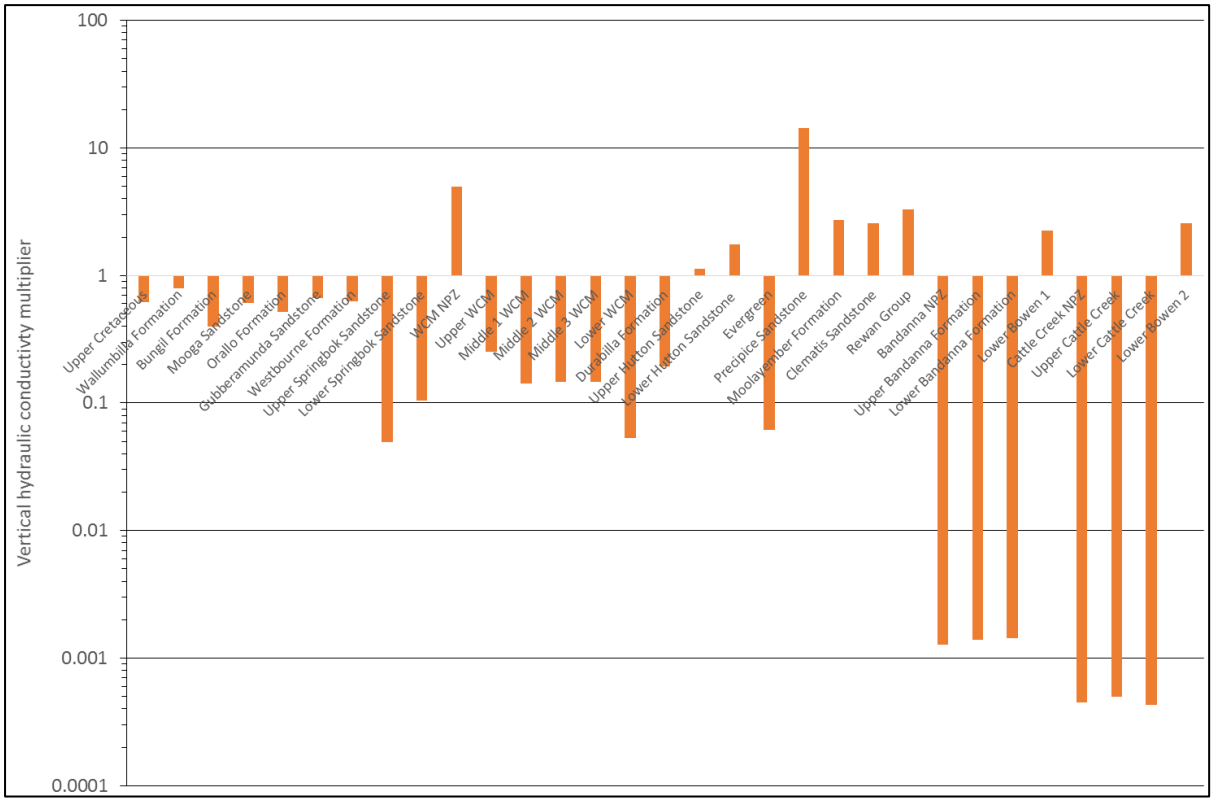

Figure 5-17 Comparison of median calibrated vertical hydraulic conductivity 2016 and UWIR 2019 models

5.9.3 Specific storage and specific yield

Calibrated specific storage and specific yield values for the mobile domain of each of the coal-bearing model layers are presented in Appendix H5 and H6 respectively. Maps of the distribution of specific storage in the remaining model layers (excluding subcrop areas that act as a proxy for specific yield given the confined layer status) and the immobile storage in coal bearing model layers, are also provided in Appendix H5. It should be noted that initial values for storage estimated according to sections 4.5.2 and 4.5.3 in the immobile domain have only been to calibrated for formations which feature in the transient calibration (i.e. model layers 8 to 19, layer 23, layers 27 to 29 and layers 31 to 33).

5.9.4 Recharge

Calibrated steady state recharge values pertaining to the 1995 steady state calibration simulation are provided as Table 5-21.

Recharge has generally been reduced during the calibration process in most modelled stratigraphic units with the total average recharge rate decreasing from 3.2 to 2.4 mm/yr during calibration. Nevertheless the calibrated values remain generally consistent with previous estimates made by Kellett et al (2003) and other authors. Consistent with current conceptual models of the CMA the model calibrated rates are also generally higher for the main aquifers in the system (such as the

Condamine Alluvium, Main Range Volcanics, Gubberamunda Sandstone and Precipice Sandstone) than for the major aquitards (such as the Westbourne Formation and Rewan Group). Pre and post calibration average values are also typically higher for formations which occur at outcrop towards the north of the CMA reflecting higher average rainfall in these areas. Whilst still relatively high the estimated long term average for the Clematis Sandstone (11.6 mm/yr) is now somewhat lower than previously estimated, largely due to the re-attribution of some of the chloride data for this aquifer to other units. As shown in Table 5-21 and contrary to most other layers long term average modelled recharge to the Precipice Sandstone was increased by a factor of two to 53.7 mm/yr during calibration and is now substantially higher than previously estimated consistent with the higher horizontal hydraulic conductivity of this layer (section 5.9.1). Whilst the revised estimated rate is high compared to previous estimates made by Kellett et al (2003), who suggested a maximum rate of 30 mm/yr, it should be noted that this previous work was based on a much smaller chloride data set than that currently available to OGIA. More than 50% of the available chloride data for samples taken from the Precipice Sandstone assessed by OGIA suggest recharge or more than 30 mm/yr, which tends to confirm that this is not a realistic upper bound for this aquifer.

It should be noted that the calibrated recharge values listed in Table 5-21 are rates which are applied at the modelled ground surface. Reference to modelled water balance results (section 5.10) confirms that in most stratigraphic units the majority of this applied recharge is subsequently rejected via modelled “drains” located at the ground surface. Therefore, as shown Table 5-22, the net recharge to each formation (defined as the sum of the net inter-formation flux and the difference between the modelled water table recharge and the modelled surficial drainage) is negligible in many cases. This model result is consistent with recent work on the Hutton Sandstone undertaken by GISERA which suggested that effective recharge to the Hutton Sandstone might be less than 3% of the rate estimated using a chloride mass balance approach (Suckow et al., 2016).

Table 5-21 Calibrated steady state recharge for each modelled formation group

Dominant formation group	Model layer(s)	Recharge multiplier	Average recharge rate (ML/yr)	Average recharge rate (mm/yr)
Condamine Alluvium	1	1.000	19,378 (19,578)	3.5 (3.5)
Non-Condamine Alluvium	1	0.500	46,595	1.4
Main Range Volcanics	1	3.300	154,554	24.9
Other Basalt	1	1.164	58,758	7.1
Cenozoic Sediments	1	0.112	22,227	0.3
Weathered Surat or Bowen	1	0.498	2,134	1.7
Upper Cretaceous	2	2.000	2,360	0.2
Wallumbilla Formation	3	1.703	10,708	1.4
Bungil Formation	4	0.898	5,076	1.4
Mooga Sandstone	5	2.000	12,447	3.8
Orallo Formation	6	0.100	1,098	0.2
Gubberamunda Sandstone	7	0.880	6,352	3.0
Westbourne Formation	8	0.106	383	0.2
Springbok Sandstone	9 – 10	0.100	570	0.1
Walloon Coal Measures	11 – 16	0.132	1,337	0.2
Durabilla Formation	17	0.132	368	0.2
Hutton Sandstone	18 – 19	0.267	10,545	0.9
Evergreen Formation / Boxvale Sandstone	20 - 22	0.273	16,102	1.3
Precipice Sandstone	23	2.000	66,113	53.7
Moolayember Formation	24	1.743	12,682	2.9

Dominant formation group	Model layer(s)	Recharge multiplier	Average recharge rate (ML/yr)	Average recharge rate (mm/yr)
Clematis Group	25	0.714	43,978	11.6
Rewan Group	26	0.100	209	0.1
Bandanna Formation	27 – 29	0.559	581	0.8
Undifferentiated Bowen Basin Strata	30 and 34	0.969	31,612	3.1
Cattle Creek	31 – 33	NA	NA	NA
Total			**526,166 (526,366)**	**2.4 (2.4)**

Notes:

1. Layer 21 which represents the Boxvale Sandstone and layers 31 to 33 which represents the Cattle Creek Formation are not present at outcrop.
2. Bracketed values refer to 1995 steady state recharge specifically; otherwise all values apply to both the 1947 and 1995 steady state simulations.

Table 5-22 Calibrated steady state net recharge for each modelled formation group

Dominant formation group	Model layer(s)	Net Recharge (ML/yr)	Net Recharge (mm/yr)
Condamine Alluvium	1	0	0
Non-Condamine Alluvium	1	0	0
Main Range Volcanics	1	14,224	2.3
Other Basalt	1	15,835	1.9
Cenozoic Sediments	1	6,890	0.1
Weathered Surat or Bowen	1	0	0
Upper Cretaceous	2	567	<0.05
Wallumbilla Formation	3	4,235	0.6
Bungil Formation	4	3,275	0.9
Mooga Sandstone	5	7,501	2.3
Orallo Formation	6	0	0
Gubberamunda Sandstone	7	3,150	1.5
Westbourne Formation	8	152	0.1
Springbok Sandstone	9 – 10	199	<0.05
Walloon Coal Measures	11 – 16	172	<0.05
Durabilla Formation	17	233	0.1
Hutton Sandstone	18 – 19	393	<0.05
Evergreen Formation / Boxvale Sandstone	20-22	531	<0.05
Precipice Sandstone	23	957	0.8
Moolayember Formation	24	0	0
Clematis Group	25	644	0.2
Rewan Group	26	0	0
Bandanna Formation	27 – 29	0	0
Undifferentiated Bowen Strata	30 and 34	0	0
Cattle Creek	31 – 33	NA	NA
Total		**16,112**	**0.1**

5.9.5 General head boundary characteristics

Summary information related to calibrated GHB heads ascribed to pilot points along the western model boundary are presented in Table 5-23, for which only minor modifications were made to initial values. The initial value for GHB conductance of 1.0E-3 m^2/d ascribed to the southern boundary was

practically unchanged by the calibration process, ranging from 8.5E-4 to 1.2E-3 m^2/d across all relevant stratigraphic units.

Table 5-23 Statistical summary of calibrated heads at pilot points for western GHB, by stratigraphic unit

Stratigraphic unit	Model layer	GHB head (mAHD)			
		Min	Max	Mean	Median
Bungil Formation	4	153.0	505.8	252.6	228.2
Mooga Sandstone	5	150.7	545.1	261.8	238.1
Gubberamunda Sandstone	7	144.0	554.9	263.9	243.0
Upper Springbok Sandstone	9	147.5	462.5	270.6	256.0
Lower Springbok Sandstone	10	147.5	412.5	268.6	256.3
Upper Walloon Coal Measures	12	363.5	541.4	422.3	393.3
Middle 1 Walloon Coal Measures	13	249.6	515.4	383.4	386.8
Middle 2 Walloon Coal Measures	14	163.1	494.4	339.7	373.3
Middle 3 Walloon Coal Measures	15	147.4	474.6	296.5	271.7
Lower Walloon Coal Measures	16	147.2	527.3	279.4	266.1
Upper Hutton Sandstone	18	260.7	612.9	417.6	391.9
Lower Hutton Sandstone	19	260.6	581.4	407.3	391.9
Boxvale Sandstone	21	464.0	522.0	498.9	499.1
Precipice Sandstone	23	430.7	678.5	539.7	522.1

5.9.6 Fault specification

Only very minor changes to the pre-calibration estimates of the fault core width and damage zone width were incurred during the calibration process. Calibrated values of fault core width and damage zone width for each of the 16 regional faults included in the model are provided in Table 5-24.

Table 5-24 Calibrated parameters for regional faults represented in the UWIR 2019 model

Fault	Fault core width (m)	Damage zone width (m)
Horrane	1.31	3.03
Wallumbilla	2.56	7.24
Bullaroo	0.72	2.96
"Fault 10"	0.68	2.81
Injune	0.75	2.92
Merivale	1.49	5.41
Arbroath - West	0.81	3.75
Consuelo	0.68	2.89
Burunga - South	0.85	3.83
Wambo	1.18	5.37
Leichardt - Central	0.70	2.45
Cockatoo	1.20	5.14
Arbroath - East	0.76	3.02
Leichardt - North	0.67	2.22
Leichardt - South	0.56	2.13
Kia Ora	0.79	2.59
Miles	0.65	2.53

Fault	Fault core width (m)	Damage zone width (m)
Moonie Goondiwindi (s1)	0.84	3.62
Moonie Goondiwindi (s3)	0.70	2.36
Moonie Goondiwindi (s5)	0.66	2.92
Moonie North Fault	0.67	2.41
Cockatoo-Connection	0.60	2.45

5.9.7 Extra parameters in coal measure layers

As described in section 0, calibration of a number of extra parameters, which apply to dual porosity or dual domain coal measures layers, is also required in the transient simulation. These are:

- enhanced hydraulic conductivity in cells where CSG wells have been installed
- the dual domain transfer rate (DDFTR)
- the Brooks-Corey exponent, *n.*

Calibrated values for enhanced hydraulic conductivity, DDFTR and the Brooks-Corey exponent are presented in Appendices H7, H8 and H9 respectively.

Enhanced hydraulic conductivity for the Walloon Coal Measures and Bandanna Formation are estimated using multipliers at pilot points, whereas the Cattle Creek Formation was parameterised using layer-wide multipliers. Maps of calibrated enhanced hydraulic conductivity are presented in Appendix H7. Average multipliers are listed for each formation in Table 5-25, showing a general reduction in pre-calibrated enhanced hydraulic conductivity for the upper and middle Walloon Coal Measures by about an order of magnitude and slightly higher calibrated values for enhanced hydraulic conductivity for the lower Walloon Coal Measures. Initial values for enhanced hydraulic conductivity for the Bandanna Formation are reduced on average by a factor two, whereas values for the Cattle Creek formation are reduced by an order of magnitude.

As described in in section 0, DDFTR was estimated using a DDFTR-to-kv-adjustment-factor using a zonal parameterisation approach for all dual porosity layers. Calibrated values of this factor are listed in Table 5-25, indicating a large reduction of the pre-calibrated ratio between DDFTR and Kv by about two orders of magnitude for the Walloon Coal Measure layers. Maps of post-calibrated values for DDFTR are shown in Appendix H8.

Similar to the estimation of enhanced hydraulic conductivity, pilot points were used to estimate the Brooks-Corey coefficient for the Walloon Coal Measures and Bandanna Formation. Maps of post-calibrated values for this property are shown in Appendix H9, exhibiting large variability for all layers. Brooks-Corey exponents estimated for the upper and lower Cattle Creek Formation are 4.3 and 1.0, respectively.

Table 5-25 Calibrated values of DDFTR-to-kv adjustment-factor and average calibrated enhanced hydraulic conductivity multipliers per formation

Coal-bearing unit (zone)	Average multiplier enhanced hydraulic conductivity	DDFTR-to-kv-adjustment-factor
Lower Springbok Sandstone	0.98	-
Walloon Non-Productive-Zone	0.99	-
Upper Walloon Coal Measures	0.15	3.91E-03

Coal-bearing unit (zone)	Average multiplier enhanced hydraulic conductivity	DDFTR-to-kv-adjustment-factor
Middle Walloon Coal Measures	0.24	1.99E-02
Lower Walloon Coal Measures	1.09	1.29E-02
Upper Bandanna Formation (West of Taroom Trough)	0.51	3.97E-01
Upper Bandanna Formation (East of Taroom Trough)	0.55	5.58E-01
Lower Bandanna Formation (West of Taroom Trough)	0.71	1.92E-01
Lower Bandanna Formation (East of Taroom Trough)	0.53	5.10E-01
Upper Cattle Creek Formation	0.10	8.87E-01
Lower Cattle Creek Formation	0.06	1.14E+00

5.10 Model water balances

5.10.1 Pre-development steady state simulation (1947)

A water balance for the pre-development or 1947 steady state simulation is provided inTable 5-26. Note that net flux into the layer is positive.

Consistent with the previous two iterations of the regional model (GHD, 2012; OGIA, 2016a) pre-development water balance results suggest only relatively minor outflows of 2,630 ML per year along the southern model boundary to the remainder of the GAB. This outflow represents less than 1% of the applied recharge; the remainder being discharged locally to shallow groundwater systems from where it may be lost as evaporation or provides baseflow to surface water courses.

5.10.2 Pre-CSG steady state simulation (1995)

A water balance for the pre-CSG development or 1995 steady state simulation is provided in Table 5-27. Note that net flux into the layer is positive.

Comparison of the pre-CSG development water balance results (Table 5-27) with those relating to pre-development conditions (Table 5-26) suggest that in the long term (i.e. once steady state conditions are established) the groundwater extraction demand of around 14,500 ML/yr will predominantly met by a reduction in the volume of water discharged to shallow systems. Water balance results also suggest that the volume of groundwater discharged along the southern model boundary will also be reduced slightly.

5.10.3 Post-CSG transient simulation (1995-2014)

Transient water balance results for the period January 1995 through to the end of the historic simulation period in December 2017 for the Walloon Coal Measures are shown in Figure 5-18. This plot suggests that the majority of the additional extraction demand of the CSG industry is currently being met from storage in the Walloon Coal Measures, with only minor increases in inflows from adjacent strata or reductions in other outflows (to surface or along the southern model boundary).

5.11 Key calibration assumptions and limitations

5.11.1 Calibrated parameter fields

As is well documented in the literature, the inverse problem of model calibration does not have a unique solution. Hence, parameters inferred through the calibration process cannot be construed to describe the “correct” system properties. They can only be construed to be estimates of system properties which are of minimised error variance (i.e. minimised potential for wrongness). The same applies to predictions made by a calibrated model in general, and the UWIR 2019 model in particular. See texts such as Menke (1984), Aster et al. (2005) and Doherty (2015c) for further details. To address for the UWIR 2019 OGIA have undertaken a predictive uncertainty analysis as described in Chapter 7.

As discussed in section 5.9.2 calibrated vertical hydraulic conductivity (Kv) in parts of a number of model layers are at their adopted upper bound values. This suggests that the model may be under-estimating this parameter in a number of aquifer layers. Unfortunately since the same upper and lower bound values have been adopted for the predictive uncertainty analysis then the uncertainty associated with the Kv of some parts of some aquifer layers is likely to be being under-estimated. Fortunately Kv is of secondary importance in these aquifer layers and calibrated Kv in the adjacent aquitard layers such as the Durabilla Formation (layer 17) is not at either upper or lower bounds.

The calibration dataset included pre-development heads at a number of sites and layers spread throughout the model domain. Conditions were not, in fact, steady state at this time. While the calibration procedure accommodated this to some extent, more exact accommodation of the transient nature of this dataset would have required full transient calibration. This was not done because of excessive model run times. Furthermore, a high degree of uncertainty accompanies estimates of non-CSG pumping rates and timing throughout the model domain. These uncertainties also afflict their steady state counterparts employed in the calibration process; indeed these uncertainties are compounded by errors associated with the steady state approximation itself.

5.11.2 Parameterisation detail

As was discussed in Chapter 2, parameterisation of the UWIR 2019 model involves two levels of upscaling. For some layers the first upscaling stage is formally accomplished through the use of numerical permeameters. For other layers it is accomplished subjectively, while taking into account results obtained through more formal upscaling implemented in permeameter layers. The second level of upscaling requires the introduction of pilot points so that regional model parameters can be adjusted during the calibration process in order that model outputs are well matched to their observed counterparts.

The necessarily regional nature of UWIR 2019 model parameters is such that they can represent only broad scale hydraulic property heterogeneity. Hence, they cannot represent local heterogeneities that may arise, for example, from alluvial channel deposits, faults, abandoned and poorly constructed wells, and other local features. At the time of writing, it is envisaged that this will be addressed through the development of a number of highly detailed models of the strata immediately over and underlying coal reservoirs to further investigate the role of faults and poorly constructed wells on propagation of CSG impacts into overlying units. Much of the fault conceptualisation work which will under-pin such a work program has already been undertaken and this will be advanced during the forthcoming UWIR cycle.

Table 5-26 Water balance in each model layer for the 1947 steady state simulation

Stratigraphic unit(s)	Model layer	Recharge (ML/yr)	Non-CSG extraction (ML/yr)	Surficial drainage (ML/yr)	Net GHB flux (ML/yr)	Net interlayer flux (ML/yr)	% Error
Alluvia, Basalt and Cenozoic Sediments	1	303,647	0	-311,525	0	7,879	0
Upper Cretaceous	2	2,360	0	-2,359	0	0	0
Wallumbilla Formation	3	10,708	0	-7,541	0	-3,167	0
Bungil Formation	4	5,076	0	-2,623	-160	-2,293	0
Mooga Sandstone	5	12,447	0	-6,213	-1,223	-5,011	0
Orallo Formation	6	1,098	0	-2,163	0	1,065	0
Gubberamunda Sandstone	7	6,352	0	-3,584	-356	-2,412	0
Westbourne Formation	8	383	0	-269	0	-114	0
Upper Springbok Sandstone	9	514	0	-424	0	-90	0
Lower Springbok Sandstone	10	56	0	-45	-11	-1	0
Walloon Coal Measures non-productive zone	11	0	0	0	0	0	0
Upper Walloon Coal Measures	12	431	0	-606	0	175	0
Middle 1 Walloon Coal Measures	13	217	0	-231	-2	16	0
Middle 2 Walloon Coal Measures	14	172	0	-170	-4	2	0
Middle 3 Walloon Coal Measures	15	207	0	-200	-4	-2	0
Lower Walloon Coal Measures	16	310	0	-304	-2	-4	0
Durabilla Formation	17	368	0	-152	0	-216	0
Upper Hutton Sandstone	18	10,322	0	-12,124	-24	1,826	0
Lower Hutton Sandstone	19	223	0	-231	-86	94	0
Upper Evergreen	20	8,991	0	-8,880	0	-111	0
Boxvale Sandstone	21	147	0	-150	3	-1	0
Lower Evergreen	22	6,964	0	-6,576	0	-388	0
Precipice Sandstone	23	66,113	0	-67,038	-763	1,688	0
Moolayember Formation	24	12,682	0	-14,012	0	1,330	0
Clematis Sandstone	25	43,978	0	-43,524	0	-454	0
Rewan Group	26	209	0	-322	0	113	0

Stratigraphic unit(s)	Model layer	Recharge (ML/yr)	Non-CSG extraction (ML/yr)	Surficial drainage (ML/yr)	Net GHB flux (ML/yr)	Net interlayer flux (ML/yr)	% Error
Bandanna Formation non-productive zone	27	0	0	0	0	0	0
Upper Bandanna Formation	28	581	0	-648	0	67	0
Lower Bandanna Formation	29	0	0	0	0	0	0
Undifferentiated Bowen Basin strata	30	25,022	0	-25,009	0	-13	0
Cattle Creek Formation non-productive zone	31	0	0	0	0	0	0
Upper Cattle Creek Formation	32	0	0	0	0	0	0
Lower Cattle Creek Formation	33	0	0	0	0	0	0
Undifferentiated Bowen Basin strata	34	6,590	0	-6,610	0	20	0
	Totals	**526,166**	**0**	**-523,536**	**-2,630**	**0**	

Table 5-27 Water balance in each model layer for the 1995 steady state simulation

Stratigraphic unit(s)	Model layer	Recharge (ML/yr)	Non-CSG extraction (ML/yr)	Surficial drainage (ML/yr)	Net GHB flux (ML/yr)	Net interlayer flux (ML/yr)	% Error
Alluvia, Basalt and Cenozoic Sediments	1	303,847	0	-307,647	0	3,800	0
Upper Cretaceous	2	2,360	-735	-1,793	0	167	0
Wallumbilla Formation	3	10,708	-444	-6,473	0	-3,792	0
Bungil Formation	4	5,076	-686	-1,801	-13	-2,576	0
Mooga Sandstone	5	12,447	-1,639	-4,946	-787	-5,075	0
Orallo Formation	6	1,098	-1,601	-1,695	0	2,198	0
Gubberamunda Sandstone	7	6,352	-3,641	-3,202	-243	734	0
Westbourne Formation	8	383	0	-231	0	-152	0
Upper Springbok Sandstone	9	514	-117	-330	4	-70	0
Lower Springbok Sandstone	10	56	-50	-41	-8	43	0

Stratigraphic unit(s)	Model layer	Recharge (ML/yr)	Non-CSG extraction (ML/yr)	Surficial drainage (ML/yr)	Net GHB flux (ML/yr)	Net interlayer flux (ML/yr)	% Error
Walloon Coal Measures non-productive zone	11	0	-26	0	0	26	0
Upper Walloon Coal Measures	12	431	-172	-484	0	225	0
Middle 1 Walloon Coal Measures	13	217	-95	-176	0	54	0
Middle 2 Walloon Coal Measures	14	172	-99	-129	-1	57	0
Middle 3 Walloon Coal Measures	15	207	-94	-159	-1	47	0
Lower Walloon Coal Measures	16	310	-119	-217	-1	28	0
Durabilla Formation	17	368	0	-135	0	-233	0
Upper Hutton Sandstone	18	10,322	-2,397	-9,929	168	1,836	0
Lower Hutton Sandstone	19	223	-361	-223	-6	366	0
Upper Evergreen	20	8,991	0	-8,869	0	-122	0
Boxvale Sandstone	21	147	-49	-137	3	36	0
Lower Evergreen	22	6,964	0	-6,565	0	-399	0
Precipice Sandstone	23	66,113	-1,888	-65,156	-732	1,663	0
Moolayember Formation	24	12,682	0	-14,000	0	1,319	0
Clematis Sandstone	25	43,978	-266	-43,334	0	-377	0
Rewan Group	26	209	0	-320	0	111	0
Bandanna Formation non-productive zone	27	0	0	0	0	0	0
Upper Bandanna Formation	28	581	-4	-647	0	70	0
Lower Bandanna Formation	29	0	-7	0	0	7	0
Undifferentiated Bowen Basin strata	30	25,022	0	-25,007	0	-15	0
Cattle Creek Formation non-productive zone	31	0	-1	0	0	1	0
Upper Cattle Creek Formation	32	0	-1	0	0	1	0
Lower Cattle Creek Formation	33	0	-1	0	0	1	0
Undifferentiated Bowen Basin strata	34	6,590	0	-6,610	0	20	0
Totals		**526,366**	**-14,493**	**-510,255**	**-1,618**	**0**	

Figure 5-18 Water balance of the Walloon Coal Measures for the transient calibration period

6 Predictive model configuration

6.1 In this chapter

This chapter describes the configuration of the predictive version of the UWIR 2019 model used to assess the cumulative impacts of CSG and P&G related water extraction.

As required under Queensland's regulatory framework for assessing and managing the impacts of P&G developments, predictive output from the UWIR 2019 model has been used to:

- define the immediately affected area (IAA) for each consolidated aquifer present within the model domain – the area where water pressures are predicted to decline by more than 5 m within the next 3 years
- define the long-term affected area (LAA) for each consolidated aquifer present within the model domain – the area where water pressures are predicted to decline by more than 5 m at any time in the future
- identify potentially affected springs – springs where the water pressure in aquifers underlying the sites of these springs is predicted to decline by more than 0.2 m at any time in the future
- predict the rate and volume of water movement between formations
- estimate the quantity of groundwater that is expected to be extracted as a result of P&G developments in the CMA.

A predictive uncertainty analysis has also been completed using the methodology outlined in section 7.2. Relevant predictions made using the model are presented in the 2019 UWIR and summarised in 7.4. Further information on predicted impacts at individual bore locations can be obtained via the OGIA bore search tool (https://www.dnrme.qld.gov.au/business/mining/surat-cma/bore-search).

6.2 Predictive model description

6.2.1 Model timing

The predictive model effectively represents a continuation of the historic transient simulation described previously in section 5.3.4. The predictive part of the simulation therefore runs from January 2018 onwards with starting conditions taken from the final stress period of the historic transient simulation (i.e. December 2017). All predictive simulations are carried out over an 8,000-year period to track the gradual recovery in groundwater levels following the planned cessation of CSG extraction in 2065-2070. A system of gradually increasing stress period lengths has been adopted as detailed below:

- 148 quarterly stress periods during the period of peak production from 2018 to 2060
- nine annual stress periods through to the planned cessation of CSG extraction in 2070
- six stress periods, each five years in length, through to 2100
- 10 decadal stress periods to 2200
- eight centurial stress periods to 3000
- seven millennial stress periods to the end of the simulation period in the year 10000.

This is considered to represent a sensible balance between providing sufficient predictive detail and tractable model run times. In particular, during the latter part of the recovery period, groundwater levels within the Surat CMA will be recovering only very slowly, so the long stress periods adopted are considered to be appropriate.

6.2.2 Future CSG extraction wells

The methodology by which existing and potential future CSG wells are represented in the model has been described previously in section 3.3.3. As described in section 3.3.3.7, future CSG wells are added to the predictive part of the simulation based on development plans received from CSG tenure holders for each 3 km^2 sub-block over which they hold tenure. Based on information provided for the UWIR 2019, tenure holders estimate that development of areas currently planned for CSG production will result in some 21,000 CSG wells being installed during the lifetime of the industry (an increase of around 3,000 compared to the UWIR 2016). These CSG wells are gradually added during the course of the predictive simulation based on the predicted start and end dates shown in Figure 3-21 and Figure 3-22.

6.2.3 Reinjection

As mentioned previously starting in January 2015, Origin has been injecting up to around 27 ML/d of treated water into the Precipice Sandstone at two sites near the Spring Gully and Ready Creek gas fields. At Spring Gully, around 20% of total water extraction from local CSG wells is reinjected via three injection bores, whilst at Ready Creek, around 84% is reinjected via 12 injection bores. The permeability of the Precipice Sandstone at both sites is understood to be relatively high, to the extent that operating pressures in the injection bores remain sub-artesian.

As described in section 2.3.5, a number of revisions were necessary to MODFLOW-USG code to simulate this process during the predictive simulations. A minimal one-stress-period lag is assumed between extraction from the relevant modelled CSG wells and reinjection, and the proportion of water reinjected has been assumed to remain static at the percentages quoted above. However, in practice this equates to a gradual decline in the volume of water reinjected since the volume of water extracted from the relevant modelled CSG wells declines with time. Based on the sub-artesian conditions observed in the injection bores, model reinjection rates start to diminish if/when the modelled head rises above the local ground surface elevation and cease altogether if the modelled head rises to 10 m above ground.

6.2.4 Recharge and other boundary condition assumptions

Calibrated long-term average recharge rates as per the 1995 steady state simulation are assumed to apply throughout the predictive period and hence static climate conditions have been assumed. All other modelled boundary conditions are consistent with the final stress period of the historic transient simulation (i.e. December 2017). Settings for the following MODFLOW packages and flow components therefore remain effectively static throughout the predictive period:

- recharge
- non-P&G groundwater extraction, as represented using the MODFLOW well package; this included transmissivity-weighted flow apportionment of all multi-layer extractions and modification of well derating variables on the basis of the calibrated horizontal hydraulic conductivity

- cross-fault resistance of faults, as represented using the MODFLOW horizontal flow barrier package
- inflow/outflow along the southern and western boundaries of the model domain, as represented using the MODFLOW General Head Boundary package
- surficial drainage as represented using the MODFLOW river package.

6.2.5 Model parameterisation

All hydraulic conductivity (including fault zones where changes to up-fault conductances are manifested as modified vertical hydraulic conductivity) and storage parameters used in the predictive model were as per the calibrated values described in Chapter 5 and illustrated in Appendix H. Calibrated parameters in coal-bearing layers for processes governing desaturation, dual porosity and enhanced conductivity also remained unchanged for the predictive simulation.

6.3 Predictive scenarios

6.3.1 Legislative scenarios

For the purposes of providing results for the 2019 UWIR, two main predictive runs or scenarios are carried out. In each case, the model simulation period is 1995 onwards so that the cumulative impacts since the commencement of CSG extraction in the Surat CMA in 1995 can be assessed. The scenarios are:

- a UWIR Base Run which includes only consumptive water extraction for non-P&G purposes (i.e. excluding all P&G water extraction)
- a UWIR P&G Production Run which includes all water use from P&G and non P&G activities, including post 2011 groundwater extraction from conventional oil and gas development, but excluding non-associated water take.

Differences between heads and fluxes extracted from the Base Run and P&G Production Run therefore identify predicted impacts associated with water extraction by current and planned CSG activities and post 2011 conventional oil and gas activities. Re-injection into the Precipice Sandstone is excluded from the P&G Production Run and predicted impacts are therefore prior to this mitigation activity.

Predictions based on a comparison of the two legislative scenario runs outlined above are presented and discussed in some detail in the UWIR 2019 and summarised below in section 7.4.

6.3.2 Other scenarios for information

For the UWIR 2019 a series of additional ‘for information’ scenarios have also been undertaken as described below. These assess the impacts of other possible CSG development scenarios and other non-CSG activities.

6.3.2.1 Additional CSG development scenarios

As described in the UWIR 2019 in addition to the main legislative CSG production scenario three further CSG development scenarios have been undertaken as follows:

- a CSG production scenario including re-injection to the Precipice Sandstone near the Spring Gully and Ready Creek gas fields

- a CSG production scenario which includes the development of a number of additional tenure areas which are currently only part way through the approvals process. This scenario includes the installation of around 23,800 CSG wells (2,800 more than in the UWIR scenario)
- a high development scenario to assess the extent to which impacts could increase if current development plans were extended to include potential CSG production areas. This high development scenario comprises some 34,000 CSG wells.

The impacts of these scenarios have then been calculated in the same way as the legislative scenario, i.e. through comparison with head and flux output from the UWIR Base Run.

7 Predictive uncertainty analysis

7.1 In the chapter

This chapter describes the methodology and outcomes of a predictive uncertainty analysis undertaken on the calibrated UWIR regional groundwater flow model described in Chapters 2 to 5.

Post-calibration uncertainty analysis was undertaken using the so-called “null space Monte Carlo” (NSMC) methodology provided by the PEST suite of software. Details of this methodology, as well as examples of its implementation in conjunction with synthetic and real-world models, are described in Tonkin and Doherty (2009), James et al. (2009), Keating et al. (2010), Herckenrath et al. (2011) and Doherty (2015). Software required for implementation of the methodology is in the public domain. It is documented by Doherty (2016a, 2016b) and can be downloaded from http://www.pesthomepage.org.

7.2 Methodology

After calibration of a groundwater model has (in theory) endowed that model with a calibrated parameter field of minimum error variance, the null space Monte Carlo (NSMC) methodology can be used to efficiently compute a suite of calibration-constrained, randomised but realistic, parameter fields. Use of this methodology is based on the premise that parameter non-uniqueness is a high contributor to predictive uncertainty. Its use is most effective if a model is endowed with a sufficiently large number of parameters to express this non-uniqueness. It is therefore assumed that calibration of the model was effected through highly-parameterised inversion supported by mathematical regularisation. It is also assumed that a sensitivity matrix (also referred to as a Jacobian matrix) has been calculated based on the calibrated parameter set.

Through singular value decomposition (SVD) of a Jacobian matrix, parameter space can be partitioned into mutually orthogonal null and solution spaces. The null space is spanned by parameter combinations that are not estimable from the calibration dataset. These are responsible for post-calibration parameter non-uniqueness. The uncertainties of these combinations are not reduced through the calibration process. In contrast, combinations of parameters which span the orthogonal-complimentary solution space are uniquely estimable from the calibration dataset. However they inherit uncertainty from errors associated with measurements from which their values are calculated. NSMC takes advantage of this partitioning of parameter space into calibration-informed combinations of parameters and calibration-uninformed combinations of parameters to make the process of calibration-constrained random parameter field generation computationally inexpensive, even for large models such as the UWIR model whose run times are lengthy.

In addition to a Jacobian matrix, another precursor to NSMC-based random parameter field generation is user-specification of prior parameter uncertainties. These are uncertainties based on information other than that forthcoming from history-matching. In many cases these can be based on expert knowledge and experience. In other cases more refined estimates of pre-calibration uncertainties may be available through geostatistical and upscaling analyses; as is discussed below, numerical permeameters were able to assist in establishing prior uncertainties for some of the parameters employed by the UWIR model.

NSMC, as implemented by the PEST suite, requires that prior uncertainties be encapsulated in one or a number of covariance matrices. Where multiple covariance matrices are employed for this purpose, each of these should pertain to a different group of parameters (for example pilot points within a single layer of the UWIR model).

Following construction of prior covariance matrices and calculation of a Jacobian matrix based on the calibrated parameter set, implementation of the NSMC methodology proceeds as follows.

- Under an assumption of model linearity an approximate posterior covariance matrix is constructed.
- The approximate posterior parameter probability distribution, comprised of this matrix and calibrated parameter values as posterior expected values, is sampled; multiple parameter fields are generated through this process.
- Because groundwater models are not linear, model runs undertaken on the basis of these parameter sets produce outputs that fit the calibration dataset reasonably well, but not well enough to deem the model as calibrated. To rectify this situation, each such parameter field is projected onto the solution and null spaces defined through SVD of the Jacobian matrix. The solution space projection of each of these fields is replaced by the parameter field associated with the calibrated model. This process generally results in parameter fields that fit the calibration dataset better than without null space projection, but still do not satisfy calibration constraints well enough for the model to be considered as calibrated.
- Each null space projected random parameter field is adjusted using regularised inversion to better fit the calibration dataset. Usually, only one iteration of adjustment is undertaken. Because this employs the same pre-calculated Jacobian matrix as that used for definition of solution and null spaces, the cost of parameter adjustment is numerically very small. Meanwhile, if the acceptance criterion for model-to-measurement misfit is reflective of measurement noise that is associated with the calibration dataset, the adjustment procedure ensures appropriate diversity of the solution space components of these random parameter fields.

Once a series of calibration-constrained random parameter fields have been obtained in this manner, all of which promulgate a good fit between model outputs and members of the calibration dataset, a model is endowed with the ability to make stochastic predictions of future system behaviour. This is achieved by making each such prediction with all of these parameter fields. A histogram can be plotted for any prediction of interest. The expected value and uncertainty of this prediction can then be calculated using this histogram.

Advantages of the NSMC methodology compared with other methods of post-calibration uncertainty analysis include the following.

- Its implementation is numerically efficient once a model has been calibrated.
- If desired, fits between model outputs and a calibration dataset can be as good as those attained through the previous calibration process.
- It is able to accommodate model nonlinearities.

As with all uncertainty quantification methods, it also has some disadvantages. These include the following.

- Its algorithm is not strictly Bayesian; nevertheless it attains nearly the same outcomes as a strictly Bayesian procedure.
- If the numerical cost of calibration is taken into account, it does not have the same efficiencies as use of ensemble methods. Use of these methods treats history-matching and uncertainty

analysis as a single, multi-parameter-field adjustment process. However ensemble methods are not without their own shortcomings; a discussion of these is beyond the scope of the present report.

7.3 Application of the methodology to the UWIR 2019 model

7.3.1 Obtaining sensitivities

Sensitivities of calibration-pertinent model outputs with respect to all parameters employed by the UWIR model were calculated by PEST using finite parameter differences. In doing this, parameters were varied incrementally from their calibrated values. Hence, in theory, the Jacobian matrix that was thus obtained represents a linearization of the model centred on parameter values of minimised post-calibration error variance.

7.3.2 The Prior Covariance Matrix

The posterior covariance matrix of model parameters, C'(**k**), can be expressed via a linearised form of Bayes equation (Christensen and Doherty, 2008):

$$C'(\mathbf{k}) = C(\mathbf{k}) - C(\mathbf{k})\mathbf{Z}t[\mathbf{Z}C(\mathbf{k})\mathbf{Z}t + C(\boldsymbol{\varepsilon})]\text{-}1\mathbf{Z}C(\mathbf{k}) \quad (3)$$

where C(**k**) is the prior covariance matrix of **k**, and is determined from expert knowledge pertaining to hydrogeological considerations and C(**ε**) is a stochastic descriptor of epistemic error (that incorporates measurement noise and structural error terms).

Table F2-1 in Appendix F2 lists parameter types employed by the UWIR model. As outlined in Table F2-1 table and discussed previously in section 5.5, some of these parameter types are layer-specific, some are zonal, some are associated with pilot points, and some fall into none of these categories.

All parameters other than those associated with pilot points were assumed to show no prior correlation. Under this assumption, their prior uncertainties can be characterised using only their standard deviations (the square of which are their variances). Hence no non-zero off-diagonal elements are required in the prior covariance matrix for these parameters. The standard deviation of each parameter was defined by dividing the difference between the upper and lower bounds adopted for calibration purposes on the assumption that the parameter was Gaussian and the parameter range spanned approximately four standard deviations (thereby representing a 95% confidence limit) up to a maximum of 0.5 in log space. Prior uncertainties for zonal and layer wide parameters are summarised in Appendix I1.

Parameter groups comprising pilot point parameters were assigned a full covariance matrix based on spatially variable variograms however. For example, for a spatially variable property such as hydraulic conductivity, it expresses both the range of values that this property is likely to take for the different aquifer materials prevailing within the study area, as well as the degree of spatial continuity that is likely to exist for this property.

Statistical correlation was represented by an exponential variogram, and hence was assumed to be a function only of pilot point separation. Covariance relationships implied by the exponential variogram are described by the equation:

$$C(h) = C(0)[1\text{-}e^{-h/a}] \quad (4)$$

where h depicts the separation between any two pilot points and C(0) expresses parameter covariance at zero pilot point separation (the variogram “sill”), this being the innate variance of the

parameter, and a is a length parameter or integral scale, which defines a variogram range of approximately 3a (Deutsch and Journel, 1992).

For all pilot point parameters, the variogram "a" value was declared as pilot-point-specific. This reflects the fact that pilot points are not capable of representing the prevailing heterogeneity of an aquifer system. Instead, this parameterisation device contains a degree of upscaling, with the extent of upscaling decreasing with increasing spatial density of pilot points. Where pilot point emplacement is dense, short range hydraulic property heterogeneity can be characterised. Alternatively, where it is sparse, only long range hydraulic property heterogeneity can be characterised. The variogram range associated with each pilot point was calculated was thereby formulated in the following manner:

- The average separation between the pilot point to which an "a" value must be assigned and its 8 closest neighbours was calculated.
- The "a" value ascribed to the variogram associated with that pilot point was designated as 25% greater than this average separation.

For parameter types represented by pilot points (excluding those associated with western GHB heads), the variogram sill (applied to the logarithm of hydraulic properties associated with pilot points) ranged between 0.01 and 0.25; this implying a standard deviation of parameter variability that could range between 0.1 and 0.5 in log space. The variogram sill for the western GHB head was specified as 100 (i.e. a standard deviation of 10 m in native space). Variograms assigned to all pilot points are isotropic.

The resulting prior uncertainties for pilot point parameters separated into different parameter types are summarised in Appendices I2 for I8.

7.3.3 Measurement noise

For calculation of the linear approximation to the posterior parameter covariance matrix, the covariance matrix that characterises measurement noise C(**ε**), was assumed to be diagonal, with elements proportional to the inverse of the squared reciprocals of weights used during the calibration process. The proportionality constant applied to all weights was such that the measurement objective function is approximately equal to the number of observations comprising the calibration dataset minus the dimensionality of the calibration solution space; refer Doherty (2015) for further details.

Implied in the level of fit that calibration-constrained stochastic parameter fields are required to attain with the calibration dataset is a stochastic characterisation of "noise" that is responsible for model-to-measurement misfit. As has already been discussed, much of this "noise" is structural. As such, it is not amenable to statistical characterisation. However, an objective function 10% greater than that attained by the calibrated parameter field was set as the constraint for attaining a sample of the posterior parameter distribution.

7.3.4 Some implementation details

The generation of posterior parameter samples for the UWIR 2019 model comprised the following steps:

1. A linear approximation to the posterior covariance matrix C'(**k**) using equation (3) was calculated using the PEST utility PREDUNC7 (Doherty, 2018) on the basis of the weighted Jacobian Matrix, C(**k**) and C(**ε**).

2. The PEST utility RANDPAR1 (Doherty, 2018) was then used to generate 500 random parameter vectors **k** derived from the posterior parameter covariance matrix C'(**k**) using a random number generator algorithm. Gaussian probability distributions were assumed for all parameters natively or for their log-10-transformations. The expected value was centred at the base calibrated model parameter value. This was necessary to achieve an adequate number of models that can be considered "calibrated". Parameter-value bounds were respected in all cases.

3. The solution space component of each random parameter vector **k** was replaced with that of the calibrated model using null space projection undertaken by the PNULPAR utility (Doherty, 2018). A solution space dimensionality of 2,000 super parameters was adopted on the basis of a singular value decomposition of the weighted Jacobian matrix using the PEST utility SUPCALC (Doherty, 2018). This corresponds to the singular value at which the ratio of lowest to highest squared singular value of the weighted Jacobian matrix is equal to 1.0E-7. (It is assumed this cut-off signifies the point at which numerical errors associated with the computation of the weighted Jacobian matrix invalidate the estimation of parameter projections).

4. The posterior probability distribution of model parameters was thereby obtained by selecting realisations for which the fit between model outputs and field measurements was considered good enough to declare a model as "calibrated" after due consideration of measurement noise and model structural errors; see Doherty and Welter (2010). It was also required that the number of these parameter fields be sufficient to provide a reasonable characterisation of posterior predictive uncertainties. So in order to achieve a workable level of numerical efficiency, each null-space projected parameter vector **k'** was subjected to only one iteration of parameter adjustment in seeking an acceptable level of model fit with the calibration dataset **h**. Parameter upgrade vectors were computed using the original "calibrated" Jacobian matrix only. The Broyden rank-one Jacobian matrix update (e.g. Skahill et al., 2009) was also undertaken after every parameter upgrade attempt to effectively maximise the potential for reducing the objective function during the re-calibration step.

In order to harvest a set of model parameter realisations that are deemed to be "acceptable", the model-to-measurement misfit for each model realisation was quantified in accordance with the total least-squares weighted measurement objective function (i.e. the sum of the multi-component objective function employed in the original base calibration, expressed herein as phi). The sum of the phi contribution across all observation groups was then compared to that of the base calibrated model. A threshold of 10% above the base calibrated model of 4.05E+05 was used to define a "acceptable level of misfit", under which the models were deemed to be "calibrated". If this was not achieved the parameter vector **k'** was rejected.

The last of these steps accommodates the nonlinear nature of the model.

7.4 Predictive uncertainty analysis results and discussion

7.4.1 Posterior probability distributions

A suite of 450 parameter fields for which the final objective function was less than 1.1 times that associated with the calibration parameter field were produced using the NSMC approach outlined above in section 7.3. These can be considered to comprise samples of the posterior parameter

probability distribution and collectively, these fields can be used to characterise the statistical properties of any model parameter. For example histograms of posterior probability distributions for zonal and layer-wide parameter types are provided in Appendix I1.

Spatial variability of the statistical properties associated with a pilot point parameters can be represented by mapping a given statistic to the location of its corresponding model parameter. Examples of these maps are provided in Appendices I2 to I8 as a pair of figures per pilot-point based parameter. The first of these figures (Figure I2-1 in Appendix I2 for example) shows the geographical distribution of the standard deviation of log (to base 10) of the pilot point parameter. The second map (Figure I2-2 for example) shows the spatial distribution of 10 raised to the power of log standard deviation. This is equivalent to the factor by which the mean parameter value at any point must be multiplied and divided to define a range which is roughly equal to its 67% confidence interval.

Posterior probability distributions for selected predictions can then be amassed by running the predictive model using the 450 calibration-constrained parameter fields. From these outputs, uncertainty statistics and the resultant “bandwidth” of the prediction can be displayed graphically as histograms and cumulative probability distributions, for example.

To interpret this abundance of outputs a statistical approach was adopted, whereby the 5th and 95th percentiles of a given output at every grid cell (or interpolated to points of interest) were computed from the 450 realisations. The values outside the 5th and the 95th percentile are considered ‘outliers’. Such an approach is common practice in probabilistic risk assessments, where a range of outcomes are produced that meet a prescribed set of risk criterion for a representative sample population. A percentile is the value of a variable (e.g. a water level) below which a given percentage of values for that variable fall. So the 95th percentile is the value below which 95% of the values for that variable may be found (and 5% are greater). Similarly, the 5th percentile represents the value below which only 5% of the values for that variable reside (and 95% are greater). Mean and median values were also computed.

7.4.2 Predicted drawdown impact

One of the primary interests of the uncertainty analysis was the impact drawdown, which is defined as the simulated groundwater level for current non-P&G activities (irrigated agriculture, stock watering and town water supplies as well as for commercial and other agricultural purposes) minus the simulated water level resulting from the further inclusion of conventional P&G and future CSG operations.

NSMC was applied to a model simulation of two future extractive scenarios over a 8000-year period (1995–10000), described in section 6.3.1, namely (i) a continuation of current activities and (ii) progressive expansion and contraction of CSG operations over the next 50-60 years. The simulation of current activities provided a spatio-temporal baseline for water level and interlayer flux response from which the comparative responses to CSG operations were subtracted to determine "impact".

Firstly, for each of the 450 NSMC simulations, the maximum simulated value of impact drawdown that occurs in every cell over 8000 years was determined, hitherto referred to as the maximum impact drawdown. Maps showing the 95th percentile, median, and 5th percentile of maximum impact drawdown in every active model cells for each aquifer unit are illustrated for key formations in Appendix I9. Conceptually, there is approximately a 5% probability that the maximum impact drawdown will be lower than the values illustrated for the 5th percentile, and approximately a 95% probability that the maximum impact drawdown will be less than the values illustrated for the 95th

percentile. As expected, the results indicate that the maximum impact drawdown is focused around CSG gas fields and impacts extend furthest in the Walloon Coal Measures (Layers 11 to 16, Appendix I9-4), Bandanna Formation (Layers 27 to 29, Appendix I9-8) and Cattle Creek Formation (Layers 31 to 33, Appendix I9-8) where extractions are directly applied.

Also of particular interest was the vertical propagation of the maximum impact drawdown envelope above and below the Walloon Coal Measures. To aid understanding of this, the total area predicted to experience maximum impact drawdown of greater than the relevant trigger threshold (2 or 5 m for unconsolidated and consolidated aquifers respectively) for the 5th and 95th percentiles are given in Table 7-1.

Table 7-1 Total area predicted to experience drawdowns of more than the 2 or 5 m trigger threshold

Stratigraphic units	Model layer(s)	Trigger threshold (2 or 5 m)	Area (km^2) (5^{th} Percentile)	Area (km^2) (95^{th} Percentile)
Cenozoic aged units	1	2	0	6
Upper Cretaceous aged units	2	5	0	335
Wallumbilla Formation	3	5	0	0
Bungil Formation	4	5	0	0
Mooga Sandstone	5	5	0	0
Orallo Formation	6	5	0	0
Gubberamunda Sandstone	7	5	0	0
Westbourne Formation	8	5	1,880	5,971
Upper Springbok Sandstone	9	5	8,844	13,601
Lower Springbok Sandstone	10	5	11,469	16,000
Upper Walloon Coal Measures	12	5	15,037	18,384
Middle Walloon Coal Measures	13 – 15	5	21,581	26,217
Lower Walloon Coal Measures	16	5	22,403	28,090
Durabilla Formation	17	5	7,613	20,689
Upper Hutton Sandstone	18	5	3,807	5,662
Lower Hutton Sandstone	19	5	2,276	5,250
Upper Evergreen Formation	20	5	90	735
Boxvale Sandstone	21	5	42	97
Evergreen Formation	22	5	74	123
Precipice Sandstone	23	5	5,537	10,368
Moolayember Formation	24	5	93	623
Clematis Group	25	5	137	578
Rewan Group	26	5	976	6,499
Upper Bandanna Formation	28	5	11,606	21,462
Lower Bandanna Formation	29	5	11,849	21,685
Undifferentiated Upper Bowen Basin	30	5	84	8,038
Upper Cattle Creek	32	5	1,076	1,696

Stratigraphic units	Model layer(s)	Trigger threshold (2 or 5 m)	Area (km^2) (5^{th} Percentile)	Area (km^2) (95^{th} Percentile)
Lower Cattle Creek	33	5	1,096	1,680
Undifferentiated Lower Bowen Basin strata	34	5	849	1,374

As shown in Table 7-1 impacts of more than the relevant trigger thresholds outside of the coal reservoirs themselves are largely limited to the Springbok Sandstone (Appendix I9-3), Hutton Sandstone (Appendix I9-5) and Precipice sandstones (Appendix I9-6).

As mentioned above the statistics presented in Table 7-1 and Appendix I9 are based on outputs from some 450 predictions. In order to confirm that the number of runs completed was sufficient to generate reliable statistics statistical convergence plots have been produced for the lower Walloon Coal Measures (model layer 16) and Bandanna Formation , as shown in Figure 7-1 and Figure 7-2. These plots have been generated by re-calculating the P5, P50 and P95 statistics for the total area impacted by more than 5 m using results from a gradually increasing number of predictive runs. As shown in these plots convergence of the key drawdown metric is relatively rapidly achieved such that there is limited variation in the statistics of predicted drawdown once data for more than 100 predictive realisations are included.

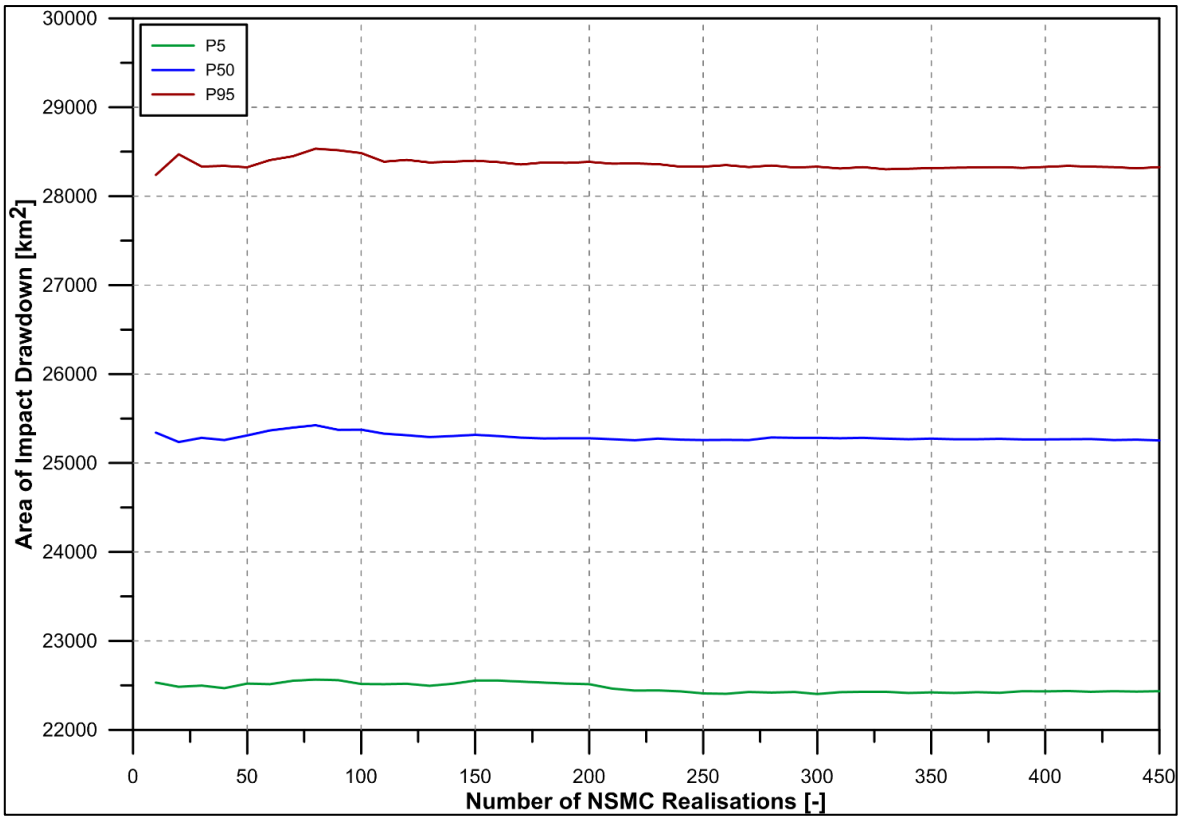

Figure 7-1 Predicted area of drawdown impacts in the lower Walloon Coal Measures, statistical convergence plot

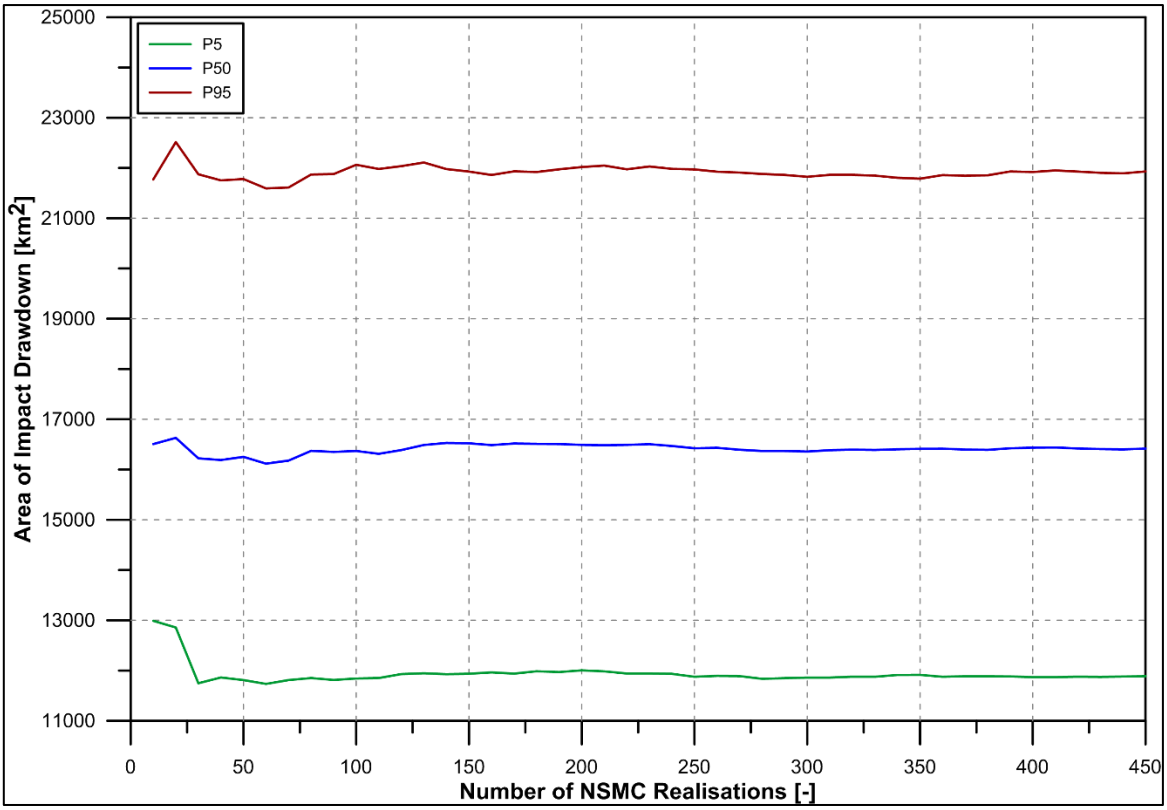

Figure 7-2 Predicted area of drawdown impacts in the lower Bandanna Formation, statistical convergence plot

Time series of predicted drawdown at selected locations within the model domain are also provided in Appendix I10.

Figure I10-1 shows predicted groundwater level impacts in the Precipice Sandstone and Bandanna Formation at two locations where these formations are understood to be in direct contact and close to areas where CSG is currently being extracted from the Bandanna Formation. As shown in Figure I10-1 impacts of up to 70 m are therefore predicted in the Bandanna Formation but leading to impacts of less than 1.6 m in the overlying Precipice Sandstone. The relatively minor impacts predicted in the Precipice Sandstone is consistent with the high permeability of this unit.

Figure I10-2 to Figure I10-5 show predicted groundwater level impacts in the Walloon Coal Measures, Springbok Sandstone and Hutton Sandstone 5 km up and down gradient and within four CSG production areas. As shown in these figures impacts of up to 500 m are predicted towards the base of the Walloon Coal Measures within production areas. However, predicted impacts on the underlying Hutton Sandstone aquifer are typically less than 2 m due to the presence of the intervening Durabilla Formation aquitard. Impacts of up to around 12 m are predicted in the Hutton Sandstone in the area south-west of Dalby (as shown in Figure I10-5) since the displacement along the nearby Horrane Fault is assessed as exceeding the thickness of the Durabilla Formation, thereby placing the Hutton Sandstone in contact with the Walloon Coal Measures. This is simulated in the groundwater model as a non-neighbour connection between model layers 16 (the lower Walloon Coal Measures) and 18 (the upper Hutton Sandstone) leading to predicted impacts of more than 5 m in the Hutton Sandstone in this area.

7.4.3 Predicted CSG water extraction

Predicted total CSG water extraction from the Walloon Coal Measures and Bandanna Formation are shown in Figure 7-3 and Figure 7-4 respectively. In addition to P5, P50 and P95 statistics based on all 450 predicted realisations results are also plotted for the 'base model'. This is a single set of predictions generated using the fully calibrated version of the model described in section 5.8.

Statistical convergence plots for the Walloon Coal Measures and Bandanna Formation are shown in Figure 7-5 and Figure 7-6 and suggest that statistical convergence is achieved after around 200 predictive realisations.

As shown in Figure 7-3 and Figure 7-4 the predicted range in volumes is relatively narrow suggesting that this prediction is subject to a relatively low degree of uncertainty. It should be stressed, however, that these predictions are based on a single CSG company development profile scenario. Potential uncertainties in the predictive scenario have instead been investigated by running an additional maximum development as described in section 6.3.2.1.

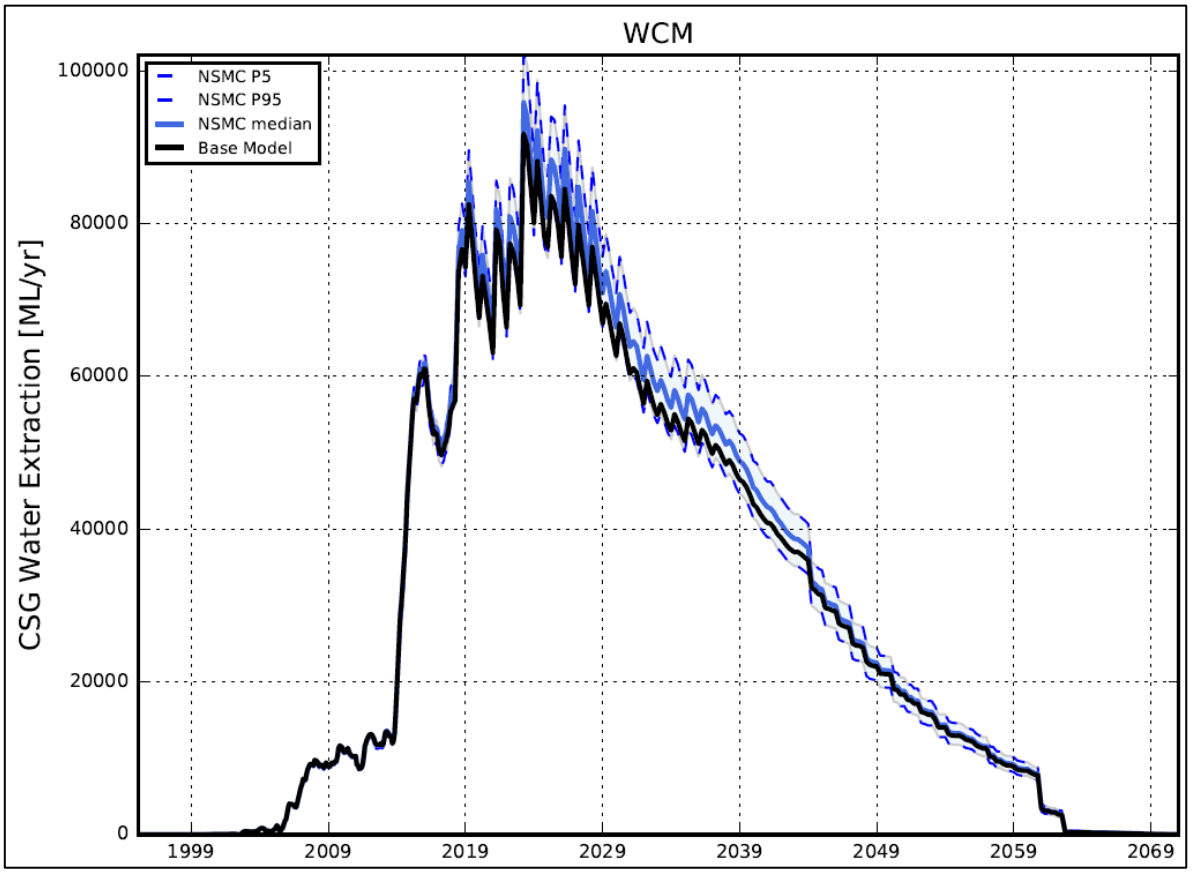

Figure 7-3 Predicted CSG water extraction, Walloon Coal Measures

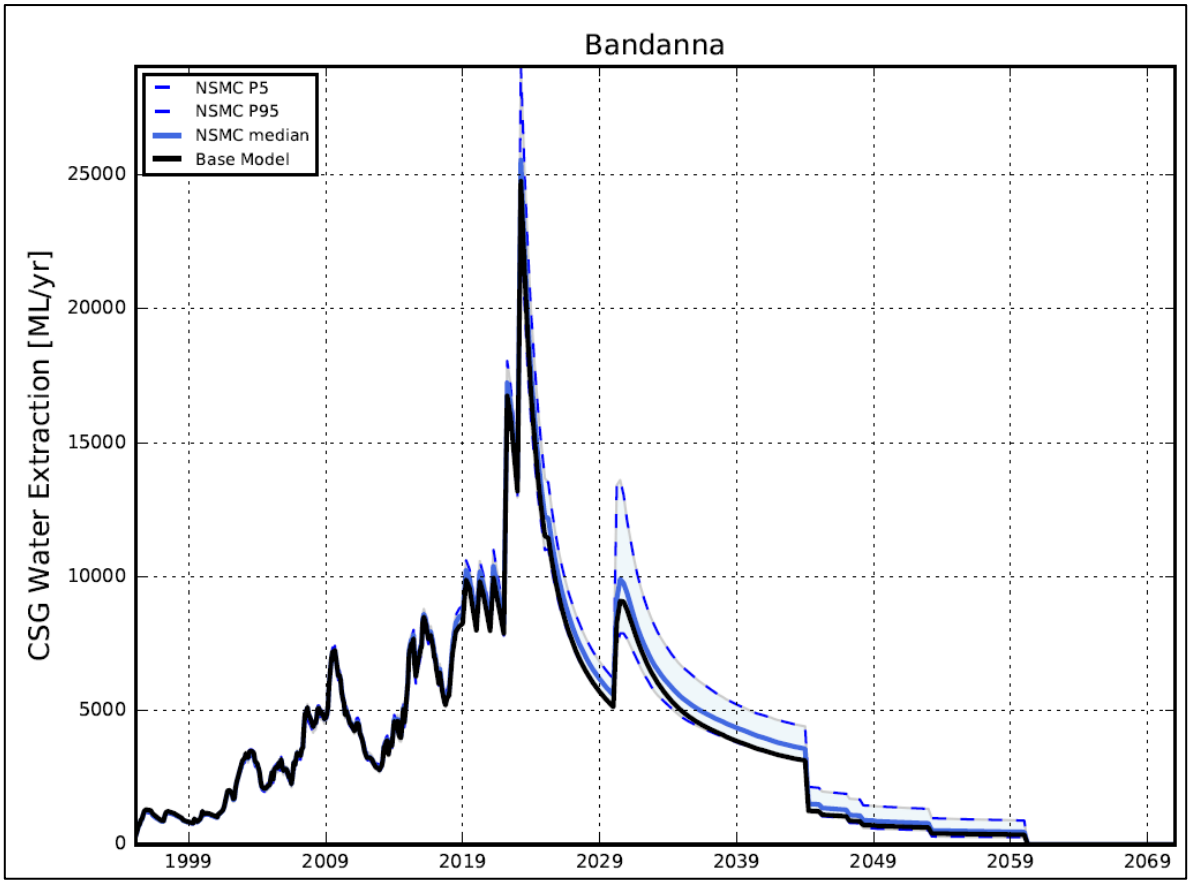

Figure 7-4 Predicted CSG water extraction, Bandanna Formation

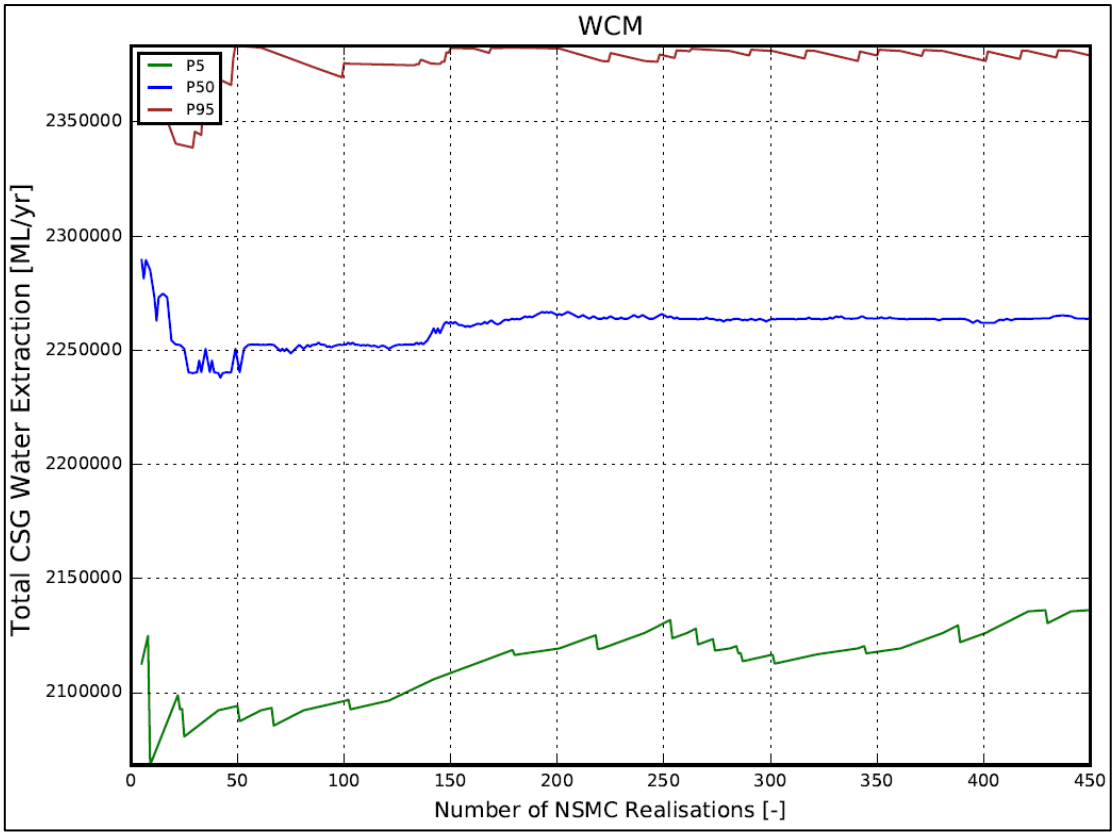

Figure 7-5 Predicted total CSG water extraction, statistical convergence plot, Walloon Coal Measures

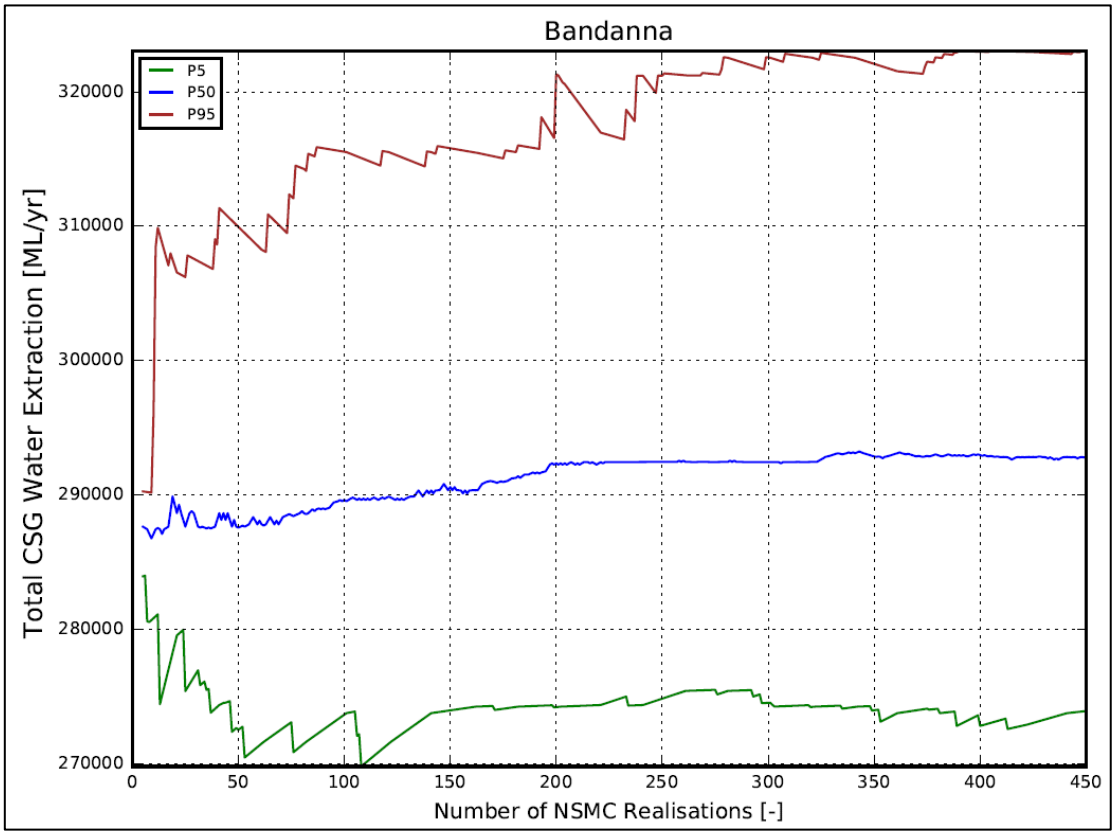

Figure 7-6 Predicted total CSG water extraction, statistical convergence plot, Bandanna Formation

7.4.4 Net flux impacts Condamine Alluvium

Predicted net flux impacts on the Condamine Alluvium based on processed outputs from all 450 predictive realisations and the fully calibrated 'base model' are shown in Figure 7-7. The key metric related to flux impacts on the Condamine Alluvium is the average impact over a 100 year period from 2011 onwards. Figure 7-8 therefore shows P5, P50 and P95 statistics for this prediction calculated based on a gradually increasing data set of realisations. As shown in Figure 7-8 convergence is generally achieved after around 200 of 450 realisations although there is some variability in the P5 and P95 statistics.

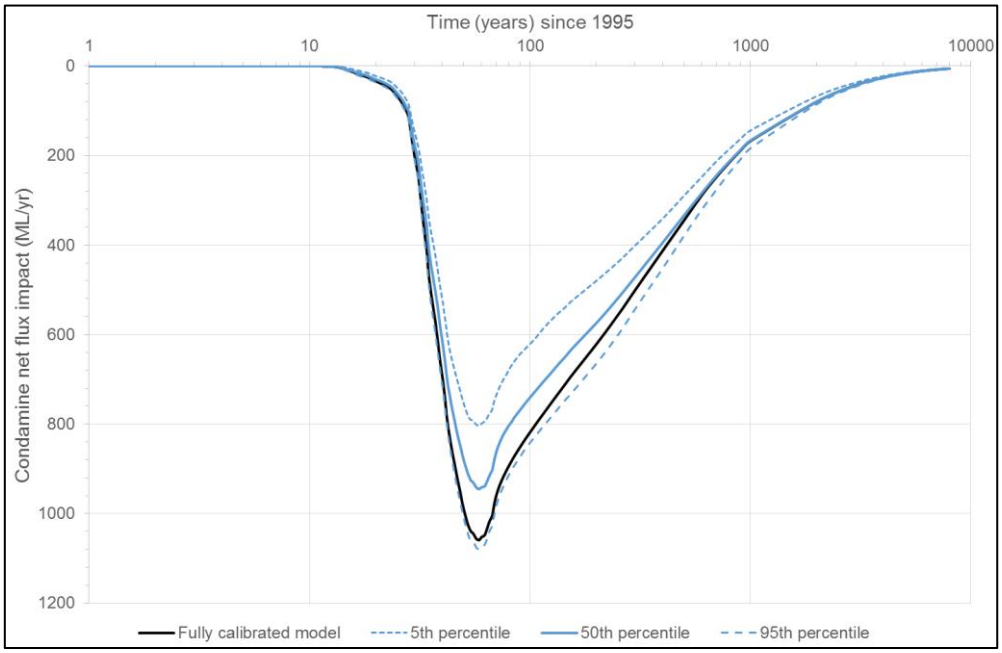

Figure 7-7 Predicted net flux impacts Condamine Alluvium

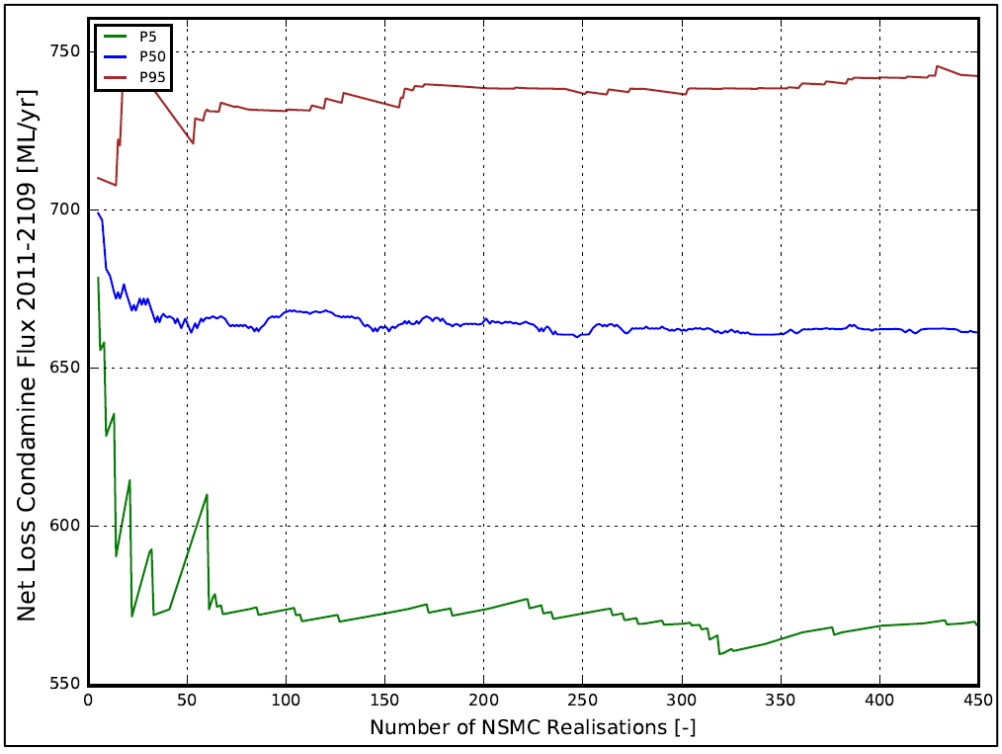

Figure 7-8 Predicted net flux impacts Condamine Alluvium, statistical convergence plot

7.5 Predictive uncertainty analysis assumptions and limitations

The uncertainty approach described above does not take into account those aspects of model construction and parameterisation (which is a form of structural noise) that may, as further information is gathered, be shown to make significant contributions to predictive uncertainty including:

- manifest knowledge gaps in the spatial disposition of aquifer units and their hydraulic boundaries
- while initial parameterisation of the majority of model layers includes a hydraulic conductivity versus depth relationship, the uncertainty associated with parameters governing this relationship was not explored explicitly during the uncertainty analysis but was instead accommodated heuristically via usage of upper and lower bounds used to define prior uncertainties that reflected this depth-dependency
- only parameters deemed estimable for the purpose of model calibration (and subsequent predictive uncertainty analysis) were explored; latent or fixed parameterisation located in areas outside the expected area of historic or future CSG influence were not included in this exercise
- uncertainty associated with the spatial continuity of faults (expressed via inter-layer juxtaposition) and their potential hydraulic effects
- notable departures from the anticipated spatial distribution and scheduling of CSG-related extractions into the future.

As such, due to the presence of structural noise, predictive uncertainties that are assessed through use of calibration-constrained stochastic parameter fields should be viewed as representing lower bounds on the uncertainties of predictions of interest rather than their true uncertainties.

In addition, the statistical characterisation of the innate variability of hydraulic properties and boundary conditions (represented by the C(**k**) matrix) employed by the model for parameter-by-parameter and cell-by-cell based stochastic field generation can never be known exactly. However, their specifications were based on field estimates and expert knowledge.

8 Conclusions

OGIA's approach to modelling has continually evolved since the UWIR 2012. The 2019 regional groundwater flow model represents the third iteration of conceptualisation, construction and calibration. Each iteration of the model is informed by a revised understanding of key hydrogeological processes or concepts operating within the Surat CMA at the time.

The first model iteration to predict impacts in the UWIR 2012 was largely based on information from previous studies. Relatively little primary data interpretation was undertaken and the model was developed using a standard version of MODFLOW 2005.

A new model was constructed for the UWIR 2016 using a number of innovative modelling techniques developed by OGIA's team and a revised conceptualisation of the groundwater flow system based on primary data interpretation. MODFLOW-USG was the modelling platform; a number of revisions were made to the standard MODFLOW-USG modelling code. These revisions included the development of additional functionality to address unique challenges in the Surat CMA:

- simulation of water desaturation due to gas production in coal seams around CSG wells
- more accurate representation of CSG wells using a descending MODFLOW drain methodology
- increased modelled permeability in areas where CSG wells screen multiple coal seams that would otherwise be separated by low permeability interburden
- simulation of reinjection of treated CSG water into the Precipice Sandstone.

8.1 Key improvements in the current model

This third and current iteration of the regional groundwater flow model used for the UWIR 2019 represents redevelopment of the previous model and includes a number of refinements to the modelling approach. Key improvements incorporated into this model are:

- development of a revised regional geology model with a 250 m grid based on geophysical log data from about 7,000 P&G wells, updated geological mapping and further constraints around the contact zones between the Precipice Sandstone and Bandanna Coal Measures
- additional model layers to explicitly represent the Boxvale Sandstone
- improved understanding of the groundwater flow system operating in the Surat CMA and the observed impacts of ongoing CSG and non-CSG extraction
- revised and updated initial model parameterisation drawing on expanded lithological and hydraulic parameter datasets
- incorporation of additional major faults (total of 22)
- inclusion of historic and future open cut coal mines at regional scale
- simulation of CSG wells partially completed into the overlying Springbok Sandstone
- inclusion of a detailed representation of permeability of the upper non-productive zone of the Walloon Coal Measures based on detailed stochastic modelling of the lithology in this key unit
- more accurate simulation of APLNG's aquifer re-injection scheme and its impacts on heads in the Precipice Sandstone

- revised and updated model calibration which includes history matching up to December 2017 of CSG and non-CSG extraction data and transient head observations for more than 480 monitoring points in CSG reservoirs and key aquifers
- post-calibration uncertainty analysis was undertaken using the so-called “null space Monte Carlo” (NSMC) approach leading to the generation of some 450 alternative parameter sets and associated impact predictions.

8.2 Model purpose and limitations

The regional groundwater flow model is designed for the specific purpose of simulating regional-scale groundwater pressure impacts caused by CSG and post-2011 P&G activities where primary mechanism for impacts in surrounding aquifers is through cross-formational flow.

The UWIR 2019 model represents a simplified representation of a complex multi layered groundwater system over an extremely large geographic area extending in three geological basins and including at least nine recognised aquifers and three separate coal reservoirs. Given current computational limits, such model must run efficiently enough to allow model calibration and predictive uncertainty analysis to be undertaken. This requires simplification and significant upscaling of system properties, both vertically and horizontally. In this context following must be considered in relation to the use of the model:

- Upscaling of system properties has been achieved by representing the majority of stratigraphic units with one or two model layers, the use of 1,500 m grid cells and the application of pilot-point spacing of more than 10 kilometres as part of the model calibration process. Although a number of local features such as geological faults and lithology variations are implicitly considered in upscaling to model grid cell scale, variations in predictions at sub-cell scale cannot be derived from the model.
- Detailed modelling of the Kenya East gas field area (see Appendix A of OGIA (2019e)) suggests that sub-regional scale models with a combination of smaller cell sizes and an increased number of model layers is required to capture local aquifer heterogeneity. In particular refinement in vertical direction is likely to be of much greater influence in simulating propagation of CSG impacts. The current regional model is likely to overestimate the rate and magnitude of impact propagation in such settings.
- Given the primary focus on simulation of cross-formational flow, generally a higher weightage is given to matching observed head differences between the formations e.g. the Hutton Sandstone and the Walloon Coal Measures. Such data prioritisation can compromise the replication of observed heads and head trends within the formations, particular given the uncertainties associated with estimated consumptive water use. Therefore, use of the model for assessing groundwater dynamics within formations should be considered within this limitation.
- Since the UWIR 2019 model aims to simulate processes in aquifers and coal reservoirs within the deeper parts of the Surat and Bowen basins, surficial groundwater flow processes have been necessarily simplified to perform the surrogate role of setting upper boundary conditions for the regional model. These simplifications include an assumption of confined groundwater flow in non-coal units (see section 3.2.6) and use of a static drainage elevation in lieu of an explicit representation of temporal stage response in rivers and creeks (see section 3.3.1); the

latter of which precludes the simulation of streamflow loss to groundwater and denudes groundwater-surface water interplay. Moreover, complex near-surface processes which also contribute to groundwater-surface water interactions such as the replenishment of soil moisture deficit in the vadose zone, surface runoff and flooding are not simulated. By design these simplifications have allowed for a conservative prediction of the impacts on shallow alluvial systems to be achieved as noted in section 3.3.1.

- Irrespective of areas such as the Condamine Alluvium where detailed modelling studies have been integrated into the regional UWIR 2019 model to reflect the additional understanding of surficial groundwater flow processes, the model is not considered to be an appropriate tool for the simulation of surface-water interaction in the Surat Cumulative Management Area.
- Away from CSG production areas, particularly in the northern part of the CMA, the underlying geological model is based on relatively fewer data sets and limited validation. This, combined with general lack of groundwater observations from the area, limits the use of the groundwater flow model for making predictions about the CSG impacts in those areas.

8.3 Uncertainties in predictions

Given the mathematical challenge of non-uniqueness in the model calibration process, its predictions are accompanied by uncertainties. Sources of predictive uncertainty for the model include the following:

- Parameters of the model are based on upscaled measurements of hydraulic properties, expert knowledge, and adjustment through the model calibration process. Information from all of these sources is not sufficient to ensure the unique estimation of model parameters. This component of uncertainty has been assessed through completion of a post-calibration uncertainty analysis as described in Chapter 7.
- Many aspects of groundwater extraction and groundwater flow can only be simulated in an approximate fashion. Examples are the approximation of dual-phase flow near CSG wells using a modified single phase flow formulation and the simplified representation of near-surface groundwater flow and coal mines using drains.
- Groundwater stresses in the Surat CMA can only be captured approximately. In particular, the model's ability to represent the impacts of non-CSG water supply extractions is affected by the lack of reliable and metered data from these extraction bores. Future CSG development is another source of uncertainty as development plans are subject to continuous change and exact locations of future CSG wells are unknown. Two additional model runs are completed to assess uncertainty in future CSG development (see section 6.3.2.1).

References

Arrow Energy, 2015. ECLIPSE modelling outputs of the Tipton field sent to OGIA on October 14th 2015. Arrow, Brisbane.

Aster, R.C., Thurber, C.H., Borchers, B., 2005. Parameter estimation and inverse problems. Elsevier Academic Press.

Babu, D.K., Odeh, A.S., 1989. Productivity of a Horizontal Well. SPE Reserv. Eng. 4, 417–421. https://doi.org/10.2118/18298-PA

Bense, V.F., Gleeson, T., Loveless, S.E., Bour, O., Scibek, J., 2013. Fault zone hydrogeology. Earth-Science Rev. 127, 171–192.

Bense, V.F., Person, M.A., 2006. Faults as conduit-barrier systems to fluid flow in siliciclastic sedimentary aquifers. Water Resour. Res. 42.

Carle, S.F., 1999. T-PROGS: Transition Probability Geostatistical Software.

Christensen, S., Doherty, J., 2008. Predictive error dependencies when using pilot points and singular value decomposition in groundwater model calibration. Adv. Water Resour. 31, 674–700. https://doi.org/10.1016/J.ADVWATRES.2008.01.003

Cooley, R.L., Christensen, S., 2006. Bias and uncertainty in regression-calibrated models of groundwater flow in heterogeneous media. Adv. Water Resour. 29, 639–656. https://doi.org/10.1016/J.ADVWATRES.2005.07.012

Corvi, P., Ehlig-Economides, C., Corbett, P., 1992. Reservoir characterisation using expert knowledge, data and statistics. Oilf. Rev. 4, 25–39.

Cui, T., Moore, C., Raiber, M., 2018. Probabilistic assessment of the impact of coal seam gas development on groundwater: Surat Basin, Australia. Hydrogeol. J. 26, 2357–2377. https://doi.org/10.1007/s10040-018-1786-2

Dagan, G., Fiori, A., Jankovic, I., 2013. Upscaling of flow in heterogeneous porous formations: Critical examination and issues of principle. Adv. Water Resour. 51, 67–85. https://doi.org/10.1016/J.ADVWATRES.2011.12.017

Deutsch, C. V., Journel, A.G., 1992. GSLIB: Geostatistical Software Library and User's Guide.

Doherty, J., 2019. PEST_HP: PEST for highly parallelized computing environments.

Doherty, John, 2018. PLPROC: a Parameter List Processor.

Doherty, J, 2018. PEST: Model-Independent Parameter Estimation User Manual Part II: PEST Utility Support Software (7th Edition).

Doherty, J., 2016a. PEST: Model-Independent Parameter Estimation. Part I: PEST, SENSAN and Global Optimisers.

Doherty, J., 2016b. PEST: Model-Independent Parameter Estimation. Part II: PEST Utility Support Software.

Doherty, J., 2015. Calibration and uncertainty analysis for complex environmental models. Watermark Numerical Computing, Brisbane, Australia.

Doherty, J., 2003. Ground Water Model Calibration Using Pilot Points and Regularization. Ground Water 41, 170–177. https://doi.org/10.1111/j.1745-6584.2003.tb02580.x

Doherty, J., Christensen, S., 2011. Use of paired simple and complex models to reduce predictive bias and quantify uncertainty. Water Resour. Res. 47. https://doi.org/10.1029/2011WR010763

Doherty, J., Hunt, R., 2010. Approaches to Highly Parameterized Inversion: A Guide to Using PEST for Groundwater-Model Calibration. https://doi.org/Scientific Investigations Report 2010–5169

Doherty, J., Welter, D., 2010. A short exploration of structural noise. Water Resour. Res. 46, 1–14. https://doi.org/10.1029/2009WR008377

Dong, J.-J., Hsu, J.-Y., Wu, W.-J., Shimamoto, T., Hung, J.-H., Yeh, E.-C., Wu, Y.-H., Sone, H., 2010. Stress-dependence of the permeability and porosity of sandstone and shale from TCDP Hole-A. Int. J. Rock Mech. Min. Sci. 47, 1141–1157. https://doi.org/10.1016/J.IJRMMS.2010.06.019

Economides, M., Brand, C., Frick, T., Leoben, M.U., 1996. Well Configurations in Anisotropic Reservoirs, SPE Formation Evaluation.

Esteban, L., Pervukhina, M., Mallants, D., Clennell, M.B., Verrall, M., Raven, M., Nguyen, D., 2015. Experimental Study of Background Permeability of Formations in the Walloon Sub Group (Surat Basin). CSIRO.

Farmer, C.L., 2002. Upscaling: a review. Int. J. Numer. Methods Fluids 40, 63–78. https://doi.org/10.1002/fld.267

Faulkner, D.R., Jackson, C.A.L., Lunn, R.J., Schlische, R.W., Shipton, Z.K., Wibberley, C.A.J., Withjack, M.O., 2010. A review of recent developments concerning the structure, mechanics and fluid flow properties of fault zones. J. Struct. Geol. 32, 1557–1575.

Fitts, C.R., 2013. Groundwater Science, 2nd ed. Elsevier, Amsterdam.

Freeze, R.A., Cherry, J.A., 1979. Groundwater. Prentice-Hall, Englewood Cliffs, NJ.

GHD, 2012. Report for Queensland Water Commission (QWC), Stage 2 Surat Cumulative Management Area Groundwater Model Report. Office of Groundwater Impact Assessment, Brisbane.

Hayes, P., Nicol, C., Underschultz, J., 2019. Precipice sandstone hydraulic property estimation from observed MAR responses, The University of Queensland Surat Deep Aquifer Appraisal Project – Supplementary Detailed Report. Brisbane, Australia.

Herckenrath, D., Doherty, J., Panday, S., 2015. Incorporating the effect of gas in modelling the impact of CBM extraction on regional groundwater systems. J. Hydrol. 523, 587–601. https://doi.org/10.1016/j.jhydrol.2015.02.012

Herckenrath, D., Langevin, C.D., Doherty, J., 2011. Predictive uncertainty analysis of a saltwater intrusion model using null-space Monte Carlo. Water Resour. Res. 47. https://doi.org/10.1029/2010WR009342

Howell, S.R., Coulibaly, K., Vaughan, R., Ryan, D., Campbell, L., Guiton, S., De Verteuil, D.I., Curum, N., 2013. The Future Of Integrated Groundwater and CSG Simulation - Modeling The Surat Basin, Queensland, Australia, in: SPE Unconventional Resources Conference and Exhibition-Asia Pacific. Society of Petroleum Engineers. https://doi.org/10.2118/167049-MS

James, S.C., Doherty, J.E., Eddebbarh, A.-A., 2009. Practical Postcalibration Uncertainty Analysis: Yucca Mountain, Nevada. Ground Water 47, 851–869. https://doi.org/10.1111/j.1745-6584.2009.00626.x

KCB, 2011. Central Condamine Alluvium, Stage IV - Numerical Modelling, Final Report. Brisbane.

Keating, E.H., Doherty, J., Vrugt, J.A., Kang, Q., 2010. Optimization and uncertainty assessment of strongly nonlinear groundwater models with high parameter dimensionality. Water Resour. Res. 46, 2009WR008584. https://doi.org/10.1029/2009WR008584

Kellett, J.R., Ransley, T.R., Coram, J., Jaycock, J., Barclay, D.F., McMahon, G.A., Foster, L.M., Hillier, J.R., 2003. Groundwater Recharge in the Great Artesian Basin Intake Beds, Queensland, NHT Project# 982713, Bureau of Rural Science.

Littleboy, M., Silburn, D.M., Freebairn, D.M., Woodruff, D., Hammer, G.L., 1989. PERFECT, A computer simulation model of Productivity, Erosion, Runoff Functions to Evaluate Conservation Techniques.

Manzocchi, T., Childs, C., Walsh, J.J., 2010. Faults and fault properties in hydrocarbon flow models. Geofluids 10, 94–113. https://doi.org/10.1111/j.1468-8123.2010.00283.x

Manzocchi, T., Walsh, J.J., Nell, P., Yielding, G., 1999. Fault transmissibility multipliers for flow simulation models. Pet. Geosci. 5, 53–63.

Menke, W., 1984. Geophysical data analysis : discrete inverse theory. Academic Press.

Moore, C.R., Doherty, J., Howell, S., Erriah, L., 2015. Some Challenges Posed by Coal Bed Methane Regional Assessment Modeling. Groundwater 53, 737–747. https://doi.org/10.1111/gwat.12276

Moore, C.R., Doherty, J.E., Howell, S., Erriah, L., de Verteuil, D., Cui, T., 2013. Challenges for upscaling hydraulic properties and processes in the coal seam gas context, CSIRO.

Nelson, PH, Batzle, M., 2013. Single-phase permeability, in: Fanchi, J. (Ed.), Petroleum Engineers Handbook. Society of Petroleum Engineers, pp. 687–726.

Niswonger, R., Panday, S., Motomu, I., 2011. MODFLOW-NWT, A Newton Formulation for MODFLOW-2005, US Geological Survey Techniques and Methods 6-A37.

OGIA, 2019a. Underground Water Impact Report for the Surat Cumulative Management Area. Brisbane.

OGIA, 2019b. Updated Geology and Geological Model for the Surat Cumulative Management Area. Department of Natural Resources, Mines and Energy, Brisbane.

OGIA, 2019c. Conceptualisation and characterisation of faults in the Surat Basin. OGIA, Department of Natural Resources, Mines and Energy, Brisbane.

OGIA, 2019d. Water extraction in the Surat Cumulative Management Area; Technical method and results. Department of Natural Resources, Mines and Energy, Brisbane.

OGIA, 2019e. Summary of Hydrogeological Conceptualisation – Surat Cumulative Management Area.

OGIA, 2019f. Fault Conceptualisation Report. OGIA, Department of Natural Resources and Mines, Brisbane.

OGIA, 2016a. Surat Cumulative Management Area Groundwater Modelling Report [WWW Document]. URL https://drive.google.com/file/d/0B5u2TKAmnh_iRlo4T0ZMOTB3WE0/view

OGIA, 2016b. Underground Water Impact Report for the Surat Cumulative Management Area, Underground Water Impact Report for the Surat Cumulative Management Area. Department of Natural Resources and Mines, State of Queensland, Brisbane.

OGIA, 2016c. Groundwater Connectivity Between the Condamine Alluvium and the Walloon Coal Measures. OGIA, Department of Natural Resources and Mines, Brisbane.

OGIA, 2016d. Hydrogeological Conceptualisation Report for the Surat Cumulative Management Area. OGIA, Department of Natural Resources and Mines, Brisbane.

Pan, Z., Connell, L.D., 2012. Modelling permeability for coal reservoirs: A review of analytical models and testing data. Int. J. Coal Geol. 92, 1–44. https://doi.org/10.1016/J.COAL.2011.12.009

Panday, S., Langevin, C., Niswonger, R., Ibaraki, M., Hughes, J., 2017. MODFLOW-USG version 1.4.00: An unstructured grid version of MODFLOW for simulating groundwater flow and tightly coupled processses using a control volume finite-difference formulation.

Peaceman, D., 1978. Interpretation of well-block pressures in numerical reservoir simulation. Soc. Pet. Eng. J. 18, 183–194.

QGC, 2014a. GEN3 Surat Basin Regional Groundwater Flow Model Calibration Report. QCLNG-BE99-WAT-PLN-000006, Brisbane.

QGC, 2014b. Walloon Subgroup.

Quental, P., Almeida, J.A., Simões, M., Amaral, H., Fernandes, J., 2012. Construction of high-resolution 3D stochastic geological models and optimal upscaling to a layer-type hydrogeological model, Ninth International Geostatistics Congress.

Rau, G.C., Acworth, R.I., Halloran, L.J.S., Timms, W.A., Cuthbert, M.O., 2018. Quantifying Compressible Groundwater Storage by Combining Cross-Hole Seismic Surveys and Head Response to Atmospheric Tides. J. Geophys. Res. Earth Surf. 123, 1910–1930. https://doi.org/10.1029/2018JF004660

Ryan, D.J., Hall, A., Erriah, L., Wilson, P.B., 2012. The Walloon coal seam gas play, Surat Basin,

Queensland. APPEA J. 52, 273–290. https://doi.org/https://doi.org/10.1071/AJ11020

Sclater, J.G., Christie, P.A.F., 1980. Continental stretching: An explanation of the Post-Mid-Cretaceous subsidence of the central North Sea Basin. J. Geophys. Res. Solid Earth 85, 3711–3739. https://doi.org/10.1029/JB085iB07p03711

Seidle, J., 2011. Fundamentals of coalbed methane reservoir engineering. PennWell Books, Tulsa, Oklahoma.

Skahill, B.E., Baggett, J.S., Frankenstein, S., Downer, C.W., 2009. More efficient PEST compatible model independent model calibration. Environ. Model. Softw. 24, 517–529. https://doi.org/10.1016/J.ENVSOFT.2008.09.011

Sperrevik, S., Gillespie, P.A., Fisher, Q.J., Halvorsen, T., Knipe, R.J., 2002. Empirical estimation of fault rock properties. Nor. Pet. Soc. Spec. Publ. 11, 109–125.

Stillwell, W.G., Seaver, D.A., Edwards, W., 1981. A comparison of weight approximation techniques in multiattribute utility decision making. Organ. Behav. Hum. Perform. 28, 62–77. https://doi.org/10.1016/0030-5073(81)90015-5

Suckow, A., Taylor, A., Davies, P., Leaney, F., 2016. Geochemical baseline monitoring. Final Report. CSIRO, Australia.

Tonkin, M., Doherty, J., 2009. Calibration-constrained Monte Carlo analysis of highly parameterized models using subspace techniques. Water Resour. Res. 45, 17–24. https://doi.org/10.1029/2007WR006678

Weatherford, 2014. Provisional Petrophysical Evaluation Report: Initial 50 Well Study of the Talinga Area.

White, J.T., Doherty, J.E., Hughes, J.D., 2014. Quantifying the predictive consequences of model error with linear subspace analysis. Water Resour. Res. 50, 1152–1173. https://doi.org/10.1002/2013WR014767

Wood, B.D., 2009. The role of scaling laws in upscaling. Adv. Water Resour. 32, 723–736. https://doi.org/10.1016/J.ADVWATRES.2008.08.015

Yielding, G., 2002. Shale Gouge Ratio — calibration by geohistory. Nor. Pet. Soc. Spec. Publ. 11, 1–15. https://doi.org/10.1016/S0928-8937(02)80003-0

Glossary

Alluvium: Deposits of clay, silt, sand, gravel, or other particulate material that has been deposited by a stream or other body of running water in a streambed, on a flood plain, on a delta, or at the base of a mountain.

Aquifer: A saturated underground geological formation or group of formations, that can store water and yield it to a bore or spring. A saturated formation that will not yield water in usable quantities is not considered an aquifer.

Aquitard: A geological formation that prevents significant flow of water due to its low permeability (e.g., clay layers or tight deposits of shale).

Basement (geological): Generally low permeability hard rock strata of igneous or metamorphic origin which lie below sedimentary rocks or sedimentary basins. In the same way the sediments or sedimentary rocks on top of the basement can be called a "cover" or "sedimentary cover".

Basin (geological): An area in which the rock strata dip from the margins toward a common centre; the site of accumulation of a large thickness of sediments.

Basin (groundwater or hydrogeological): A groundwater system made up of multiple aquifers, may be equivalent to a geological basin.

Consolidated aquifer: A water bearing aquifer made of consolidated rock such as sandstone, coal, limestone or granite.

Conventional petroleum and gas: Petroleum and gas that is generally found in permeable formations such as sandstone trapped in reservoirs by an overlying low permeability rock formation, or within geological structures that allow the petroleum and gas to concentrate or pool.

Deposition: The laying down/settling of material (clay, sand, rock) carried by wind, water, or ice.

Depressurisation: The extraction of groundwater by pumping to decrease pressure in the groundwater system or reduce groundwater head.

Drawdown (noun): The difference between the groundwater pressure before and after pumping or depressurisation.

Drill stem test: A procedure used to test the surrounding geological formation through the drill stem when a petroleum well is drilled. It is used to estimate the productive capacity, pressure, porosity or permeability of a petroleum producing formation.

Dual-phase flow: The simultaneous flow of two substances through porous material; for example when gas and water are flowing through a geological formation to a well.

Elevation: Height above a set point usually in relation to a standardised sea level or datum.

Erosion: The wearing down or washing away of the soil and land surface by the action of water, wind, or ice.

Fault (geological): A break in a geological formation along which some measurable movement, or displacement, has occurred typically due to tectonic movement and uplift of the earth's crust (see also ‘Fracture’).

Formation (geological): A sediment or rock, or group of sediments or rocks. Geologists often group rocks of similar types and ages into named formations, for example the Hooray Sandstone of the Great Artesian Basin.

Fracture (geological): A minor break in a geological formation with no measurable movement, or displacement (see also 'Fault').

Groundwater: Also known as underground water. Water found in the cracks, voids, pores or other spaces between particles of clay, silt, sand, gravel or rock within the saturated zone of a geological formation.

Groundwater database: A database maintained by DNRME that stores information relating to registered groundwater bores drilled within the state of Queensland.

Groundwater flow model: A set of equations, which, subject to certain assumptions, quantify the physical processes active in a groundwater system. While a model cannot simulate the detailed reality of the groundwater system, its behaviour approximates that of the actual system and is used to simulate that behaviour.

Head (groundwater): Groundwater level or pressure.

Horizon (geological): A bedding surface where there is marked change in the lithology within a sequence of sedimentary or volcanic rocks, or a distinctive layer or thin bed with a characteristic lithology or fossil content within a sequence.

Hydraulic gradient: The difference in water pressure or water level across one or more formations over a unit distance. The hydraulic gradient indicates which direction groundwater will flow, and how rapidly.

Hydrogeology: The study of how groundwater moves, how it is distributed and how it interacts with rock.

Hydrostratigraphy: The identification of units on the basis of hydraulic properties.

Immediately Affected Area: The area of an aquifer within which water levels are predicted to fall, due to water extraction by petroleum tenure holders, by more than the trigger threshold within three years. The trigger thresholds are specified in the Water Act as five metres for consolidated aquifers (such as sandstone) and two metres for unconsolidated aquifers (such as sand). Within the Immediately Affected Area, there is significant risk that the supply of water from a bore tapping the formation will be impaired within three years.

Interbedded: Where beds, or layers, of geological material of different lithology or properties are layered together.

Lithic: Geological deposits or sedimentary rocks that contain abundant fragments of previously-formed rocks.

Lithology: The physical characteristics of rock, with reference to qualities such as colour, composition and texture.

Long-term Affected Area: The area of an aquifer within which water levels are predicted to fall, due to water extraction by petroleum tenure holders, by more than the trigger thresholds at any time in the future. The trigger thresholds are specified in the Water Act as five metres for consolidated aquifers (such as sandstone) and two metres for unconsolidated aquifers (such as sand).

Measures (geological): A series of coal-bearing rocks, such as the Walloon Coal Measures.

Model domain: The areal extent of the regional groundwater flow or associated geological model.

Mudstone: An extremely fine-grained sedimentary rock consisting of a mixture of clay and silt-sized particles.

Numerical permeameter: Local-scale block models of the subsurface developed to derive effective formation scale hydraulic properties from detailed lithological data.

Outcrop (noun): A geological formation or rock strata exposed at the ground surface.

Outcrop (verb): To be exposed at the ground surface.

Permeable: Capable of transmitting water through porous rock, sediment or soil.

Permeability: A property of a soil, sediment or rock indicating how easily water will be transmitted through it under a hydraulic gradient.

Permeameter: See 'numerical permeameter'.

Petroleum tenure holder: An entity that holds an authority to prospect and/or a petroleum lease under the *Petroleum and Gas (Production and Safety) Act 2004*.

Potentially affected spring: A spring where the water level in the underlying aquifer is predicted to fall by more than 0.2 metres at any time in the future.

Production area: The area from which petroleum and gas is planned to be produced.

Recharge: The process of water flowing into an aquifer.

Sediment: Material suspended in water or deposited from suspension. The plural form, sediments, is applied to all kinds of deposits from the waters of streams, lakes and seas.

Sedimentary basin: A geological basin containing a sequence of mainly sedimentary rocks.

Sequence (geological): A sequence of geological events, processes, or rocks, arranged in chronological order.

Shelf (geological): A narrow surface of basement rock shaped like a shelf.

Siltstone: Fine-grained sedimentary rock consisting of consolidated silt.

Simulation period: The timeframe over which the groundwater predictions are made using the groundwater flow model.

Spring complex: A group of spring vents located close to each other. The vents are located in a similar geology and are fed by the same aquifer. No adjacent pair of spring vents in the complex is more than 10 km apart.

Spring vent: A single point in the landscape where groundwater is discharged at the surface. A spring vent can be mounded or flat and can also present as wetland vegetation, with no visible water at the location of the spring.

Steady state conditions: Conditions representing the long-term average hydrological balance of the groundwater system.

Strata: A series of layers of rock in the ground (singular: stratum).

Stratigraphic Unit: a volume of rock of identifiable origin and relative age range that is defined by the distinctive and dominant, easily mapped and recognisable petrographic, lithologic or palaeontologic features (facies) that characterise it.

Stratigraphy: The arrangement or layering of rock strata (stratification).

Sub-basin (geology): A smaller depression or accumulation of sediments within a larger basin; for example, the Surat Basin is a sub-basin of the Great Artesian Basin.

Trough (geological): An elongated, linear structural depression or narrow basin that is not steep-walled.

Uncertainty analysis: A technique for assessing the effect of uncertainty on prediction, using multiple realistic parameter sets to generate a large number of predictions which can then be statistically analysed to provide a measure of uncertainty in model prediction.

Unconfined aquifer: An aquifer with no overlying low permeability layers that restrict water movement into the aquifer. The water level in an unconfined aquifer is known as the water table.

Unconsolidated aquifer: An aquifer comprised of material that has not been turned into rock, such as sand.

Unit (geological): See ‘stratigraphic unit’.

Vertical permeability: The property of a formation indicating how easily or rapidly water is transmitted vertically.

Well field: An area within a petroleum lease with multiple wells used for P&G extraction.


Queensland
Government